Session II: Prestressed concrete pressure vessels

SESSION II SITZUNG II SESSION II

Caissons en béton précontraint

Spannbeton-Druckbehälter

Prestressed Concrete Pressure Vessels

CHAIRMAN: Prof. W. Zerna, Bochum, Germany

CO-CHAIRMAN: Prof. R.N. White, Cornell University, Ithaca, USA

Leere Seite
Blank page
Page vide

IABSE
AIPC
IVBH

SEMINAR on:
«CONCRETE STRUCTURES SUBJECTED TO TRIAXIAL STRESSES»
17th-19th MAY, 1974 - ISMES - BERGAMO (ITALY)

On the design of massive structures for nuclear plants

Über dem Proiekt der massiven Strukturen für nukleare Anlagen

Du projet de structures massives pour des installations nucleairs

G. BALLIO, A. CASTELLANI, L. FINZI
Istituto di Scienza e Tecnica delle Costruzioni
Politecnico di Milano (Italy)

1. INTRODUCTION

From the civil engineering point of view, the design of thermonuclear power plants raises particular problems, especially those concerned with stress analysis, structural detailing, and construction techniques.

In fact, the presence of highly radioactive substances in the vessel, the primary circuit, the fuel deposit and elsewhere gives overriding importance to the sealing of the building, even under the most severe loads. Furthermore, even if the distances between floors, or the centre-to-centre distances between columns and vertical walls in these buildings are similar to those in large modern factories, the loadbearing structures, slabs, beams, columns and walls are particularly thick. This is in part due to the requirements of biological shielding and the need to make the building missileproof, but it is also the consequence to a large extent of the vast loads involved. Inside the containment structures there may be pressures in the range of dozens of ton $\bar{m}^2$ while the outside may be subject to meteoric or military activity that can be translated into pressures 10 to 30 times greater than those due to wind. Finally, there may be mass horizontal forces, that, further exasperated by the rigidity of the structure, can be four

to six times greater than those laid down in Italy for 1st class seismic zones. As a result, even for buildings of modest transversal and longitudinal dimensions, the effects provoked by changes in temperature and by shrinkage are significant.

On the whole, the structures of nuclear buildings are massive and heavily braced, or even they are of the box type. It follows that great importance must be attributed not only to the foundation soils but also to the soil-structure interaction.

There are also cases of buildings in which the size itself of the ground plan dimensions becomes a factor of importance, further increasing the effects of inelastic variations in volume. This is true for the turbo-pedestals which, for 1000MW, can be 80m long, and for foundation mats, which tend to be interconnected in order to control safely the effects of differential settlements, which in turn condition the behaviour of the ducts connecting the various blocks of the building.

Besides thermal stresses and concrete shrinkage, earthquakes, wind and hurricanes, and pressure accidents, there are also, of course, the effects of dead weight and working loads. Besides these, there are also the local effects, which may well be measured in hundreds of tons, such as jet forces, the effects of pipe whipping, the fall of equipments during erection or substitution (fuel cask drop) and the action of internal missiles.

When therefore a single member has to be checked, a suitable combination has to be worked out of the most unfavourable overall loading conditions together with the most unfavourable local loads.

There are no established criteria on which to base the formation of these combinations, since many of these events involved are so rare, or even new, that information is insufficient for a statistical approach.

As a result, when in doubt it is normal to check all the combinations of possible events, laying down, for any one structure, tests for dozens of loading combinations.

Thus the structural designer is obliged to design buildings on the basis of a selection of loading conditions that seem decisive, and then to check them for the envelope of all the very many combinations possible. This is essential, since the structures involved are always highly redundant in which, of course, the elastic weights of the parts play an important role in the state of stress.

The obvious consequence is that, even where adequate computational instruments are available, the final stress analysis may lead to results that are locally very different from those allowed for at the design stage. This implies strengthening the steel reinforcing, with resulting problems of congestion.

Anyway, these structures are generally highly reinforced because it is better to reduce as much as possible the stiffness of individual members in order to minimise the conspicuous

effects of temperature and shrinkage on the one hand, and, on the other, the so-called "edge" effects that arise to guarantee compatibility with adjacent elements.

To sum up, for the civil engineer, nuclear power stations differ from other constructions in the following ways:

1) the need to ensure perfect sealing in the most severe conditions;
2) the importance of inelastic variations in volume;
3) the type of massive, box structures involved;
4) the size of the loads weighing on the ground;
5) the need to check the structure for a considerable number of loading combinations;
6) the congestion of the reinforcing.

The designer will thus have certain unusual problems in working out the behaviour patterns of reinforced concrete structures, in calculating and constructing them.

As to the basic structure of reinforced concrete buildings, since the elements involved are mostly subjected to two - and three-dimensional states of stress, two problems arise: defining the partialisation surface and the ultimate strength of the concrete, the latter having wide variations for three-dimensional states of stress; defining its behaviour when subjected to thermal stresses.

As to calculation, it seems necessary to turn to finite element processes, since these structures cannot be thought of as frames. Furthermore, as the computation methods become more sophisticated, in order to establish congruence between structural elements of different kinds and behaviour, strong local stresses arise. A non linear analysis thus becomes necessary to ensure a perfect seal in spite of these forces. However, since the design is generally conditioned by these problems of sealing, it is not necessary to take the non-linear analysis to the point of collapse.

Because of the large number of loading combinations,it seems tempting to computerise the design as much as possible, leaving it to a computer code to sort out the severest loading combinations and the necessary controls. The present authors have their doubts about this, since it would seem to lead to a formal respect for the controls to the detriment of sound design.

Lastly, the considerations already mentioned, but even more, the need to respect the regulations in the controls, often lead to a congestion of reinforcing, even when thick or bundled bars are used. In this situation, detail drawings and tight control over the erection become important.

2. GAP BETWEEN STRESS ANALYSIS AND DESIGN

More and better computer methods are gradually becoming available for the approach by finite elements.

Until recent times it was considered a success to be able to transform a problem from discrete to continuous, but today the finite element method leads to a reversal of this process.

Thus, for example, a circular slab of constant thickness subject to generic concentrated and distributed loads and resting on Winkler type soil, may be studied by dividing it into finite elements,each seen as perfectly homogeneous, elastic and isotropic.

A computer will deal with this problem,though with some effort, and gives stress and strain states which, since they refer to finite elements, have to be re-converted to the continuous system.

So parameters like displacements, which are of an integral nature, can be worked out with good approximation without artificial discontinuities. On the other hand local factors, i.e. the stress strain state, are given as discontinuities and averages.This makes their interpretation uncertain and personal.

The fact that computers can be used giving apparently exact solution makes this process extremely attractive, especially when very many loading combinations are involved as is in fact the case for nuclear structures.

However, the present authors would like to point out that there is still a lot of work to be done in this field. In fact,of the four blocks shown in fig.1, no.3 has received a great deal of attention, but much less work seems to have been done on no.2 and no. 4.

What this all comes to is that at the end of the operation the structural designer is faced with tens of thousands of figures from which it is difficult to form an overall picture of the real behaviour of the structure and so of the reliability of the result.As a process it is vitiated by a series of rules of thumb, both before and after, that make it like the mythical "colossus" with feet of clay and,in this case, a tutty neck.

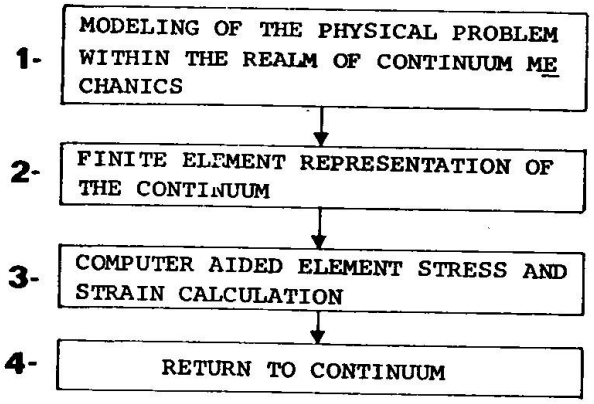

fig.1.

This state of affairs is, of course, known to those doing research in this field, and attention is now being directed to improving the ways

by which finite elements may be used for interpreting what is in reality a continuum - for us, reinforced concrete. The present authors find it strange that, in a field in which so much importance is rightly given to reliability, so little interest is placed in researching the suitable finite element models for concrete.

It has even been suggested that certain structural problems could be dealt with by using two different computer programs for the finite element approach, so that one would be a check on the other. It may be true that practical experience well applied can be of great help in processing data, but it is equally true that two uncertainties do not make one certainty.

The present authors feel that, after all, knowledge in this field being what it is at the moment, the basic study for a nuclear building must be carried out with reference to the real continuous system, working, when necessary, on ranges of values attributed to the paramenters involved, so as to form an overall picture of the structural response.

Along with this approach, a numerical analysis by the finite element approach would also be suitable, carried out with reference to a restricted group of loading conditions already singled out as the most severe to be expected, and applied to those parts of the structure where the continuous structural arrangement adopted may really prove defective: interface areas between different structural elements, sudden changes in thickness, load concentrations etc.

The last point to be considered will be the methods for checking the calculations, both for the total structure and for the details.

In the first, overall case, a general analysis by finite elements could be used, with reference to a few carefully chosen loading conditions, or else experiments could be made on a model. In the case of details, test models could be used of those critical areas that had previously been analysed by finite elements (see fig.2).

Coming back to the four blocks shown in fig.1 which summarise the necessary processes for structural analysis by finite elements, it is worth pointing out the marked but little known anisotropy of reinforced concrete when subject to two and three-dimensional stresses.

So, for example, in a foundation mat subdivided, along its thickness, into five layers, the upper and lower layers would be heavily reinforced, much less so the three internal layers. How can this be accounted for in the calculations?

Or again, in areas subject to tensile stress, microcraking may arise, thus altering the ways in which the structural element might deform. How can this be allowed for?

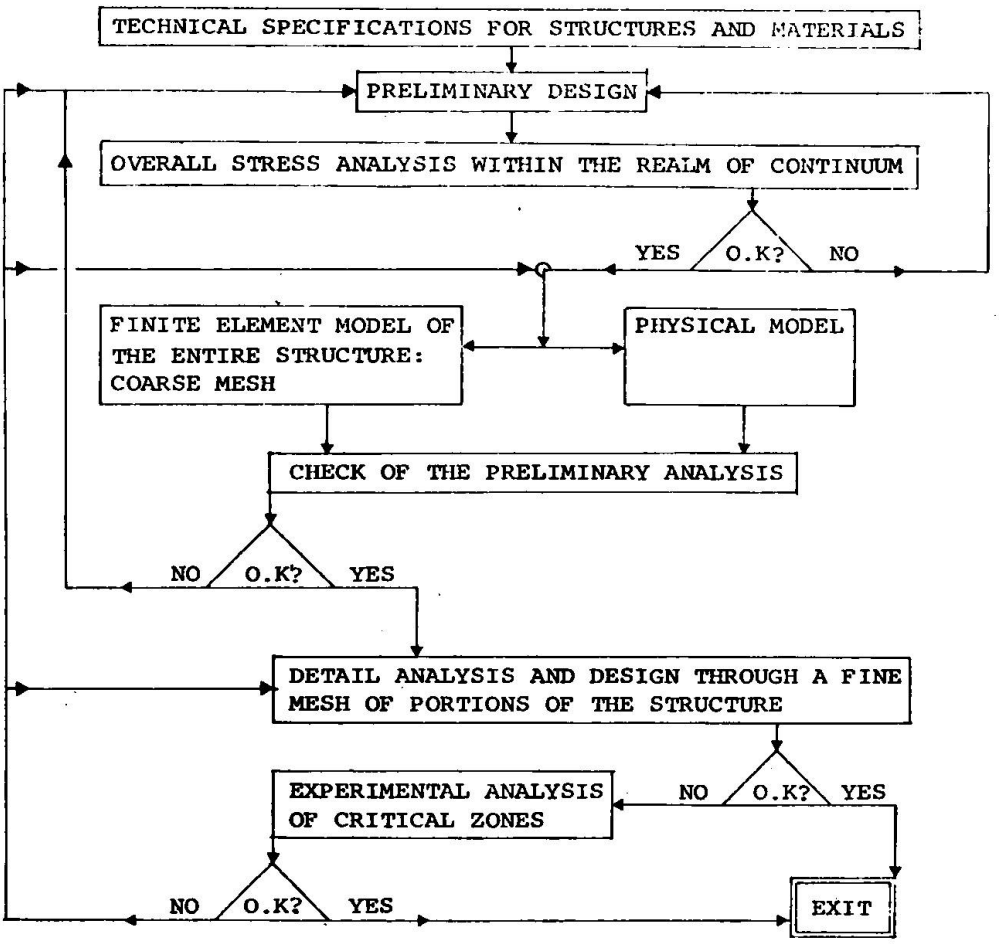

fig.2.

Looked at in this way, the problem would pose unanswerable questions and, purely from the point of view of control calculations, no solution would be possible. Something has to be done about the mathematical layout of the calculation model. That is to say, the evaluation of the stiffness must be in harmony with the design criteria for the reinforcing, i.e. concrete has to be considered as if cracked.

However, this is no simple matter, since it implies a study of all loading combinations plus an iterative examination of mathematical models according to the state of stress. Furthermore, it means that at least biaxial cracking must be allowed for, and, at least so far as the present authors know, this is still an open question, both theoretically and experimentally. There have been many studies, some quite recent, on the domains of resi-

stance [1,2,3,4] , and on how unreinforced concrete behaves when cracked [5,6,7,8] , but not much is known about the distribution and width of cracks in reinforced concrete. Furthermore, it seems of doubtful value to make unconditional assumptions, for calculation purposes, about structural rigidities under the hypothesis of cracked concrete, without being able to estimate dangers (leakage, corrosion) that can be quantified only when more is known about the width and spacing of the cracks. Designers and licensing authorities must therefore examine the problem together in order to base simplified calculation and checking methods on what real experience there is in this field.

3. THERMAL EFFECTS

This section will be concerned with three main arguments:

1) the heat transfer law across a massive concrete wall;
2) the elastic properties of the concrete related to changes in temperature;
3) the stress analysis.

As to the first topic, consider an infinite wall of thickness d, initially at a uniform temperature. When it is exposed to cooler air on both faces, the heat transfer from concrete to the air up to the instantt can be expressed, under certain assumptions,

1) $$\Delta Q = Q_0 \exp(-\frac{k}{d^2} t)$$

where k is a suitable constant depending on the heat capacity and conductivity of the concrete. Eq.1. says that the time constant for the temperature variation is inversely proportional to the square of the thickness d .For instance for a 15 cm thick wall, 90% of the heat in the concrete will be last to the air in 1,5 h. For a 1 m thick wall this amount of heat would be lost in 3 days and for a 1.5 m thick wall in a week. Another implication of the above assumption is that at the surface of a thick exterior wall the temperature of the concrete follows almost completely the daily variations of air temperature, while 60 cm from the surface only 10% of the daily surface temperature is felt in the concrete.

The consequences of such thermal behavior are twofold:

1) in a thick external wall the surface is often defenceless against stress cracking,
2) the structural stresses due to the average temperature rise of the entire cross section are to be related to the air temperature averaged over a few days or a week.

In fact, consider a temperature variation of 25°C acting so fast on the surface of a thick wall that the interior of the

wall could be thought of as insensitive to it.

For a concrete with 300.000 Kg/cm^2 elastic modulus E, without cracking, the surface stresses would vary to about 75 Kg/cm^2 in both horizontal and vertical directions. The concrete can quite easily take such a stress wehn in compression, but cannot be relied on when in tension (in the horizontal direction assume no stress for dead load). In this latter case cracking is therefore nearly unavoidable; it is only possible to control the width and the distance of fissures by means of a suitable disposal of reinforcing.

On the other hand the overall behavior of the structure is only related to the average temperature rise of the entire cross section, which shows a smaller temperature change in both cases 1) and 2), depending on the heat transfer law.

As to leakage control, in the above picture the surface cracking due to temperature changes is confined to a relatively thin superficial region. That is, the surface, even cracked, protects the structural integrity of the concrete below it.

The "thermal shock" just mentioned may represent the effect of an accident of any sort or a noticeable daily excursion to which the interior concrete of a thick wall cannot take up.

Apart from the accident conditions which are confined to the reactor building, the seasonal temperature cycles only affect the state of stress of a structure very slowly provided that its exterior walls are thick enough to make them sensitive to the mean weekly variations only. Now as is well known, the elastic modulus of normal elasticity depends on the time history of the loads: instantaneous loading are related to a value of which is nearly the double of the value to be accounted for where the loading history is accomplished in some months, see for instances the Figs. 3 and 4. The data there reported refer to arch dams where similar and more severe problems are encountered.

As to figs. 3 and 4 it may be noticed:

1) according to the available data, even after 5 years, the concrete offers greater rigidity when acted on by instantaneous loading, although the ratio between instantaneous and substained rigidity decreases as the concrete ages;
2) there is evidence of a general trend toward the increase of the modulus as the concrete ages.

The first of these observations suggests that the seasonal effects on a thick walled structure are to be taken into account with a reduced modulus of elasticity, all along the structure life. On the other hand, according to the second consideration, every effect shares a different elastic behaviour for different structural age, in particular temperature cycles produce more severe

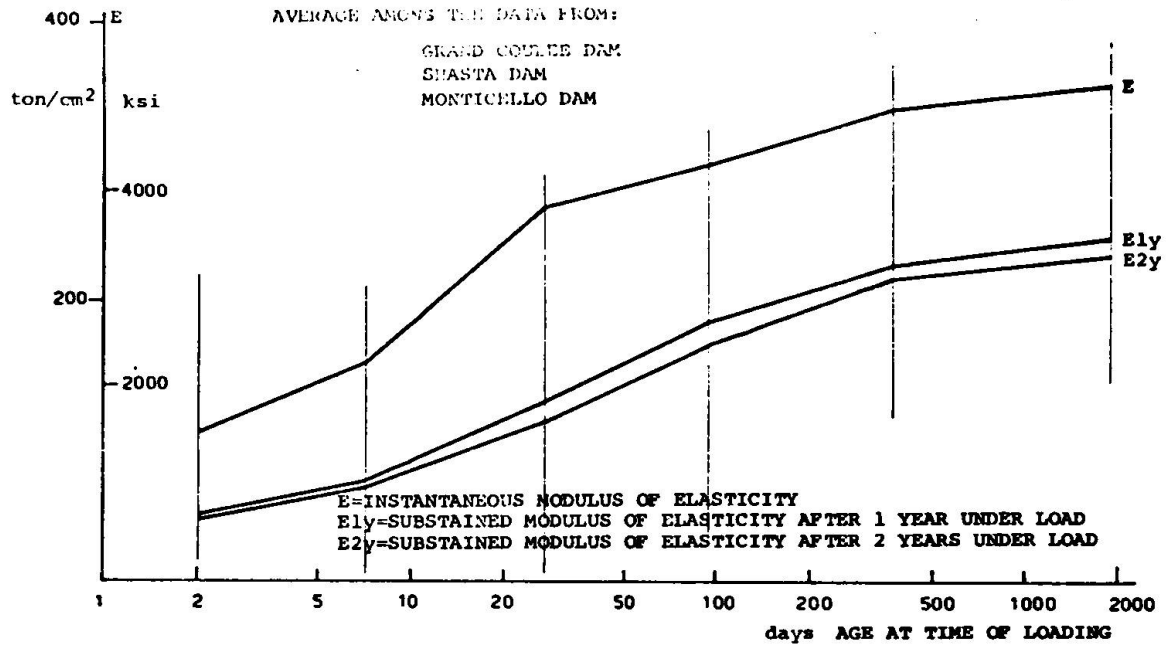
400
E
ton/cm2
ksi
4000
200
2000
AVERAGE AMONG THE DATA FROM:
GRAND COULEE DAM
SHASTA DAM
MONTICELLO DAM
E
E1y
E2y
E=INSTANTANEOUS MODULUS OF ELASTICITY
E1y=SUBSTAINED MODULUS OF ELASTICITY AFTER 1 YEAR UNDER LOAD
E2y=SUBSTAINED MODULUS OF ELASTICITY AFTER 2 YEARS UNDER LOAD
1
2
5
10
20
50
100
200
500
1000
2000
days AGE AT TIME OF LOADING

Fig.3

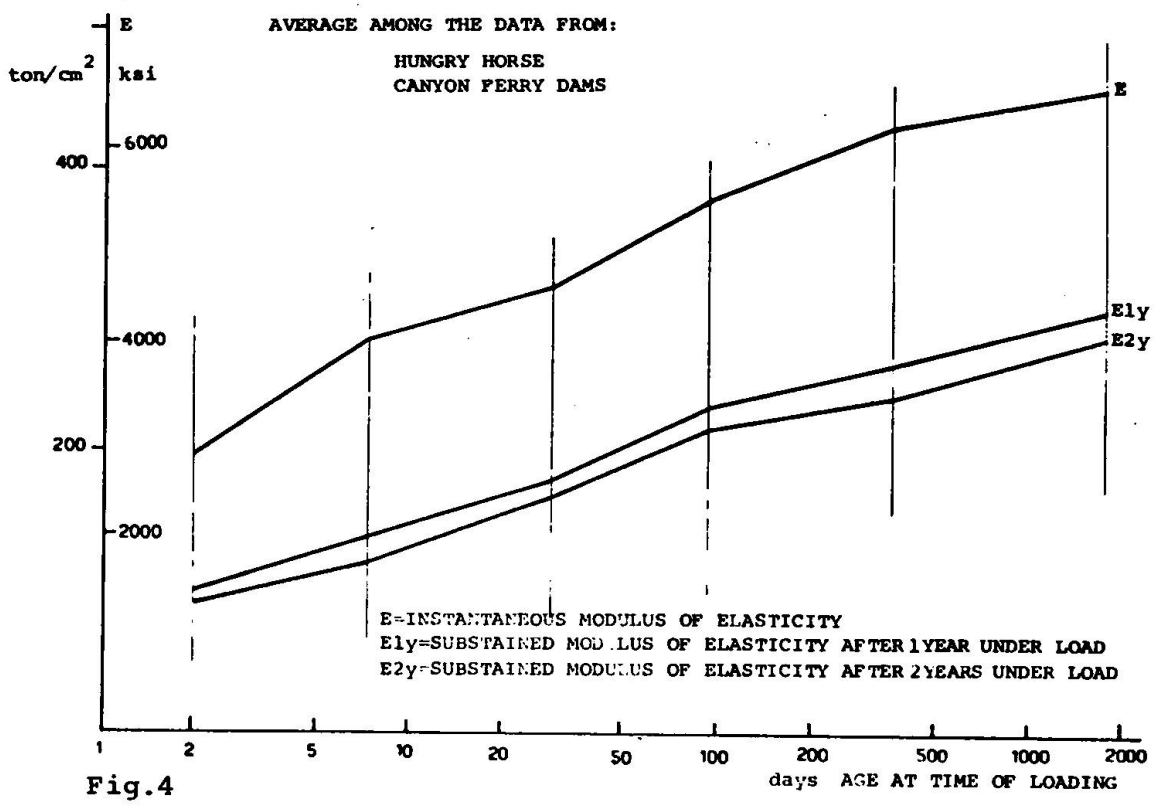
E
ton/cm2
ksi
400
6000
4000
200
2000
AVERAGE AMONG THE DATA FROM:
HUNGRY HORSE
CANYON FERRY DAMS
E
E1y
E2y
E=INSTANTANEOUS MODULUS OF ELASTICITY
E1y=SUBSTAINED MODULUS OF ELASTICITY AFTER 1YEAR UNDER LOAD
E2y=SUBSTAINED MODULUS OF ELASTICITY AFTER 2YEARS UNDER LOAD
1
2
5
10
20
50
100
200
500
1000
2000
days AGE AT TIME OF LOADING

Fig.4

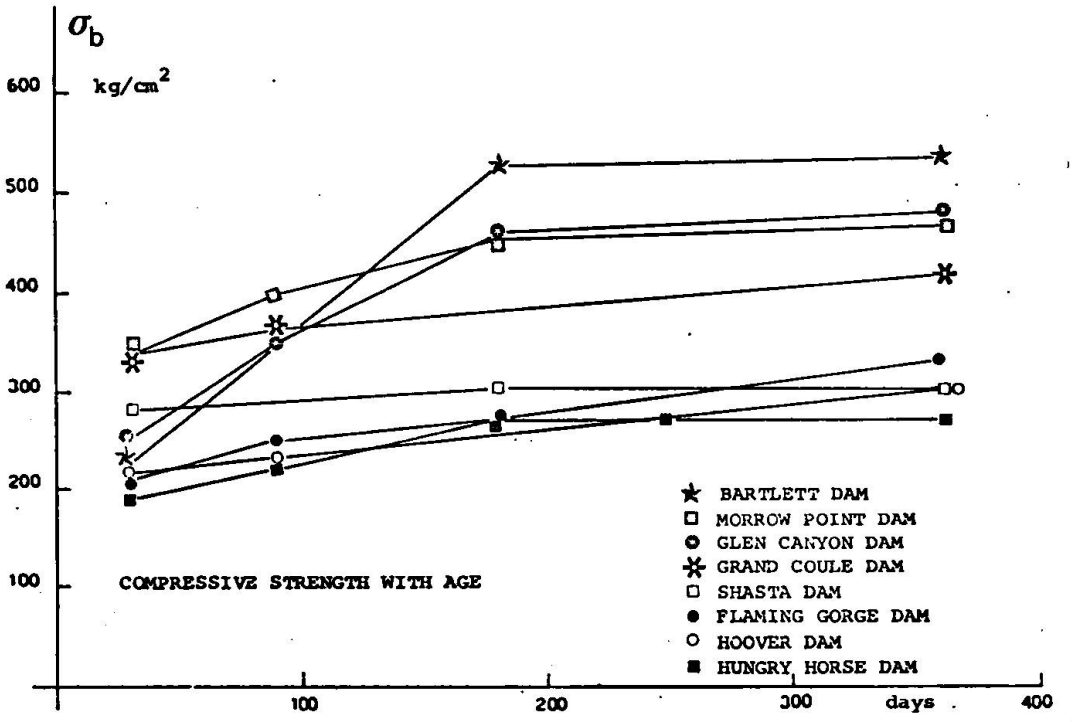

fig.5

effects when the elastic moduli are increased.

As to the safety analysis it may be further mentioned:

1) the strength of the concrete also increases with age, see for instance fig.5, (the shear strength shows similar tendencies);
2) the stresses due to applied loads, to be superimposed on temperature stresses, are not affected by a uniform increase of structural rigidity, so that, in theory, a variety of the loading combinations ought to be considered, depending on the age of the concrete.

As far as loading combinations and the relevant stress analyses are concerned, the lack of something equivalent to the ASME 3 code - Nuclear Vessel - is evidente. In fact, the ACI Committee 349, Code - Design Criteria for Reinf. Concrete Nuclear Reaction Cont. Structures - allows a nonlinear approach in the stress evaluation, which means that one can rely on the material ductility., although this occurs in the greatest portion of cases with

the formation of crackings. But ACI Committee 349 does not allow peak stresses to be disregarded, as ASME 3 Code does, so that,in theory it is possible to rely on ductility provided that one is able to show in each case the relevancy of cracking.

It must be further mentioned that the stress release due to section partialization is to be taken into account, for the sake of coherence; in fact this is the physical model for any reinforcement design.

In particular, the conventional elastic analysis technique is not directly suited to application in a containment structure,where severe strain effects at discontinuities lead to cracking.

4. DISCONTINUITY EFFECTS

A typical discontinuity effect occurs where axial expansion of a slab produces large local bending and circumferential traction in a cylindrical containment structure.

For the containment structure of Fig.6, let p be the undeter-

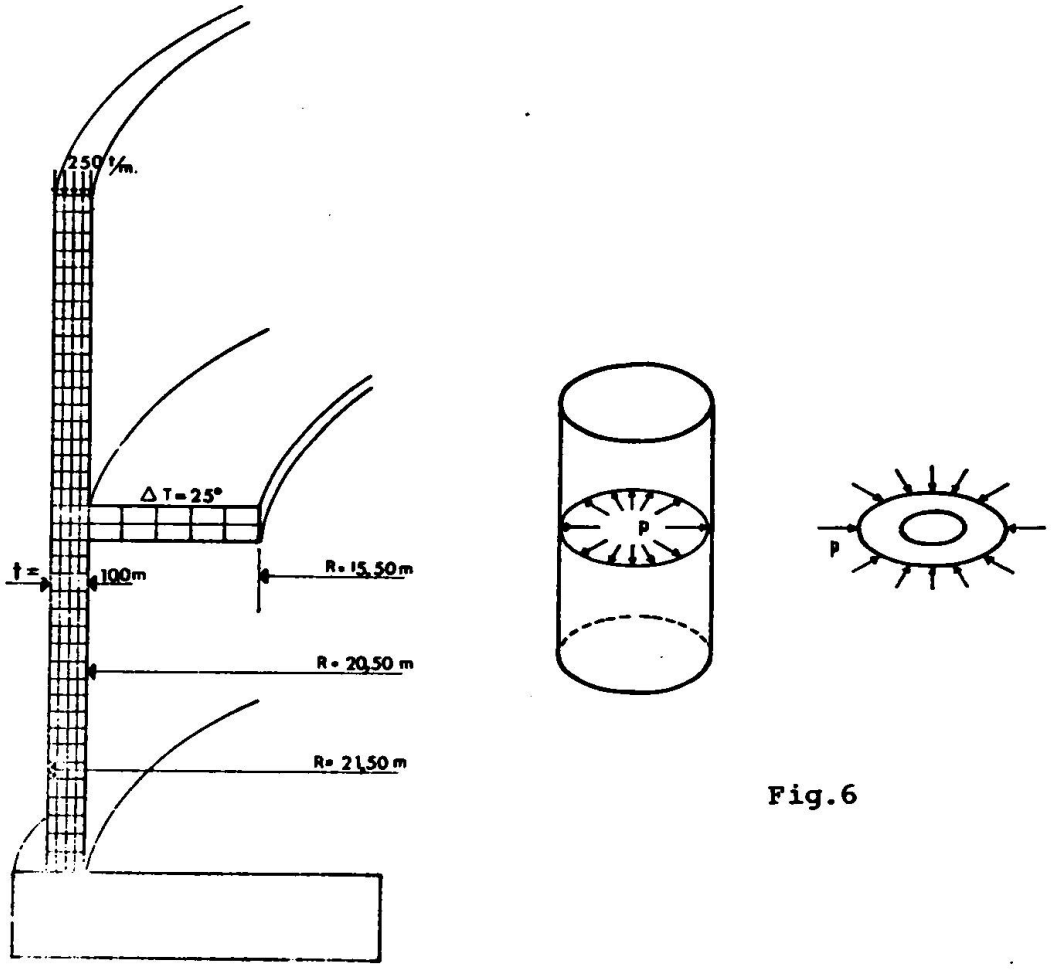

Fig.6

minate action exchanged between the slab and the shell.As a first approximation, the radial displacement produced by p on the slab may be disregarded, in comparison to the same quantity for the shell, i.e., the slab radial expansion may be taken as $s_r = \alpha \Delta T R$

Under this hypothesis, according to the thin elastic shell theory: $p = \frac{2\alpha\Delta T}{R\lambda} E t$

and the shell longitudinal moment is:

$$M_\ell = \frac{p}{4\lambda}\left[e^{-\lambda x}(\cos\lambda x + \sin\lambda x)\right] - \frac{p}{2}\left[\frac{1}{\lambda} e^{-\lambda x}\sin\lambda x\right]$$

where:

$$\lambda \simeq 1{,}3 \Big/ \sqrt{Rt}$$

The maximum value of M_ℓ is the well known expression:

$$\bar{M}_\ell = 0{,}294\,\alpha\Delta T E t^2$$

In the same way the following maximum values are computed:

$$\bar{M}_c = \nu \bar{M}_\ell$$

$$\bar{N}_c = \alpha \Delta T E t$$

Such a procedure leads generally to unacceptable designs even if a reduced modulus of elasticity has been used to account for creep releasing. The suitability of a nonlinear analysis is therefore evident.

The plastic analysis of shells by finite element methods have been extensively tried out [9,10] . The procedure is also applied in commercially available computer codes (Nastran,Feast 3, Poco..)

As to tridimensional reinforced concrete structures, the procedures so far quoted and the relevant codes are not directly applicable owing to the brittle nature of the tensile behaviour of the concrete. A few models for such a behaviour have been proposed [11,12,13] . In view of the smoothed stress pattern in the considered example, such models may be substantially simplified.

Without going into detail, the aim is to produce, in the final step, a mesh in which, for any element, the rigidities both circumferential and longitudinal are consistent with the stress levels. A shear transfer across cracks is allowed, other than the dowel action provided by the reinforcement, according to some recent investigations [14] .

The main results - see Fig.7 - are as follows.

- Circumferential actions N_c, which are to be feared in that fissures are not closed by dead load, are substantially reduced by the appropriate analysis. This is due to the fact that small

	thin shell elastic teory [Eq.1]	elastic analysis	inelastic analysis
N_c [t/m]	500	183	51
M_c [tm/m]	29,4	34.5	4.2
S [mm]	5.1	2.53	3.8

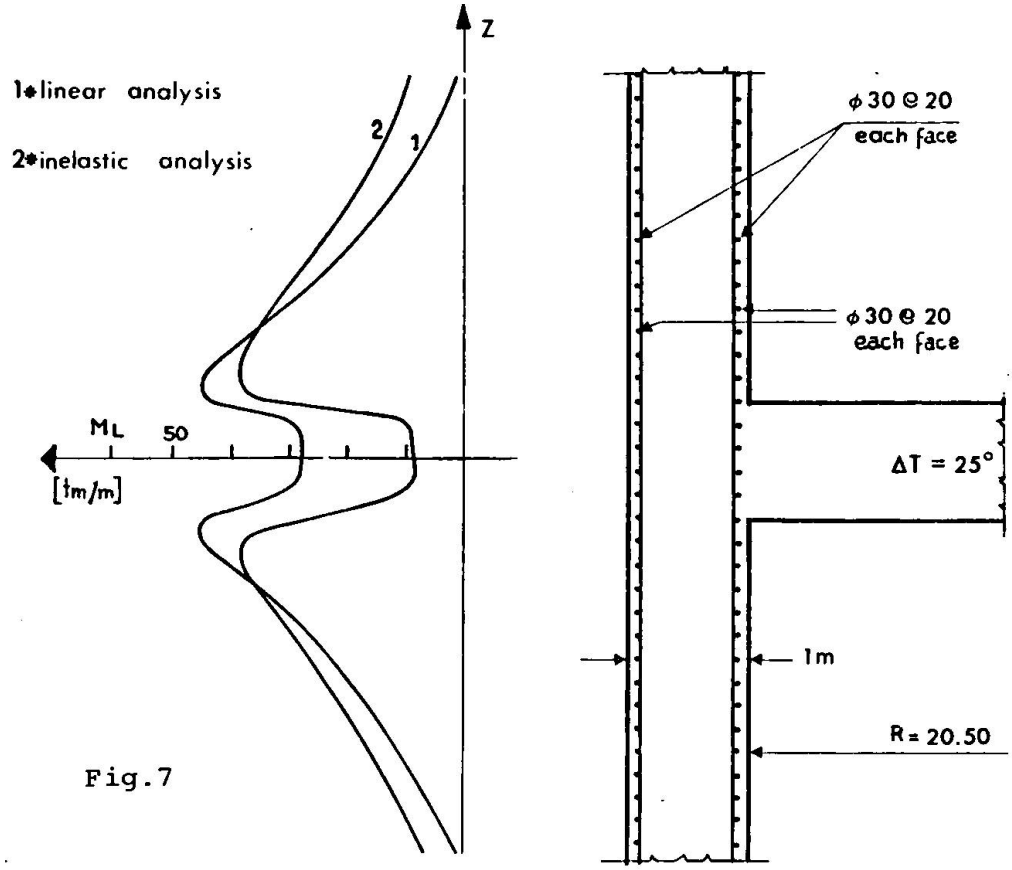

Fig.7

inelastic strains, but all along the circumference and through out the entire shell thickness, are allowed. The same happens for circumferential moment M_c.

- On the contrary an elastic analysis gives values of longitudinal moments M_ℓ not far from those obtained through a non linear approach. May also be that the latter are greater than the former, if the shell radial stiffness is not meaningless compared to the slab.This holds obviously if one takes into account the

same mesh both for the elastic and inelastic approach.
- On the contrary if the thin shell theory is directly used, a peak value for the longitudinal moments M_ℓ appears which is far greater than reality.

In conclusion the above example points out that a non linear approach gives vanishing values for M_c and N_c while proper values for M_ℓ can be obtained through a linear analysis provided that the model is not based on the thin shell theory when this is not suitable.

5 - TURBO PEDESTAL

The peculiar limit state to which this kind of structure is referred is the deformation under dynamic loading due to machine vibrations. While the pertinent level of stresses is generally fairly low, deformations are source of heating and wearing on the bearing supports and finally of machine misperformances.

The conventional approach is based on the analysis of the first three vibration modes or, which is equivalent, on the analysis of the sidewise lateral rigidity see fig.8. The fair beha-

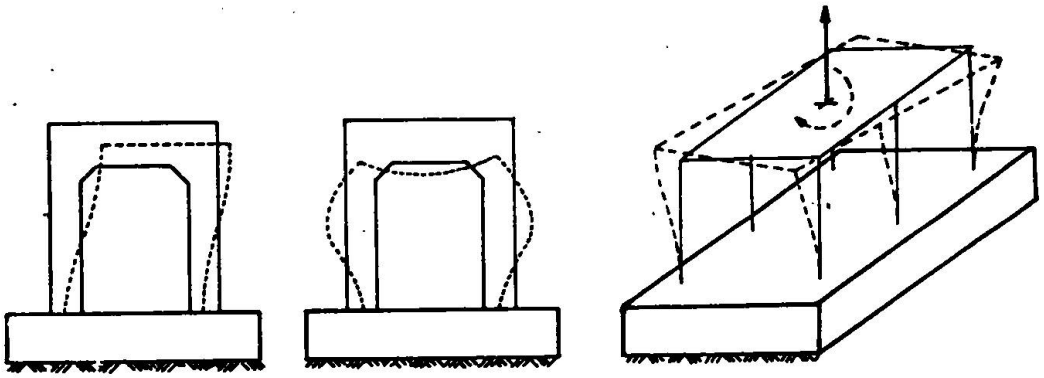

fig.8.

viour of small and medium sized pedestals is at the basis of such an approach. In fact for these structures higher modes of vibrations, others than those considered are seldom excited. So, disregarding them is allowed, even if deformation of the shaft and the relevant poorperformances mainly influence the higher modes.

When the dimensions of the pedestals are increased, up to 40 60 m in length, the structure is generally undertuned in its overall behaviour. On the other hand higher modes become critical, which implies that the conventional approach is not sufficient.

The analysis for the behaviour at higher modes of vibration faces several difficulties.

- If the analysis shows that the higher modes are undertuned for the initial value of the modulus of elasticity, this may no longer be true as the concrete ages, see Fig.3. So that the only reliable situation is the one in which all higher modes, other than those in fig.8, are overtuned.
- Shrinkage and temperature stresses, both for seasonal or functional reasons, are quite important due to the large dimensions of the structures. Unless a strictly elastic analysis is satisfied, the structure may differ from the mathematical model on which dynamical analysis is based. An elastic verification of shrinkage and temperature stresses allowing a suitable tensile strength for the concrete is therefore advisable. On the other hand, an inelastic analysis based on stress release due to concrete cracking, leads to meaningless stresses for such structures.
- The shape of the pedestal pertains more to bi or tridimensional structures than to a frame structure, so that the finite element approach or a physical model approach is compulsory. It must be mentioned in this regard that the Italian National Council for Electric Energy - ENEL - has for several years tested its plants with such techniques, mainly by means of the ISMES facilities.
- The rigidity of the machine itself contributes to the structural rigidity of the working slab. There is a lack of experimental evidence in this regard.

An advisable design would make the structure as rigid as possible in order to have it overtuned for higher modes even for the initial value of the modulus of elasticity. Thus the overtuning will hold all through its structural life provided that shrinkage and thermal effects are properly arranged. This tendency has led in some G.E. plants to linking the foundation mat to the turbine building mat. The foundation deformation, in fact, is proved to contribute significantly to pedestal rigidity, see Fig.9. A further progression of this tendency is given by an integrated system where the turbine pedestal is rigidly connected to the surrounding building at every level. A bearing wall, box system structure fulfils this arrangement. A very accurate lay out of the plant must be devised before hand for this kind of structure.

6. DETAILING

In one-dimensional structures normally the state of stress alone conditions the dimensions and geometrical layout of the reinforcing. In massive concrete constructions the reinforcing spatial mesh (dimensions and geometrical layout) is instead heavily conditioned by design choices of a technical kind, such as:

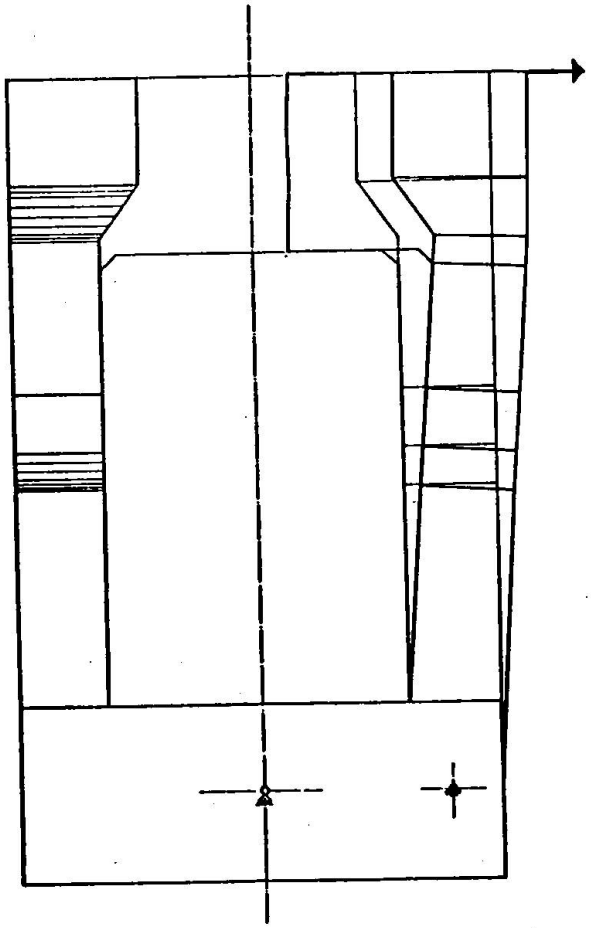

fig. 9

- the real possibilities of effectively arranging the steel reinforcing
- the practicability of casting, and the possibility of correct and adequate vibration.

These reservations dictated by the need to ensure correct erection, often become actual conditions of feasibility. Even if this cannot yet be proved theoretically, the present authors feel that a structure with a slightly undersized reinforcement, but correctly cast and erected, is preferable to one that has formal agreement with the verifications, but with a congestion of reinforcing that would jeopardize the quality of the casting and the real possibilities for checking it.

Some attempt will now be made to clarify those problems that are inherent in the designing and geometrical layout of the reinforcing, with reference to two typical examples: foundations mats and containment structures.

6.1. FOUNDATION MATS

Foundation mats are generally rectangular or circular, cover a wide area, and are from 2 to 4 meters thick. From the static point of view, a severe condition is generally that of earthquake which would partialise the supporting soil, thus subjecting the mat to considerable bending moments and shear forces. Furthermore, axial forces may arise at the same time, due to temperature changes, shrinkage and, in the case of containment structures, accident pressures.

However, the basic state of stress is typical that of bent slabs.

To a large extent, practical technology conditions the geometrical arrangement of the reinforcing.

In rectangular mats, it seems natural to make the main reinforcing with bars arranged parallel to the sides, and in several layers. No great difficulties arise here.

Circular mats,on the other hand, may have radial-circumferencial layout of reinforcing.This seems an obvious choice,but leads to serious problems concerning the distance between the bars,since this will not only affect the flexural behaviour of the mat, but may lead to congestion near the centre.As a result,it may well be a good idea to use an orthogonal cartesian mesh instead of a polar mesh.

This is normally done for the lower reinforcing of the mat, but is not suitable for the top, as it would militate against the axial symmetry of the dowels for the containment structure.

As to the design of the reinforcing, let us consider that the analysis provide, in the area to be reinforced, as a result of loading combinations, a triaxial state of stress characterised by high values for the main stress tensions.

How does this help to design the reinforcing?

Not enough information is available on the strength of reinforced concrete since, so far as the authors know, research has been mainly directed towards states of bi and triaxial compression characteristic of structures in prestressed concrete. There seems to be only one way out: use the calculation criteria valid for one-dimensional inflected structures, deduce the bending and shear forces acting on the whole section in two directions at right angles to each other (cartesian or polar), and calculate separately the tractions in both directions at the level of the reinforcing bars. Then add them vectorialy and resolve in the two components corresponding to the mesh fixed beforehand.

The same can also be said for absorbing shear forces which may often be too strong for the concrete, in that it is subject at the same time to normal tension stresses, even if they are not very great.

All this goes to show that, at the moment, there is a considerable qualitative and conceptual gap between analysis by finite element programs and the empirical and over-simplified control criteria.

When one passes to a technological examination of what has been done so far, two points stand out.

- Most of the reinforcing is arranged in the upper and lower layers of the mat, some metres apart.
- The dimensions of the foundations call for casting several thousand of cubic metres of concrete.

Plans for casting therefore constitute a problem that cannot be ignored. There seem to be two possible solutions: cast the mat

has a series of horizontal layers, or make it up in full depth blocks following a ground-plan division.

The first solution has the advantage that it reduces to a minimum the heat arising from dehydratation,and also helps in laying out the upper level of reinforcing, which could rest on the layer below. On the other hand it clashes with site practice which tries to avoid interference between casting and the positioning of the reinforcing, and above all increases the problems,often not easily quantifiable, of differential shrinkage between one layer and the next. The second solution offers advantages both in terms of statics and completion times, but implies real loadbearing metal structures that have to support the upper layers of the reinforcing, and will be lost in the casting (fig.10).

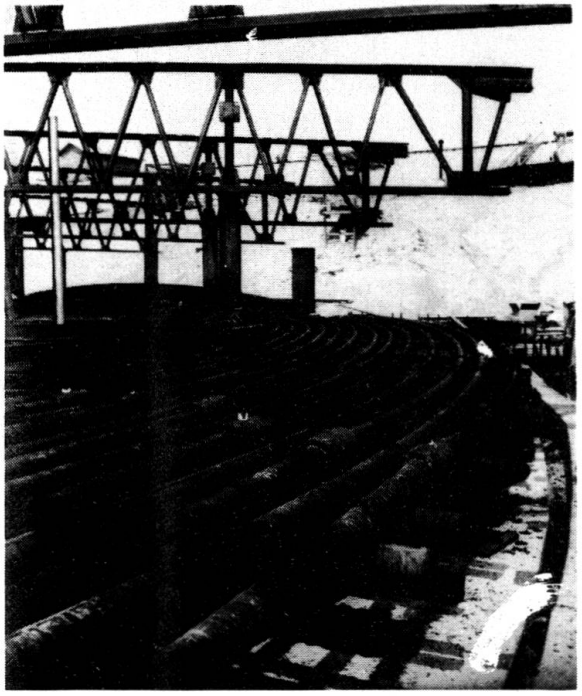

fig. 10

Furthermore,the block solution leads to greater heating in the concrete during setting, and so calls for particular expedients, such as the preventive cooling of the aggregate, or even a real refrigeration plant, that will inevitably be lost in the casting.

These problems,which could well seem even more serious and limiting than the real calculation of the foundation, make it worthwhile to ask whether there may not be solutions other than the massive slab.

In fact, a box structure of greater dimensions but reduced mass could be used, provided that a close study was made of the differential shrinkage between upper and lower slabs, as well as the distribution of concentrated loads.There is, however, another technique, recently tried out, that is perhaps even more interesting. This exploits the contribution of the metal structures needed to support the steel rods or at least makes the most of the co-operation between a steel space frame and the concrete casting of mat. In other words, and from the point of view of statics, the designer could make the best of all that was to be learned from the various stages and requirements of erection, in order

to design a real metal space structure reinforced by bars embedded in the casting with both local and integrating functions.

There would certainly be great economic advantages, a reduction in completion time, and a simpler static structure without those uncertainties that arise when concrete is subjected to shear forces and at the same time to tension and bending. This is a modern solution, that has recently been successfuly tried out in works of some importance [15] .

6.2. CONTAINMENT STRUCTURES

Containment structures in reinforced concrete generally take the form of a cylinder or a truncated cone. It follows that here too the form conditions the geometrical layout of the reinforcing. This should be arranged according to the directrices and generatrices (circumferential and longitudinal reinforcing). Furthermore it will often be necessary to provide for a double helical space mesh suited to absorbing shear forces in the membrane, especially in earthquake zones. This is because the containment structure must be checked for an accompaning high internal pressure leading to a basic state of tensile stress both longitudinally and circumferencially. In such conditions the formation of efficient diagonal rods under compression becomes doubtful. The membrane stresses could be easily checked statically. Great problems, however, would arise when studying secondary effects corresponding to points where there was no continuity or where there were openings, since here the state of stress would once again have to be studied in three-dimensional terms, with all those uncertainties and difficulties already listed for mats. In these areas there would also be the risk of such a congestion of reinforcing that successful casting would be jeopardized. The basic cause of this congestion lies in having to provide adequate reinforcing against longitudinal and circumferencial bendig and radial shear (i.e. related to the thickness). This is particularly important for the openings, where the main reinforcing, arranged so as to absorb membrane stresses, has already been deviated. This is also true for the connection between the containment structure and the foundation mat.

The designer is thus obliged to make the best to provide all the reinforcing resulting from calculations. It would be useless to try to increase its thickness locally, since this would mean adding to the local rigidity, which could imply a higher value for the internal actions, which would in turn call for more reinforcing.

All of this, added to the ideas expressed at the end of section 4, leads the authors to suggest the following concept for designing the reinforcement. Calculate:

a) the internal membrane forces on models that take into account noncracked concrete;
b) the internal membrane forces on models that take into account cracked concrete;
c) secondary internal forces, bending and shear, on the same models as in b).

The dimensions of the reinforcing will follow the normal theory for reinforced concrete in the most unfavourable combination between (a+c) and (b+c). The result would certainly be a balanced situation in which congruence would be satisfied at the price of cracking due only to those internal forces that originate in the congruence itself.

7. CONCLUSION

The major items to be further developed in the future for improving the design and erection of reinforced concrete structures may be summarised as follows:

- A reduction in the conceptual gap between calculating the state of stress and designing the structure
- Interchange of ideas between structural and mechanical engineers in order to reach a more realistic evaluation of leakage in the event of craks in concrete, and to arrive at a more rational arrangement for the piping.
- A combined study, by both designers and licensing authorities, to findmore realistic calculation models.
- An analysis up to define the limits of reinforcement congestion.
- A study of those solutions that allow for the use of prefabricated steel frames that co-operate with the concrete in order to reduce the problems of placing the reinforcement.

REFERENCES

1 F. Bremer: ON A TRIAXIAL STRENGTH CRITERIUM FOR CONCRETE,ACI Sp 34,1972 pag.283-294.

2 V. Hansson, K. Schimmelpfenning: CONCRETE STRENGTH IN MULTI-AXIAL STRESS STATES,ACI Sp 34,1972 pag. 295-311.

3 D. Linse: STRENGTH OF CONCRETE UNDER BIAXIAL SUSTAINED LOAD, ACI Sp.34,1972 pag 327-333.

4 S. Stockl: STRENGTH OF CONCRETE UNDER UNIAXIAL SUSTAINED LOADING, ACI Sp 34,1972 pag.313-326.

5 H.H. Kupfer, M.K. Hilsdorf: BEHAVIOUR OF CONCRETE UNDER BIAXIAL STRESSES, ACI Journal August 1969, pag.656-662.

6 O. Buyukozturk, A.H. Nilson, F. Oslate: STRESS STRAIN RESPONSE AND FRACTURE OF A CONCRETE MODEL IN BIAXIAL LOADING, ACI Journal August 1971 pag.590-599.

7 T.C.Y. Liu, A.H. Nilson, F.O. Slate: STRESS STRAIN RESPONSE OF CONCRETE IN UNIAXIAL AND BIAXIAL COMPRESSION, ACI Journal, May 1972 pag.291-295.

8 P. Launay, M. Gachon: STRAIN AND ULTIMATE STRENGTH OF CONCRETE UNDER TRIAXIAL STRESS, ACI 1972 SP 34 pag.269-282.

9 H. Argiris, K.E. Buck, I. Grieger, K.J. William: DISCUSSION ON FINITE ELEMENT ANALYSIS FOR PRESTRESSED CONCRETE REACTOR VESSELS, CONCRETE FOR NUCLEAR REACTORS, Vol.1, ACI Special Publication SP-34, Detroit, Michigan 1972.

10 Chen Pang Tan: A STUDY OF THE DESIGN AND CONSTRUCTION PRACTICES OF PRESTRESSED CONCRETE AND REINFORCED CONCRETE CONTAINMENT VESSELS, Report F-C2121,Franklin Institute Research Lab., Philadelphia, April 1969.

11 I. Holand, E. Munkeby: ANALYSIS OF ORTHOTROPIC REINFORCE CONCRETE STRUCTURES , ASCE Journal of the Struct. Div. Vol.97, no.ST10, oct.71.

12 H. Nilson: NONLINEAR ANALYSIS OF REINFORCED CONCRETE BY THE FINITE ELEMENT METHOD, ACI Journal Vol.65,N.9,Sept.1968.

13 S. Berg, P.G. Bergan, I. Holand: NONLINEAR FINITE ELEMENT ANALYSIS OF REINFORCED CONCRETE PLATES, Conference on Structural Mechanics in Reactor Technology, M.3/5,Berlin, 1973.

14 R.N. White, P. Gergely, J.P. Laible, O.A. Fajarolo: SEISMIC SHEAR TRANSFER ACROSS CRACKS IN CONCRETE NUCLEAR REACTOR CONTAINMENT VESSELS, 5WCEE Session 7-A,Rome 1973.

15 E. Leporati, V. Nascé: IL MODELLO DEI NODI DEL SUPERBACINO DI GENOVA. To be printed on Costruzioni Metalliche, 1974.

SUMMARY

The Authors, as involved in the structural design of some recent Italian Nuclear Plants, point out the following items that seem to be widely open to discussion:

- Gap between threedimensional elastic stress analysis and design of reinforced concrete structures.
- Interaction between microcracking and stresses due to loading conditions when combined with temperature effects.
- Interface problems between parts of a massive structure analysed through different mathematical models.
- Liability of the finite element approach for dynamic analysis of turbo-pedestals.
- Congestion of rebars and connected problems of detailing and pouring.

ZUSAMMENFASSUNG

Die Autoren die mit dem strukturellen Projekt von eigigen neuen italienischen nukleare Anlagen beschaftigt sind, machen auf folgende Punkte aufruerksam die offen zur Diskussion stehen:

- Raum zwischen dreidimensionalen analytischen elastischen Belastungen und Projekt von verstarkten konkreten Strukturen.
- Zwischenaktion zwischen Mikrocracking und Belastungen verursacht durch Ladungskonditionen wenn sie mit Temperatureffekten kombiniert sind.
- Probleme zwischen Teilen einer massiver Struktur, die durch verschiedene mathematische Modelle analysiert wurden.
- Annaherender Spielraum der endlichen Elemente fur die dynamische Analysen der Turbo-Sockel.
- Inanspruchnahme der Armaturen und daraus folgendenProblemen der Detaillierung und des Betonieren.

RESUME

Les Auteurs, étant engagés dans le projet structural de plusieurs récentes installations nucléaires italiennes font remarquer que les points ci dessous restent ouverts à une ample discussion:

- lacune entre l'analyse élastique à trois dimensions de l'effort et le projet de structures en béton armé.
- Interaction entre microcracking et efforts dus aux conditions de chargement lorsque combinés avec des effets de température.
- Problèmes de liaison entre les parties d'une structure massive analysés à l'aide de différents modèles mathématiques.
- Crédibilité de l'approche à l'aide d'éléments finis pour l'analyse dynamique de turbo-piédestaux.
- Congestion des armatures et relatifs problemes de détail et de coulage.

Leere Seite
Blank page
Page vide

IABSE
AIPC
IVBH

SEMINAR on:
«CONCRETE STRUCTURES SUBJECTED TO TRIAXIAL STRESSES»
17th-19th MAY, 1974 - ISMES - BERGAMO (ITALY)

Small Scale Models of PCPV for High Temperature Gas Reactors. Modelling Criteria and Typical Results

Modèles en échelle réduite de caissons en précontraint pour réacteurs à gaz à haute température. Techniques de reproduction et résultats typiques

Kleinmasstab-modelle von Spannbetonbehälter für Hochtemperatur-gas Reaktoren. Modelltecniken und Versuchergebnisse

Prof. Ing. E. FUMAGALLI, Director of ISMES - Bergamo Italy
Mr. G. VERDELLI, Laboratory of pressure vessel tests, ISMES

1. INTRODUCTORY REMARKS

1.1 For the static tests on PCPV, there have been used up to now, two main types of models which utilize different techniques and serve different experimental purposes: one is the model in resin which allows tests to be carried out in the elastic range as an alternative to calculation processes; the other one is the concrete model, especially devised for failure tests.

The geometrical scales for concrete models usually range from 1/10 to 1/30 (refs. 1 ÷ 5). However, there are many examples of reproduction on a larger scale.

Smaller scale ratios allow, at a same cost and at a same time schedule, the test of many more models so that the design can be improved through further experimental stages on the various subsequent models.

However, a small scale reproduction imposes some limits on the modelling. For instance, the concrete model does not correctly reproduce the stresses due to the fact that the dead load, cannot be modelled. At any rate the impact of the only dead load on the general state of stress is negligible.

Besides that, a small scale model needs in some cases a simplified schematization of the cable pattern which usually leads to an im-

provement of the cable specific power. This brings to light the practical possibility of adopting, for the prototypes, such high powered unit cables (in the range of 1,000 - 2,000 tons) (refs. 6 and 7).

With regard to the choice of the concrete for the models, that requires the reduction of the size of the aggregates, advanced researches are carried out in many laboratories, sometimes at a very sophisticated level.

However, there are some limits of approximation to the physical reality, suggested by the purposes and the nature of the tests.

Generally, it may be considered sufficient that the characteristics of the concrete selected for the models fit into the dispersion range of the properties of the normal concrete (max aggregate size 3 cm).

Furthermore, always within the limits and the aims of the research, it is not necessarily required that all the properties of the material be fully respected.

For example, it does not seem logical at all, to reduce the grain size of the aggregates in the true scale ratio. This leads to worst conditions in the model as far as the crack distribution is concerned; on the contrary the mechanical properties must be imperatively respected.

A correct scaling down of the aggregates means that there is an increase in the percentage of cement mortar. In turn larger percentage of cement mortar increases the creep of the material and, because of a great evaporation due to the higher water content, also its shrinkage. A theoretically correct reproduction of the conglomerate is not, therefore, obtainable in practice, and the maximum size of the aggregates is usually determined in function of the clearances between the reinforcing steel bars and cable ducts.

In addition, the correlation between the model and the prototype becomes more and more difficult because of the different lives experienced by the two structures. In fact, during the design stage, the model must necessarily be tested in the shortest time; whereas the prototype comes into use some years after its building.

For the model, it is therefore impossible to take into account the changes which arise in the properties of the material due to the long standing (in any case the ageing of the concrete is a minor effect).

In addition, for the small scale models it must be evidenced that the correct modelling of the liner, whose behaviour is so important for the true structure, can hardly be achieved.

The research through the models on creep and shrinkage effects does not seem, at present, to offer and adequate reliability.

1.2 The main purpose of the model testing is the estimation of the safety margins of the structure.

Since several years researches on the strength of concrete under multiaxial stresses have been carried out on specimens with encouraging results, with the aim of making it possible to correlate the local tensor of the stresses with the collapse values and then to deduce the local safety factor.

Nevertheless, a failure test on the model gives a more reliable overall safety factor of the structure, because it takes into account the plasto-viscous type of deformation processes, which are strongly accentuated in triaxial stress conditions, and consequently the stress redistribution coming from these processes. Such plasto-viscous effects can also be observed in triaxial test on concrete specimens, when the failure is mainly due to shear stresses.

Therefore, the problem is how to select the criteria for the carrying out of the ultimate tests. The failure tests of explosive type (pressured gas) arise some important problems in connection with the intrinsic difficulty to learn the failure mechanism during the explosive phase. An endurance collapse test does not reproduce the possible failure mechanism of the prototype. The failure tests usually carried out are of a relatively fast type (1 - 2 $Kg/cm^2/min.$) and they consist of a gradual increase of the internal pressure, and of the step by step deformation and cracking processes measurements, up to the structural collapse.

1.3 It is usually difficult to obtain a complete picture of the state of stress from the tests performed in the working range. Since the structure under test is usually stiff, the deformations to be measured are very small.

Besides that, it is difficult to obtain strain or deflection measurements on the internal surface, because of the existance of a liner under pressure, and on the external surface because of the existence of the cable anchor heads, ribs and penetrations.

The measurement of the strains and thus the evaluation of the stresses, are therefore rather incomplete.

However, the adoption of continuous lines of small strain gauges has proved to be quite valid.

In this way, for instance, the congruence between the summation of the local strains and the total deflections may be checked. A comparison between this kind of measured results and calculation predictions (ref. 8) becomes thus possible to some extent.

1.4 To conclude, it is worth of pointing out a few disadvantages caused by the schematization of the prestressing system needed to satisfy the reduced scale of the model.

The cable of the model,reduced in accordance with the scale ratio, leads to an improvement of load losses because of a greater impact of the cable head settlements. This means the performance of frequent

checking and, sometimes, additional restressing interventions.

1.5. As to measurements of surface stresses in the elastic field, due to the internal pressure, the testing made on a non-prestressed epoxy resin model may be of some interest. The high Poisson ratio of the resins (about 0.4) can be reduced to values ranging from 0.25 to 0.30 with the addition of suitable aggregates.

The main advantage of these epoxy resin models consists of the fact that the effects of their penetration on the axisymmetric structure can be measured by drilling in sequence on the same model.

Some tests made at ISMES (Experimental Institute for Models and Structures) on epoxy resin models have been quite satisfactory.

However, as it has been already said, the modern trend of the research in this field is to emphasize the failure tests.

This interest is due to the need to determine the failure mechanism of the structure and the relevant safety margins that cannot be satisfactorily derived from the calculation tools.

The present paper describes the most recent researches carried out at ISMES on the failure tests of the PCPV small scale models.

The tests have been carried out for CPN (Nuclear Design and Construction Center) of ENEL (Italian State Electricity Board) as a part of the general research programme sponsored by DSR (Studies and Research Direction) of ENEL, with the aim of investigating more advanced techniques in the field of prestressed concrete vessels models for nuclear reactors.

2. MODEL TESTING TECHNIQUES

2.1. The tests carried out at ISMES in the last 10 years in the field of prestressed concrete vessels for nuclear reactors include:

a) concrete models (complete or portions) in scale 1 : 20;

b) epoxy resin models in scale 1 : 50;

c) photoelastic plain models for the study of details (areas concerning the penetrations, gussets, etc.).

Some of the techniques which have been used at ISMES for concrete models as well as the main results of the tests, with particular reference to the most recent model are included in this part of the report (figs. 1 and 2). As regards the concrete models tested until now, the following techniques and simplifications were used.

2.2. Liner

A reduced scale steel liner (actual thickness 2 - 4 cm)

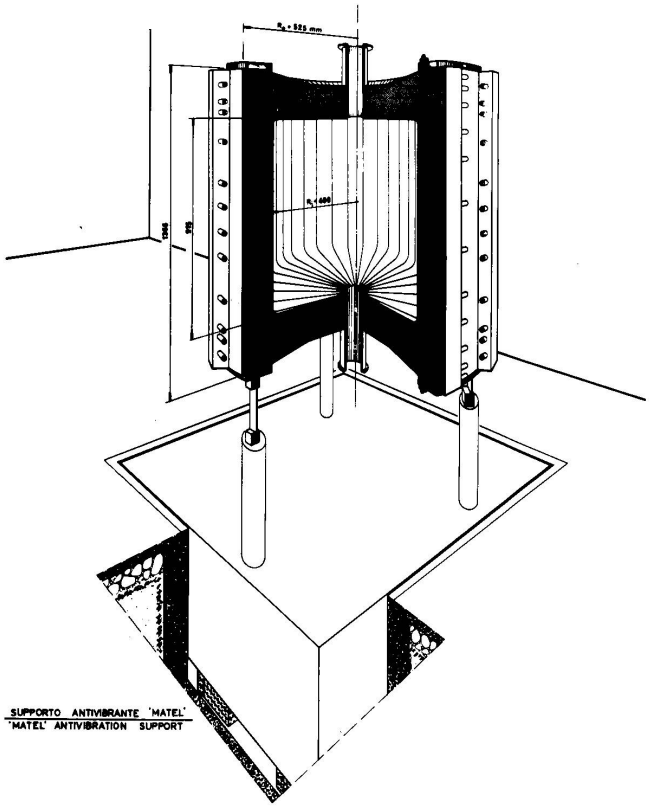

FIG. 1 ARRANGEMENT OF THE MODEL FOR TESTING
DISPOSITION DU MODELE POUR LES ESSAIS
EINRICHTUNG DES MODELLS FÜR DIE VERSUCHE

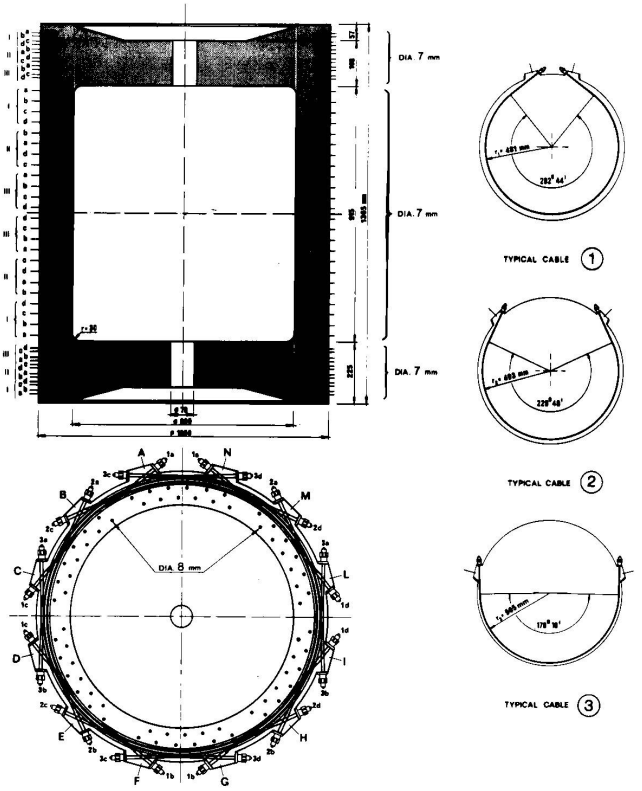

FIG. 2 LAYOUT OF PRESTRESSING CABLES
SCHEMA DES CABLES DE PRECONTRAINTRE
MODELL VORSPANNUNG

showed a brittleness at weldings, especially in the range of the large deformations occurring during the ultimate tests.

After a number of unsuccessful experiments during which sealed rubber bags were used, it was decided to replace the steel liner with a more ductile copper liner (ref. 9) allowing larger deformations and thus leading to the collapse of cable systems.

2.3 Prestressing cables

A correct reproduction of the prestressing system is very important. The solution adopted for the models consists in the use of the same harmonic steel wires of the actual structure 6 - 7 - 8 mm in diameter (which is the same diameter as that of the wires chosen for the prototype).

In order to distribute the prestressing loads uniformly the monowire cables were used.

2.4 Mild-steel reinforcement

The mild-steel reinforcement installed near the liner and outer surfaces so as to distribute the cracks are reproduced in the model by electro-welded steel netting. The reinforcement in the stress concentration areas, such as the penetrations and gussets, is obtained with steel cages of small diameter wires (Ø 3 - 5 mm).

2.5 Instrumentation

The measurements are especially difficult, considering that the concerned deformations are slight. Several attempts to obtain information from the inside of the castings and the surface of the liner were made, which gave rather unreliable results.

Furthermore, taking into account that the internal instruments and their connections cause discontinuities leading to the starting of the cracks, only external measurements were taken, measuring only the temperature distribution by means of several thermocouples located inside.

As far as the measurement of the deflections is concerned at first the measurements were taken by using an external rigid reference frame. These instruments, placed one opposite the other on the frame, measured the diametrical and axial deflections to produce the average value.

Later, an intrinsic measurement system of the deflections was preferred, fixing a series of displacement transducers to four rigid invar frames anchored directly onto the model. The transducers are arranged in two orthogonal diameters on each slab and along the four corresponding generatrixes on the cylindrical walls. Fig. 3 clearly shows the arrangement of the measuring system.

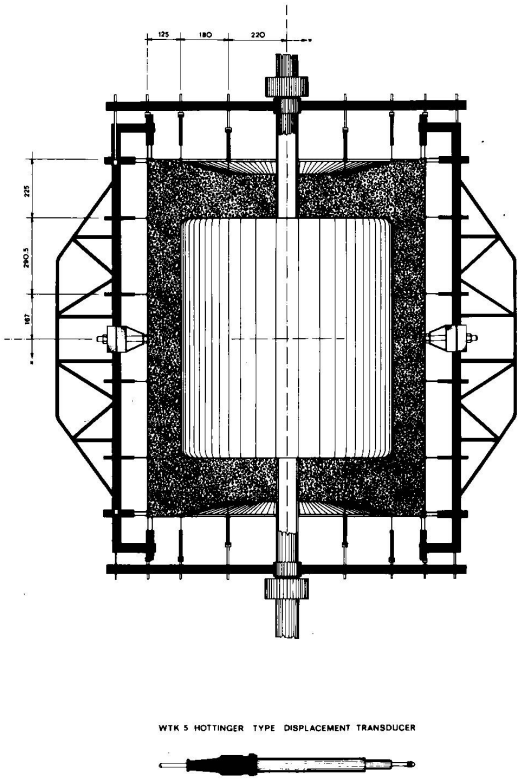

FIG. 3 APPARATUS FOR MEASURAMENT OF DEFLECTIONS
TREILLIS DE MESURE DES DESPLACEMENTS
MESSVORRICHTUNG DER VERSCHIEBUNGEN

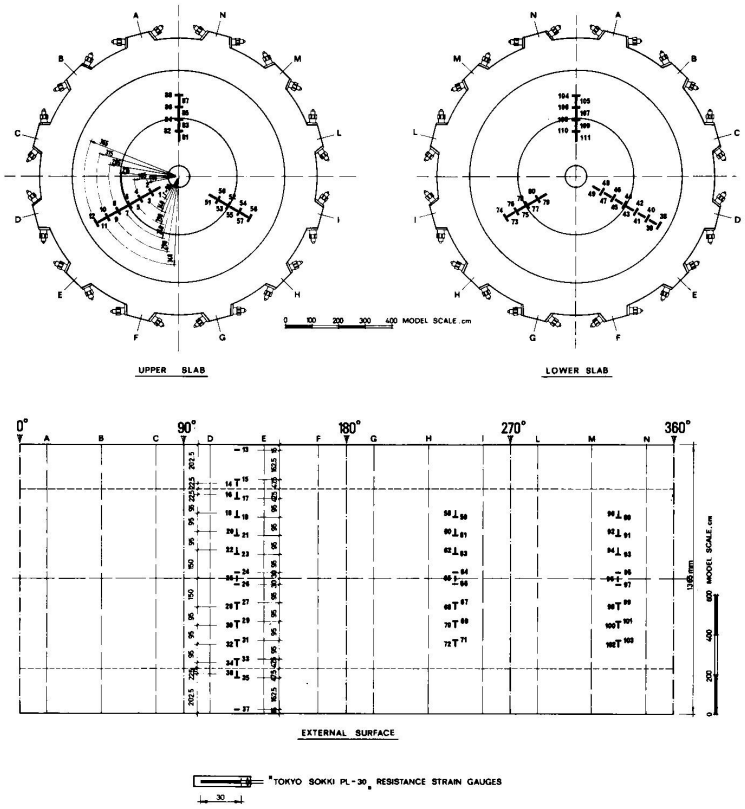

FIG. 4 LAYOUT OF RESISTANCE STRAIN GAUGES
POSITION DES JAUGES A FIL RESISTANT
ADNORDNUNG DER DEHNUNGSMESSSTREIFEN

It should be pointed out that this arrangement allows the true deformed surface of the structure under test to be determined.

2.6 Pressurization system

Internal hydrostatic pressure is applied to the model. The system consists of an oil pump (flow rate 10 lt/min) capable of operating up to 400 Kg/cm^2, connected to an interchange oil-water piston. An electronic operated pumping station allows the pressure to be regulated with a motorized valve. The final value of the pressure can be reached in a previously chosen length of time, with steps of 0,1 Kg/cm^2.

2.7 The tests on concrete models carried out at ISMES in recent years include:

a) prestressed concrete model of vessel for the "Dragon Project" (HTGR type)

b) prestressed concrete model of vessel for the THTR project.

The results obtained from the tests of the above - mentioned model b) suggested the opportunity to complete the tests on partial models of the structure: i. e. the end slabs and the barrel. The main purpose of the additional researches was to assess the behaviour of the single structural elements up to collapse. On the basis of the results, it was decided to carry out other experiments on three models with thin walls.

On the first model, conventionally named CPS 3/1, where penetrations both of barrel and slabs were reproduced, tests were completed by the beginning of 1972. The failure of the model was due to the collapse of the hooping cables at a pressure of 119 Kg/cm^2.

The other two models, CPS 3/2 and CPS 3/3, were built at the same time and were similar to the previous model in shape and size, with the exception of:

a) the penetrations were not reproduced

b) the prestressing installation was schematized so as to make the structure as axisymmetric as possible

c) the steel of the prestressing cables which in these two models was replaced with stabilized steel.

The only difference between CPS 3/2 and CPS 3/3 is related to the barrel hooping cables (ϕ 6 mm for CPS 3/2, ϕ 7 mm for CPS 3/3) and the vertical cables (ϕ 7 mm and ϕ 8 mm, respectively).

3. DESCRIPTION OF CPS 3/3 MODEL

3.1 The model, shown in fig. 1, reproduces the project plan of a prestressed concrete vessel for a "THTR" gas reactor. The vessel is

cylindrical with two flat closure end slabs. The inside part is lined with a metal liner. The concrete is prestressed vertically and horizontally with systems of monowire cables as in the BBR System. The operating pressure of the reference prototype is 40 Kg/cm^2.

A damper system (fig. 1) of "Matel" rubber bricks, on which the supporting concrete block of the model stands, allows a good isolation as regards accidental external dynamic actions. The concrete block leaning on the rubber bricks supports the model by means of a flexible system of steel pipes and blades which offers a negligible radial restraint.

Table I (see page 10) lists the main characteristics of the model. The casting of the model was carried out in one stage.

3.2 Measuring instruments

The instrumentation of the model is summarised in the following Table II:

Type of measurement	Type of instrument	No.
Deflections of the cylindrical wall and slabs	Inductive displacement transducers. Hottinger type W1 and W5	80
Strains measured on the outer sufaces	Electrical resistance strain gauges Sokki Kenkyujo type	111
Pull check in the prestressing cables	Load cells ISMES type	41
Temperature distribution in pours	"Thermoelectric" type thermocouples	24
Internal model pressure	Hottinger type extensimetric pressure cells P 3 M 50 and P 3 M 200	2

During the tests the readings of the above instruments were carried out at the speed of 1 point a second, with Hottinger commutation apparatus with automatic recording. The values are also independently recorded on perforated tape and then elaborated on an HP Computer.

Moreover, multichannel pen recorders were used for a real time reading of the more representative instruments.

During the ultimate tests an acoustical noise emission recorder was used in order to record the intensity of the crack propagation versus the rising pressure.

TABLE I

GEOMETRICAL DATA		Scale	1 : 20
		Total height	H = 136,5 cm
		Internal height	h = 91,5 cm
		Slab thickness	hs = 16,8 cm
		Height of prestressed band of slabs	hp = 22,5 cm
		Outer radius	Re = 52,5 cm
		Inner radius	Ri = 40,0 cm
CONCRETE	Composition	Grain size curve	cubic
		Aggregates	Torre del Lago sand up to 1 mm Limestone fragments from Zandobbio up to 8 mm
		Cement	Portland 425 - water/cement ratio 0,475
	Mechanical properties	At the time of testing approx. 1 year after casting	
		Compressive strength	(test specimen 16 x 16 x 16 cm) R_{cc} = 530 Kg/cm^2
		Tensile strength	(cylindrical test specimen ϕ 10, h = 20 cm, Brasilian test) R_{ct} = 32 Kg/cm^2
		Young modulus	(up to 120 Kg/cm^2, E_c = 400.000 + 420.000 Kg/cm^2
PRESTRESSING	Mechanical properties	Prestressing system	BBR
		Monowire cables	stabilized steel ϕ 7 - 8 mm
		Proportionality limit	K_s = 0,1% = 151,3 Kg/mm^2 ϕ 7 mm 143,7 Kg/mm^2 ϕ 8 mm
		Yield limit	K_s = 0,2% = 153,0 Kg/mm^2 ϕ 7 mm 146,0 Kg/mm^2 ϕ 8 mm
		G. U. T. S.	K_{rag} = 175,0 Kg/mm^2 ϕ 7 mm ϕ 8 mm
		Young modulus	E_a = 21.000 Kg/mm^2
	Layout	Vertical cables	36 x 2 = 72 monowire cables ϕ 7 mm
		Slab cables	Hooping monowire cables ϕ 7 mm, nos. 3 hooping for each layer (Layout patent ENEL, Dr. Scotto). Total nos. 12 layers for each slab 12 x 3 x 2 = 72 anchor heads on 12 anchor ribs at 30°. (ref. 10).
		Barrel cables	Hooping monowire cables arranged as for slabs.
	Initial pulls	Vertical cables	5208 Kg (58,9% UTS) per cable
		Slab cables	5541 Kg (82;3% UTS) per cable
		Barrel cables	4122 Kg (61,2% UTS) per cable
		Average friction coefficient of the hooping cables	f = 0,15 . (^)
		Cable ducts	mild steel ϕ 8 - 10 mm (slab barrel) ϕ 10 - 12 mm (vertical)
		Liner	Annealed copper bag 3 mm thick

(^) Determined by experimental measurement on models.

4. TEST PROCEDURE

The tests carried out on the model can be summarized as follows:

4.1 Prestressing

The prestressing sequence has been chosen so as to obtain the better distribution of the stresses induced by the cable pulling during the different stages and to avoid any tensile stresses in the structure (fig. 5). Instrumentation reading:

- resistance strain gauges on the external surface of the model;
- load cells on cable anchor heads.

Before carrying out the pressure tests, due to the losses in the cables, the prestressing was repeated to restore the required theoretical conditions.

4.2 Internal pressure tests

The internal pressure tests were carried out as follows:

a) First pressure cycles (0 - 40 Kg/cm^2): by means of a multi-channel pen recorder, some typical measuring instruments were read in order to check the behaviour of the model.

b) Pressure cycles in working conditions (5 - 40 Kg/cm^2) at ambient temperature. All the measuring instruments were read.

c) Pressure cycles in working conditions (5 - 40 Kg/cm^2) internal water temperature 44°C (Δt across the wall: 10°C).

d) Test with increasing pressure up to starting of clearly visible cracks, internal water temperature 44°C. First visible crack pressure 90 Kg/cm^2.

e) Pressure cycles as in c).

f) Overpressure test, up to 115 Kg/cm^2. Internal water temperature 44°C.

g) Pressure cycles as in c).

h) Collapse test. Internal water temperature 44°C. Collapse pressure 140 Kg/cm^2.

5. TEST RESULTS

5.1 Prestressing

In the diagrams of fig. 6 the pull losses of several cables of the three models at the anchor heads are shown both during and after the prestressing stages. With regard to the evaluation of these losses the observations already made in the introductory remarks should not be for-

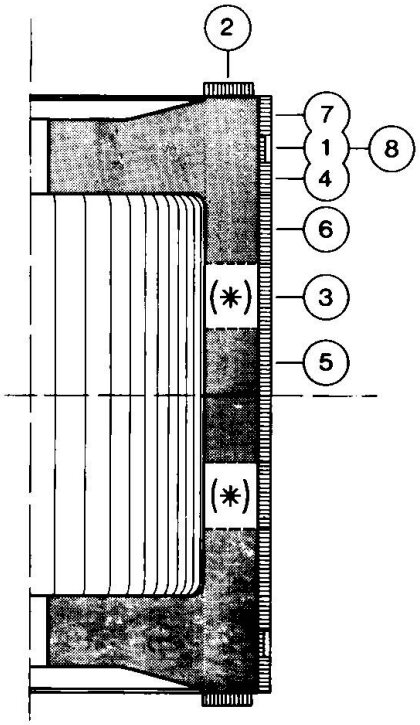

FIG. 5 PRESTRESSING SEQUENCE

SEQUENCE DE PRECONTRAINTE

FOLGE DER VORSPANNUNG

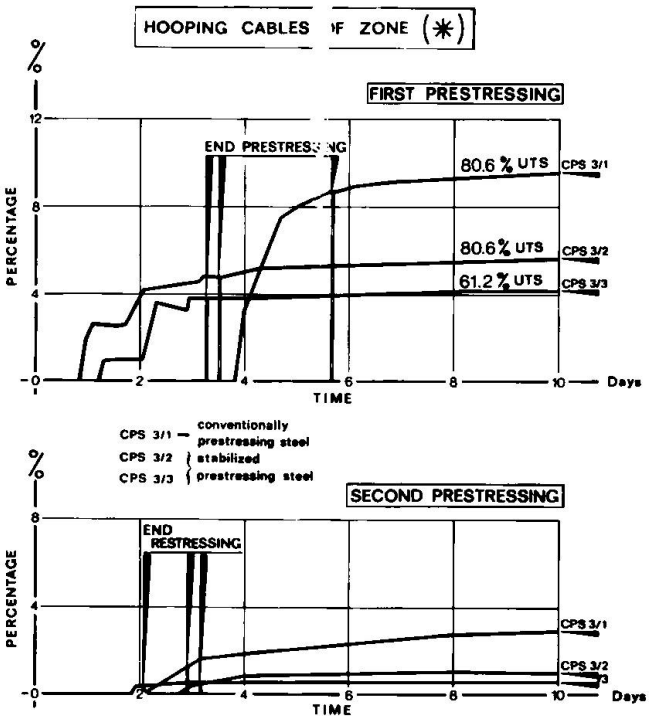

FIG. 6 LOAD LOSSES AT CABLE ANCHOR HEADS

PERTES DE PRECONTRAINTE MESUREE AUX TETES D'ANCRAGE

KRAFT VERLUSTE AN DEN VERANKERUNGEN

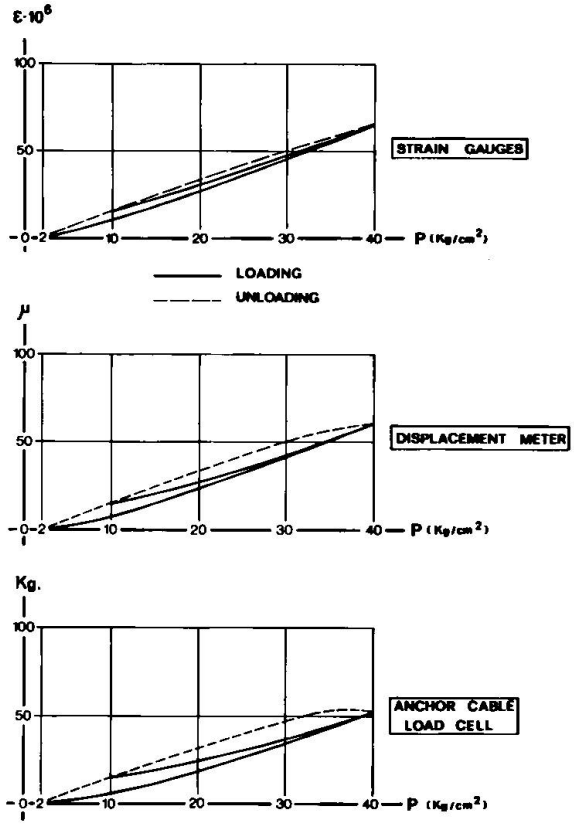

FIG. 7 TYPICAL BEHAVIOUR OF THE MODEL DURING LOADING CYCLES

COMPORTAMENT TYPIQUE DU MODEL PENDANT LES CYCLES DE PRESSION

TYPISCHES VERHALTEN DES MODELLS WÄHREND DEN VERSUCHEN

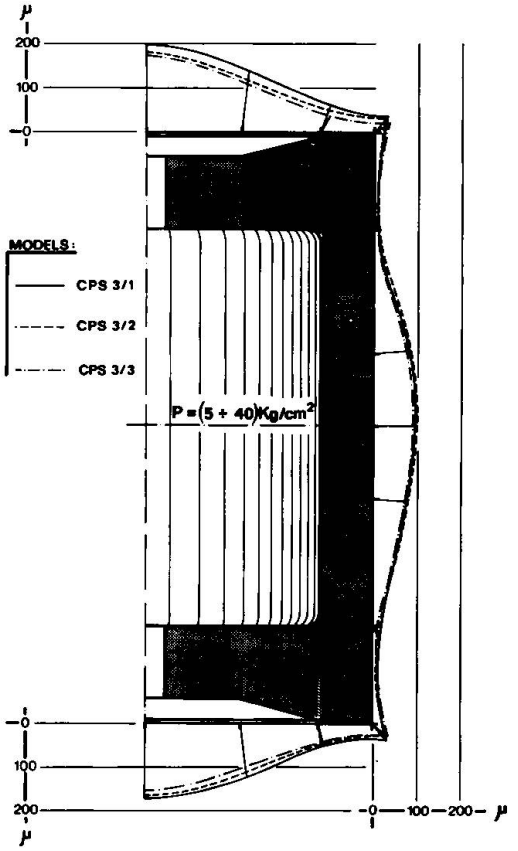

FIG. 8 COMPARISON BETWEEN THE OUTSIDE SURFACE DEFLECTIONS FOR AN INTERNAL PRESSURE

COMPARAISON ENTRE LES DEFORMATIONS DE LA SURFACE EXTERIEURE POUR L'EFFET D'UNE PRESSION

VERGLEIG ZWISCHEN DEN VERSCHIEBUNGEN FÜR INNENDRUCK

gotten. In fact, owing to the short length of the cables of the model, even a small settlement of the anchor heads leads to a not negligible pull loss.

However, although in qualitative terms, it can be ascertained that the use of stabilized steel gives lower losses than normal steel. In fact, being the pulling of the cables over the 80 % of their G. U. T. S. they showed losses not greater than 5 - 6% after prestressing (in comparison with the 10% of normal steel) and smaller than 1, 5% after the restressing.

5.2 Pressure tests

As regards pressure tests in the range of working conditions and up to the collapse, carried out as per paragraph 4. 2, it should be noted that:

5.2.1 After the first pressure cycles the load - deformations diagrams for the working conditions even developping hysteresis loops, as shown in fig. 7, are repeatible as long as the prefixed upper and lower load limits remain unchanged.

5.2.2 During the first cracking tests, for pressures over 65 Kg/cm^2 the first microcracks was experienced along the central band of the barrel, as the strain measurements shown in fig. 9 indicate.

The development of this process is also evidenced by the deflection measurements in figs. 10 and 11. However, the cracks appeared clearly visible only from the above said pressure of 90 Kg/cm^2 (crack width $0,1 \div 0,2$ mm).

In spite of microcracks the behaviour of the structure, coming back to the working condition limits, remains elastic and practically linear, very similar in fact to the original behaviour (ref. to fig. 12). This is due to the fact that the steel of the cables remains still elastic and the cracks affect only a cortical external limited region of the PCPV.

5.2.3 Over pressure test up to 115 Kg/cm^2 showed an increase in the state of cracking, limited however to the central band of the barrel due to the fact that the behaviour of the cable was still totally elastic.

Coming back to the working condition limits the structure does not recover its previous elastic behaviour (ref. to fig. 12) but the new curve, under cycling in the working pressure range, is mantained fairly well.

In fig. 13 radial displacements in the equatorial area of the barrel are shown, measured for the different overpressure test cycles. As may be seen, the values of these displacements, although following different paths, practically concide at the maximum pressure point reached in the previous cycle. The same behaviour is evidenced also in the measurements of the load increase in the vertical prestressing cables (see fig. 14).

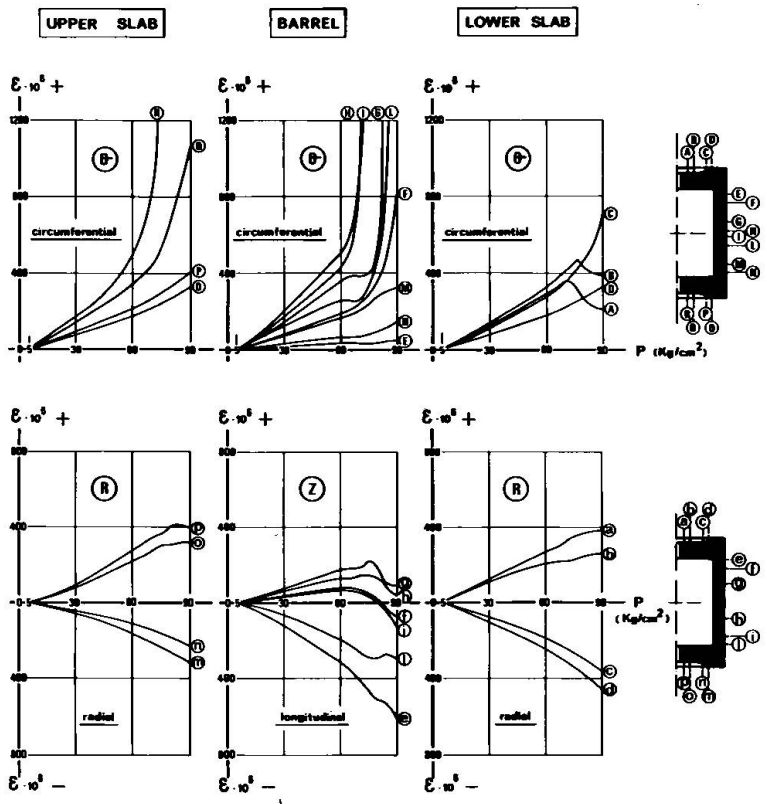

FIG. 9 STRAINS
DEFORMATIONS
DIAGRAMME DER $\varepsilon_R - \varepsilon_\theta - \varepsilon_Z$

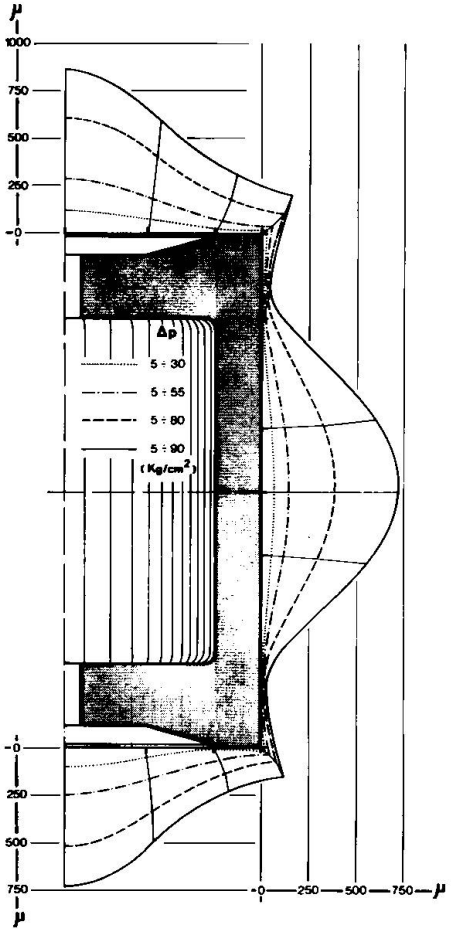

FIG. 10 DEFLECTIONS OF THE OUTSIDE SURFACE AT VARIOUS PRESSURE
DEPLACEMENTS DE LA SURFACE EXTERIEURE A DIFFERENTS NIVEAUX DE PRESSION
VERSCHIEBUNGEN FÜR VERSCHIEDENE DRUCKE

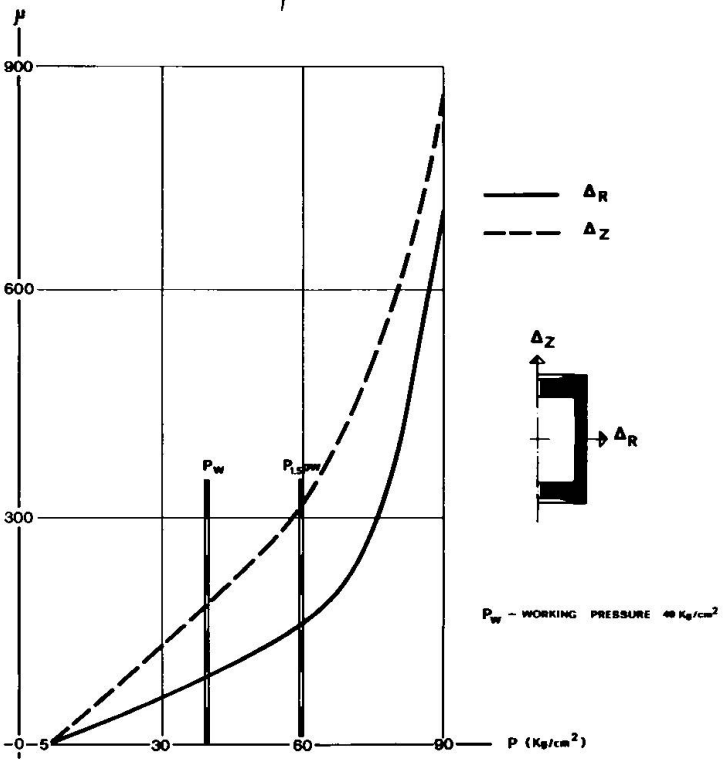

FIG. 11 TOP SLAB AND AEQUATOR DEFLECTIONS
DEPLACEMENTS AU POINT CENTRAL DE LA DALLE ET A L'EQUATEUR
VERSCHIEBUNGEN DES ÄEQUATORES UND DER DECKE

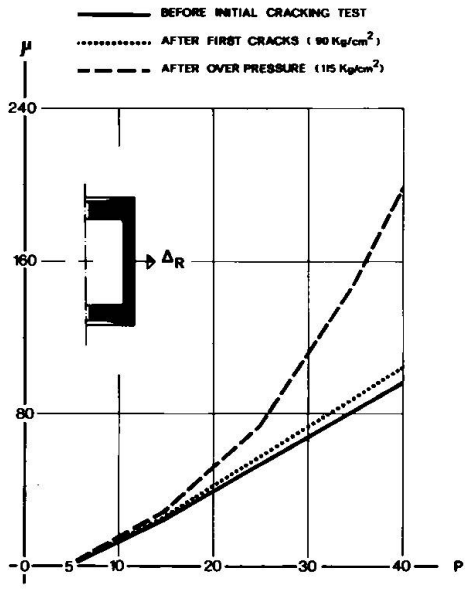

FIG. 12 AEQUATOR DEFLECTIONS AT WORKING PRESSURE
DEPLACEMENTS A L'EQUATEUR DANS LE DOMAINE DES PRESSIONS DE TRAVAIL
VERSCHIEBUNGEN DES ÄEQUATORES AND DEN DIENSTBEDINGUNGEN

OVERPRESSURE CYCLES AND COLLAPS TEST

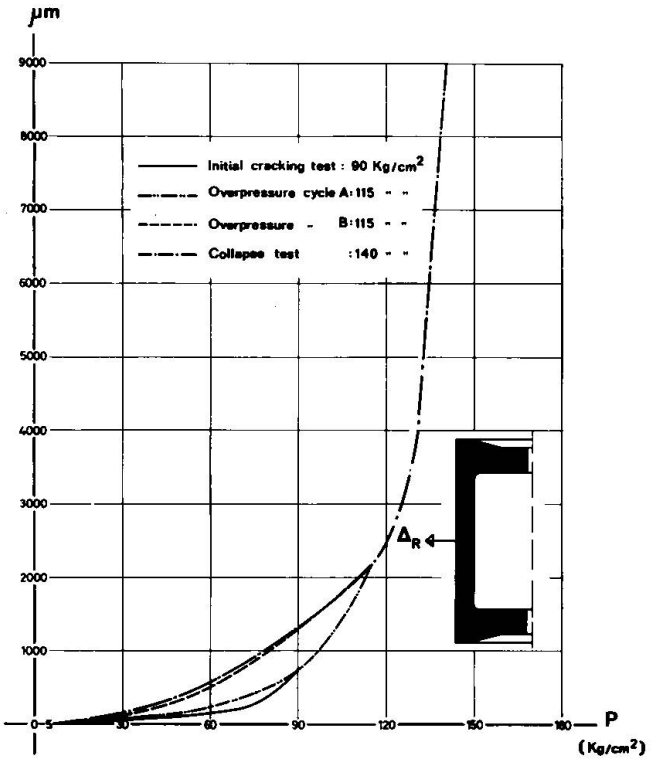

FIG. 13 AEQUATOR DEFLECTIONS
DEPLACEMENTS A L'EQUATEUR
VERSCHIEBUNGEN DES ÄEQUATORES

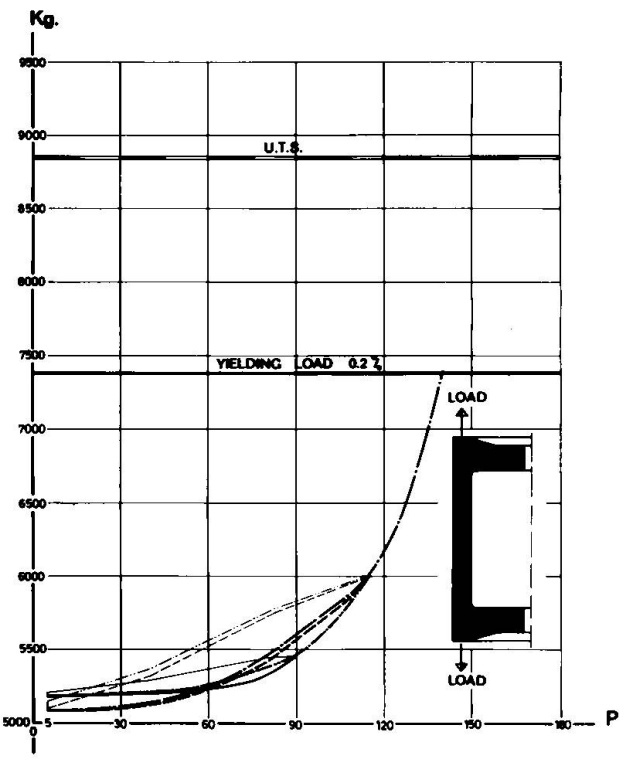

FIG. 14 VERTICAL CABLE ANCHORAGE LOADS
COMPORTEMENT DES CABLES DE PRECONTRAINTE VERTICALE
KRÄFTE IN DEN VERTICALENKABELN

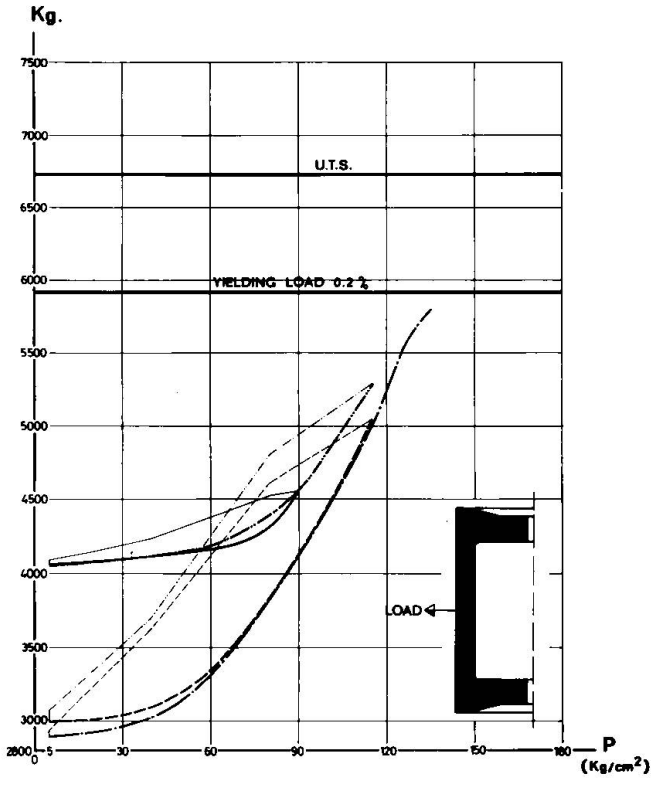

FIG. 15 HOOPING CABLE ANCHORAGE LOADS
COMPORTEMENT DES CABLES DE PRECONTRAINTE HORIZONTALE
KRÄFTE IN DEN KREISKABELN

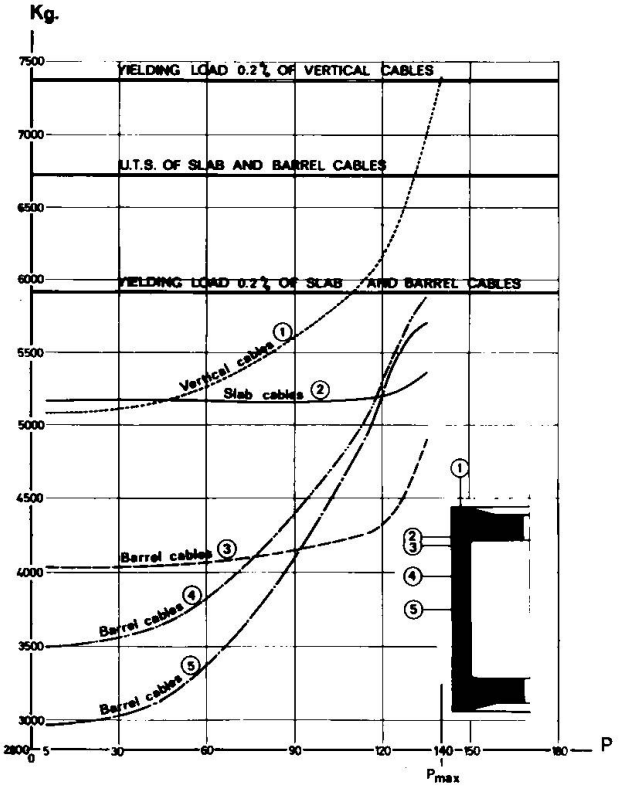

FIG. 16 COLLAPSE: CABLE ANCHORAGE LOAD
ESSAIS DE RUPTURE: COMPORTAMENT DES CABLES
KRÄFTE IN DEN KABELANKERN

As far as the hooping cables of the central band of the barrel are concerned, the considerations are analogous with the exception of the pulling decrease on the anchor heads (fig. 15). This decrease pull is probably due to a large extent to a more homogeneous load distribution along the cables, which in the prestressing stage it is not possible to obtain owing to the frictional effects.

5.2.4 In fig. 16 the average load increases in the collapse test of the vertical and hooping cables are shown. As can be seen, the hooping cables of the central band of the barrel almost reach the yield limit, whilst the load in the barrel hooping cables near the slabs increases considerably only in the final stage (more than 120 Kg/cm^2) mainly due to a process whereby the barrel and the end slabs tend to disconnect, as the rapid increase in the vertical cables load also suggests. The final collapse (140 Kg/cm^2) occurred with a complete failure collapse of the central part of the upper slab (fig. 17).

This type of unexpected failure (the previous model experienced the tendons failure) was due to the yield of the wires of the hooping of the cable system of the slab, whose diameter, unlike made for the wires of the other cable systems of this model (barrel hooping cables and vertical cables), had not been increased.

This means that the collapse mode can be driven by designers. For instance increasing the safety margins of the slab hooping cable system it was possible to avoid the structural collapse of the slab itself.

REFERENCES

(1) E. Torielli, F. Scotto "PCPV Experiment on Small Models"
Euratom Conference, Brussels, November 1967.

(2) W. Rockenhauser, T. E. Northup, R. O. Marsh
"Pressure Test and Evaluation of a Model Pressure Vessel"
Conference on Prestressed Concrete Pressure Vessels, paper 38, London 13-17 March 1967.

(3) J. W. Hornby, G. F. Verdon, Y. C. Wong
"Testing the Oldbury Vessel Model"
Conference on Prestressed Concrete Pressure Vessels, paper 41, London 13-17 March 1967.

EXTERNAL SURFACE CRACK PATTERN

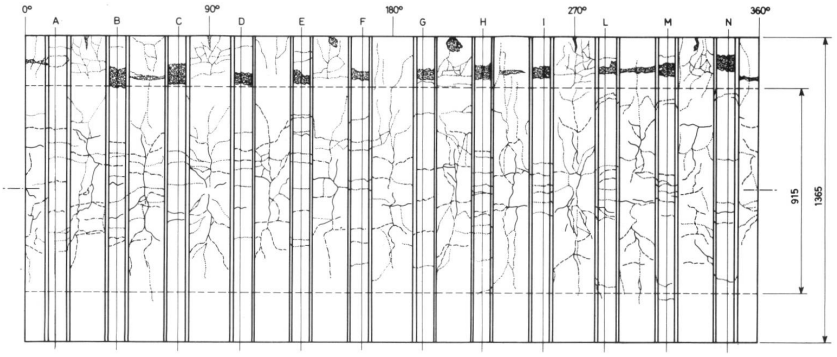

90 Kg/cm² 115 Kg/cm² 115 Kg/cm² 140 (COLLAPSE TEST)

UPPER SLAB COLLAPSE AREA

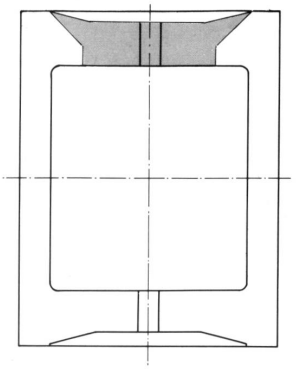

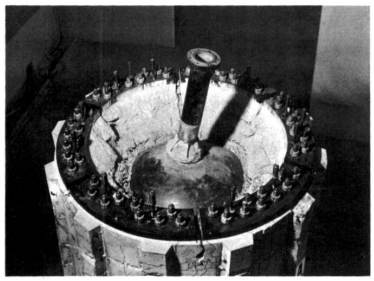

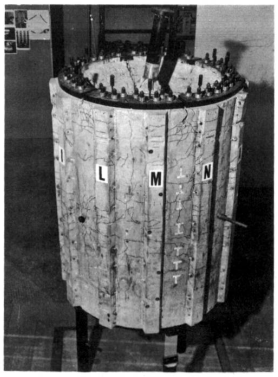

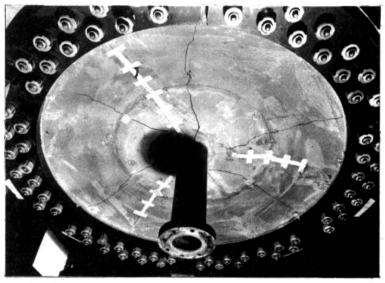

FIG. 17 MODEL AFTER COLLAPSE TEST
MODELE APRES L'ESSAI FINAL A RUPTURE
DER MODELL NACH DEN BRUCHVERSUCHEN
: 140 Kg/cm²

(4) F. Scotto — "Concrete Behaviour under Combined Stresses up to Failure. Test Results on Small Dimension Prestressed Concrete Pressure Vessel Models"

ACI - Seminar "Concrete for Nuclear Reactors", Berlin 5-9 October 1970.

(5) F. Scotto — "Tiny-Walled 1 : 20 Prestressed Concrete Pressure Vessel Model for THTR Reactor Type"

Paper H5/4, First International Conference on Structural Mechanics in Reactor Technology, Berlin, September 1971.

(6) E. Fumagalli, G. Verdelli — "Static Tests on a Small Model of Prestressed Concrete Pressure Vessel for THTR Nuclear Reactor' - Safety Aspects of PCPV"

Delft, December 1970.

(7) F. Scotto — "Thin-Walled Prestressed Concrete Pressure Vessel for High Temperature Reactors: Experimental Investigations on Three 1 : 20 Scale PCPV Models and Design Philosophy Proposals"

Paper H4/5, Second International Conference on Structural Mechanics in Reactor Technology, Berlin, 10-14 September 1973.

(8) M. Fanelli, R. Riccioni, G. Robutti

"Finite Element Analysis of PCPV"

IABSE Seminar, Bergamo 17-19 May 1974.

(9) F. Scotto — "Techniques for Rupture Testing of Prestressed Concrete Vessel Models"

Proceedings of the Conference organized by The British Nuclear Energy Society in London, 10-11 July, 1969.

(10) F. Scotto — "An Improved System of Hooping Cables"

Conference on Prestressed Concrete Pressure Vessels, paper 3, London 13-17 March 1967.

SUMMARY

In this report the general principles ruling the models and static experimentation on prestressed concrete pressure vessels are described. Critical observations with regard to schematization principles adopted for models, testing methods and finally the reliability of the results are discussed.

The report deals with the testing techniques used at ISMES for three models of prestressed concrete pressure vessels with thin walls for "THTR" gas reactors.

The final part of the report describes more in detail the tests and results on the third model (CPS 3/3).

RESUME

Dans ce rapport on décrit les principes généraux qui règlent les modèles et l' expérimentation statique pour les caissons en béton précontraint. A ce propos, on développe des observations critiques sur les principes de la schématisation utilisée pour les modèles, les méthodes de essai et, enfin, la crédibilité des résultats obtenus.

Le rapport est accompagné d' une documentation sur les techniques d' expérimentation développées à l' ISMES pour trois modèles de caissons en béton précontraint avec parois minces pour réacteurs à gaz "THTR".

Enfin, on décrit - plus en détail - les essais et les résultats du troisième modèle (CPS 3/3).

ZUSAMMENFASSUNG

In diesem Bericht sind die algemeinen Richtlinien beschrieben, die bei der Ausführung von Modellen und statischen Versuchen über Behälter aus Spannbeton beachtet werden. In diesem Zusammenhang, werden kritischen Betrachtungen entwickelt über die für die Modelle angewandten Schematisierungs-Richtlinien, die Versuchsbedingungen und, zum Schluss, über die Glaubwürdigkeit der erreichten Ergebnisse.

Dem Bericht ist eine ausführliche Dokumentation beigelegt, über die Versuchstechniken, die ISMES für die Modelle eines dünnwandigen Behälters aus Spannbeton für "THTR" Typ-Reaktor (3 Modelle) angewandt hat. Im letzten Teil werden die Versuche und die Ergebnisse bezüglich des dritten Modelles (CPS 3/3) eingehender beschrieben.

Leere Seite
Blank page
Page vide

IABSE
AIPC
IVBH

SEMINAR on:
«CONCRETE STRUCTURES SUBJECTED TO TRIAXIAL STRESSES»
17th-19th MAY, 1974 - ISMES - BERGAMO (ITALY)

Finite Element Analysis of Prestressed Concrete Pressure Vessel

Analyse par éléments finis de caisson en béton précontraint pour réacteurs nucléaires

Analyse Begrenzter Element von Reaktordruckbehältern aus Spannbeton

Prof. Ing. Michele FANELLI - ENEL, Hydraulic and Structural Research Center
Via Gattamelata 34 - 20149 Milano, Italy

Dr. Ing. Roberto RICCIONI - ISMES, Viale Giulio Cesare, 29 - 24100 Bergamo, Italy

Dr. Ing. Giorgio ROBUTTI - ISMES, Viale Giulio Cesare, 29 - 24100 Bergamo, Italy

SUMMARY

The present report is related to some studies carried out on the strain-stress behaviour of prestressed concrete pressure vessel for nuclear reactors.

At first, a finite element model is introduced in order to simulate the behaviour of an equivalent physical model of the prestressed reactor vessel under examination.

Then, an average concrete elastic modulus is calculated using the information obtained by the comparison between displacements of physical and mathematical models, as well as the results from experimental tests made on concrete specimens of the same kind of the physical model.

At last, the strain-stress state of the structure is analyzed in the operating conditions under the action of fast loads. Time depending effects are not taken into account.

RESUME

Dans cette mémoire on étudie le comportement des contraintes et déformations d' un caisson en béton armé précontraint type "HTR" pour réacteur nucléaire.

On commence par la description du modèle mathématique à é-

léments finis simulant le modèle physique du caisson qu' on veut examiner.

Ensuite on effectue la détermination du module élastique du béton en se servant soit des renseignements tirés de la comparaison entre les déplacements donnés par le calcul et ceux donnés par le modèle, soit des mesures faites en laboratoire sur des éprouvettes de béton.

On termine par l' étude des champs de contrainte et de déformation dans la structure en régime d' exploitation sous l' action de changes instantanées.

ZUSAMMENFASSUNG

In diesem Bericht wird das Spannungs-und Verformungs-Verhalten eines Behälters aus Spannbeton für "HTR" Typ - Kernreaktor studiert.

Anfangs wird das mathematische Begrenzter Elemente-Modell beschrieben, welches das physikalische Modell des in Frage stehenden Kernreaktors simuliert.

Aufeinanderfolgend, wird das Betons-Elastizitätsmodul ermittelt, mit Hilfe der Auskünfte, die sich aus dem Vergleich der durch die Berechung bestimmten Verschiebungen mit den durch das Modell bestimmten Verschiebungen ergeben, sowie mit Hilfe der durch Laboratoriumsversuche auf Betonproben erhaltenen Auskünfte.

Zum Schluss, werden die Spannungen und Verformungen der Struktur unter Schnelllast-Bedingungen studiert.

1. INTRODUCTION

The problems concerning the design of PCPV for nuclear reactors show, at present, a great interest.

Some physical models on 1 : 20 scale of a tiny-walled prestressed concrete pressure vessel for Gas Reactor (1), (2), (3) have been made and tested by ISMES (Experimental Institute for Models and Structures) in Bergamo. Such models have been devised and commissioned by CPN (Nuclear Design and Construction Center) of ENEL (Italian State Electricity Board).

Also some finite element mathematical models of the same structures were made by ISMES in strict cooperation with CPN and CRIS (Hydraulic and Structural Research Center) of the R & D Dept. of ENEL with the following purposes:

- to calibrate the mathematical models on the basis of the results obtained from the physical models;
- to evaluate the stress-strain state and the local safety factor of the structure in operating conditions;

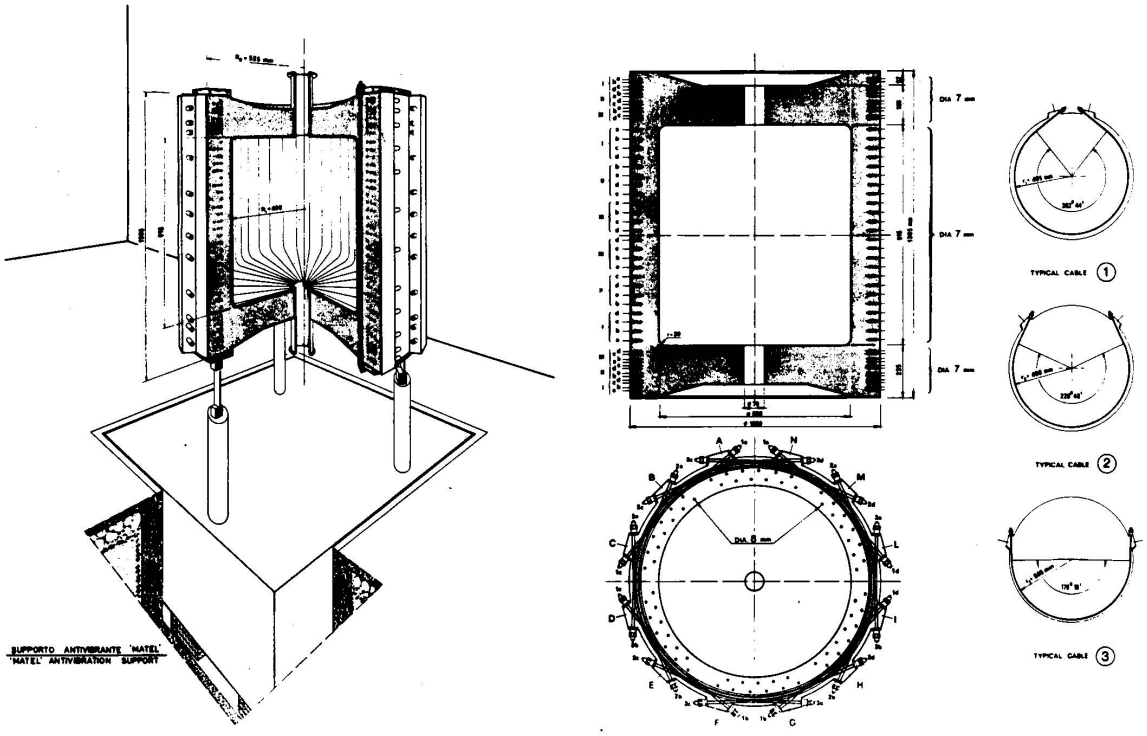

FIG. 1
Geometrical data and prestressing cables system. - Données géométriques et système des cables de précontrainte. - Geometrische Angaben und Vorspannungskalen-System.

In order to make a comparison between the physical and the mathematical models and to evaluate the stress-strain state in working conditions, a physical model without penetrations and an axysimmetric mathematical model in linear-elastic behaviour have been studied. Fig. 1 shows the geometric data of the model and the prestressing cable system pattern.

2. FINITE ELEMENT SIMULATION OF PCPV

Prestressed concrete pressure vessels are usually structures of relevant complexity because of the presence of penetrations, steel reinforcements, prestressing cables, anchoring plates, cable ribs, etc.

The elastic stress-strain analysis of such structures, based on finite element method, has not shown conceptual differences with respect to the analysis made for homogeneous continua (4), (5).

In fact, for a given finite element mesh, the stiffness matrix of each element "i" is defined as follows:

$$\left[K_i\right] = \int_{Vol} \left[B\right]^T \left[D\right] \left[B\right] \, dvol$$

where the matrix $\left[B\right]$, which represents the link between the strain and the nodal displacements depends on the type and the geometric shape of the element, while the matrix $\left[D\right]$ represents the elastic properties of the material.

Once known the stiffness of each element, the stiffness matrix $\left[K\right]$ of the whole structure is built assembling the stiffness matrixes of each element. The $\left[K\right]$ matrix relates the external forces acting at the nodes to the nodal displacements.

In order to study the behaviour of the model under consideration, it was necessary to define the stiffness matrix $\left[K_i\right]$ of the different types of elements, as shown in fig. 2, that is:

- quadrangular and triangular axisymmetric isoparametric solid elements capable of simulating concrete behaviour. All the basic expressions are indicated in (6);
- quadrangular and triangular isoparametric elements capable of simulating the anchoring cable ribs. Due to the presence of the ribs, the structure cannot be considered perfectly axisymmetric. In order to restore the axial-symmetry, special elements with a meridian stiffness equivalent to that of the ribs have been defined, having suitable thickness ΔR and "fictitious" elastic modulus E_r. Since the ribs did not present circumferential deformation ε_θ, the stiffness matrix $\left[D\right]$ has been adequately modified;
- Hoop bars able to simulate the action of circunferential cables on barrel and slabs. The bars are schematized with a point, and they

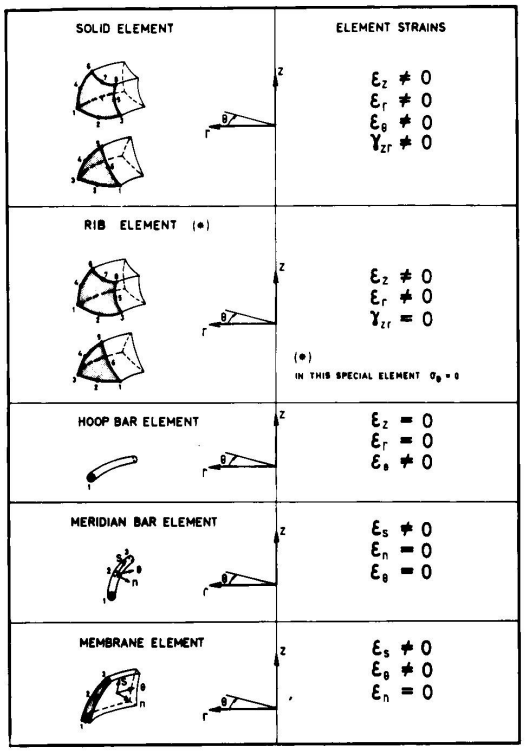

FIG. 2
Finite elements used for axisymmetric PCPV analysis.
Eléments utilisés pour l' analyse statique du caisson.
Begrenzte Elemente zur statischen Analysis von Behältern.

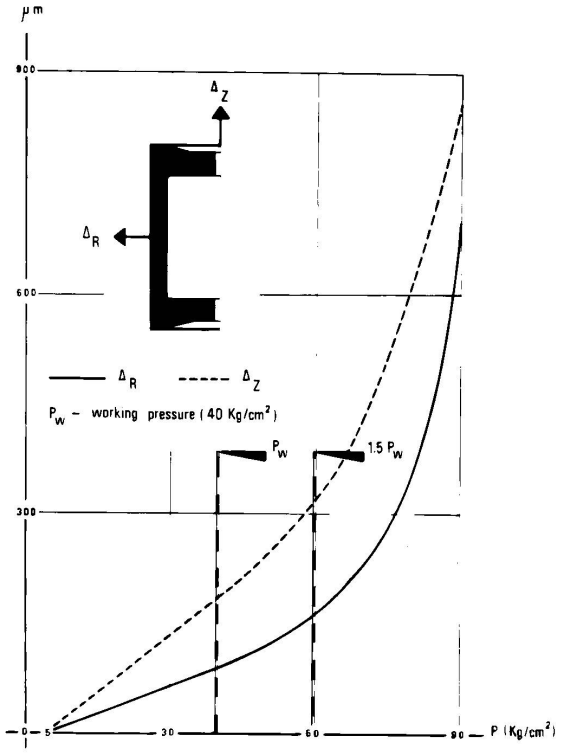

FIG. 3
Equatorial and top cap deflections versus pressure.
Déplacements de la section équatorielle et de la plaque d' extrémité en fonction de la pression.
Aequatorschnittes-und Plattenvershiebungen in Hinsicht auf den Innendruck.

have stiffness only in the circunferential direction. Their strain is defined as: $\epsilon_\theta = u/r$. The determination of the strain matrix $[B]$ is, in this case, immediate;

- meridian bars capable of simulating the action of the cables lying on the meridian plane. They are schematized as a continuous line and have stiffness in the s direction tangent to the bars. The strain matrix $[B]$ links, in this case, the strain ϵ_s, defined in local axis, to the nodal displacements defined in global axis;
- membrane elements capable of simulating a liner of assigned thickness. These elements have stiffness in the circunferential direction and in s direction, tangential to the membrane in the meridian plane. The strain matrix $[B]$ links, in this case, ϵ_s and ϵ_θ strains, defined in local axis, to the nodal displacements defined in global axis.

3. DESCRIPTION OF THE PCPV PHYSICAL AND MATHEMATICAL MODEL

The tests carried out on the physical PCPV model have been performed in the elastic and non-elastic fields up to the model collapse (3). These tests have practically defined up to the working pressure (40 Kg/$/cm^2$) an internal "pressure-displacements" relationship (fig. 3) of a linear elastic type, while the first cortical microcracks were detected at a pressure of about 70 Kg/cm^2.

The purpose of the mathematical model was the investigation of the stress-strain state in working conditions. With the results obtained from the behaviour of the physical model it was possible to schematize, with a good approximation, the behaviour of concrete, as linear elastic.

The geometrical symmetries of the structure were taken into account in building up the finite element mesh shown in fig. 4. The mesh consisted of:

- 269 second order isoparametric elements to simulate the concrete;
- 29 second order isoparametric elements to simulate the ribs;
- 39 elements to simulate the radial prestressing cables;
- 21 elements to simulate the meridian prestressing cables;
- 36 elements to simulate the internal copper liner.

The computer programs used for the mathematical model and available at ISMES, were:

- GEOTAV 2 to set up and draw the finite element mesh on plotter
- AXITEN 3 to evaluate the stress-strain state
- BICAMP 3 to evaluate the temperature distribution
- DIPLA 13 to draw the results automatically on plotter.

4. ESTIMATE OF THE CONCRETE ELASTICITY MODULUS

In this phase of calculation, attempt was made to give an estimation of the average elastic modulus of the concrete by a comparison between measured and calculated displacements.

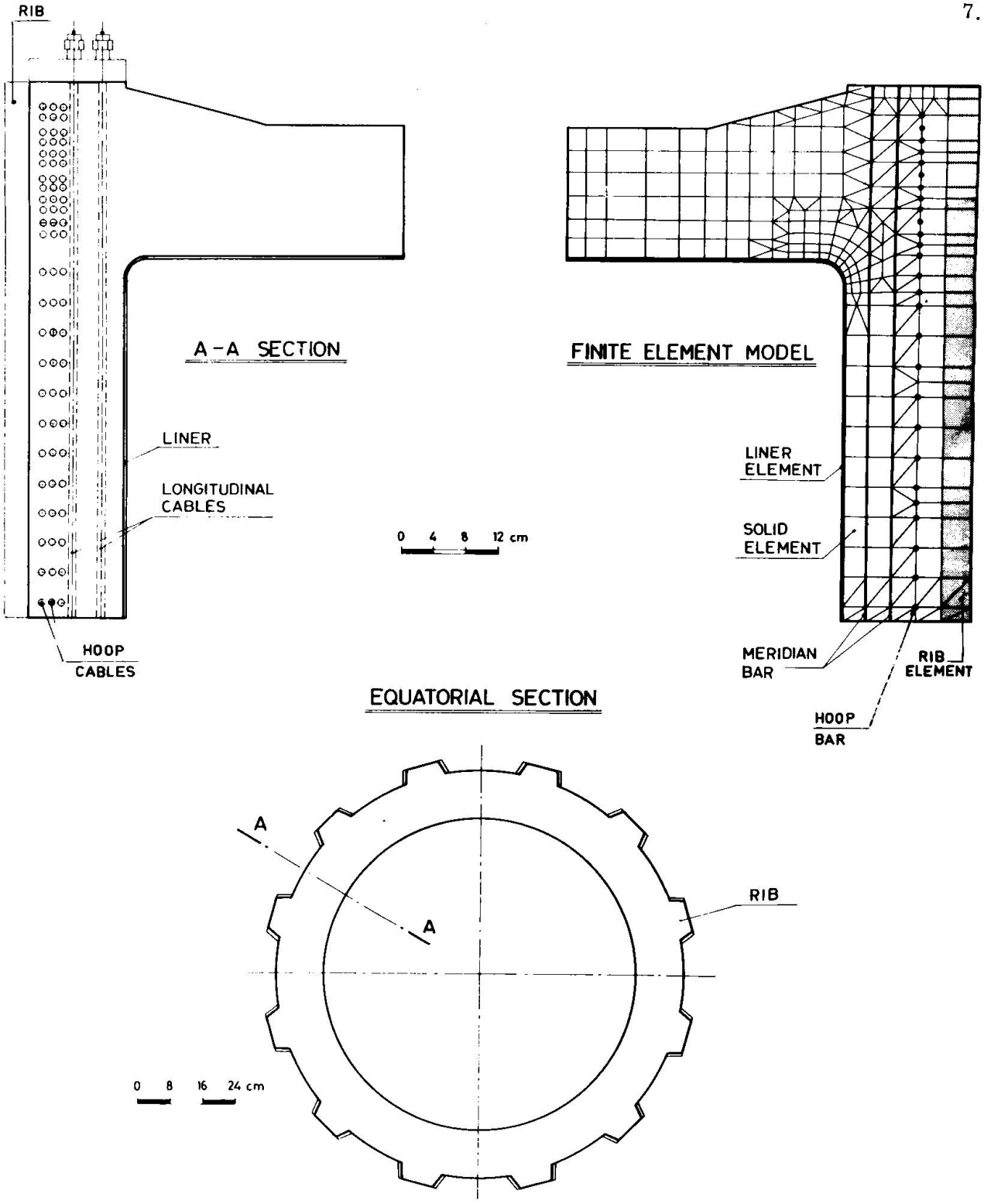

FIG. 4

Equatorial and meridian sections of the vessel and finite element mesh.

Sections équatorielles et méridiennes du caisson, avec réseau d' éléments finis.

Meridian-und Aequatorschnitte des Behälters mit Begrenzter Elemente-Masche.

Such value has been subsequently verified by the results of uniaxial compression tests performed on same samples of the same concrete utilized for the physical model.

The logical scheme of this calculation phase is briefly outlined in fig. 5.

Practically, reference was made to the measured displacements at some points of particular interest on the vessel, relative to an internal pressure variation $\Delta_p = 10$ Kg/cm^2.

For the same pressure variation, displacements at the same points were calculated assuming that the elastic concrete modulus E_c is respectively 400,000 - 410,000 - 430,000 Kg/cm^2, and the steel modulus E_f equal to 2,100,000 Kg/cm^2.

In each particular case a concrete modulus $E'_c = E_c/K'$ was evaluated by means of the least square method in order to have calculated displacements as close as possible to the measured ones.

If δ_{ic} and δ_{im} are the calculated and measured displacements at point "i", the value K' was determined in order to minimize the function:

$$\phi(K) = \sum_{i=1}^{N} (K\ \delta_{ic} - \delta_{im})^2$$

where, the above summation has been extended to the N points at which displacements were measured. The following values were found:

- for $E_c = 400,000$ Kg/cm^2; $K' = 0.932739$; $E'_c = 428,834$ Kg/cm^2;
- for $E_c = 410,000$ Kg/cm^2; $K' = 0.955781$; $E'_c = 428,968$ Kg/cm^2;
- for $E_c = 430,000$ Kg/cm^2; $K' = 1.0005$; $E'_c = 429,934$ Kg/cm^2.

Finally, at the third attempt it was found that the concrete modulus definying a value $K' = 1$ is about 430,000 Kg/cm^2. The comparison between displacements evaluated by finite element model and those measured on the physical model is shown in fig. 6.

To evaluate the reliability of this kind of procedure, the values so found were verified by means of other experimental data.

At the Niguarda Laboratories of CRIS in Milan, some uniaxial compression tests were carried out on samples of the concrete used for the physical model. It was thus possible to evaluate the variation of the secant modulus versus the uniaxial stress.

With the finite element model previously used it was possible to calculate at every nodal point the triaxial state of stress for the loading combinations of total prestress with a gas pressure variation $\Delta_p = 10$ Kg/cm^2.

Among the three principal nodal stresses, the one of maximum compression was selected, assuming that in this direction, the stress state can roughly be considered the closest to the uniaxial one.

On the basis of such compression value, the modulus has been

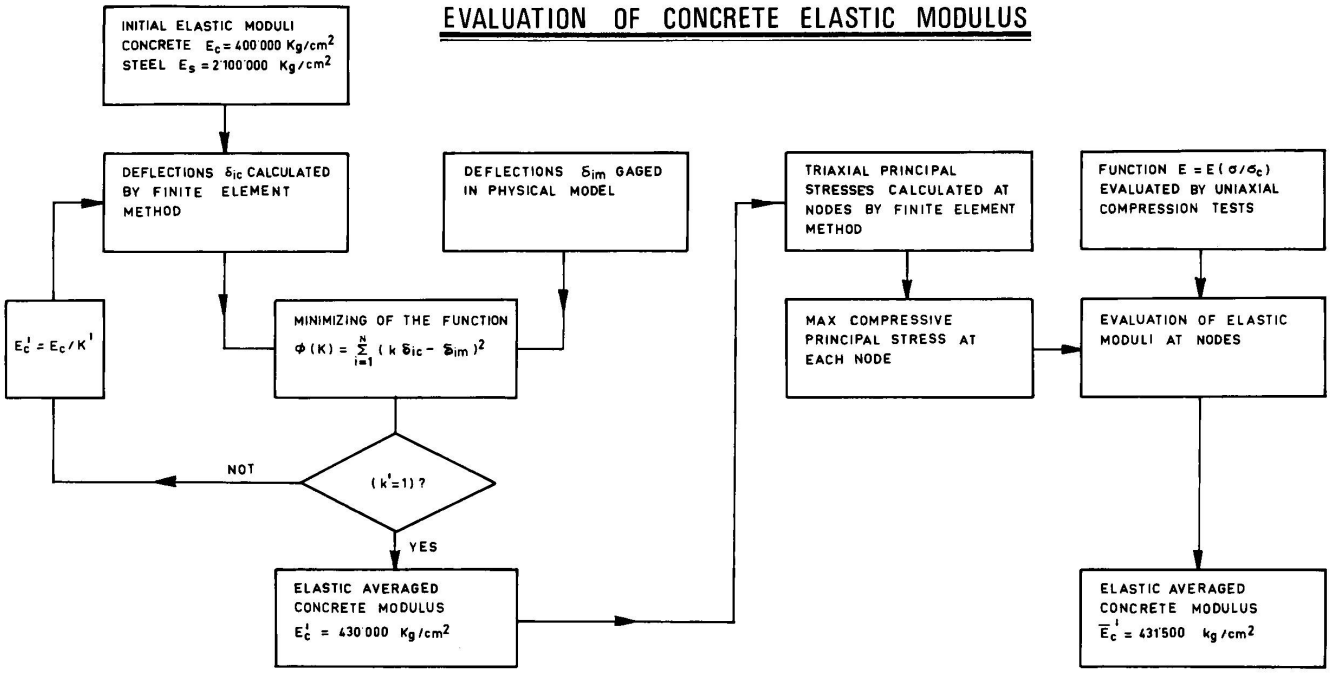

FIG. 5

Logical scheme to evaluate the concrete modulus.

Schème logique pour évaluer le module élastique du béton.

Logisches Schema zur Berechnung des Betons-Elastizitätmoduls.

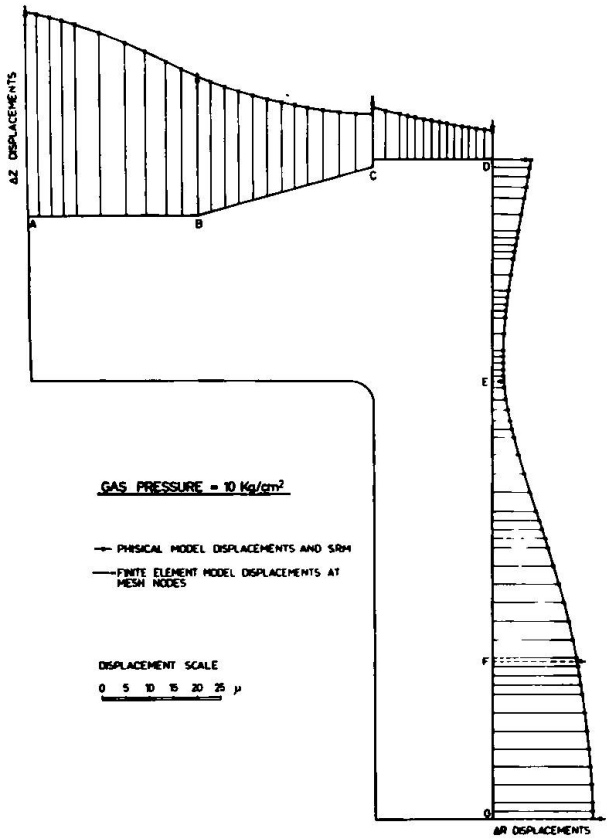

FIG. 6

Finite element and physical model displacements.

Déplacements du modèle à éléments finis et du modèle physique.

Verschiebungen des Begrenzter Elemente-und physikalischen Modelles.

———— o ————

determinated at each nodal point through the experimental relationship as shown in fig. 7a.

By averaging the nodal values, an elastic modulus $\overline{E'}_c = 431,500$ Kg/cm^2 was found. This value fairly agrees with the value $E'_c = 430,000$ Kg/cm^2 previously obtained.

Contour lines of the elastic modulus, obtained by plotting the above-mentioned nodal values, are shown in fig. 7b.

5. ANALYSIS OF THE STRESS-STRAIN STATE OF THE STRUCTURE IN WORKING CONDITIONS

Further analysis consisted in studying the stress-strain behaviour of the structure in the working conditions under the action of fast loads. Therefore, the typical time-dependent phenomena of concrete like shrinkage and creep, were not considered.

The structural loading conditions are the following:

SECANT MODULUS $E = E(\sigma/\sigma_c)$

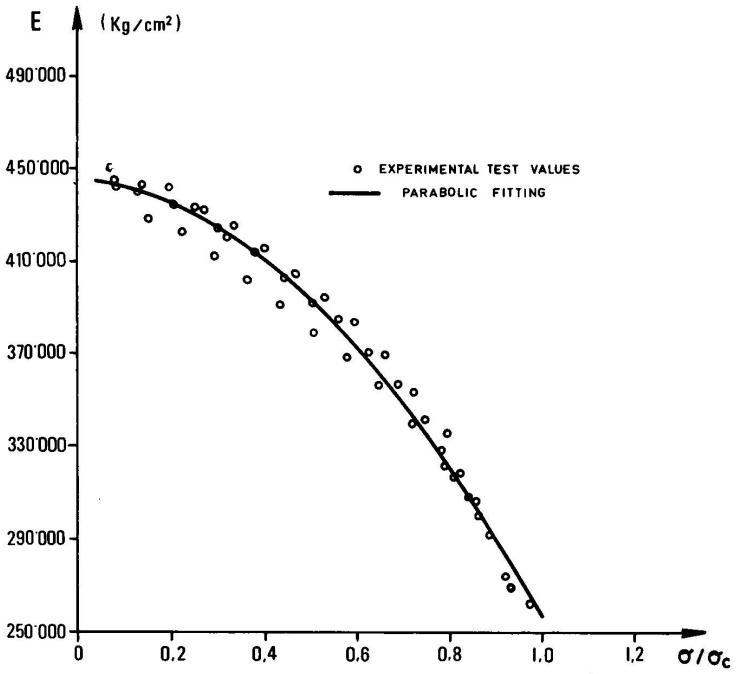

FIG. 7 a
Function $E = E(\sigma / \sigma_c)$
Fonction $E = E(\sigma / \sigma_c)$
Funktion $E = E(\sigma / \sigma_c)$

ELASTIC MODULUS CONTOUR LINES

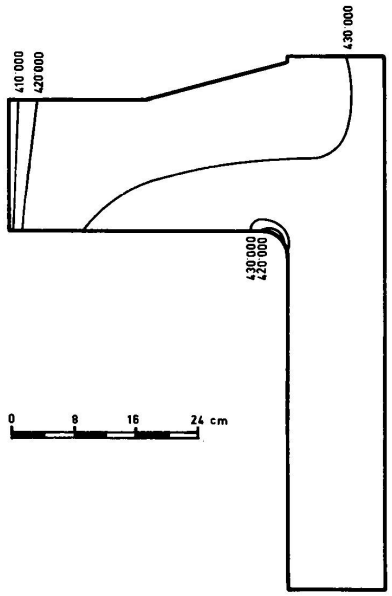

FIG. 7 b
Elastic modulus contour lines for the structure.
Lignes d' égale valeur pour le module élastique dans la structure.
Elastizitätlmoduls-Niveaulinien im der Struktur.

a) The cable pulling sequences up to total prestress.

By means of computer calculations, it was possible to evaluate the optimum cable pulling sequence, i.e., the sequence avoiding tensile stresses acting locally in the structure, during an intermediate stage of prestressing.
Fig. 8 shows the prestressing sequences for the structure and the contour lines of the safety factor for the subsequent stages of prestress until the total pulling is over. In order to calculate the local safety factor, the Mohr - Caquot theory (7) has been taken into account. The intrinsic curve shown in fig. 9 was determined on the basis of the values of the tensile ultimate strength $\sigma_{rt} = 32$ Kg/cm^2 and the compressive ultimate strength $\sigma_{rc} = 525$ Kg/cm^2 derived from uniaxial tests.
Fig. 10 shows the principal stress patterns acting on the meridian plane, and the contour lines for the three principal stresses for the total prestress.

b) The operating conditions where the following actions are combined:

- Total prestress
- Gas pressure (40 Kg/cm^2)
- Temperature difference between inner and outer wall assumed as $T_i - T_o = 10^oC$.

For the evaluation of the thermal stress state generated in the structure, temperature values at mesh nodes were obtained with a finite element program solving field problems governed by Laplace's equation.
Fig. 11 shows the isothermal contour lines for the structure. In fig. 12 are shown the patterns of the principal stresses acting on the meridian plane and the contour lines of the three principal stresses for the operating conditions. The local safety factors shown in the same figure are quite satisfactory.

6. CONCLUSIONS

The main purpose of the present study was the evaluation of the stress-strain state and the local safety factor of the structure during the construction phase and in the working conditions, assuming an elastic behaviour for the materials. To this end it was necessary to define the elastic moduli of the materials under consideration which being the input data of the problem conditioned all the calculation results. Information on the rheological behaviour was at hand both for the physical model and concrete samples. Thus, it was deemed advisable to utilize this kind of information to evaluate the elastic modulus values of concrete and then compare the obtained values.

The study, which in its preliminary phase, was a study of con

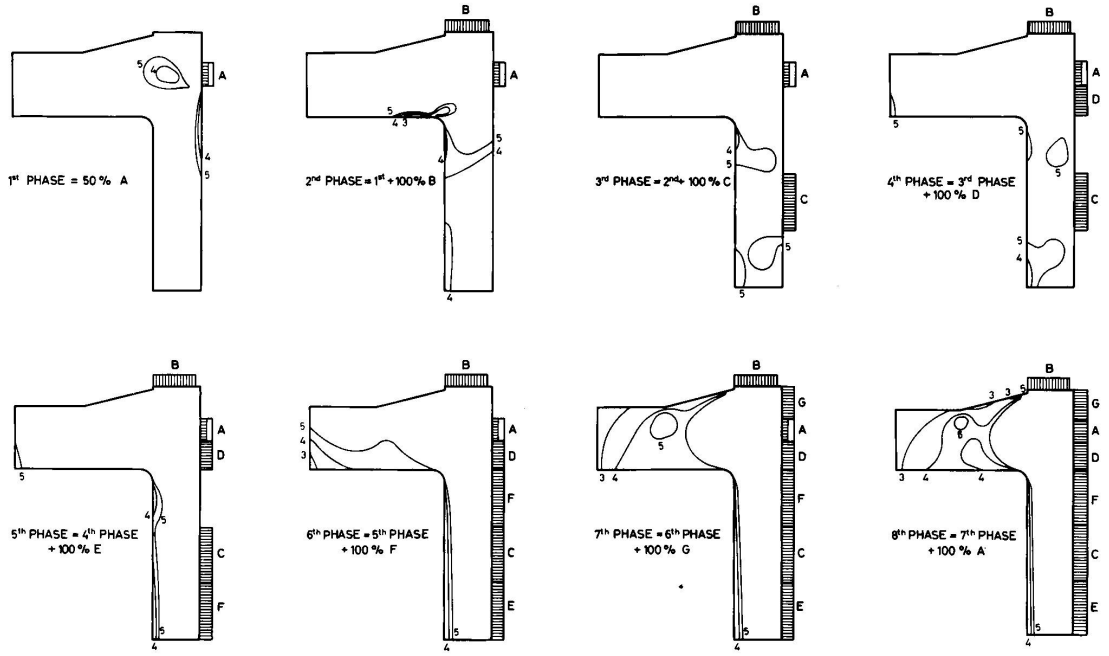

FIG. 8
Safety factor contour lines in prestressing sequence. - Lignes d' égale valeur pour le coéfficient de sécurité pendant les opérations de précontrainte. - Sicherheitskoeffizients-Niveaulinien während der Vorspannung.

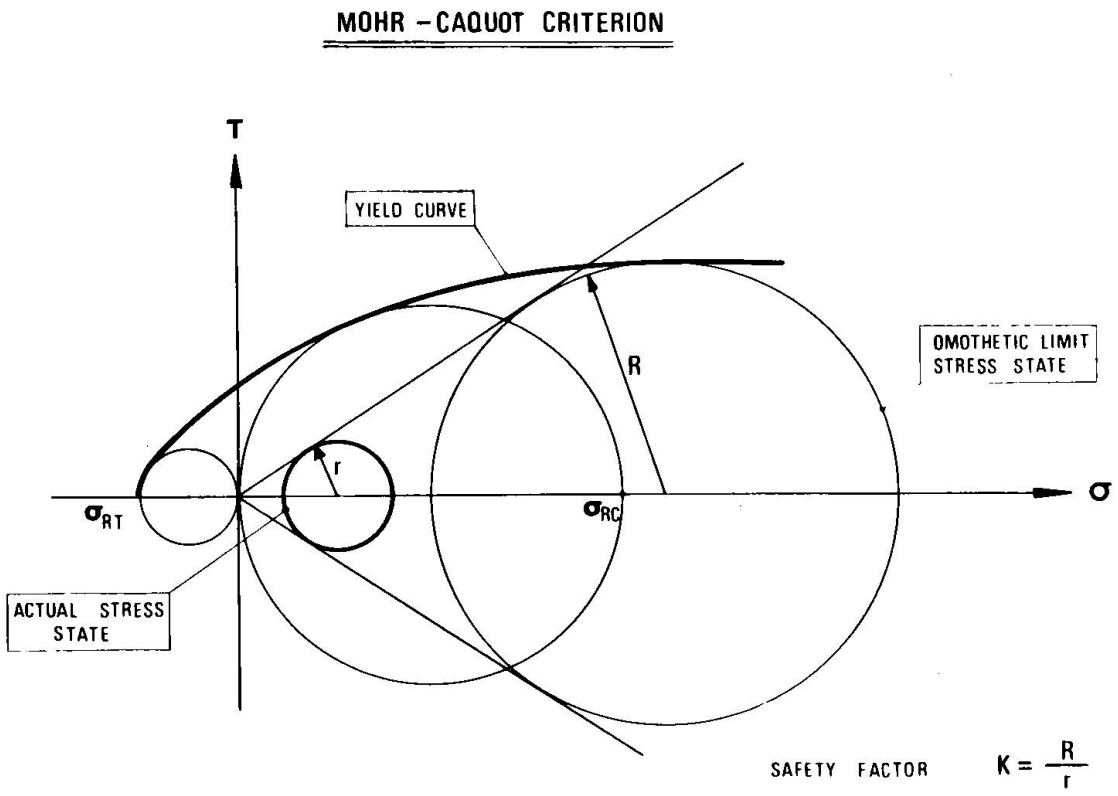

FIG. 9

Mohr-Caquot criterion and safety factor definition.

Critère de Mohr-Caquot et définition du coefficient de sécurité.

Mohr-Caquot-Kriterium und Sicherheitskoeffizients-Bezeichnung.

O

catenation and interaction between the mathematical model and the experimental results, evidences the limits and possibilities of the various types of information and therefore, the necessity of complementaring of physical, rheological and mathematical models one with each others. The results confirm the validity of the linear elastic approach for the structure for the operating conditions.

In the above mentioned conditions, for all the points of the structure the safety factor values are satisfactory, confirming what experienced on the physical model, that is, no crushing, cracking or sliding are to be expected in the bulk of the structure.

As far as the safety factor is concerned, the Mohr - Caquot theory was adopted, whose limitations are well known. In fact, that theory neglects the principal intermediate stress. More recent studies (8), (9), (10) give results more in agreement with the concrete behaviour under triaxial state of stresses, considering also the effect of the principal intermediate stress and the two different collapse modes (brittle and shear failure).

PRESTRESSING ONLY

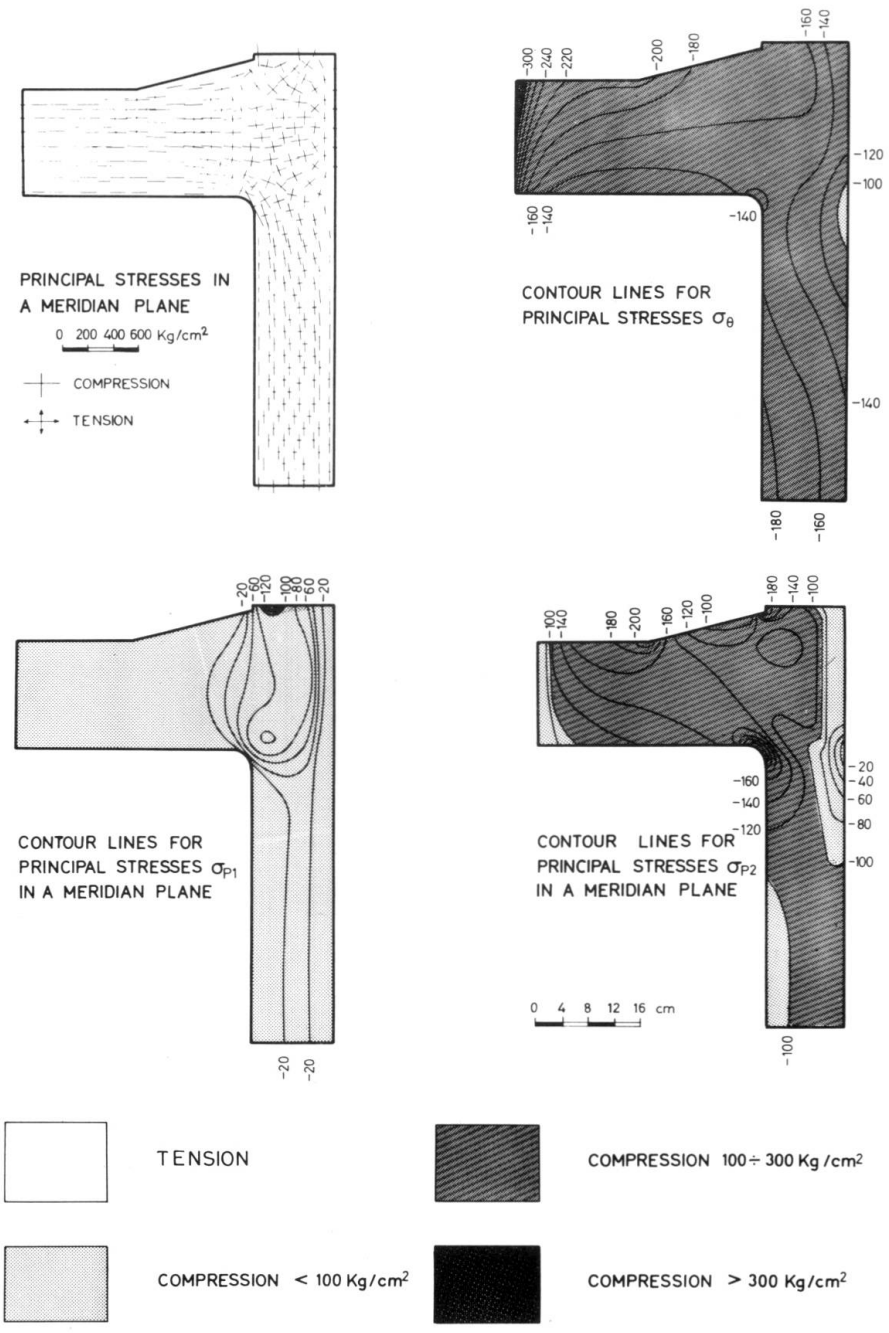

FIG. 10

Principal stress patterns and contour lines of the principal stresses for prestressing only.

Croix et lignes d' égale valeur pour les contraintes principales en régime de seule précontrainte.

Hauptspannungs trajektorien-Schema und Hauptspannungs Niveaulinien nur unter Vorspannungs- Bedingungen.

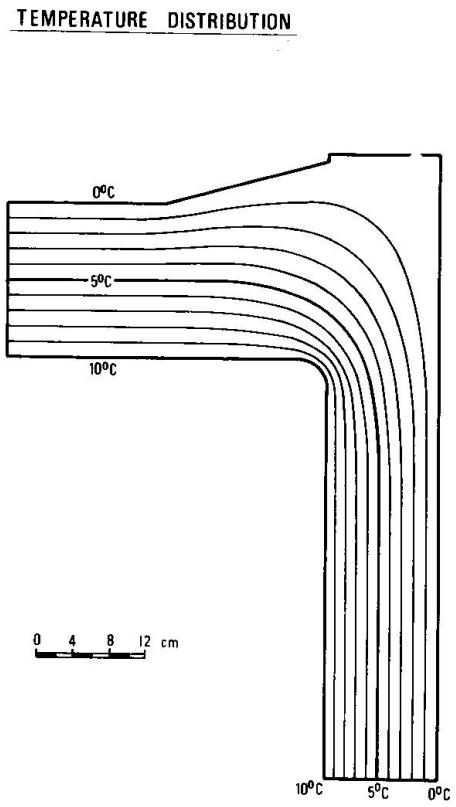

FIG. 11

Contour lines of the temperature distribution.

Lignes isothermes pour la distribution de températures.

Niveaulinien für die Temperaturverteilung.

For the structure under consideration, it is felt that the safety factor should be defined.on the basis of a more realistic rheological model, taking into account as well the fact that the external actions (pressure and temperature) act on a prestressed structure subjected to a triaxial state of stresses.

The logical development of the present work will be the studies of the structure in non-linear conditions up to the collapse limits, taking care of the viscous-elastic characteristics of the concrete in such conditions.

PRESTRESSING + GAS PRESSURE (40 kg/cm²) + TEMPERATURE VARIATION ΔT=10°C

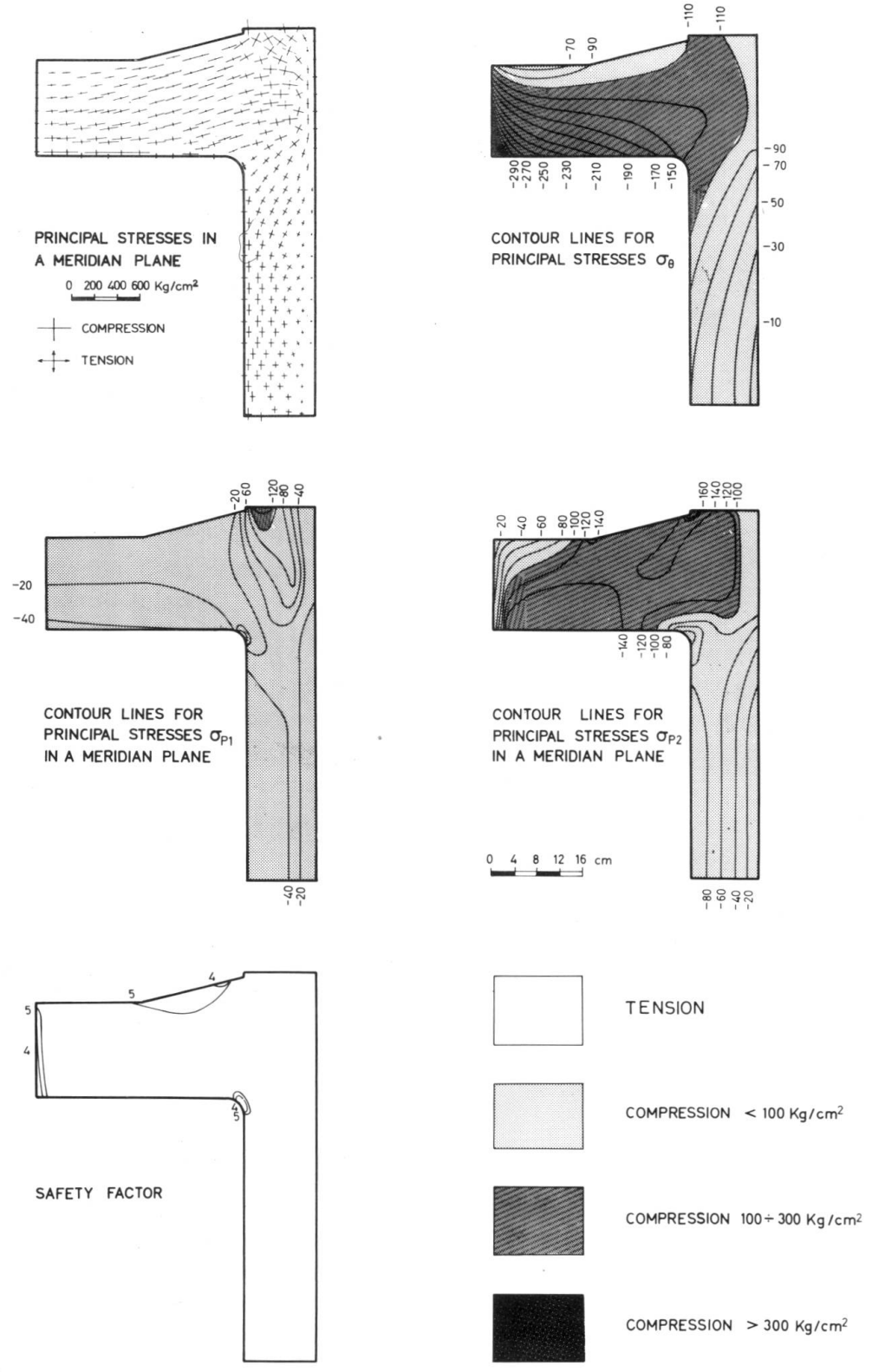

FIG. 12

Principal stress patterns and contour lines of the principal stresses and safety factor in working condition. - Croix et lignes d' égale valeur pour les contraintes principales et le coéfficient de sécurité en régime d' exploi tation. - Hauptspannungs trajektorien- und Hauptspannungs und Sicher- heitskoeffizients Niveaulinien im Betriebszustande.

REFERENCES

(1) F. Scotto — "Tiny- Walled 1 : 20 Prestressed Concrete Pressure Vessel Model for THTR Reactor Type"

Paper H5/4, First International Conference on Structural Mechanics in Reactor Technology, Berlin, September 1971.

(2) E. Fumagalli, G. Verdelli — "Static Tests on a Small Model of Prestressed Concrete Pressure Vessel for THTR Nuclear Reactor - Safety Aspects of PCPV"

Delft, December 1970.

(3) E. Fumagalli, G. Verdelli — "Small Scale Model of PCPV for High Temperature Gas Reactor - Modelling Criteria and Typical Results"

IABSE Seminar on Concrete Structures subjected to Triaxial Stresses, Bergamo, May 1974.

(4) J.H. Argyris, G. Faust, J.H. Roy, J. Szimmat, P. Warnke, K.J. Willam

"Finite Elemente zur Berechnung von Spannbeton-Reaktordruckbehältern"

Issue No. 234, DAfStb, 1973.

(5) E. Schrem — "Computer Implementation of the Finite Element Procedure"

ONR Symposium on Numerical and Computer Methods in Structural Mechanics, University of Illinois, 1971.

(6) O.C. Zienkiewicz — "The Finite Element Method in Engineering Science"

McGraw-Hill, 1971.

(7) A. Caquot — "Idées actuelles sur la résistance des matériaux"

Le Génie Civil, 1930/11.

(8) B. Saugy

"Contribution à l' étude théorique du comportement non linéaires des structures massives en béton armé sous charge rapide"

Bulletin Technique de la Suisse Romande, n. 22, Novembre 1969.

(9) L. Ianda

"Triaxial State of Stress of Concrete Structures"

Proceedings of the First International Conference on Structural Mechanics in Reactor Technology; Vol. 4, Part. H 1/2, Berlin Wo., 1971.

(10) P. Bertacchi, R. Bellotti

"Experimental Research on Deformation and Failure of Concrete under Triaxial Loads"

RILEM International Symposium I 3, Vol. I - p. 37-52, Vol. IV, p. 54 - 65, October 1972, Cannes.

Leere Seite
Blank page
Page vide

IABSE
AIPC
IVBH

SEMINAR on:
« CONCRETE STRUCTURES SUBJECTED TO TRIAXIAL STRESSES »
17th - 19th MAY, 1974 - ISMES - BERGAMO (ITALY)

Analysis and Behaviour of Triaxially Prestressed Concrete Components for Prestressed Concrete Pressure Vessels

Analyse et comportement de composantes pour caissons en béton précontraint triaxialement

Analyse und Verhalten der dreiachsigen Spannbeton-Komponenten für Spannbeton-Druckbehälte

F.K. GARAS, Ph.D., B.Sc., M.I.C.E.
Head of Structures Research Laboratory,
Taylor Woodrow Construction Limited, Southall, Middlesex, U.K.

1. INTRODUCTION

The two nuclear power stations at present being constructed at Hartlepool and Heysham(1) in the United Kingdom have twin advanced gas-cooled reactors with 1250 MW electric output per station. They are being constructed by British Nuclear Design and Construction for the Central Electricity Generating Board and are the first commercial stations to incorporate the use of the podded boiler concept. In the type of prestressed concrete pressure vessel which has been adopted, the boilers and gas circulators are housed in vertical pods in the walls of the vessel. The advantage of this type of design is that the boilers can later be removed for maintenance, should this ever be required in service.

During the lifetime of the vessel it will be subject to complex mechanically and thermally induced stress conditions. In certain zones of the vessel the stresses may be higher than those normally accepted in conventional structures. Thus there was a need for considerable experimental verification during the development of the pressure vessel structure. The paper deals with only one aspect of the triaxial stresses where the concrete is under the combined action of high shearing forces and biaxial restraint.

2. VESSEL DESCRIPTION

The vessel is cylindrical in form with an external diameter of 25.9 m (85 ft) and overall height of 29.3 m (96 ft) and is vertically and circumferentially prestressed. Circumferential prestress is provided by wire winding the cylindrical surface of the vessel. The end slabs and the walls are 5.5 m (18 ft) and 6.4 m (21 ft) thick respectively. (See Fig. 1.)

The boilers are contained in eight circular cavities of 2.74 m diameter and are housed within the wall of the pressure vessel. Several hundred penetration tubes are also incorporated throughout the concrete mass.

The boiler closure, which forms an integral part of the complete boiler unit, is a prestressed concrete component. In addition to the primary function of closing the upper end of the boiler pod, the closure supports the boiler heat transfer surface by means of a central axial spine tube, and carries penetrations for the steam and feed tail pipes. (See Fig. 2.)

By constructing the closure of prestressed concrete it became possible to apply the same safety philosophy and criteria to the closure as were applied to other parts of the vessel. The closure is prestressed by circumferential wire winding, but additionally, substantially unstressed wire is wound on to provide a passive radial restraint to the concrete plug. The passive restraint ensures that the closure, without prestress, has a load carrying capacity in excess of the design ultimate load.

3. END SLABS AND BOILER CLOSURES

3.1. Design Problems

The end slabs and boiler closures are geometrically deep in relation to their span; the shear span to depth ratios are 2.39 and 1.62 respectively. High operating pressures results in higher shear forces than normally accepted in conventional structures. Their strength is, however, enhanced by the use of hoop prestress.

In the assessment of the ultimate strength of the end slabs and boiler closures, the shear stresses were found to be dominant in determining the mode of collapse. The particular mode of failure is greatly influenced by the behaviour of the concrete under complex states of stress.

Because of the complexity in the behaviour of thick elements under high shear stresses, designers tend to be very conservative in their selection of allowable stress and hence their requirements for a factor of safety. This is due to the lack of knowledge of the distribution of stresses in the compression zone, and of the capability of the concrete to withstand these stresses. The current practice is to adopt methods used for conventional structures which are primarily subjected to flexure. These methods usually ignore the high shear stresses which can be mobilised and the triaxial state of stress which occurs in this type of structure, resulting in an uneconomic design.

3.2. Assessment of Shear Resistance

Because of the low span to depth ratio, flexural failure is unlikely to occur in the end slabs and boiler closures. Shear failure is a characteristic of thick slabs and occurs before the flexural capacity is exhausted. In order to understand the failure mechanism in deep structural members, the following points should be considered:

(i) the shear stresses are more dominant than those due to flexure

(ii) the geometry of the section induces stresses which are essentially three-dimensional

(iii) just prior to failure the strength of the member is dependent on the resistance of an element of concrete subject to triaxial compression with shear - a state of stress which as far as the author is aware has not fully been studied.

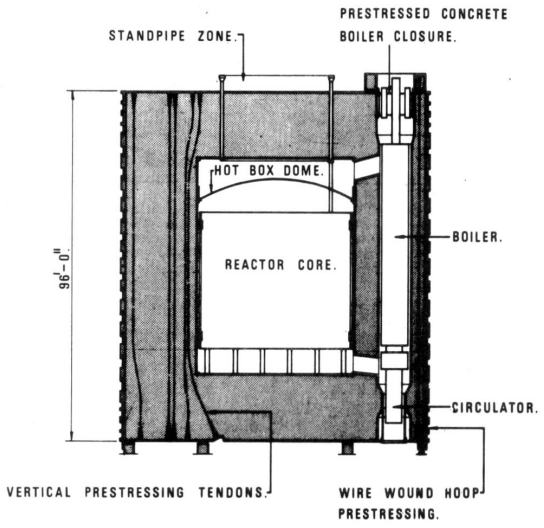

Fig. 1

SECTION THROUGH HARTLEPOOL / HEYSHAM PRESSURE VESSEL.

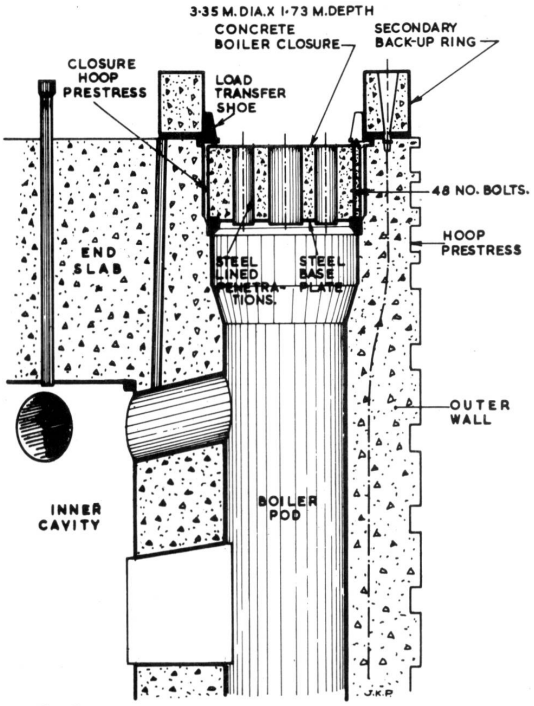

Fig. 2

CONCRETE BOILER CLOSURE IN THE HARTLEPOOL PRESTRESSED CONCRETE PRESSURE VESSEL

3.3. Shear Components

As an aid to the understanding of shear mechanism the components of the internal shear resistance which balance the total shear force generated by the applied forces at the point of failure are identified. In restrained slabs the total shearing force 'F' is resisted by the component forces shown in Fig. 3.

3.3.1. Shear Resistance of the Compression Zone 'Fc'

From the author's experimental work(2) it was found that at the point of failure the depth of the compression zone was reduced to about 15% of the original depth of the slab, see Fig. 4.

The contribution of this component may be assessed using the relationship between the biaxial compression and the shear stresses based on the parametric study which was carried out by the author(3). Using this information and determining the depth of the compression zone, the shear resistance of the compression zone was found to be 45% of the total.

3.3.2. Shear Transfer by the Vertical Components of the Aggregate Interlock within the Tension Zone 'Fg'

This action develops because of a shear displacement parallel to the direction of the shear planes. When a crack forms in the section the shear displacement causes the larger aggregate particle to act as dowels. Smaller crack widths increase the significance of aggregate interlock, and since this is a function of the aggregate itself the properties of the aggregates are important.

From the behaviour of end slabs examined by the author(2) the calculated crack width prior to failure was about 0.003 in (0.08 mm). By extrapolation using Fenwick's work(4) on the contribution of the aggregate interlock in resisting shear forces, this value was found to be in the range of 50% of the total shear force.

3.3.3. Shear Transfer by Dowel Action of Bonded Reinforcement 'Fd'

At present there is no adequate method of assessing the magnitude of this component but because of the low steel percentage its contribution to the shear resistance was found to be very small(2).

3.4. Method of Analysis

To develop general design rules for deep restrained sections, two approaches were possible:

(i) to develop a mathematical approximation to the particular mode of failure observed from the testing of elements under certain boundary conditions, i.e. find a solution for each type of shear failure.

(ii) to undertake a parametric experimental study and relate all results non-dimensionally; this could lead to an empirical formula based on a statistical analysis of the data.

The second alternative was more realistic although the amount of available data on the ultimate load behaviour of restrained and unrestrained deep elements is still too limited to enable comprehensive design rules for shear to be developed.

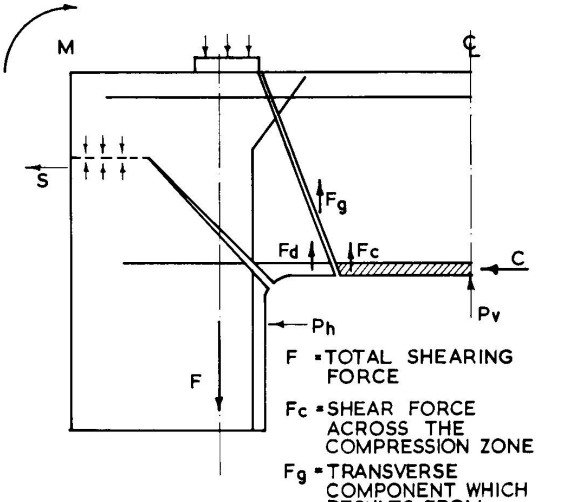

$F = Fc + Fg + Fd$

F = TOTAL SHEARING FORCE

Fc = SHEAR FORCE ACROSS THE COMPRESSION ZONE

Fg = TRANSVERSE COMPONENT WHICH RESULTS FROM INTERLOCKING OF AGGREGATE PARTICLES ACROSS CRACK

Fd = TRANSVERSE FORCE INDUCED IN THE MAIN REBAR AND PRESTRESS WIRES BY DOWEL ACTION

FIG. 3

MECHANISM OF SHEAR FAILURE

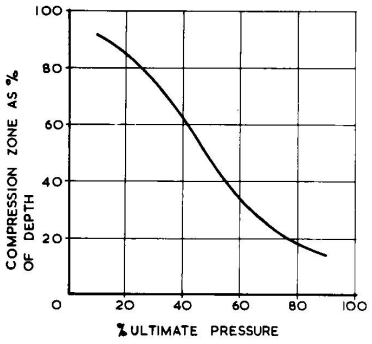

FIG. 4

REDUCTION OF DEPTH OF COMPRESSION ZONE WITH PRESSURE

4. EXPERIMENTAL INVESTIGATION OF END SLABS

4.1. General

During the last eight years an extensive study was carried out into the behaviour of end slabs in cylindrical prestressed concrete pressure vessels. To date, 23 end slab models have been constructed and tested to failure. The test programme, which was described in an earlier paper[2] was designed to examine the effect of the variation of the major parameters on the ultimate strength of failure of end slabs, e.g. hoop prestress level, penetrations lined or unlined and pressurised penetrations, boundary conditions and sustained elevated temperature. Fig. 5 shows a cross section of the pile cap model clamped to the test base. A rubber chamber was used to produce water pressure and to act as a liner between the pile cap and the base slab.

From these studies, and assessing most of the published work on end slab behaviour, it became apparent that the possible mode of failure is the classical shear plug failure. Shear or sliding planes are developed such that a central plug is forced outwards and isolated from the main annulus of concrete. The position of the failure plane is governed, on the outer face, by the location of the vertical prestress, the inclination of the plane by the hoop prestress and span to depth ratio.

4.2. Behaviour of End Slabs Prior to Failure

The general behaviour of an end slab is described in Fig. 6 where the central deflection, as a percentage of the value of the ultimate is plotted against percentage of maximum pressure. The flexural behaviour of the slab may be divided into three stages. The first stage, elastic, is defined by the pressure at which the first radial cracks formed on the external surface. This pressure is almost twice the design pressure whilst the central deflection was equivalent to about 5% of the maximum (1/450 of the depth). Furthermore, tensile strains of the order of 3000 microstrain have been measured at the outer face of the slab before any visible cracking was observed.

The second stage, elastoplastic, was characterised by the development of external flexure cracks. The crack started at the centre of the slab and spread towards the edges of the model; on average they were fully developed at about three times the design pressure (74% of the ultimate strength). Further pressures caused secondary cracks to appear between the major radial cracks and accompanied by a rapid increase of deflection due to yielding of the tensile reinforcement in the central region.

In the final stage, yielding of the reinforcement was fully developed along all the radial cracks and the deflections increased considerably with a small increase in pressure; the maximum deflection varied between 10 and 12.5 mm (0.4 and 0.5 inch).

Although the flexural plastic stage was well advanced, it did not result in failure as another mode interceded, i.e. a central plug of concrete was extruded through the circular slab. (See Fig. 7.)

4.3. Summary of Results

The following are general comments obtained from the experimental investigation:

(a) An increase in the thickness of the slab in relation to its span has a dominant effect on the ultimate strength.

(b) Provision of hoop prestress or lateral restraint increases the ultimate strength of the slab but the rate of increase of strength progressively falls. At the magnitude of prestress required for producing acceptable stress levels under

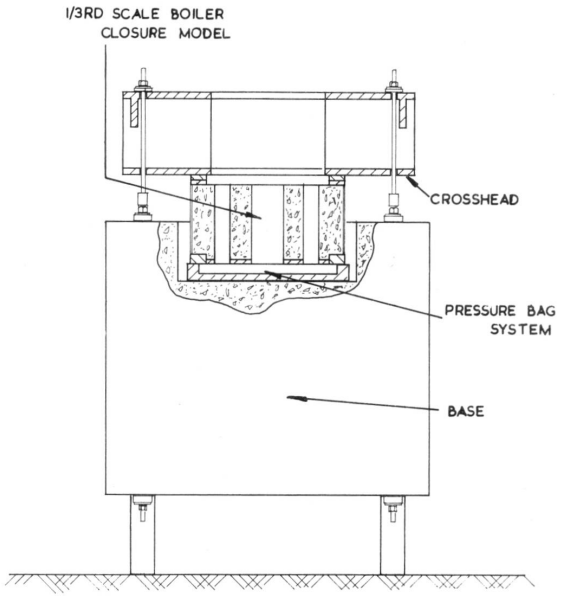

FIG. 11

TEST ARRANGEMENT FOR $\frac{1}{3}$RD SCALE MODEL BOILER CLOSURE

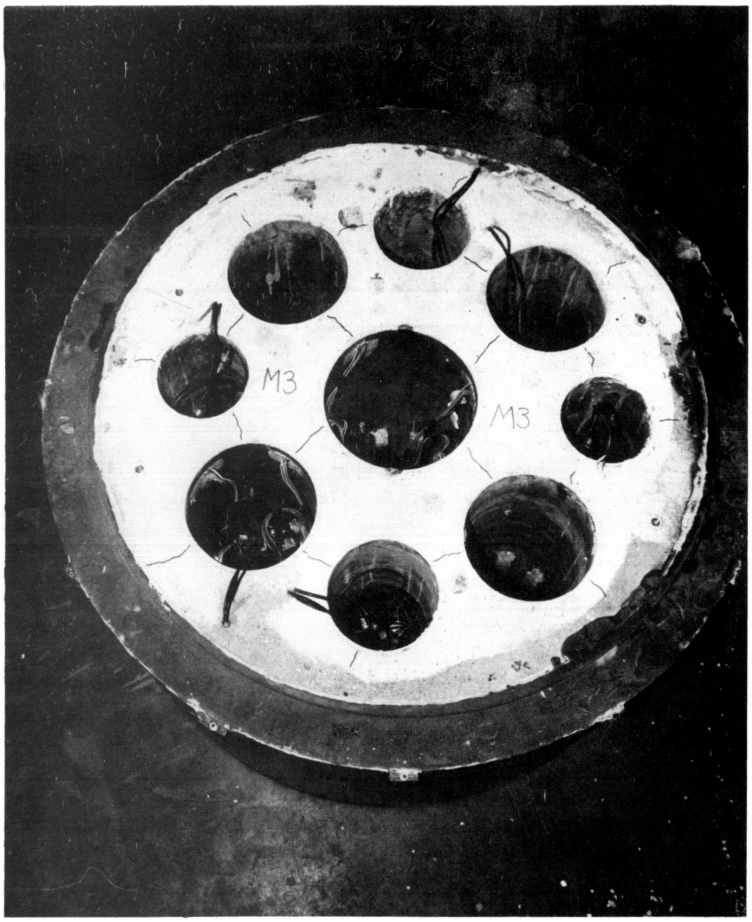

FIG. 12 1/3rd Scale Model Boiler Closure Crack Patterns

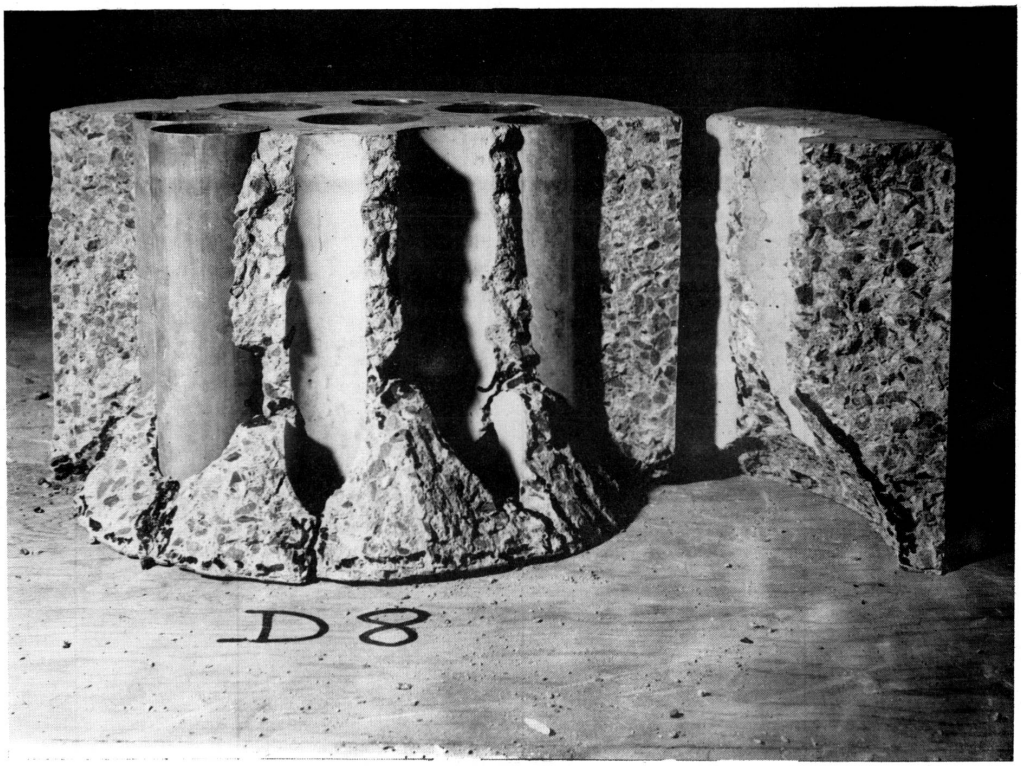

FIG. 10 1/10th Scale Model Boiler Closure Showing Failure Planes

reactor working conditions the ultimate strength is not significantly affected by variation of the hoop prestress.

(c) When penetrations are incorporated in the slab, the liners partly compensate, by dowel action, for the loss of the area of concrete acting in shear. The loss of strength due to the introduction of a standpipe array is therefore not severe (17.5% loss in cross sectional area resulted in about 10% reduction in the ultimate shear strength).

(d) Surface reinforcement equivalent to 0.44% of the cross sectional area of the slab only increased the ultimate shearing strength by 3% presumably because of the dowel forces.

(e) By reducing the level of hoop prestress at transfer from 4.1 to 2.5 N/mm^2 (600 to 360 lb/sq.in.) whilst maintaining the same area of steel, the difference between the ultimate shear strength was only 10%.

(f) Sustained temperature has no effect on the ultimate shearing strength of concrete.

(g) For similar shapes of models the ultimate shear strength has been found to be approximately proportional to the square root of the cylinder strength of the concrete.

4.4. Ultimate Shear Strength Equation

An attempt was made to obtain an analytical expression which would give better correlation with the available published data on end slabs, including the author's work, and which takes into consideration the effect of the lateral prestress, depth of slab, diameter of pressurised area, as well as the strength of the concrete.

The following expression was found to fit the test data of 36 end slab models reasonably well:

$$P = 77 \frac{d}{D} \sqrt{f_c} + 10\left(1 - \frac{D}{\phi}\right)^{\frac{1}{2}} \sqrt{f_h}$$

where P = ultimate pressure in lb/sq.in.
f_h = lateral prestress at transfer in lb/sq.in.
d = depth of slab
D = internal diameter of pressure vessel
f_c = cylinder compressive strength in lb/sq.in.
ϕ = outer diameter of pressure vessel

This equation is based on a small number of tests and can only be considered to be applicable to structural members similar to the test results and where lateral prestress is applied. With additional data a more generally applicable expression similar to the above could be developed.

5. DESIGN DEVELOPMENT OF BOILER CLOSURE

5.1. Analysis and Design of Closure

In developing the structural design of the closure, model analysis was preferred to a purely theoretical approach. The closure contains several closely spaced steel lined penetrations and other steel components. The combined effect of operating pressure and the active prestress produces a complex triaxial state of stress within the structure. An ultimate load analysis incorporating cracking and plasticity of the concrete is very difficult due to the limitation of establishing applicable criteria of failure for concrete. The only alternative was therefore to undertake model studies.

Initial examination of the design was based on a simplified axi-symmetric Dynamic Relaxation analysis under operating pressure and various extreme boundary conditions. This was supported by a rapid but extensive series of tests of 1/10th scale models to determine the likely effects of various parameters on the functional and ultimate behaviour of the closure. The intensity of prestress, quantity of circumferential steel, the effect of penetration liners, the system of support and other relevant factors were all examined. The guidance obtained from these models enabled a final design to be chosen.

As final confirmation, four fully representative 1/3rd scale models were tested to establish the load factor of the closures and then to investigate the effects on operational and overload behaviour of both cycled and sustained pressure and temperature.

5.2. 1/10th Scale Models

5.2.1. Test Programme and Procedure

The experimental programme described in Table 1 was phased to examine the following main parameters which are likely to affect the behaviour of the closure under working and overload conditions. The models were simplifications of prototype designs but were still representative for obtaining general conclusions. Sixty models were tested using the experimental arrangement shown in Fig. 8.

TABLE 1 1/10th Scale Secondary Closure Models - Test Programme

Shear Span (mm)	Prestress (N/mm2)				
	None	Passive		Active 6.2	Steel Casing
		0.5	1.0		
229	*	*	*	*	*
290			*	*	*

* Two models tested with this combination of parameters.

To reduce the frictional restraint at the bearing ring, and achieve uniformity of bearing, a resin/polytetrafluorethylene interface was included on certain specimens.

The geometry of the specimens, penetrations and liners were scaled from an early prototype design in which the span to depth ratio was 1.27. Where the introduction of a reduced bearing area was incorporated into the tests, this ratio was increased to 1.42. The prototype closure design was finally fixed at 1.61. The penetration geometry has remained substantially unchanged.

Prestress was applied by a wire winding machine and consisted of close pitched windings of 0.94 mm (0.036 inch) diameter wire.

For active restraint, prestress was applied to give a mean stress on the cross section of 6.2 N/mm^2. This was achieved by one layer of wire approximately 165 turns wound at 65% of the ultimate tensile strength of the wire (U.T.S.) and anchored by pins set into the concrete.

The quantity of passive restraint required was estimated from the author's previous work on shear(3). In general, two layers of 165 turns were applied, with a limited examination on specimens with one layer. A nominal

tension only was applied to maintain uniform wire lay; this was equivalent to about 4% of the U.T.S. of the wire.

Load to simulate the gas pressure was applied to the specimen via. heavy steel circular plattens of the diameters indicated in Fig. 8, the largest being equivalent to the total area which would be pressurised in the prototype. The reaction was taken by annular bearing rings.

An hydraulic system was also used with some of the models and consisted of a rubber platten operated by a pressurised oil filled diaphragm such that a uniform pressure was applied to the gas face of the model closure.

5.2.2. General Behaviour

The following are general comments on the behaviour of the models:

(a) The specimens initially behaved elastically in flexure until sufficient over pressure was applied to overcome the prestress compression and/or tensile strength of the concrete at the free face. (Fig. 9.)

(b) Radial dilations indicated that there was a substantial reserve of strain capacity in either active or passive prestress when shear failure occurred.

(c) Flexural cracks developed at the free face and the disposition was governed by the major penetrations which act as stress raisers. The elements so formed were held in equilibrium by the elastic external restraint and the high compressive stress state developed in the uncracked concrete adjacent to the gas face.

(d) As the closure continued to flex elastoplastically, the vertical shear stresses within the concrete increased. At the same time the shear capacity of the uncracked concrete at the gas face was significantly increased by the high lateral compressive stresses developed in this region.

(e) The shear strength was finally exceeded in the ligament between adjacent penetrations where this pitch-point has significantly concentrated the shear stresses.

(f) In the majority of the tests the mode of failure was by vertical shearing of the concrete along a plane formed by the pitch circle of the outer ring of penetrations. (Fig. 10.) Initial development of this plane, indicated by a rapid increase in the rate of vertical deflection did not occur in passively prestressed specimens until pressures above three times design was attained. In specimens having active prestress, this pressure was in excess of six times the design value.

(g) The use of polytetrafluorethylene in some of the tests only reduced the stresses by about 7% in the case of prestressed specimens.

(h) In the case of unlined penetrations the strength was reduced by about 23%

5.3. 1/3rd Scale Models

5.3.1. Test Programme and Procedure

Four 1/3rd scale models were tested using the arrangement shown in Fig. 11. The models simulated the prototype design as closely as was

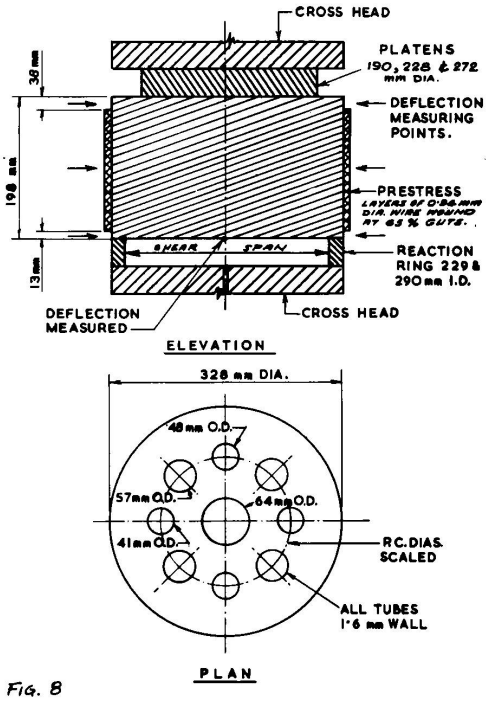

FIG. 8

TEST ARRANGEMENT FOR 1/10TH SCALE BOILER CLOSURE.

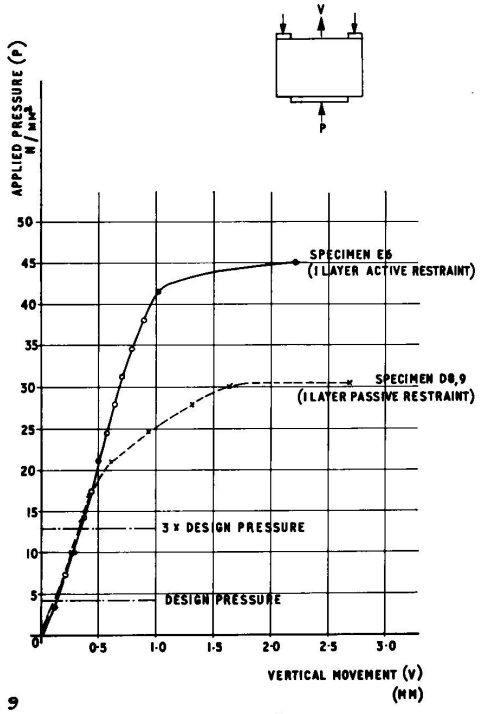

FIG. 9

SHEAR DEFORMATION CURVES FOR $\frac{1}{10}$TH SCALE MODEL SECONDARY CLOSURES

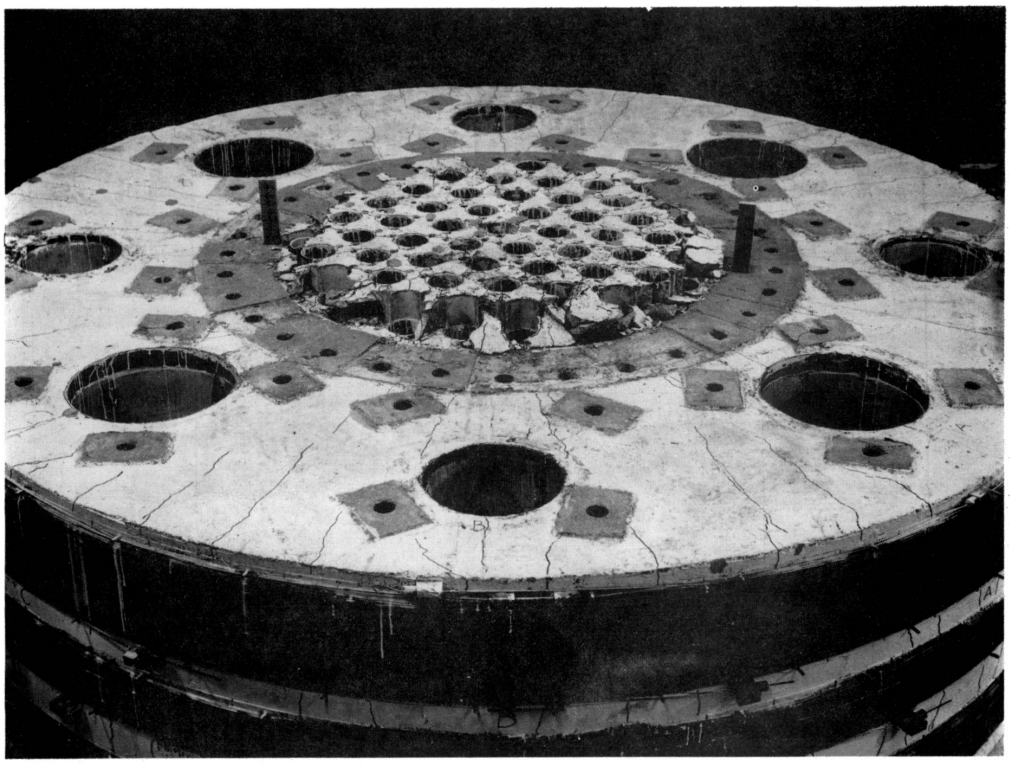

FIG. 7 Failure of Perforated Cap (Model M3)

FIG. 5

CROSS SECTION OF END SLAB MODELS SHOWING TEST ARRANGEMENT

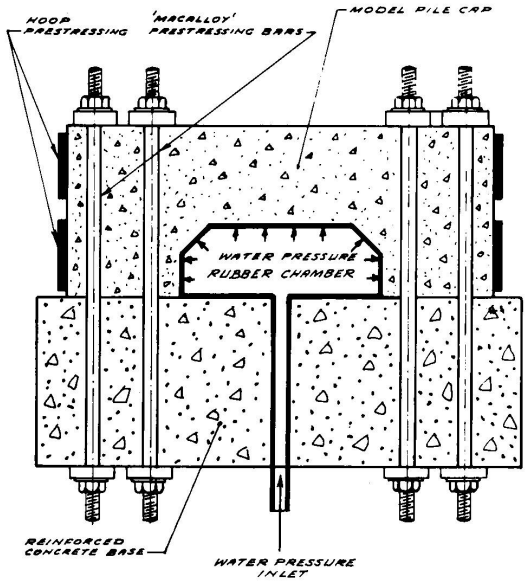

FIG. 6

FLEXURAL BEHAVIOUR OF END SLAB

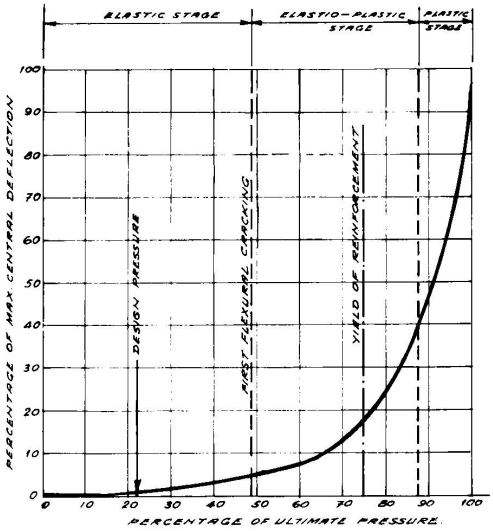

experimentally practicable. The test programme described in Table 2 was designed to examine the short and long term behaviour of the closure.

TABLE 2 1/3rd Scale Models - Test Programme

Model	Prestress	Loading
M1	Passive	Short term up to 6 times design pressure at ambient temperature.
M2	Active	Short term up to 6.5 times design pressure at ambient temperature.
M3	Active & Passive	(i) Sustained 50°C and 7 N/mm^2 pressure for a period of 9 months. (ii) Overload test.
M4	Active &	(i) 54 temperature cycle between 24°C and 50°C. (ii) 10 temperature cycle combined with pressure cycle between 0 and 7 N/mm^2. (iii) 10 pressure cycle and ambient temperature. (iv) Overload test.

The prestress consisted of close pitched windings of 0.94 mm diameter wire, one wire representing almost exactly the scaled area of one prototype 2.6 mm (0.104 inch) diameter wire. Each layer of wire was individually anchored.

The passive restraint consisted of six layers and, when combined with active prestress, it was wound at a nominal tension designed to compensate for creep, shrinkage and elastic shortening. In the test in which passive prestress was examined in isolation, windings were at a tension of approximately 5% of the wire U.T.S. to facilitate uniformity of lag.

The gas pressure was simulated by water pressure applied at the lower surface of the model closure through a contained reinforced rubber pressure chamber. Pressure was applied over an area equivalent to that lying within the inner sealing ring of the prototype.

The reaction was taken via. the bolt system to a structural steel crosshead restrained by 42 No. 32 mm Macalloy bars.

In the prototype, the main source of heat occurs at the gas face, and this was simulated in the models by resistance elements cast into the concrete 50 mm from the pressurised face. Each element was duplicated.

The rate of temperature rise to 50°C did not exceed 5°C per hour to avoid thermal shock. Under temperature cycling, the models were allowed to cool naturally along the diameter and the adjacent sides. Strains were measured in the concrete and on a number of selected penetrations.

5.3.2. Results and Behaviour of Models

The following are very brief comments obtained from the test results:

(a) Models M1 and M2 withstood maximum pressures of 26 and 29.5 N/mm^2 without failure which gave a load factor of 5.90 and 6.55 respectively.

(b) At the maximum pressure, both M1 and M2 were tending towards the anticipated shear plug failure.

(c) At pressures varied between 5.5 and 9.5 N/mm^2 fine radial cracks were observed in three of the four ligaments between the main and superheater penetrations of models M1 and M2. These cracks (Fig. 12) were fully developed, but with a maximum crack width of 0.25 mm, at pressures of 13 and 16 N/mm^2 for models M1 and M2 respectively. All cracks, however, appeared to exhibit complete recovery on depressurisation.

(d) At five times the design pressure, the central deflections for models M1 and M2 were only 0.036% and 0.18% respectively of the depth of the models. (Fig. 13.)

(e) Both M3 and M4 were shown to be structurally stable after sustaining the severe overload conditions for the tested period. Up to four times the design pressure the central deflections of these models were very similar to those of M2. (Fig. 14.)

(f) The rate of creep development for models M3 and M4 was shown to be substantially that predicted from control specimens(5). (Fig. 15.)

(g) In the final tests, both M3 and M4 withstood pressures of six times the design pressure without failure. Subsequent sectioning revealed negligible fracture, and both models were considered capable of withstanding higher overload pressures.

(h) Model behaviour was compared with that predicted by the axi-symmetric analysis. Under the simplest loading conditions, e.g. hoop prestress only, measured hoop strains in zones of mass concrete were within 4% of the predicted values.

5.4. Comparison Between 1/3rd and 1/10th Scale Model Behaviour

Small scale models were used to optimize the main parameters for the final design of the boiler closure. These parameters were then incorporated in the 1/3rd scale models. Direct comparison between the behaviour of the two scales of models is limited by variations in some of the key factors, e.g. depth, loading and boundary conditions and material properties. However, supplementary tests on the 1/10th scale models showed that none of these variations influenced the ultimate strength by more than 15%. Thus, if these factors are taken into consideration, a realistic comparison is possible.

6. CONCLUSIONS

6.1. The paper describes the behaviour of structural components in which stresses are utilised, to greatly enhance the shear strength of deep concrete sections.

6.2. Two examples are given of the use of model analysis as a design tool in determining the long term and ultimate load behaviour of complex structural components. This technique will continue to be a basis for designing such structures until our fundamental knowledge of concrete behaviour under multiaxial stress states is more rigorously defined.

Fig. 13 - COMPARISON OF CENTRAL VERTICAL DEFLECTIONS FOR 1/10 & 1/3 SCALE CLOSURE MODELS.

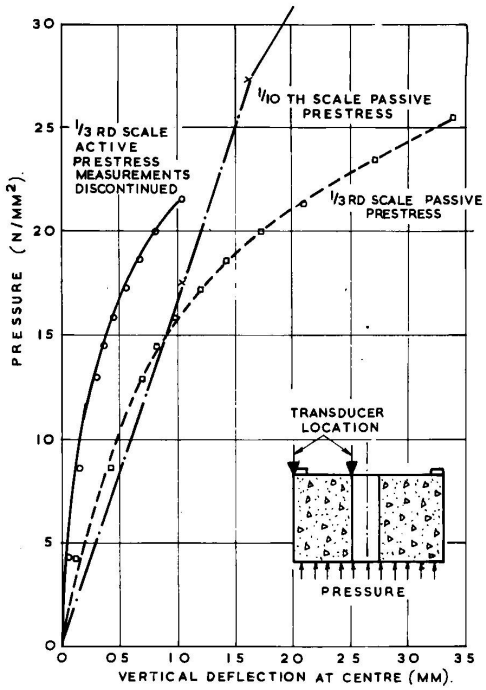

Fig. 14 - ONE THIRD SCALE CLOSURE MODELS M2, M3, M4. CENTRAL VERTICAL DEFLECTION IN FINAL PRESSURE TESTS.

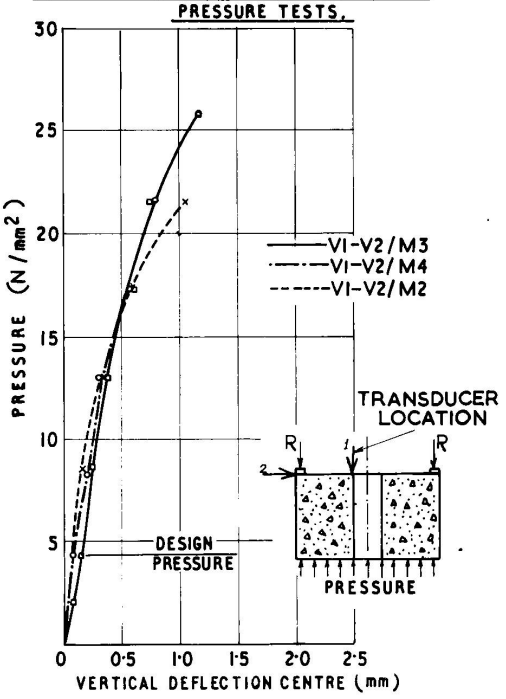

MODEL M3 GAS FACE

THEORETICAL & MEASURED HOOP STRAINS

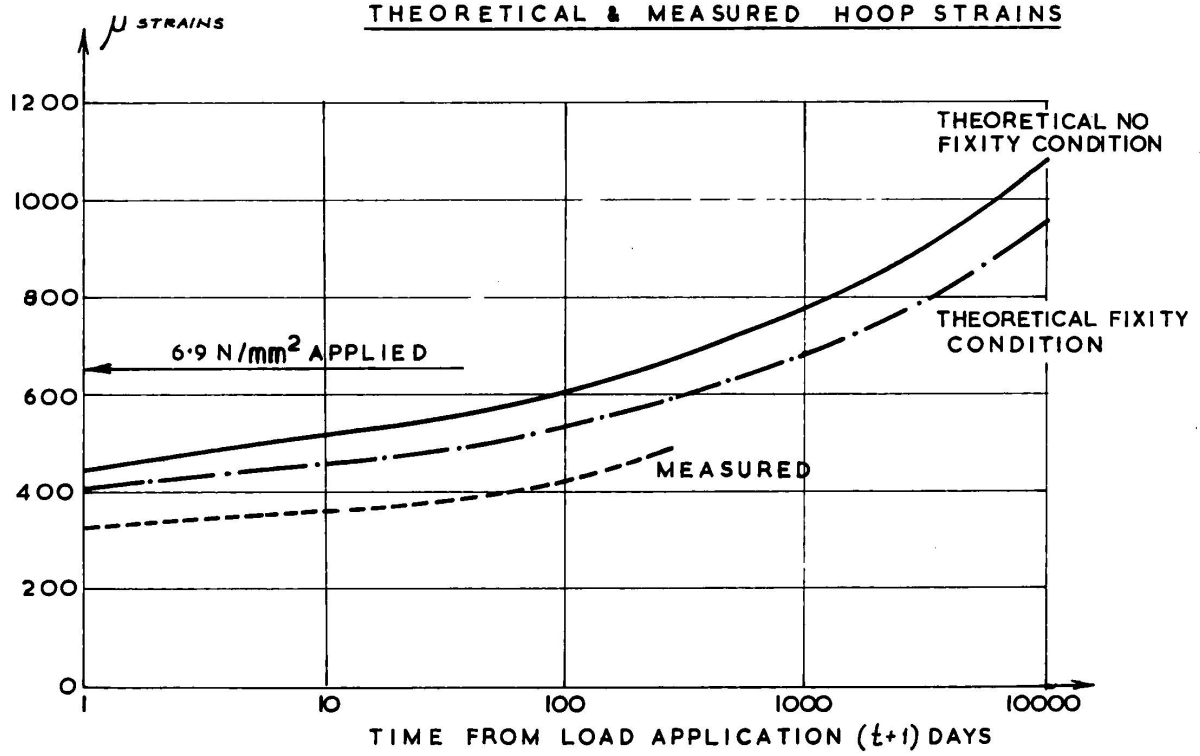

FIG. 15

7. REFERENCES

(1) Burrow, R.E.D. and Williams, A.J. "Hartlepool AGR Reactor Pressure Vessel" Nuclear Engineering International, Nov. 1969.

(2) Langan, D. and Garas, F.K. "Behaviour of End Slabs in Cylindrical Prestressed Concrete Pressure Vessels" Proceedings of the First International Conference on Structural Mechanics in Reactor Technology, Berlin, 1972.

(3) Langan, D. and Garas, F.K. "The Failure of Concrete Under the Combined Action of High Shearing Forces and Biaxial Restraint" International Conference on Structures, Solid Mechanics and Engineering Design in Civil Engineering Materials, Southampton, April 1969.

(4) Fenwick, R.C. and Paulay Thomas, "Mechanism of Shear Resistance of Concrete Beams" Journal of the Structural Division, Proceedings of the American Society of Civil Engineers, Oct. 1968.

(5) Browne, R.D. and Blundell, R. "The Behaviour of Concrete in Prestressed Concrete Pressure Vessels" Proceedings of the First International Conference on Structural Mechanics in Reactor Technology, Berlin 1972.

ACKNOWLEDGEMENT

The author wishes to thank Taylor Woodrow Construction Limited for permission to publish this paper.

SUMMARY

The paper describes the mechanism of the shear resistance in restrained concrete elements. Details are given of two experimental investigations where shear stresses were dominant. In the first, the general behaviour of 23 end slab models is summarised and an empirical formula is introduced which was found to fit most of the available data on this subject. Secondly, the paper describes model tests undertaken to aid the design of a boiler closure. Sixty 1/10 scale models were tested to give a quick assessment of the influence of main structural parameters. These were followed by short and long term studies on four realistic 1/3 scale models to confirm the final design. Details of the investigation are given together with the general behaviour of the models during various stages of testing.

RESUME

Le rapport décrit le méchanisme de résistance au cisaillement des éléments contenus en béton. On donne des détails sur deux études expérimentales dans lesquelles les efforts de cisaillement étaient dominants. D' abord on résume le comportement général de 23 maquettes de dalles de fermeture et on présente une relation empirique qui s' est démontrée en accordance avec la plus part des résultats expérimentaux à disposition au sujet.

Ensuite le rapport décrit des essais sur maquettes réalisés afin d' aider le projet de fermeture de chaudière. On a essayer 60 maquettes en échel le 1 : 10 afin d' obtenir une évaluation rapide de l' influence des paramètres structuraux plus importants. Ensuite on a réalisé des études de longue et courte durée sur 4 maquettes réalistiques en échelle 1 : 3 pour confirmer le projet final. On donne des détails sur les études réalisées et sur le comportement des maquettes durant les différentes phases d' essai.

ZUSAMMENFASSUNG

Der Artikel beschreibt den Mechanismus des Schnittwiderstandes in Spannbeton-Komponenten und schildert die Einzelheiten von zwei Versuchsstudien, in denen Schnittbelastungen vorherrschend waren. Zuerst wird in Kürze das Verhalten von 23 Betonsohlen-Modellen beschrieben und eine empirische Formel eingeführt, die auf die meisten, für diesen Fall zur Verfügung stehenden Resultate passt.

Es folgt eine Beschreibung der Tests an Modellen, die eigens dafür angefertigt wurden, um einen Boilerverschluss zu entwerfen. Sechzig Modelle im Mass-Stab 1 : 60 wurden getestet, um schnell den Einfluss der wichtigsten Struktur-Parameter bewerten zu können. Darauf folgen kurz- und langfristige Studien an vier realistischen Modellen im Mass-Stab 1 : 3, um die Gültigkeit des endgültigen Modells zu bestätigen. Die durchgeführten Studien und das allgemeine Verhalten der Modelle während der verschiedenen Test-Phasen werden ausführlich beschrieben.

IABSE
AIPC
IVBH

SEMINAR on:
«CONCRETE STRUCTURES SUBJECTED TO TRIAXIAL STRESSES»
17th-19th MAY, 1974 - ISMES - BERGAMO (ITALY)

The Effects of Localised Steady and Cyclic Over-Heating in the Oldbury Concrete Pressure Vessels

L'influence de surèchauffement localisé tant permanent que cyclique des caissons en béton précontraint de la centrale nucléaire d'Oldbury

Die Auswirkungen stetiger und periodischer örtlicher Überhitzung in den Spannbetondruckbehältern von Oldbury

I.W. HORNBY B. Sc. (Eng.), C. Eng., M.I.C.E.
Central Electricity Research Laboratories, Leatherhead, U.K.

G.D.T. CARMICHAEL B.Sc. PhD., C. Eng., M. I. Mech. E.
Berkely Nuclear Laboratories, Berkeley, U.K.

J. IRVING B. Sc.
Generation Development and Construction Division, Cheltenham, U.K.

1. INTRODUCTION

The nuclear power programme in Great Britain has gathered considerable momentum since its start in the mid 50's. Nuclear stations with a total capacity of 5300 MW(e) are now complete; stations of a further 6600 MW(e) capacity are under construction. Of this 11900 MW(e), 70%, is from stations utilising prestressed concrete pressure vessels (PCPVs) to contain the primary gas circuit.

The first station in Great Britain to use a concrete vessel was at Oldbury-on-Severn, which has been operational since 1967. The two vessels at this station, in common with all subsequent British designed vessels, are lined internally with a mild steel membrane. This liner is tied to the concrete with closely pitched hook bolts or studs. The liner and concrete temperatures are controlled by a network of cooling pipes at or near the liner/concrete interface together with insulation on the liner/gas interface. These measures are designed to limit the concrete temperatures to less than 65°C with a reactor gas temperature in excess of 350°C.

During the commissioning tests of the Oldbury vessels, several localized areas of the steel liner reached temperatures higher than the design level of 65°C. In one area the thermocouples indicated a peak temperature of 180°C. The high temperature regions or 'hot-spots' were attributed to a small number of local shortcomings in the performance of the as installed thermal insulation. Consequently attempts were made to improve the insulation performance without major redesign. It was accepted that some less severe hot-spots would be likely to remain even after these improvements.

It was recognized that these hot-spots would induce high thermal stresses in the concrete and a theoretical study was made to determine the effect these stresses would have on the overall structural integrity of the vessel. This study showed that there was no cause for concern about the safety margin against failure of the vessel, but it was possible that cracking could occur in the concrete close to the liner. It was therefore considered that a practical test was necessary to demonstrate that, if cracking occurred, it would be limited in extent and the liner would remain fixed to the concrete by the retaining bolts.

Examination of the hot-spots recorded during the commissioning tests showed that the highest temperatures occurred around the upper boiler instrument penetrations. Calculations showed that the stresses and strains imposed on the liner and adjacent concrete would be more severe at these positions than at any others under the most critical loading conditions. It was therefore decided to test a full scale model of this region under conditions which were similar to those experienced in the vessel during reactor operation.

2. PRELIMINARY CALCULATIONS AND TEST PROPOSALS

The first step in designing the model was to determine the stresses occurring in the vessel. It was essential that the stress analysis should include the effects of creep of concrete since experimental evidence[1] suggested that this could have a significant effect on the behaviour of the vessel. In the method chosen[2] the effect of creep of concrete on stress in the vessel was assessed by finding the steady state stress solution[1]: the stresses found by this method are the bounding values as creep strains become large.

Stresses in the vessel at the four positions shown in Fig. 1 were compared for the six loading conditions detailed below. At two of these positions there were several hot-spots whilst, for comparison, the other two positions were in areas operating under normal conditions.

The four positions considered were:-

A Mid wall

B Upper boiler instrument penetration (hot-spot of 180°C)

C Carbon shield block (hot-spot of 90°C)

D Centre of top slab

The critical loading conditions considered (see Fig. 2) were:-

1. Before initial start-up (prestress only)

2. Half pressurised, vessel cold

3. Early operating conditions (prestress plus full pressure plus temperature).

4. Long term operating conditions (allowing for stress relaxation due to creep).

5. Shut-down after a long period of operation (vessel cold and depressurized, showing reversal of thermal stress).

6. Restart from condition 5 (vessel cold plus half pressure plus prestress).

The computed radial, hoop and vertical stress histories at the four positions are shown in Fig. 2.

It is apparent from Fig. 2 that in general there are two unavoidable critical loading conditions:-

(a) At initial start-up (loading case 3), when high compressive stresses occur.

(b) During the shut-down cycle (loading cases 5 and 6), when high tensile stresses occur.

The worst tensions actually occur when repressurising after a shut-down (loading case 6). The results in Fig. 2 show that under all loading conditions the upper boiler instrument penetration (position B), sustains the highest stresses. For this reason the model was chosen to simulate this position with a hot-spot at approximately 180°C. This simulation would also show the effects of stress concentration due to the penetration. The analysis of the vessel showed that the highest stresses occur in the hoop and vertical directions, the maxima being very similar in these two directions. The choice of a model with equi-biaxial stresses approximately equal to these stresses was therefore justifiable.

The actual model chosen is illustrated diagrammatically in Fig. 3 and is described later in the paper. In order to verify further that the model was representative a separate stress analysis was undertaken. The resulting stress profiles at the simulated penetration were compared with those computed for the vessel during a typical reactor start-up/shut-down cycle. The calculations showed that a steep stress gradient behind the liner is caused by the temperature gradient between the liner and the cooling water pipes which are positioned 100 mm into the concrete. The tensile stresses predicted under loading case 6 greatly exceed the tensile strength of the concrete and cracking would be expected. The results obtained from this preliminary comparison showed that reproduction of the appropriate prestress and temperature pattern in the model would produce a similar stress and strain situation to that in the vessel.

It was proposed that the main body of the model would be heated to a temperature distribution simulating the operational thermal conditions at the upper boiler instrument penetration of the vessel and finally cooled to simulate loading case 6. The expected variation in the overall stress gradient through the vessel wall due to creep relaxation during the operational period would be simulated in the model by removing some of the prestressing as the test proceeded. It was considered unnecessary to simulate the effect of gas pressure normal to the liner since no contribution to any mechanism of failure could be envisaged from this source, the stresses exerted normal to the surface being negligible in

comparison to those parallel to the liner. At the end of the test an examination of the liner and adjacent concrete would be made. Cores would be taken to obtain an indication of the condition of the concrete, and dye injected into the concrete to indicate the extent of cracking.

The opportunity would be taken to include instruments which would measure significant phenomena such as structural strain, temperature, vapour pressure and moisture content of the concrete. The formation of cracks in the concrete would also be monitored.

3. DESCRIPTION OF MODEL

The model is shown diagrammatically in Fig. 3 and Fig. 4, shows the model before concreting. It consisted of a cylindrical disc of concrete 365.8 cm diameter and 152.4 cm thick, mounted with its central axis vertical. The bottom of the concrete was faced with a 12.7 mm thick steel liner, attached to the concrete with 38.1 cm long hook bolts at 30.5 cm equipitch. Fins 10.2 cm high were welded at right angles to the liner at 30.5 cm centres on which were mounted the pairs of cooling water pipes. These ran from north to south across the disc, except for the central pair which curved round the east side of the central penetration.

The boiler instrument penetration was 'sleeve' reinforced with 27.3 cm O.D. steel tube, 14.3 mm thick, thickened locally where it was welded to the liner. The tube was water cooled by two spirally wound pipes welded to its outer surface.

The details of the liner, cooling water system and penetration were similar to those in the Oldbury vessel, except that the large radius curve of the vessel wall was omitted.

The concrete was to the same specification as that used in the Oldbury pressure vessel, the aggregate being obtained from the same pits. Details of the mix are given in Appendix I. Casting was undertaken in two lifts on successive days. After curing, the sides and top of the model were coated with Araldite resin X83/44 to minimise moisture loss. The moisture condition of the model therefore simulated the likely moisture condition of the vessel.

The region of the model local to the hot-spot was subdivided into four quadrants by moisture barriers 10 cm high, sealed to the liner. By this means it was hoped to prevent the dye injected into one quadrant affecting another quadrant.

After curing for 28 days the model was prestressed by wire winding with 2.6 mm diameter high tensile steel wire. The total initial force in the wire over the surface was 13.0 MN, giving an average radial stress in the concrete of 4.5 N/mm^2 after allowing for losses. This value had been computed as being representative of vessel conditions. Part of the prestress over the bottom 30.5 cm was wound in three predetermined bands which could be removed when required to simulate stress redistribution due to creep strain. The first of these three bands was removed 43 hrs after the start of the first test, the remaining two bands 15 days later. This represented a total reduction of prestress over the bottom area of approximately 49%.

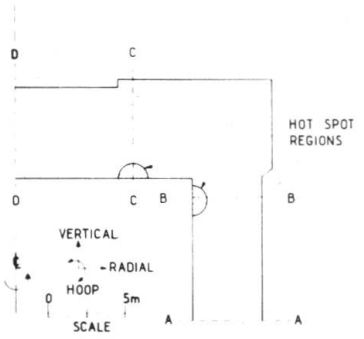

VERTICAL SECTION THROUGH TOP HALF OF VESSEL

KEY

A-A	MID-WALL
B-B	UPPER BOILER INSTRUMENT PENETRATION
C-C	CARBON SHIELD BLOCK
D-D	CENTRE OF TOP SLAB

FIG. 1. OLDBURY VESSEL – SECTIONS CONSIDERED IN THE PRELIMINARY CALCULATIONS

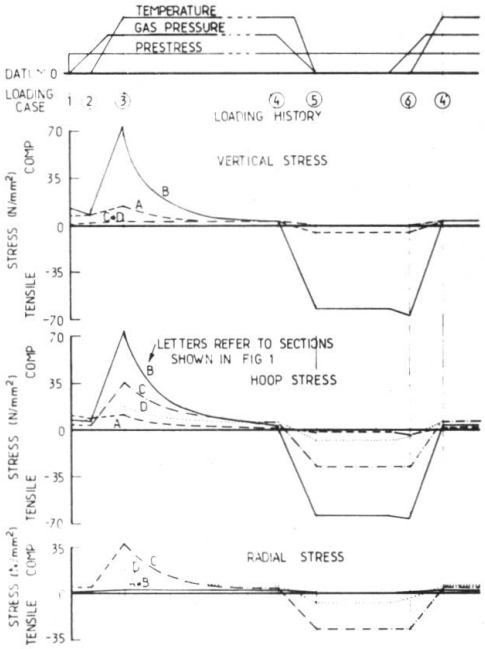

FIG 2 OLDBURY VESSEL - APPROXIMATE STRESS HISTORIES AT THE LINER FACE OF VESSEL SECTIONS A-A, B-B, C-C, AND D-D SHOWN IN FIG 1

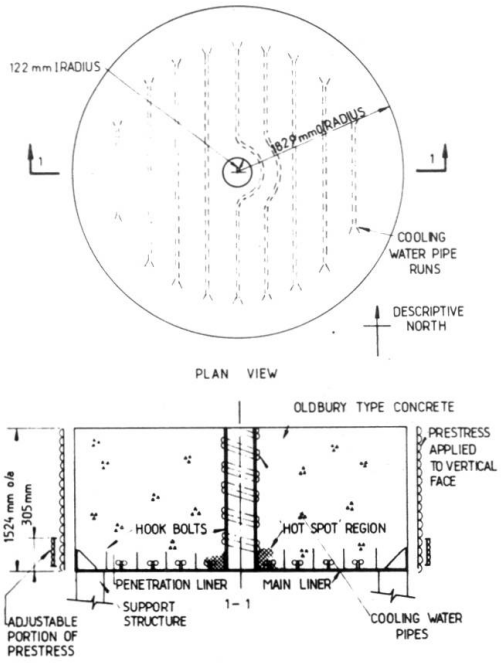

FIG. 3 MODEL – GENERAL ARRANGEMENT

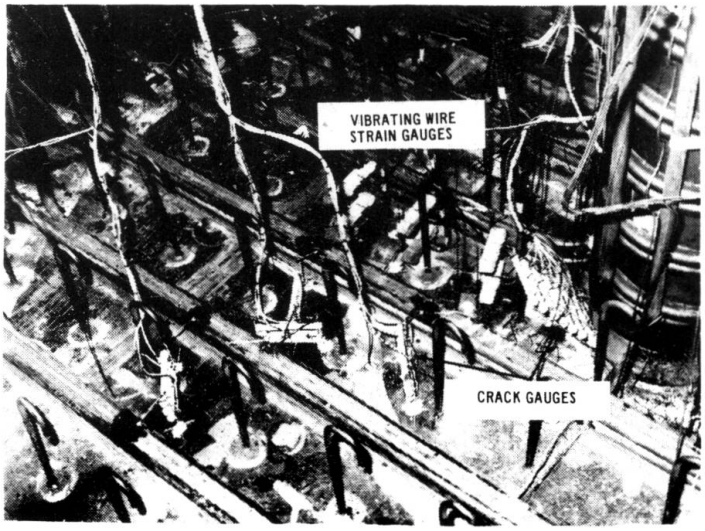

FIG. 4 VIEW OF MODEL DURING CONSTRUCTION, SHOWING INSTRUMENTATION

Heat was applied to the liner and penetration using 'Pyrotenax' electric heating cables backed with insulation. The heaters were arranged in zones for each of which temperature controls were provided.

Facilities were provided to supply cooling water at $20^{o}C \pm 1^{o}C$ at a velocity of 0.5 m/s through the cooling pipes.

4. INSTRUMENTATION

Eighteen 'Perivale' type 641 vibrating wire strain gauges were positioned as shown in Fig. 5. The gauges were used to measure the strains occurring in the concrete during the tests.

155 Chrome-Alumel thermocouples were fitted, 23 of which were used to control the heaters.

Seventy-eight pairs of crack gauges were fitted. These were specially developed for the experiment at C.E.R.L.,[3] and were designed to indicate the onset of cracking. The gauges respond both to the opening and closing of cracks.

Twelve C.E.R.L. moisture gauges, positioned as shown in Fig. 5 were used to determine the moisture gradients in the concrete during the tests.

Twelve pressure gauges were fitted to measure the vapour pressure during heating at the liner/concrete interface and the cooling pipe/concrete interfaces. Three gauges were also positioned to measure the vapour pressure at the boiler penetration/concrete interface.

Injection nipples were positioned on the liner and on pipes leading to the cooling pipe level to facilitate the injection of dye after each test. This technique, developed specially for the experiment, enabled the position of cracks to be determined from cores taken after each test. The presence or absence of dye in cracks would indicate whether these had occurred before or after the coring operation.

5. TEST PROCEDURE

In the first test a thermal profile was established which was similar to that at the upper boiler instrument penetration of the Oldbury vessel R.1. This profile with a maximum temperature, at the hot-spot, of $172^{o}C$ was maintained for three months. The second test consisted of fifteen thermal cycles each of 48 hours duration between 30^{o} and $178^{o}C$. The temperature range of each cycle was controlled to correspond approximately to the range of temperatures that the hot-spot region of the liner would be subjected to, during the reactor start-up/shut-down cycle. The third test was a further over heating test but with the hot-spot maintained at a maximum temperature of $300^{o}C$ for 28 days.

After each test an examination was made of the model. Blue dye was injected into one quadrant of the model at a number of points, a maximum pressure of 0.7 N/mm^2 being maintained at the pump during this injection. Some of the dye injection nipples led to the liner/concrete interface while others led through the cooling pipe fins directly to the cooling pipe/concrete interface.

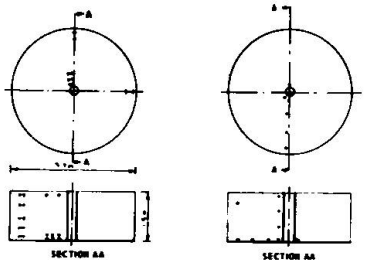

FIG. 5 VIBRATING WIRE STRAIN GAUGE (LEFT) AND MOISTURE GAUGE POSITIONS

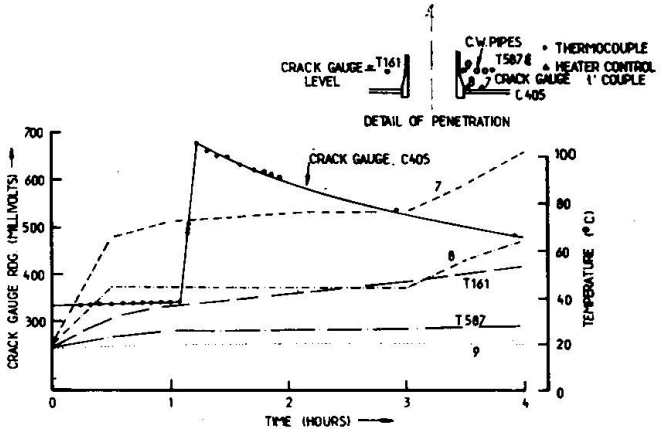

FIG 6 TEST 1 - CRACK GAUGE READINGS IN FIRST 4 HOURS OF TEST

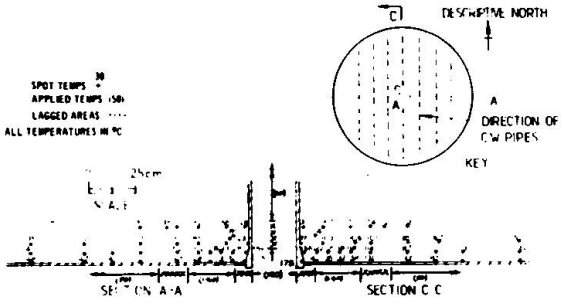

FIG 7 TEST 2 - RECORDED TEMPERATURES AT 24 HOURS AFTER START OF 1st CYCLE

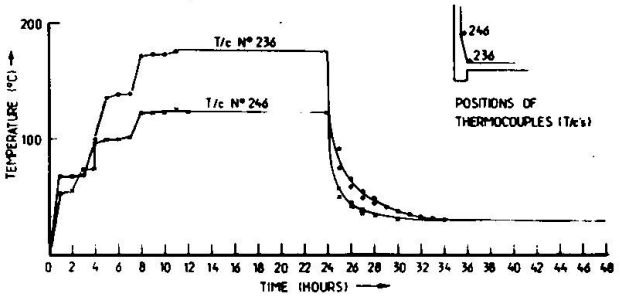

FIG 8 TEST 2- RECORDED TEMPERATURE VARIATIONS AT HOT-SPOT DURING 1st CYCLE

Concrete coring followed, from which a study of the dyed cracked surfaces could be made. Certain cores were also used to determine the compressive and tensile strength of the concrete.

Measurements to determine the ultrasonic pulse velocity between adjacent core holes and between the central penetration and core holes were made at different depths. These measurements were compared with ones obtained from control specimens.

6. RESULTS

Test 1

Results from the first test have been reported elsewhere[4] but, as they have a bearing on the vessel behaviour during the subsequent tests, they are briefly reiterated in this paper.

One pair of crack gauges showed a significant change in reading 65 minutes after the start of the first test. A plot of one of these gauge readings is shown in Fig. 6. The readings indicated the formation of a crack wider than 0.5 mm which decreased to zero as the test proceeded.

The coring and dye injection indicated the presence of a horizontal crack extending to approximately 500 mm radius at a level of 110 mm from the liner - i.e. cooling water pipe level. The cores also showed dye penetration on the cooling pipe-fin/concrete interface and in many cases the liner/concrete interface.

Test 2

The temperature distribution applied to the liner is shown in Fig. 7, which also shows the maximum temperatures recorded during the first cycle. The temperature variation at two positions in the model during one 48 hours cycle is shown in Fig. 8.

The strain variation at two gauge positions, at 24 hour intervals, during this test are shown in Fig. 9.

None of the crack gauges indicated cracking. Those gauges which had changed during the transient heating of test 1 showed no change in test 2.

The coring checked the limits of the original horizontal crack and found that these limits remained unchanged. Two cores had fine vertical hair cracks on their bottom face penetrating up to a depth of 50 mm. The cracks were random and not interconnected.

Test 3

Steady state temperatures recorded by the thermocouples are shown in Fig. 10.

The strain changes occurring in the hoop gauges adjacent to the central penetration are shown in Figs. 11 and 12. These figures also show the total strain history of these two gauges during the three tests.

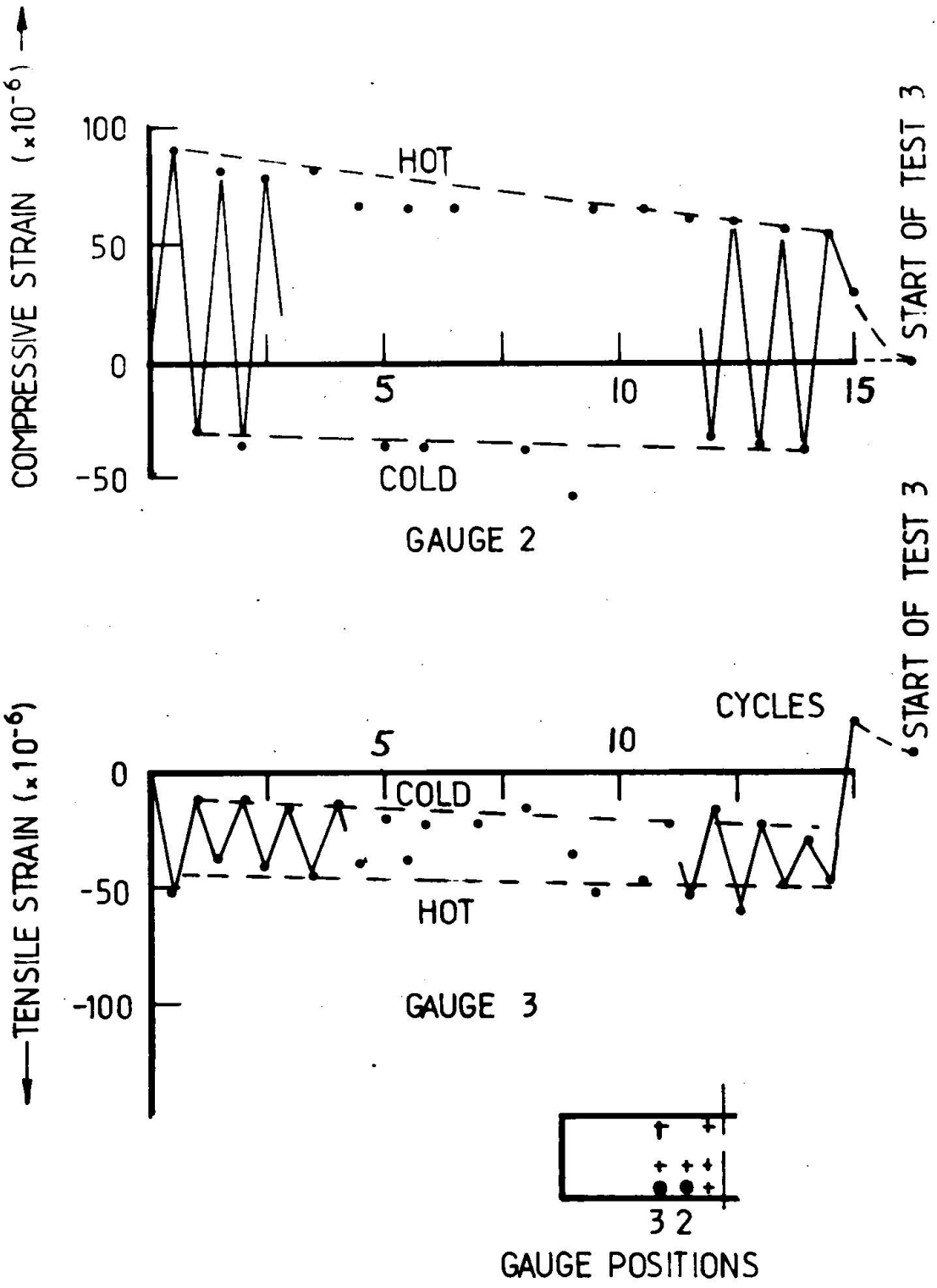

FIG.9 TEST 2 - RECORDED STRAINS AT GAUGES 2 AND 3 AT 24 HOUR INTERVALS

As in test 2, no further cracking was indicated by the crack gauges, and coring again confirmed that the extent of the original horizontal crack remained unchanged.

7. DISCUSSION

The cores taken during the first test included ones which penetrated the central pair of cooling pipes (see Fig. 13 and position of core 1/3). For the second test these pipes were isolated and consequently the concrete temperatures local to the central penetration were higher than normal. The conditions imposed on the concrete in this test were therefore more arduous than those experienced in the Oldbury vessel. (See Section AA of Fig. 7).

Very little strain change was recorded between the beginning and end of the test. Most gauges showed a trend in the tensile direction the maximum being 35×10^{-6} strain units. Results from two of the gauges in the zone of the crack (Nos 2 and 3) are shown in Fig. 9 and show no residual strain soon after the end of the test. These plots are again illustrated in Figs. 11 and 12. An interesting change occurred at the position of gauge 2. The thermal strain became compressive during the heating up part of the cycle whereas it was tensile during test 1 (Fig. 11). It is thought that this anomalous behaviour was due to the change of temperature distribution resulting from the absence of cooling water flow in the pipes mentioned above.

The cores taken after the test confirm the presence of the horizontal crack at a similar level to that found in test 1. This crack is clearly shown in Fig. 14. The extent of the crack in the NE quadrant after test 2 was similar to that in the SE quadrant in test 1. It is therefore considered that the original crack had not extended as a result of the thermal cycling. The presence of the hairline cracks in cores 2/3 and 2/5 is thought to be due to shrinkage induced by moisture movement.

The results of this test can be applied to the Oldbury vessel since temperatures will change in a similar but less severe manner during the reactor start-up and shut-down cycle. In the actual vessel, the hot periods will be of longer duration than those experienced by the model and this may lead to differences in behaviour due to creep strain. It has been observed[5], however, that the Oldbury vessel is not subject to large changes in creep strain during reactor operation. It can, therefore, be concluded that cracks which occur in the upper boiler instrument penetration of the Oldbury vessel and which are of a similar kind to those found in test 1 will not propagate further due to reactor cycling.

During test 3 the maximum temperature applied to the model was $305^{\circ}C$ at the junction of the main liner and penetration. As in test 2, because of the isolated central cooling pipes the high temperature zone extends more deeply into the concrete than would occur with full cooling capacity. This test, therefore, simulates not only the effect of a high temperature hot-spot but also failure of the cooling water supply local to the hot-spot.

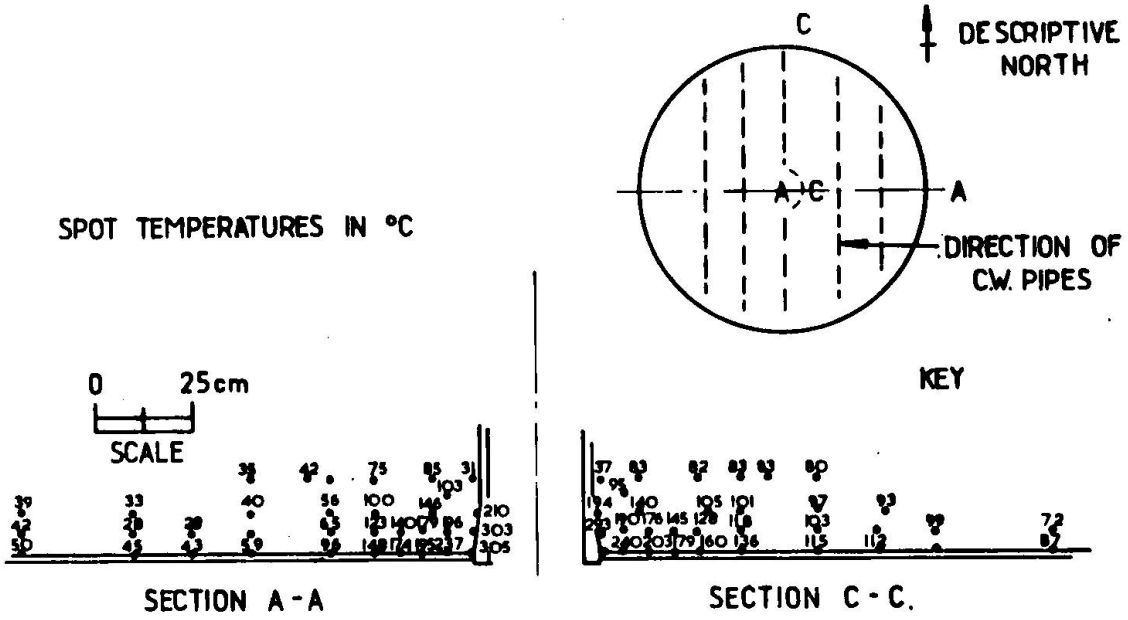

FIG. 10 TEST 3 TEMPERATURES IN THE MODEL AVERAGED FROM VALUES AT DAYS 21, 22, 24, AND 28.

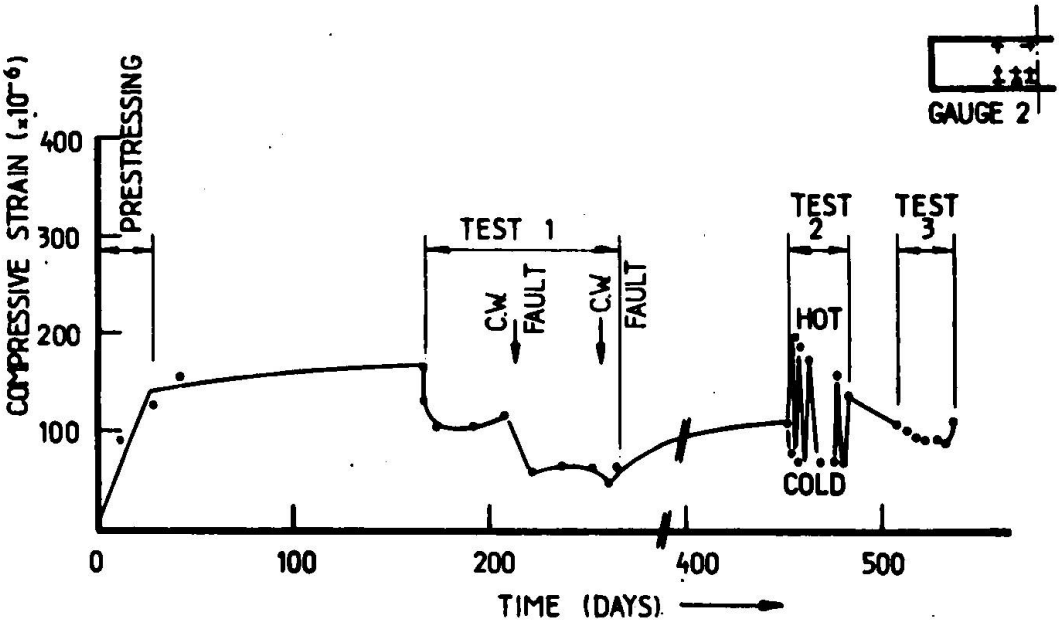

FIG.11 RECORDED STRAINS AT GAUGE 2 OVER COMPLETE HISTORY OF MODEL.

The strains which occurred in test 3 show little change during the heated period. It can be seen from Figs. 11 and 12 that there was little change in strain between the end of test 1 and the end of test 3. There was, therefore, little additional permanent deformation in the model caused by either thermal cycling or over-heating.

The cores taken after this test confirmed the presence of the horizontal crack found in the previous tests. The extent of the crack in the NW and SW quadrants after test 3 was similar to that found in the other quadrants. It is therefore considered that the original crack had not extended as a result of the high temperature test.

It is to be expected that a similar temperature excursion in the upper boiler instrument penetration area of the Oldbury vessel, even with local cooling water failure, would not result in damage to either the liner or the concrete.

8. CONCLUSIONS

The cracks formed during the first transient heating of the model were not increased by thermal cycling between 30°C and 178°C.

Maintaining the hot-spot at 305°C for 28 days did not increase the original cracking.

It can be deduced from the model results that cracking is likely to have occurred at the upper boiler instrument penetration of the Oldbury vessel. The cracking will be limited to a depth of 100 mm from the liner which will remain fixed to the concrete by the retaining hook bolts. This cracking will be unlikely to extend during reactor start-ups and shut-downs. Hot-spot temperatures of 300°C could be tolerated at the upper boiler instrument penetration, even with blockage of local cooling water pipes.

9. ACKNOWLEDGEMENT

This paper is published by permission of the Central Electricity Generating Board.

10. REFERENCES

1. Ross, A.D., England, G.L. and Suan, R.H.
Prestressed Concrete Beams under Sustained Temperature Crossfall.
Mag. Conc. Res., 1965, 17, Sept. 117-126.

2. Lewis, D.J. and Irving, J.
Operational Stresses in Nuclear Prestressed Concrete Pressure Vessels.
Civ. Eng. and Pub. Wks. Rev., 1968, 63, Part 1, 673-676, Part 2, 793-796.

3. Hornby, I.W. and Wilson, J.M.
Instrumentation Techniques in Large Scale Concrete Models.
Proc. Conf. on Model Techniques for PCPVs, BNES, London 1969, p3-6.

4. Irving, J., Carmichael, G.D.T. and Hornby, I.W.
A Full-Scale Model Test of Hotspots in the PCPVs of the Oldbury Nuclear Power Station (to be published).

5. Carmichael, G.D.T. and Hornby, I.W.
The Strain Behaviour of Concrete in PCPVs.
Mag. Conc. Res., 1973, 25, March 5-16.

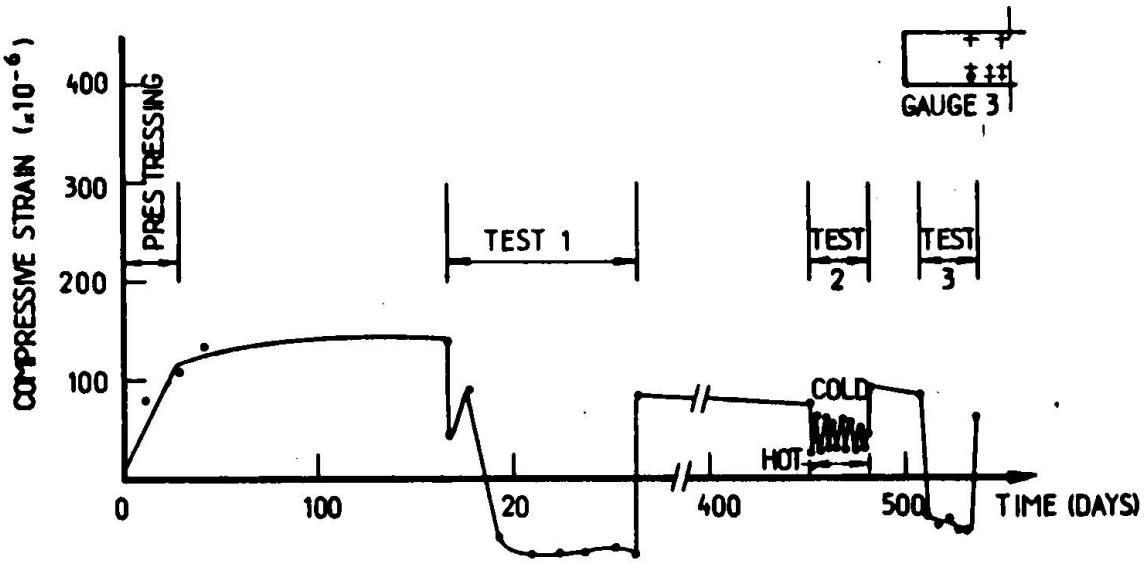

FIG 12 RECORDED STRAINS AT GAUGE 3 OVER COMPLETE HISTORY OF MODEL

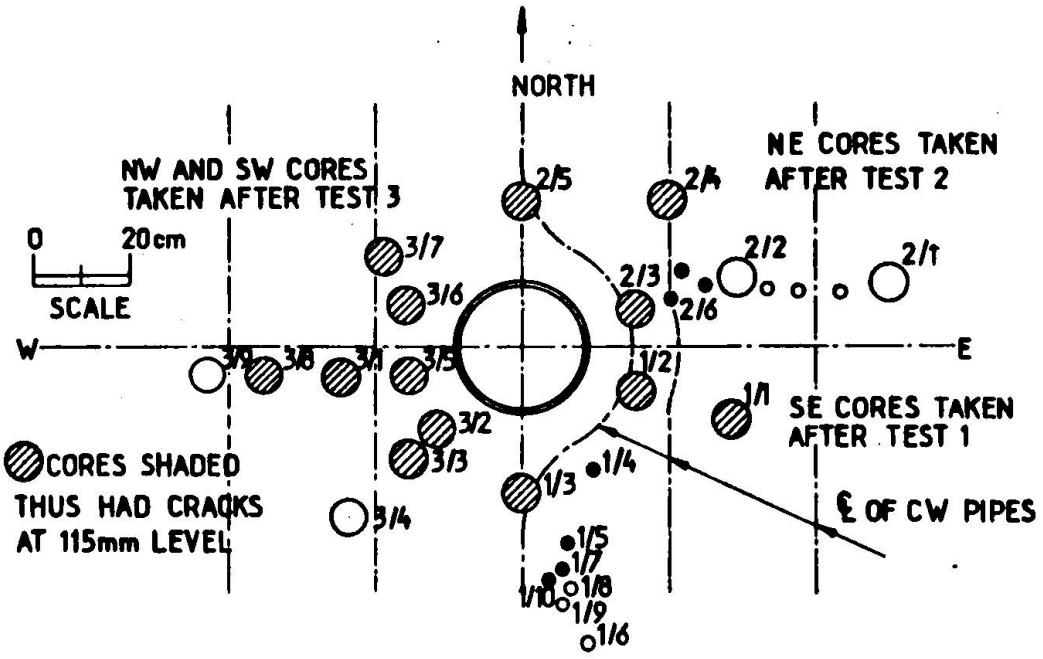

FIG.13 POSITIONS OF CORES TAKEN FROM MODEL

APPENDIX I - MATERIALS

1. DETAILS OF CONCRETE MIX

Design of mix:-

1:5.1/0.47, 19 mm maximum size aggregate
Minimum 28 day strength 41.4 N/mm^2
Target average 49.6 N/mm^2
Standard deviation 4.0 N/mm^2

Mix used:-

1:2.0:3.1/0.47 w/c
Sulfacrete cement
Ball mill put sand in zone 2 of BS 882
'Cromhall' limestone in two grades - 19 to 9.5 mm and 9.5 to 4.75 mm
½% Sika Plastocrete

2. MATERIAL PROPERTIES USED IN THEORETICAL ANALYSIS

Steel:-

Young's modulus: 207.0 kN/mm^2
Poisson's ratio: 0.3
Coefficient of linear thermal expansion: 10.0 µm/mdegC
Thermal conductivity: 41.6 W/m deg C
The steel was assumed to be perfectly elastic and not to creep or plastically deform at the prevailing stresses and temperatures.

Concrete:-

Young's modulus: 43.1 kN/mm^2
Elastic and Creep Poisson's ratio: 0.18
Coefficient of linear thermal expansion: 8.0 µm/m deg C
Thermal conductivity: 1.75 W/m deg C

SUMMARY

During commissioning tests for Oldbury Nuclear Power Station it was found that 'hot-spots' with temperatures in excess of design values occured in the concrete at a small number of positions immediately behind the concrete pressure vessel liner. An experimental investigation was conducted to ascertain the seriousness of damage, if any, to the liner and concrete which would result from these hot-spots.

The investigation consisted of testing a full-scale model of the region of the vessel local to the upper boiler instrument penetration where the highest liner temperatures had been recorded. Three tests were undertaken. In the first test a thermal profile with a hot-spot representing conditions in the vessel was established and maintened for three months. A second test consisted of fifteen thermal cycles, each of 48 hours duration. The third was an over-heating test with an applied liner temperature distribution similar to that of the first and second tests but

with the hot-spot maintened at a maximum temperature of 305°C for 28 days. After each test the model was thoroughly examined for signs of damage by cutting out sample cores and by ultrasonic probing.

This paper describes the cyclic and over-heating tests and discusses the significance of the results with respect to full scale pressure vessel behaviour.

It is concluded that limited cracking of concrete may have occured in the Oldbury vessels at modest temperatures during the first heating cycle, but that these cracks will not extend during further cycles or at hot-spot temperatures as high as 300°C. The cracks formed will not impair the integrity of the liner or vessel.

SOMMAIRE

Lors des essais de réception de la centrale nucléaire d' Oldbury, des points chauds d' une température nettement plus élevée que celles prévues ont été rélevés à plusieurs endroits dans le caisson au droit de la peau d' étanchéité. On a effectué une étude expérimentale pour évaluer toute avarie de la peau d' étanchéité et du béton résultant de ces points chauds.

On a réalisé trois essais sur maquette en vrai grandeur de la partie du caisson à proximité de la pénétration supérieure recevant les instruments des échangeurs de chaleur, à l' endroit sur la peau d' étanchéité où se trouvent les températures les plus élevées.

Pour le premier essai on a établie sur la maquette un profil de températures comportant un point chaud tel à reproduire les conditions dans le caisson qu' on a maintenu pendant trois mois.

Pendant le deuxième essai la maquette a subit 15 cycles thermiques de 48 heures chacun.

Pour le troisième essai on a procédé à un echauffement pour établir un profil de températures sur la peau d' étanchéité comparable à celui des essais précédents, le point chaud cependant étant maintenu à une température maximale de 305°C pendant 28 jours. Chaque essai a été suivi d' un examen minutieux de la maquette avec prélèvement des carotes et l' emploi de techniques à ultra sons pour en évaluer les avaries.

On décrit les essais de suréchauffement tant permanents que cycliques et on discute la signification des résultats obtenus vis-à-vis du comportement du caisson même.

On tire la conclusion que le béton des caissons à Oldbury ait pu être fissuré à des températures peu élevées dès le premier cycle thermique mais que les fissures ne se propageraient pas pendant les cycles ultérieurs ou à des températures de point chaud allant jusqu' à 300°C. Les fissures existantes ne compromettrons pas l' intégrité structurelle ni de la peau d' étanchéité ni du caisson.

ZUSAMMENFASSUNG

Im Laufe der Inbetriebnahmprüfungen für das Kernkraftwerk

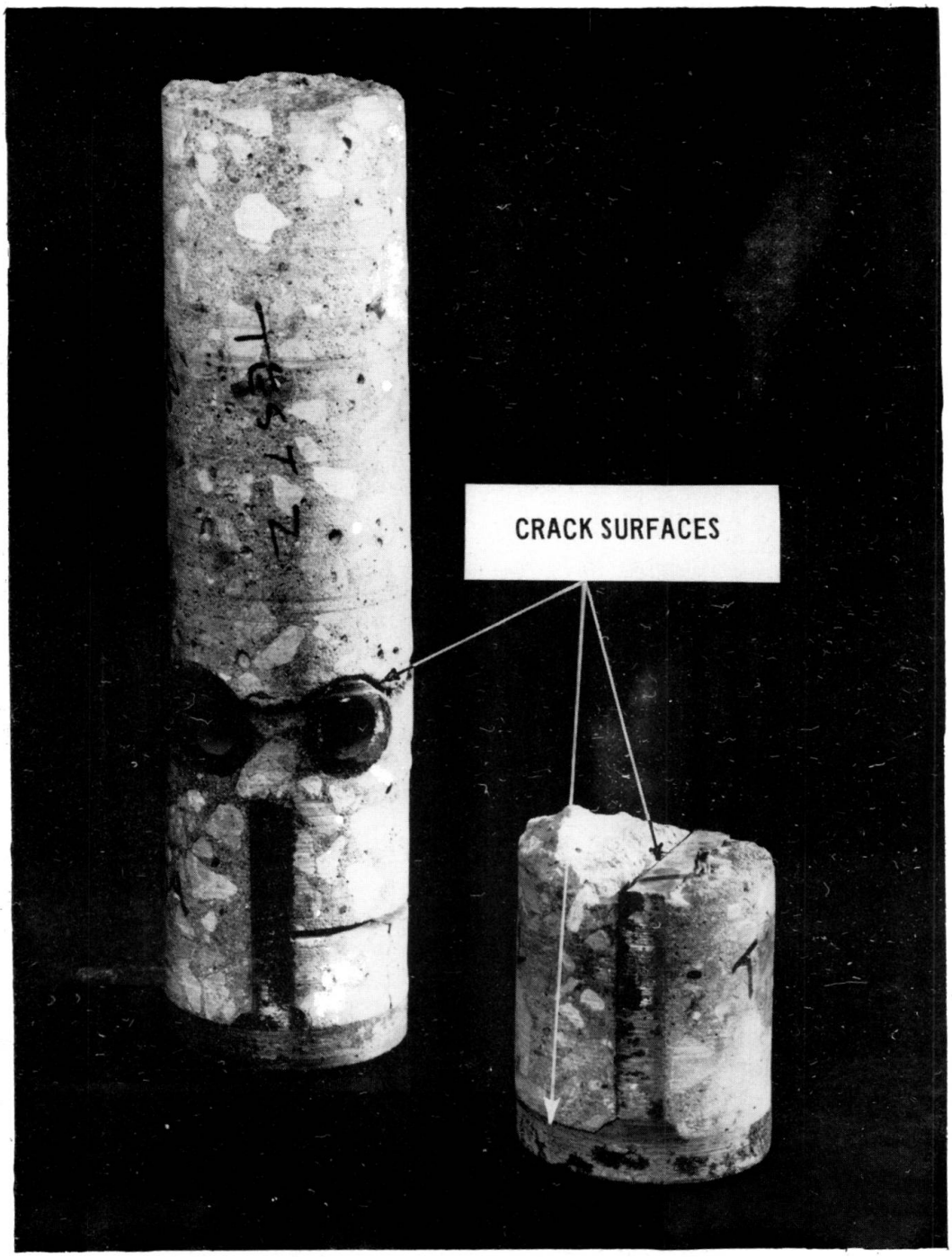

FIG. 14 CORES 1/3 (RIGHT) AND 2/5 SHOWING CRACK SURFACES

ZUSAMMENFASSUNG

Im Laufe der Inbetriebnahmeprüfungen für das Kernkraftwerk Oldbury wurden an mehreren Punkten unmittelbar hinter dem Spannbetonbehälter-Liner sogenannte Heissstellen mit die Auslegungswerte überschreitenden Temperaturen festgestellt. Es wurden Versuche durchgeführt, um das Ausmass etwaiger durch diese Heissstellen bedingter Schäden am Liner und Spannbeton zu bestimmen.

Im Rahmen der Untersuchungen wurde ein Modell natürlicher Grösse der im Bereich der oberen Durchführung für die Kesselinstrumentierung befindlichen Behälterzone geprüft, in der die höchsten Linertemperaturen verzeichnet worden waren. Es wurden drei Versuche durchgeführt. In dem erstem Versuch wurde ein Wärmeprofil aufgenommen, wobei die den Bedingungen an dem Behälter entsprechende Heissstelle drei Monate lang aufrechterhalten wurde. Der zweite Versuch umfasste 15 Wärmezyklen von je 48 Stunden Dauer. Der dritte Versuch bestand in einem Überhitzungstest. Die Verteilung der Linertemperaturen war dabei ähnlich wie in dem ersten und zweiten Versuch, doch wurde die Heissstelle 28 Tage lang auf einer Höchsttemperatur von 305° C erhalten. Nach jedem Versuch wurde das Modell durch Entnahme von Probekernen und Ultraschallsondierung gründlich auf Anzeichen von Schäden untersucht.

Dieser Bericht behandelt die Temperaturwechsel- und Überhitzungsversuche und die Bedeutung der Ergebnisse, was das Verhalten der Druckgefässe natürlicher Grösse anbelangt.

Man gelangte zu dem Schluss, dass in dem Spannbeton der Druckbehälter von Oldbury während der ersten Aufheizungsperiode bei mässigen Temperaturen in begrenztem Umfang Risse entstanden sein mögen, dass sich diese Risse aber während weiterer Zyklen bzw. bei Heissstellentemperaturen bis 300° C nicht weiter ausbreiten würden. Die gebildeten Risse werden die Verwendbarkeit des Liners bzw. des Behälters nicht beeinträchtigen.

LIST OF FIGURES

FIGURES

VERZEICHNIS DER ABBILDUNGEN

Leere Seite
Blank page
Page vide

IABSE
AIPC
IVBH

SEMINAR on:
«CONCRETE STRUCTURES SUBJECTED TO TRIAXIAL STRESSES»
17th-19th MAY, 1974 - ISMES - BERGAMO (ITALY)

Spannbetondruckgefäss mit Heisser Dichthaut und Beton Erhöhter Temperatur

Prestressed concrete pressure vessel with hot liner and concrete of elevated temperature

Caisson en béton précontraint avec peau d'étenchéité chaude et béton à température élevée

A. NESITKA J. NÊMET
Reaktorbau Forschungs- und Baugesellschaft
A-2444 Seibersdorf, Osterreich

1. Einleitung, Konstruktion

Der Bau eines Spannbetonbehälters zur Prüfung von Komponenten von Kernreaktoren am Forschungszentrum Seibersdorf der Österreichischen Studiengesellschaft für Atomenergie durch eine Gruppe österreichischer Industriefirmen ist der Anlaß zu diesem Bericht [1]. Die Beanspruchungen in vielen Bereichen des Behälters sind mehrachsial. Verformungsmessungen unter diesen Beanspruchungen werden durchgeführt. Über Konstruktion, Berechnung, Überlegungen, die mehrachsialen Beanspruchungen betreffend, soll berichtet werden.

Die Bauart des Behälters ist so, daß sowohl Versuche für gasgekühlte Reaktoren durchgeführt, als auch die Zustände bei wassergekühlten Reaktoren geprüft werden können.

Aus der Übersicht in BILD 1 können die Hauptabmessungen und die wesentlichen Konstruktionsteile ersehen werden.

Von anderen Spannbetondruckgefäßen unterscheidet sich das hier beschriebene dadurch, daß die Dichthaut durch keine Wärmeisolierung geschützt ist und der vollen Temperatur des Kühlmittels ausgesetzt wird. Dies ist auch ein Weg, Spannbetondruckgefäße für wassergekühlte Reaktoren zur Anwendung zu bringen.

Die Temperatur des Kühlmittels, ca. 300° C, führt zu Zwängspannungen in der gegen den Beton unverschieblich gehaltenen Dichthaut. Um diese

Zwängung zu verringern, wird die Temperatur im Beton auf 1oo bis 12o° gebracht. Der Innendruck wurde mit 1oo bar angesetzt. Er entlastet die Dichthaut von Temperaturzwängung und den Beton von den Druckbeanspruchungen des Lastfalles Vorspannung. In BILD 2 sind Temperaturverlauf und Druck für die berechneten Lastfälle dargestellt.

Die hohe Temperatur im Beton bringt eine wesentliche Verstärkung und Beschleunigung der Kriechvorgänge in diesem mit sich. Es soll vermieden werden, aus diesen Verformungen größere Druckbeanspruchungen in die Dichthaut zu bringen. Zu diesem Zweck wird vor kraftschlüssiger Verbindung zwischen Dichthaut und Isolierbeton einerseits und Spannbeton andererseits dieser einem Kriechvorgang unter voller Vorspannung und einer dem Betriebszustand entsprechenden Temperatur unterworfen.

Dieses Vorkriechen dauert ca. 1oo Tage. In dieser Zeit sollten ca. 6o % der Kriechverformung nach $1o^4$ Tagen unter Temperatur und Vorspannung erreicht worden sein. BILD 3 zeigt den Verlauf der Kriechkurve für versiegelte Probekörper unter der angegebenen Temperatur, extrapoliert bis $1o^4$ Tage. Eingetragen ist die Zeit des Vorkriechens. Nach Kraftschluß, durch Füllen der Fuge durchgeführt, wird vorerst die Temperatur auf Raumtemperatur bleiben, die Vorspannung kleiner sein als während des Vorkriechens, da durch teilweises Nachlassen und Wiederaufbringen der Vorspannung ein Teil von ihr in Isolierbeton und Dichthaut gebracht wird. Wenn in dieser Zeit Kriechen eintritt, so nur in geringem Ausmaß. Nach Inbetriebnahme wird die Temperatur wieder erhöht, der Innendruck jedoch verringert die Beanspruchung im Spannbeton auf Bruchteile. Die Messungen werden zeigen, ob geringes weiteres Kriechen oder ein Rückkriechen einsetzt.

Zur Konstruktion sei noch vermerkt, daß die Spannglieder ohne Verbund sind, so daß sie zu beliebiger Zeit nachgespannt oder auch ausgewechselt werden können. Das Relaxationsverhalten des Spannstahles 16o/18o wurde untersucht. Der Verlauf ist in BILD 4 für gegebene Spannung und Temperatur dargestellt.

2. Statische Berechnung

Die statische Berechnung liefert für Bauzustand, Gebrauchs- und Ausnahmezustände Spannungsbilder, die in BILD 5 bis BILD 9 für verschiedene Stellen und Lastzustände angegeben sind.

Die Zylinderfestigkeit des Betons kann nach 9o Tagen mit β_{c9o} = 6oo kp/cm2 als gesichert angesehen werden. die erhöhte Temperatur

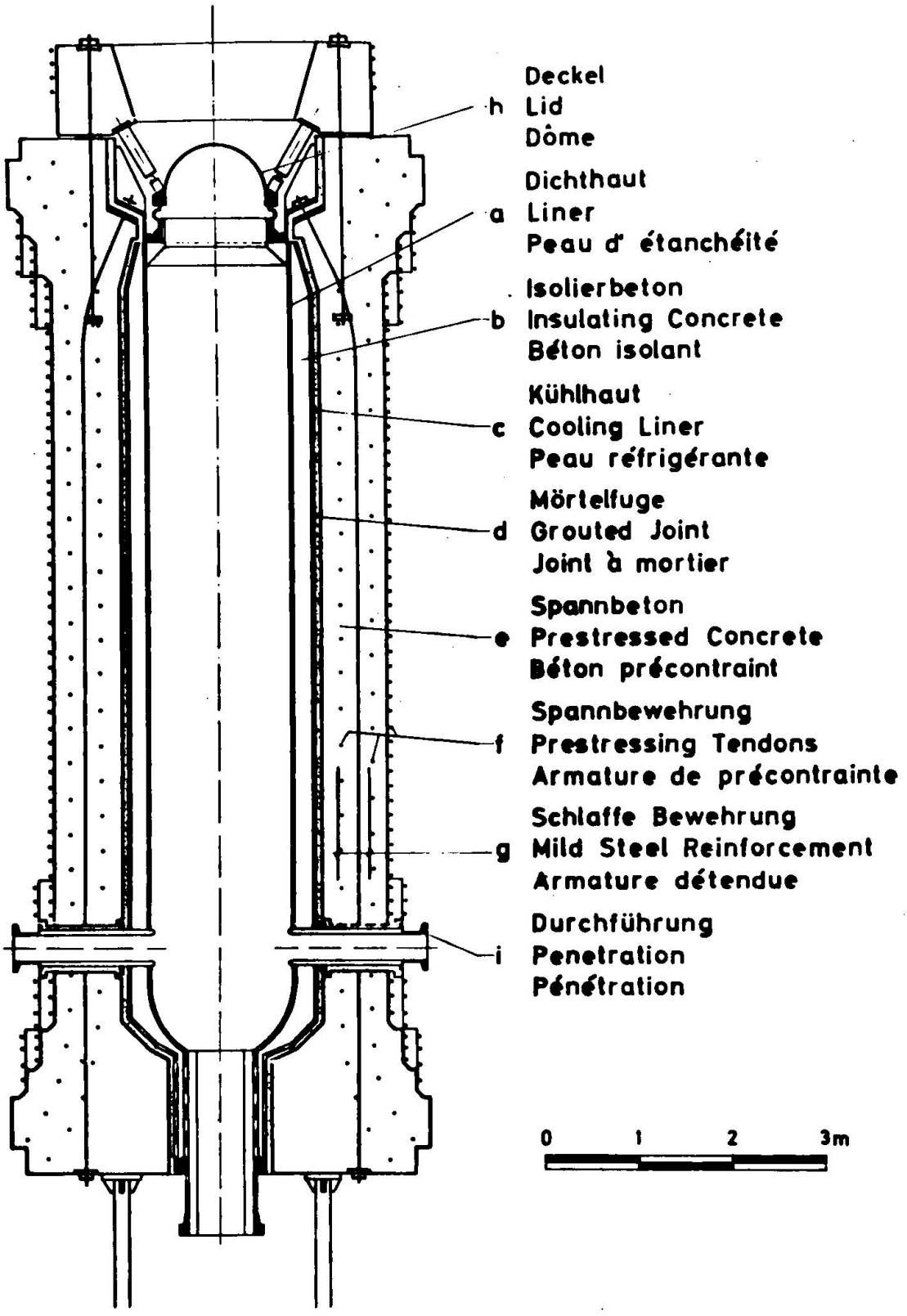

Bild 1 Spannbetonbehälter Seibersdorf
Prestressed Concrete Pressure Vessel Seibersdorf
Caisson en béton précontraint Seibersdorf

bringt einen Abfall der Festigkeit, der versuchsmäßig kontrolliert wurde. Zum Nachweis der Sicherheit wird eine Zylinderfestigkeit β_{c90} = 4oo kp/cm2 angesetzt.

Nach dem deutschen Normenentwurf für Reaktordruckgefäße aus Spannbeton ist die zulässige Druckspannung

$$\sigma_{zul} = \frac{4oo}{2,1} = 19o \text{ kp/cm2}$$

Diese Beanspruchung wird an den in den vorstehenden Bildern dargestellten Stellen z.T. wesentlich überschritten.

Der mehrachsige Nachweis soll hinreichende Sicherheit bestätigen.

Bei Betrachtung kann unterschieden werden zwischen linienförmig oder quasi linienförmig sich ausdehnenden Gebieten solcher Beanspruchungen und flächenförmig sich verbreiternden Bereichen. Ferner kann unterschieden werden zwischen Beanspruchungen, die nur fallweise kurzfristig, anderen, die über beschränkte Zeit, und solchen, welche während der gesamten Gebrauchszeit des Gefäßes vorhanden sind.

Auf diese Merkmale und die Frage, ob Kriechvorgänge im Beton Spannungsumlagerungen und Abbau der Zwängung bewirken können, oder ob der Spannungszustand unter unmittelbarem Einfluß einer äußeren Last praktisch nur von dieser abhängig und unveränderlich ist, sollte bei Beurteilung des Sicherheitsfaktors und der gemessenen Verformungen geachtet werden.

3. Nachweis der Sicherheit bei mehrachsiger Beanspruchung

3,1 Es sollen hier primär nicht Bruchtheorien behandelt oder verglichen werden. Die auf Versuchen basierenden Kriterien für das Eintreten des Versagens werden zum Nachweis der Sicherheit des Spannbetonbehälters angewandt.

Die an ihm noch durchzuführenden Messungen, die sich über Jahre erstrecken, können erst zu späterem Zeitpunkt in ihrer Aussage beurteilt werden. Die Sicherheitsbeiwerte, die es zu ermitteln gilt, werden mit Hilfe von Diagrammen aus dem Schrifttum bestimmt und miteinander verglichen. Aus diesem sollen Arbeiten nachstehender Autoren verwendet werden:

Yoshiji Niwa, Shoichi Kobayashi und Wataru Koyanagi speziell über Leichtbeton; [2]

V. Hansson und K. Schimmelpfennig die Kurvenscharen für beschränkte Bereiche von Spannungsverhältnissen angeben; [3]

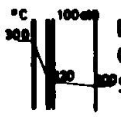

Betrieb
Operation
Service

Druckentlastung, Gas
Pressure Relieve, Gas
Décharge de pression, gaz

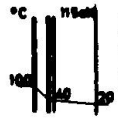

Prüfdruck
Test Pressure
Pression d'épreue

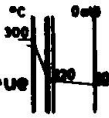

Heiß, drucklos
hot, pressure relieved
chaud, sans pression

Druckentlastung, Wasser
Pressure Relieve Water
Décharge de pression, eau

Bild 2
Lastfälle
Loading Conditions
Conditions de charge

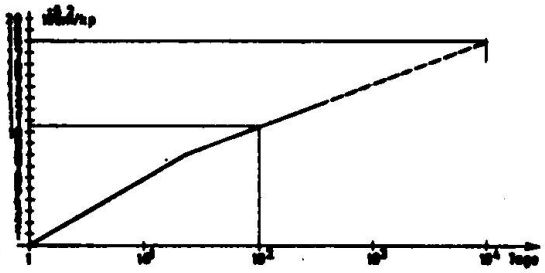

Bild 3
Kriechkurve des Betons
Creep of Concrete
Fluage du béton

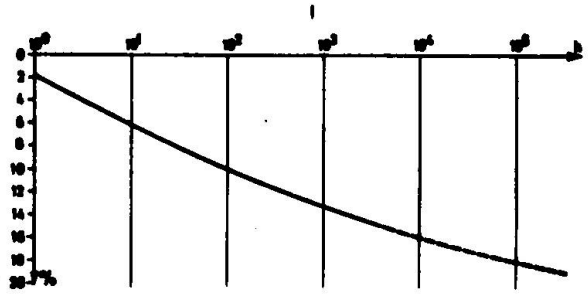

Bild 4
Relaxation des Spannstahles
Relaxation of the Tendons
Relaxation des armatures de précontrainte

J. P. Magnus und A. Audibert [4]
die eine geschlossene Form für den gesamten Bereich von Spannungsbeziehungen, Druck und Zug, veröffentlichen.

Beim Nachweis wird beachtet, daß der Spannungszustand einer kritischen Grenze sich dadurch nähern kann, daß alle Hauptspannungen gleichzeitig anwachsen, oder daß dies nur bei einer Hauptspannung geschieht, was von der Art der Ursache abhängen kann.

3,2 Innenseite des Isolierbetons an der Dichthaut, vgl. Bild 5

Temperatur: 300° C, Zylinderfestigkeit β_c = 400 kp/cm2. Die Beanspruchung tritt für den Lastfall "heißer, druckloser Behälter" im ganzen Isolierbetonmantel auf. Dies ist ein Ausnahmezustand von beschränkter Dauer. Er rührt vor allem aus Zwängung durch Temperatur her, bei deren Anstieg alle drei Hauptspannungen wachsen.

Um Fig. 11 aus [2] verwenden zu können, wird gesetzt:

$\sigma_1 = \sigma_2 =$ - 240 kp/cm2 $\qquad \frac{\sqrt{2} \cdot \sigma_1}{\sigma_0} = 0{,}848$

$\sigma_3 =$ - 45 kp/cm2

$\sigma_0 =$ - 400 kp/cm2 $\qquad \frac{\sigma_3}{\sigma_0} = 0{,}113$

Diese Verhältnisse bestimmen auf der Bruchzustandsfläche

$\frac{\sqrt{2} \cdot \sigma_1^*}{\sigma_0} = 4{,}40$ und die vorhandene Sicherheit

$\underline{\underline{\nu}} = \frac{\sigma_1^*}{\sigma_1} = \underline{\underline{5{,}2}}$

Ebenfalls in [2] unter Fig. 13 wird das Bruchkriterium, nur abhängig von σ_1 und σ_3, also unter Außerachtlassen der mittleren Hauptnormalspannung, dargestellt. Damit folgt

$\frac{\sigma_1 + \sigma_3}{\sigma_0} = 0{,}713 \qquad \frac{\sigma_1 - \sigma_3}{\sigma_0} = 0{,}488$

Diese Verhältnisse bestimmen wieder

$\frac{\sigma_1^* + \sigma_3^*}{\sigma_0} = 4$ und die vorhandene Sicherheit

$\underline{\underline{\nu}} = \frac{\sigma_1^* + \sigma_3^*}{\sigma_1 + \sigma_3} = \underline{\underline{5{,}6}}$

also von dem erstermittelten nur um 7 % abweichend.

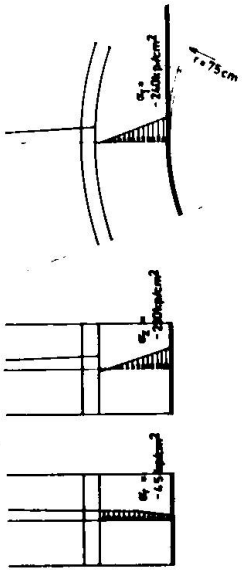

Bild 5

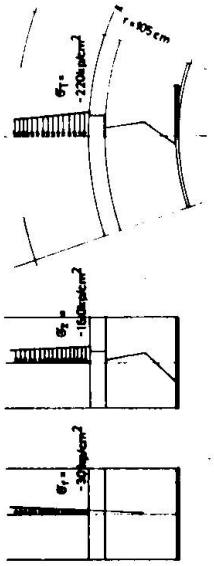

Bild 6

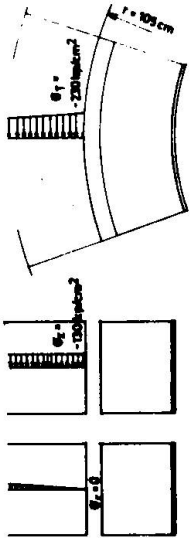

Bild 7

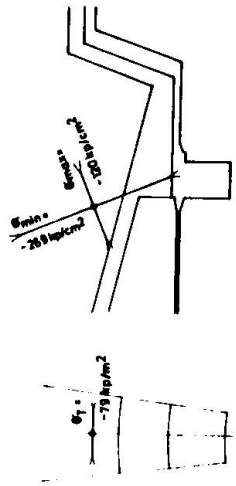

Bild 8

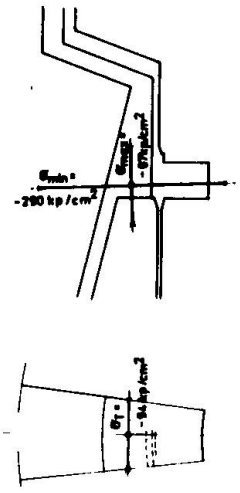

Bild 9

3,3 Innenseite des Kiesbetonmantels, vgl. Bild 6

Temperatur 12o° C, Zylinderfestigkeit β_c = 4oo kp/cm2. Die Beanspruchung tritt kurzfristig unter Druckentlastung bei wassergekühltem Gefäß im gesamten Kiesbetonmantel auf, wieder nur während beschränkter Frist. Die Spannungen rühren vor allem von der Vorspannung her.

3,31 Prüfung nach [3], Fig. 5

σ_1 = - 3o kp/cm2 $\qquad \frac{\sigma_1}{\sigma_3}$ = o,136

σ_2 = - 16o kp/cm2 $\qquad \frac{\sigma_2}{\sigma_3}$ = o,727

σ_3 = - 22o kp/cm2 $\qquad \frac{\sigma_3}{\beta_c}$ = o,55

Aus der Kurventafel folgt

$\frac{\beta_{r3}}{\beta_c}$ = 3,6o und die vorhandene Sicherheit

$\underline{\underline{\nu}} = \frac{\beta_{r3}}{\sigma_3} = \underline{\underline{6,55}}$

3,32 Prüfung nach [4], Fig. 21

σ_1 = 22o kp/cm2 $\qquad k = \frac{\sigma_2}{\sigma_1}$ = o,73

σ_2 = 16o kp/cm2

σ_3 = 3o kp/cm2 $\qquad \frac{\sigma_1}{\sigma_{o'}}$ = o,55o

$\sigma_{o'}$ = 4oo kp/cm2 $\qquad \frac{\sigma_3}{\sigma_{o'}}$ = o,o75

Es wird angenähert die Kurve k = o,75 verwendet. Sie ergibt

$\frac{\sigma_1^*}{\sigma_{o'}}$ = 5 und die vorhandene Sicherheit

$\underline{\underline{\nu}} = \frac{\sigma_1^*}{\sigma_1} = \underline{\underline{9,1}}$

einen Wert, der wesentlich höher liegt als bei 3,31.

3,4 Innenseite des Kiesbetonmantels, vgl. Bild 7

Temperatur 12o° C, Zylinderfestigkeit β_c = 4oo kp/cm2. Die Beanspruchung tritt während der Zeit des Vorkriechens, d.h. ca. 1oo Tagen, an der gesamten Innenfläche des Kiesbetons auf. Die Spannungen kommen aus Vorspannkräften.

3,41 Prüfung nach [7], Fig. 5

$\sigma_1 = 0$ $\qquad \frac{\sigma_1}{\sigma_3} = 0$

$\sigma_2 = -130$ kp/cm2 $\qquad \frac{\sigma_2}{\sigma_3} = 0{,}565$

$\sigma_3 = -230$ kp/cm2 $\qquad \frac{\sigma_3}{\beta_c} = 0{,}575$

Aus der Kurventafel folgt

$\frac{\beta_{r3}}{\beta_c} = 1{,}16$ und die vorhandene Sicherheit

$\underline{\nu} = \frac{\beta_{r3}}{\sigma_3} = \underline{2{,}02}$

3,42 Prüfung nach [4], Fig. 21 (Bezeichnungen wie dort)

$\sigma_1 = 230$ kp/cm2 $\qquad k = \frac{\sigma_2}{\sigma_1} = 0$

$\sigma_2 = 0$ $\qquad \frac{\sigma_1}{\sigma_0'} = 0{,}575$

$\sigma_3 = 130$ kp/cm2 $\qquad \frac{\sigma_3}{\sigma_0'} = 0{,}325$

$\sigma_0' = 400$ kp/cm2

Aus Kurve $k = 0$ folgt

$\frac{\sigma_1}{\sigma_0'} = 2{,}3$ und die vorhandene Sicherheit

$\underline{\nu} = \frac{\sigma_1^*}{\sigma_1} = \underline{4{,}0}$

ein Wert, der fast doppelt so groß ist wie bei 3,41.

3,5 Innenseite des Kiesbetons hinter Dichthautabschluß, Bild 8

Temperatur 120° C, Zylinderfestigkeit $\beta_c = 400$ kp/cm2. Die Beanspruchung tritt langdauernd bei normalem Betrieb auf. Eine Erhöhung der Temperatur des Dichthautflansches vergrößert vor allem die etwa radial wirkende Spannung, es soll daher nur ihr Anwachsen beurteilt werden.

Prüfung nach 3 , Fig. 5

$\sigma_1 = -79$ kp/cm2

$\sigma_2 = -120$ kp/cm2

$\sigma_3 = -269$ kp/cm2

Durch probeweise Wahl von ν wird gefunden

$$\nu = 3{,}48$$

dafür ist

$$\frac{\sigma_1}{\nu \cdot \sigma_3} = 0{,}084, \qquad \frac{\sigma_2}{\nu \cdot \sigma_3} = 0{,}128 \text{ und}$$

$$\frac{\beta_{r3}}{\beta_c} = 2{,}34 = \frac{\nu \cdot \sigma_3}{\beta_c}$$

3,6 Verpreßte Fuge hinter Dichthautabschluß, Bild 9

Temperatur 12o° C, Zylinderfestigkeit β_c = 4oo kp/cm2. Die Beanspruchung entspricht der im Kiesbeton nach 3,5. Wie dort wird nachgewiesen:

σ_1 = - 67 kp/cm2
σ_2 = - 94 kp/cm2
σ_3 = - 29o kp/cm2

Durch probeweise Wahl von ν wird gefunden

$$\nu = 3{,}o$$

3,7 Diskussion der Nachweise

3,71 Leichtbeton (3,2)

Der Umstand, daß die mittlere Hauptnormalspannung ohne Einfluß zu sein scheint, kann an der anderen Art des Leichtbetons - im Gegensatz zum Kiesbeton - liegen, Kräfte aufzunehmen bzw. zu Bruch zu gehen [5] . In der Zellenstruktur der Feinmörtelmatrix brechen zuerst jene Zellenwände, die in ungünstiger Richtung zu den äußeren Kräften liegen. Solche Elemente für sich betrachtet sind in Querrichtung nur mit der Korneigenfestigkeit des Leichtzuschlages belastbar. Diese liegt bei 14o bis 32o kp/cm2 [6]. D Verhältnis der Spannungen zueinander im Element ist anders und ungünstiger als im Gesamtkörper und führt so zu früherem Bruch als bei Kiesbeton. Die Spannungen nach BILD 5 würden, nach [3]. Fig. 5, also einem für Kiesbeton sicheren Kriterium beurteilt, eine Sicherheit von etwa 7,5 aufweisen.

Es beweist sich hier offenbar eine Einschränkung der Laststeigerung unter mehrachsiger Beanspruchung, welche u.a. auch dazu führt, daß umschnürte Säulen aus Leichtbeton nicht zugelassen sind oder auch, daß bei Leichtbeton Würfel- und Zylinderfestigkeit in vielen Fällen praktisch gleich groß sind.

Es zeigt sich hier wieder der Einfluß der Eigenfestigkeit der Zuschlagskörner des Leichtbetons auf dessen Festigkeit, im Gegensatz zum normalen Kiesbeton, bei welchem die Festigkeit vorwiegend vom Wasserzementfaktor abhängig ist.

3,72 Regelteil des Zylindermantels

3,721 Innenseite Kiesbeton bei Druckentlastung (3,3)
Auffallend ist der beachtliche Unterschied zwischen den nach zwei verschiedenen Kriterien ermittelten Sicherheiten.
Bei Betrachtung von [3], Bild F 7, wird deutlich, daß der auf den ersten Blick nicht entscheidend verschiedene Verlauf der Bruchzustandsfläche durch den flachen Schnitt mit einer aus dem Ursprung kommenden Geraden wesentlich andere Werte ν geben muß.
Es werden dabei die Kurven nach [7] nach den dort veröffentlichten Versuchsergebnissen mit denen nach [4] als gleich vorausgesetzt, da sie auf denselben Versuchen aufgebaut sind. Von Bedeutung mag die Lastaufbringung sein, geschmierte starre Stahlplatten bei [7], Bürstenplatten bei [8], welche Versuche den Bereich in der Nähe der biaxialen Beanspruchung bei [3] wesentlich mitbestimmt haben.
Die wesentliche Bedeutung der Größe der kleinsten Hauptnormalspannung bei Spannungszuständen in der Nähe des biaxialen wird besonders deutlich.

3,722 Innendruck bei Vorkriechen (3,4)
Hier, beim zweiachsigen Spannungszustand, wird der Unterschied der beiden ermittelten Sicherheiten noch wesentlich stärker. Es gelten die Ausführungen von oben.

3,73 Bereich des Dichthautabschlusses

3,731 Innenseite Kiesbeton (3,5)
Der gewählte Vorgang, nur die größte der Hauptnormalspannungen anwachsen zu lassen, um die Sicherheit zu beurteilen, ist ein Grenzfall. Tatsächlich wird auch die mittlere Hauptnormalspannung durch die behinderte Querdehnung wachsen, was in etwas geringerem Maß auch für die kleinste Hauptnormalspannung gilt.

Es kann notwendig werden, mit steigender Last durch eine Reihe von Rechengängen die Änderung des Spannungszustandes zu verfolgen, um die Sicherheit zutreffend beurteilen zu können.

3,732 Fugenmörtel (3,6)
Für diesen Punkt gilt was oben gesagt wurde mit dem Zusatz, da die kleinste Hauptnormalspannung überwiegend Temperaturzwängung als Ursache hat. Ein Anwachsen der Temperatur wird auch sie anheben.

3,733 Es sei für beide Punkte, 3,5 und 3,6, noch vermerkt, daß die Temperaturzwängung, welche die überwiegende Ursache der Spannungen ist, keine nachdrängende Last darstellt, daher Relaxation aus örtlich verstärktem, nicht mehr lastproportionalem Kriechen eintreten kann.

3,74 "Sicherheit"

Der Faktor ν wurde in den vorangegangenen Punkten als "Sicherheit" bezeichnet. Er wurde unter Bedachtnahme auf die Art der La ermittelt, stellt aber in jedem Fall das Verhältnis einer Bruchspannung zu einer Gebrauchsspannung dar. Als Sicherheit könnte m ebensogut auch das Verhältnis von Bruchlast zu Gebrauchslast bezeichnen, was nicht immer, insbesondere nicht bei Spannbeton, gleichbedeutend mit dem Spannungsverhältnis sein muß.

Die Ursachen eines Spannungszustandes sind meist vielfältig, im vorliegenden Fall können es sein Eigengewicht, Vorspannkräfte, Innendruck, Temperatur. Die beiden erstgenannten bleiben nach Erbauung des Behälters konstant oder nehmen mit der Zeit ab, die letztgenannten unterliegen u.U. mancherlei Änderung und Lastzyklen. Es müssen hier Fragen der Werkstoffermüdung mitüberlegt werden [4] bzw. das Langzeitverhalten betrachtet werden. Es ist, wi eingangs schon erwähnt, zu überlegen, ob bei wachsender Beanspruchung durch Kriechen begrenzter Bereiche Lastumlagerungen eintreten können, um die "nachdrängenden" Lasten nach Abbau von Spannungsspitzen in breiterem Bereich zu tragen bzw. um "nicht nachdrängende" Zwänglasten abzubauen.

Die gefundenen Werte ν sind, wenn man vom Bauzustand 3,4 absieht für die untersuchten Stellen als etwa gleichwertig zu beurteilen berücksichtigt man die örtliche Ausdehnung der Spannungszustände

4. Methoden der Spannungs- und Verformungsmessung

4,1 Um das Verhalten von Beton und Dichthaut bei mechanischer und thermischer Belastung zu erfassen, werden folgende Geber und Meßeinrichtungen eingebaut:

a) Widerstands-Dehnmeßgeber (12o Ohm) in Viertelbrückenschaltung mit eingebautem Thermoelement Cu-Constantan im Isolierbeton.

b) Saiten-Dehnungsmeßgeber im Spannbeton, die Empfängerspule als Widerstandsthermometer verwendet.

c) Widerstands-Dehnmesser (Freigitter-DMS zur Flame-Spray-Montage, 5oo Ohm) in Viertelbrückenschaltung auf Dichthaut und Deckel mit eingebautem Ni-CrNi-Thermoelement.

d) Mechanische Meßeinrichtungen, radiale Invarstäbe zur integralen Prüfung der Veränderung der Dicke des Isolierbeton- bzw. Kiesbetonmantels.

e) Hydraulische Meßgeber zur unmittelbaren Spannungsmessung im Kiesbeton, an spannungsgleichen Stellen mit den Saitendehnungsgebern angeordnet.

f) Thermoelemente vom Typ Cu-Constantan zur Prüfung des Temperaturverlaufes.

g) Meßpunkte für Setzdehnungsmessungen an der Oberfläche und an der Innenseite der Dichthaut.

h) Dynamometer zur laufenden Prüfung der Spannkraft an den Ankerstellen einer Anzahl von Spanngliedern.

i) Vorkehrungen für die geodätische Vermessung des Behälters an diesem, dem Fundament und in der Umgebung.

4,2 Die im Isolierbeton und Kiesbeton angesetzten Geber nach 4,1a, b und e sind in dichter Anordnung in jenem Bereich des zylindrischen Teiles eingebaut, der durch seine geometrische Form und das Fehlen von Störstellen eine möglichst gute Vergleichbarkeit von Berechnung und Messung erwarten läßt. Gruppen von Meßgebern liegen dort jeweils an mehreren Punkten, auf einem Radius angeordnet, so daß zu den Spannungsbildern entsprechende Verformungszustände in drei Achsrichtungen bestimmt bzw. die Spannungen überprüft werden können. Die Gruppen von Gebern bilden entweder Achskreuze, oder, wo irgend möglich, Tetraeder, so daß jeweils je Achsrichtung eine Mehrzahl von Messungen vorliegt.

Neben den Meßstellen im Regularteil sind solche noch an Punkten mit Abweichungen von der Zylinderform, etwa bei den seitlichen Durchbrüchen, vorhanden.

Was die Aufnahme und Verwertung der Meßdaten betrifft, wird auf [1] verwiesen.

4,3 Erfahrungen über das Langzeitverhalten solcher Meßgeber konnten an einem vorweg hergestellten Versuchsring, einem 1 m hohen Schuß des Zylindermantels, [1], gesammelt werden, die wesentlich über das hinausgingen, was an kleinen Probekörpern festgestellt werden konnte.

Die hohe Temperatur, das feuchte Milieu mit dem dieser Temperatur entsprechenden Dampfdruck, das chemische Verhalten des Betons gegen Kunststoff, machten zusätzliche Schutzmaßnahmen an diesen Gebern erforderlich, die mit beachtlichem Aufwand verbunden waren. Der erwartete Erfolg muß sich erst beweisen, es kann daher auch an dieser Stelle bzw. zu diesem Zeitpunkt darüber noch nicht berichtet werden.

4,4 Parallel zu den Messungen am Versuchsbehälter laufen im Labor solche an Probekörpern aus Bauwerksbeton, an welchen die Entwicklung der Festigkeit, des statischen und dynamischen E-Moduls und der Querdehnzahl, das Schwinden und Kriechen bei Last und Temperatur, wie sie dem Zustand im Bauwerk entsprechen, gemessen werden.

5. Ergebnis der Messungen

Hier kann vorerst nur über solche berichtet werden, die am Versuchsring gefunden wurden. Sie zeigen, überraschend, trotz der späteren Ausfälle und Versuche der Reaktivierung, brauchbare bis gute Übereinstimmung, wobei diese durch Variationen von E-Modul und Querdehnzahl, entsprechend kurzfristigen Kriechvorgängen, wesentlich verbessert wurden.

6. Schrifttum

[1] Berichte der Österreichischen Studiengesellschaft für Atomenergie Ges.m.b.H.
Erster bis vierter Zwischenbericht zum Gemeinschaftsprojekt Spannbetonbehälter-Heliumversuchsstand 'beschränkte Verbreitung'

[2] Yoshiji Niwa, Choichi Kobayashi and Wataru Koyanagi
Failure Criterion of Lightweight Aggregate Concrete
Subjected to Triaxial Compression
Memoirs of Faculty of Engineering,
Kyoto University, Japan
Vol XXIX, Part II, April 1967

[3] V. Hansson und K. Schimmelpfennig
Concrete Strength in Multiaxial Stress States.
American Concrete Institute Seminar
Concrete for Nuclear Reactors, Berlin 1970

[4] J. P. Magnas et A. Audibert
Critères de résistance du béton sous sollicitations multiaxiales
Annales de l'institut technique du bâtiment et des travaux publics
Supplément à No 287 Novembre 1971

[5] G. Wischers und M. Lusche
Einfluß der inneren Spannungsverteilung auf das Tragverhalten
von druckbeanspruchtem Normal- und Leichtbeton
beton 8/72

[6] H. Weigler und S. Karl
Stahlleichtbeton
Bauverlag, Wiesbaden und Berlin, 1971

[7] P. Launay, H. Gachon, P. Poitevin
Deformation et résistance ultime du béton sous étreintes triaxial
Sixième Congrès International de la Précontrainte
Prag 1970

[8] H. Kupfer, H. K. Hilsdorf, H. Rüsch
Behavior of Concrete under Biaxial Stresses
ACI Journal August 1969

Zusammenfassung

Es wird über den Entwurf und den Bau eines Spannbetondruckbehälters mit heißer Dichthaut und Beton von erhöhter Temperatur zur Prüfung von Reaktorkomponenten berichtet. Für die aus der statischen Berechnung folgenden mehrachsigen Spannungszustände wird die Sicherheit gegen Bruch ermittelt und diskutiert. Die eingebauten Vorrichtungen zur Spannungs- und Verformungsmessung werden beschrieben.

Summary

There ist given a report on the design and construction of a presresse concrete pressure vessel with hot liner and concrete of elevated temperature for testing components of nuclear reactors. The state of stresses resulting from the structural analysis is multiaxial. The factor of security against failure is calculated and dicussed. The devices, installed for measuring stresses and strains are described.

Resumée

Un caisson en béton précontraint avec une peau d'étanchéité chaude et béton à température élevée, pour éprouver des composantes des réacteurs nucléaires est décrit. L'état d'étreinte, resultant du calcul statique, est multiaxiale. Les facteurs de sécurité sont calculés et discutés. Les indicateurs pour mesurer les étreintes et les déformations sont décrits.

IABSE
AIPC
IVBH

SEMINAR on:
«CONCRETE STRUCTURES SUBJECTED TO TRIAXIAL STRESSES»
17th-19th MAY, 1974 - ISMES - BERGAMO (ITALY)

Caisson Bugey I et ses maquettes. Auscultation et exploitation des mesures prises pendant les essais

Bugey I pressure vessel and scale models. Instrumentation and utilization of the measurements carried out during the testing period

Spannbetondruckbehalter Bugey I und die Versuchsmodelle. Instrumentierurg und Auswertung der Bemessungen während der prüfungszeit

par M. Jacques LEMASSON - Spie-Batignolles / Citra
13, Avenue Morane-Saulnier - Velizy (78 140) - France

I - INTRODUCTION

La présente communication est relative à l'exploitation des mesures prises pendant les essais effectués sur le caisson BUGEY 1 et sur ses maquettes. Avant de présenter les résultats correspondants nous rappellerons brièvement les caractéristiques et l'historique de ces ouvrages. D'autre part, nous passerons en revue les types de capteurs adoptés, leur implantation et les méthodes d'exploitation des mesures.

II - LE CAISSON EN BETON PRECONTRAINT BUGEY 1 ET SES DEUX MAQUETTES AU 1/5e

1 - Description du caisson

Le caisson en béton précontraint de la centrale nucléaire BUGEY 1 a été construit de 1967 à 1970. Le réacteur qu'il contient est du type uranium naturel- graphite-gaz, la puissance électrique est de 560 MWe (voir figure 1). Les essais précédant la mise en service ont eu lieu de juin 1971 à janvier 1972

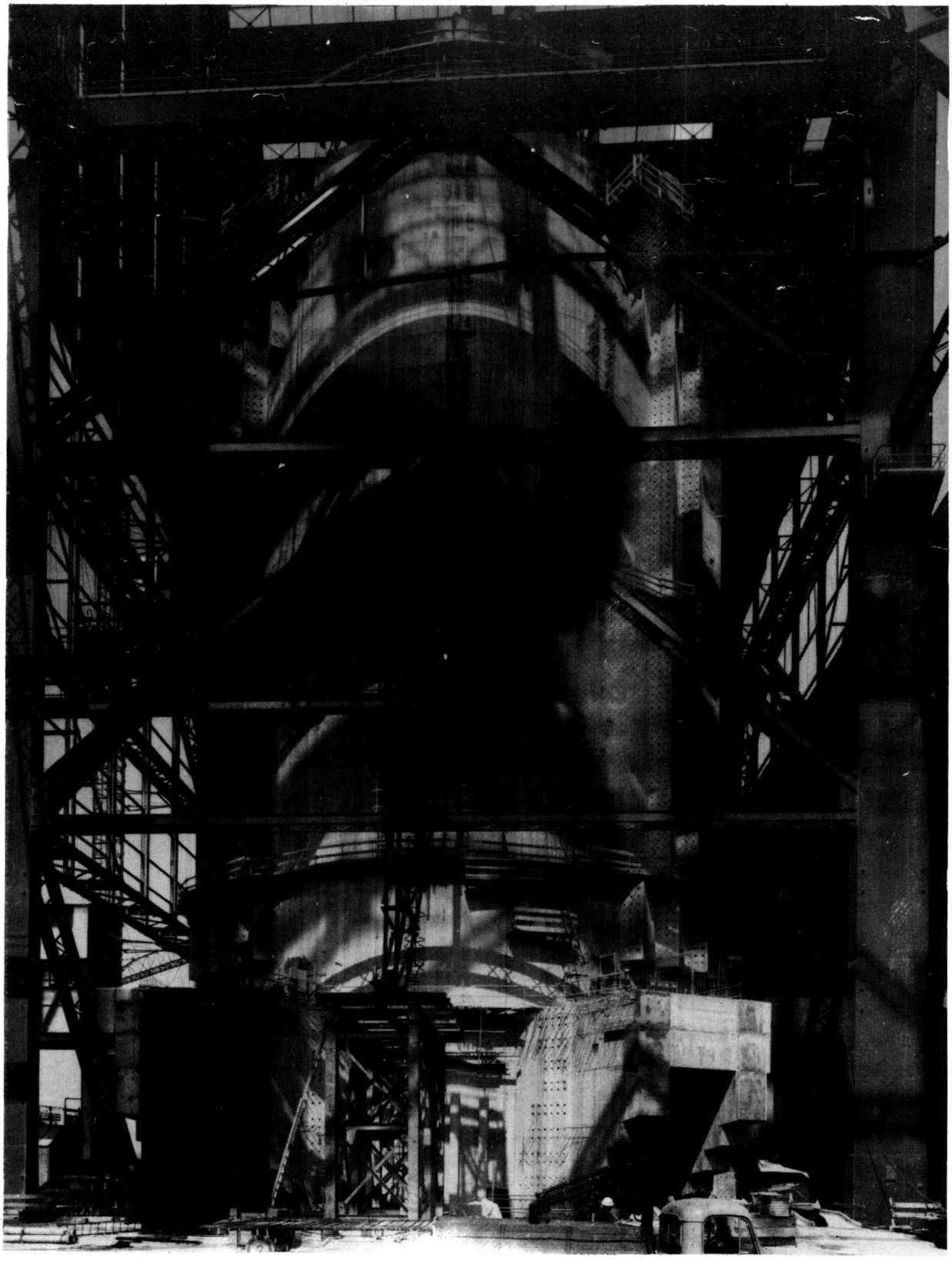

Figure 1 Caisson BUGEY 1 en construction.
Pressure vessel BUGEY 1 in construction.
Druckbehälter BUGEY 1 im Aufbau.

Cet ouvrage est remarquable par ses dimensions et par les sollicitations auxquelles il est soumis en service. Les figures 2 et 3 schématisent le coffrage et la précontrainte de l'ouvrage. Les caractéristiques principales sont :

- Diamètre intérieur	17,10 m
- Hauteur intérieure	40,125 m
- Epaisseur de la paroi cylindrique	5,50 m
- Epaisseur des dalles des fonds	7,50 m

La précontrainte est assurée par 4 200 t de câbles du type BBRB 54 Ø 7 placés sous gaines injectées. L'ouvrage est revêtu intérieurement d'une peau d'étanchéité en acier de 25 mm d'épaisseur portant un calorifuge et un circuit de refroidissement. La dalle supérieure est perforée de 942 puits formant le "bloc tubulaire supérieur" : cette disposition interdit le passage de câbles radiaux.

2 - Sollicitations

Le caisson doit pouvoir supporter, dans les conditions de service une pression interne absolue de 46 b et une différence de température entre faces interne et externe du béton de 35°C.

3 - Sécurité, contraintes admises

On ne saurait manquer de rappeler l'importance de la notion de sécurité pour de tels ouvrages. A l'époque à laquelle le caisson a été entrepris il n'existait pas de réglementation particulière pour ce type de structure, soumise à un gradient thermique important (depuis, une codification a été précisée par l'Arrêté Ministériel du 15 juin 1970). Par référence aux ouvrages dépendant du Ministère des Travaux Publics le domaine de sécurité du béton a été déduit du domaine de résistance par une réduction homothétique dans le rapport de 1 à 0,42. D'autre part, la pression entraînant la ruine de l'ouvrage devait rester supérieure à 2,5 fois la pression de service. Enfin, comme il s'agissait d'un appareil à pression, le Service des Mines a fait procéder à un essai sous 1,1 fois la pression de service (50,6 b).

4 - Calcul

Le caisson peut être assimilé à un corps de révolution. Toutefois, le rapport des épaisseurs des parois au diamètre ne permet pas de traiter la structure comme une coque mince. SFAC (aujourd'hui CREUSOT LOIRE) et CITRA (aujourd'hui SPIE-BATIGNOLLES et CITRA FRANCE) ont établi en commun un programme de calcul thermoélastique à deux dimensions qui a permis de traiter ce problème. Ce programme se réfère à la théorie de l'élasticité linéaire et utilise la méthode des éléments finis. Développé depuis -notamment pour les structures tridimensionnelles- ce programme a été le départ du sytème de calcul sur ordinateur baptisé "TITUS".

5 - Données numériques relatives aux matériaux

Elles ont fait l'objet d'une expérimentation étendue. Pour le béton, l'on a notamment mesuré les modules de déformation instantanés et différés à trois températures, la résistance mécanique, le retrait, la dilatation thermique. Les paramètres suivants ont par suite été introduits dans les calculs

E_i = 400 000 b

$E_{\infty} = \frac{E_i}{3}$ sous précontrainte

$E_{\infty} = \frac{E_i}{2}$ sous chargement thermique

σ'_{28} = 400 b

σ_{28} = 34 b

α = 8×10^{-6} Coefficient de dilatation

- CAISSON . BUGEY.1.
- PRESSURE VESSEL . BUGEY.1.
- DRUCKBEHÄLTER . BUGEY.1.

- Coupe Verticale
- Vertical Section
- Vertikalschnitt

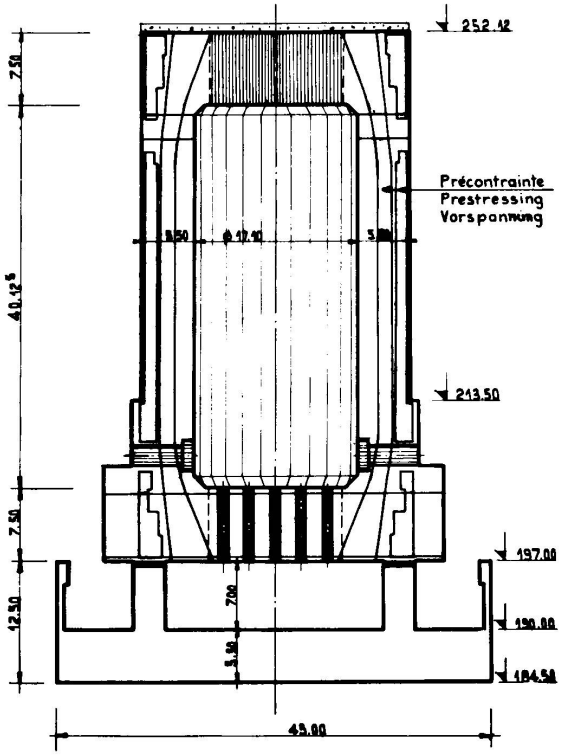

figure .2.

Ech : 0.003

- Coupe Horizontale
- Horizontal Section
- Horizontalschnitt

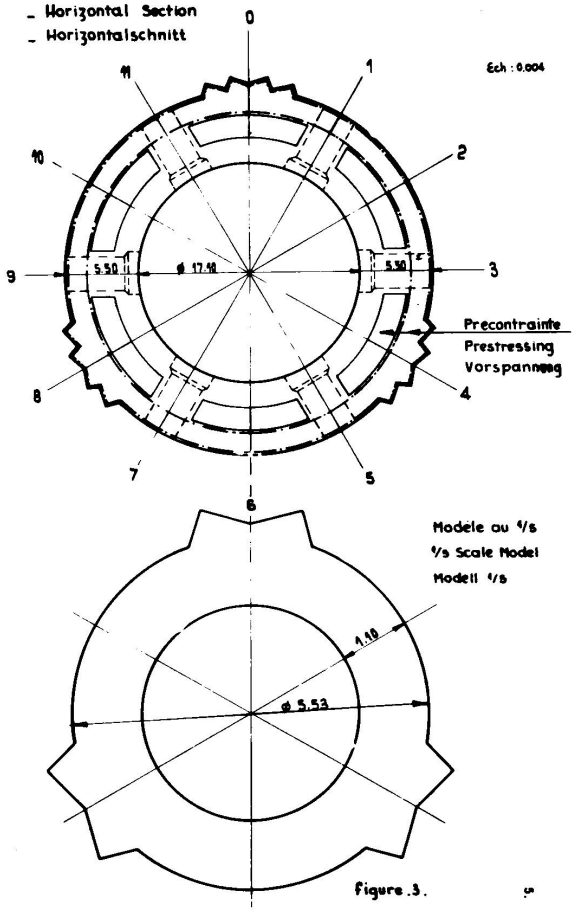

figure .3.

Le coefficient de frottement des câbles de précontrainte dans leurs gaines a été mesuré sur un banc circulaire de diamètre comparable à celui du caisson. La valeur de 0,18 a été retenue.

Le "bloc tubulaire supérieur" forme un complexe béton-acier dont les propriétés ont dû être mesurées sur une maquette particulière. La mesure des déformations sous étreinte circulaire a permis l'obtention des données suivantes

E_i (BTS) = 0,75 E_i (béton seul)

E_{∞} (BTS) = E_{∞} (béton seul)

6 - Maquettes du caisson

Compte tenu de l'état des connaissance et de l'impossibilité de procéder à des essais de réception de l'ouvrage sous pression fortement majorée (ce qui entraînerait la fissuration), il a été décidé de construire deux maquettes complètes. L'échelle du 1/5è a été retenue car elle permet notamment l'emploi d'un béton "réel" (0/15) dont les caractéristiques ne s'éloignent pas de celles du prototype. En outre il reste possible dans ces conditions de placer des capteurs dans le béton sans apporter de perturbations locales (à ce jour les appareils sûrs restent encombrants).

La maquette n°1, dite "froide", était destinée à des essais en pression poussés jusqu'à rupture (obtenue à 124 b).

La maquette n°2, dite "chaude" était plus particulièrement destinée à l'étude des chargements thermiques. Elle a servi à de multiples expériences jusqu'à sa rupture obtenue pour ΔT = 100°C et p = 137 b.

Outre la vérification globale de la validité du calcul, ces maquettes ont, en parallèle avec l'expérimentation "sur éprouvette", servi à l'établissement des paramètres détaillés ci-dessus en II-5.

III - INTERET DE L'INSTRUMENTATION

Le résumé qui vient d'être fait montre tout l'intérêt qu'il y a à disposer d'informations recueillies "in situ" grâce à un dispositif d'auscultation étoffé. Deux buts principaux peuvent lui être assignés : la surveillance et l'information. Vis-à-vis de la sécurité, on peut citer le contrôle des calculs et de leurs données, le pilotage des essais de réception, la surveillance de la durabilité de l'ouvrage. Vis-à-vis de l'information on peut retenir particulièrement l'appréciation des "effets d'échelle" entre éprouvettes et structures massives, l'étude du retrait et du fluage des parois épaisses soumises à un gradient thermique, etc, ..

IV - APPAREILLAGE UTILISE

1 - Pour le caisson

1.1 - Mesures globales de position et de déformation

1.11 - 4 pendules inversés placés suivant deux diamètres. Ces appareils mis au point par EDF (DTG) fournissent des verticales repères. Des tables de lecture sont situées à mi-hauteur du caisson et au niveau de la dalle supérieure

1.12 - 6 repères de nivellement topographique

1.13 - 3 bases de lecture de longueur au fil Invar

1.2 - Mesure des températures

706 thermocouples (dont 446 dans le béton, du type PYROTENAX T 10 C)

1.3 - Mesure des déformations locales

1.31 - 318 extensomètres à corde vibrante (témoins sonores) du type TELEMAC F2 (longueur 254 mm)

1.32 - 250 rosettes d'extensomètres à fil résistant collées sur la peau d'étanchéité métallique

1, 4 - Mesure des forces de précontrainte

20 dynamomètres montés sur 6 câbles verticaux (une extrémité) et 7 câbles horizontaux (deux extrémités), du type SERIM. Ces appareils sont placés sous les ancrages, la mesure s'effectue par l'intermédiaire d'un anneau comprimé équipé de jauges électriques. Notons que les gaines des câbles correspondants ne peuvent être injectées : elles sont balayées en permanence par un courant protecteur d'air sec.

1, 5 - Mesure de la teneur en eau du béton

15 hygromètres. Ces appareils mis au point par EDF (SERNUTH) déduisent l'humidité du béton de sa résistance électrique.

2 - Pour les maquettes

Les deux maquettes ont reçu une instrumentation similaire, adaptée à leur but respectif, notamment :

Maquette n°1 = 238 témoins sonores, 10 thermocouples
Maquette n°2 = 250 " " 133 "

Les témoins sonores étaient du type TELEMAC C 90, (longueur 120 mm

3 - Salle de mesures

Une salle d'enregistrement automatique des lectures a été installée pour le caisson et pour les maquettes. Une lecture complète des appareils conduit au recueil de plus de 1 000 informations. Seules de telles installations permettent de "saisir" l'état de contrainte lorsque la pression varie rapidement.

V - REMARQUE SUR L'IMPLANTATION DES EXTENSOMETRES

Il faut savoir placer efficacement et ceci quel que soit l'ouvrage instrumenté un certain nombre de capteurs, limité par les possibilités budgétaires. Il faut en outre se rappeler les deux buts : surveillance et information, qui peuvent être contradictoires. Dans un ouvrage cylindrique type BUGEY 1 une solution apparue comme bonne est d'équiper largement une section méridienne, et légèrement 5 autres. Il faut éviter le "saupoudrage" qui empêche les corrections par continuité. De même, les points de mesure doivent être groupés en files d'au moins 4 ou 5, perpendiculaires aux parements du béton.

Enfin, on utilisera les symétries pour réduire le nombre de capteurs placés en chaque point de mesure. On pourra voir cette disposition sur la figure 8 . Dans tout ouvrage -surtout s'il s'agit d'un caisson nucléaire- les contraintes thermiques, particulièrement en régime transitoire, peuvent être importantes : il est toujours nécessaire de placer un thermocouple à chaque point de mesure extensométrique.

VI - PROGRAMME DE MESURES

Il est important de prévoir à l'avance un calendrier des mesures, le relevé de tous les appareils étant faits à l'occasion d'états de sollicitation caractéristiques. Il est notamment indispensable, en vue de l'exploitation des mesures de relever les "zéros" avant ou après une phase d'essai. Pour le caisson BUGEY 1, dans la période qui intéresse la présente communication, le déroulement des opérations principales a été le suivant : (voir figure 4)

Précontrainte	6 - 1969 à 4 - 1970
Essais en air sans pression	6 - 1971
Essais en CO_2 en pression	8 - 1971 à 12 - 1971
Essai final (Service des Mines)	1 - 1972

Les lectures exploitées vont du "zéro avant précontrainte" au "zéro après essai final". Elles correspondent à un an et demi du premier âge du caisson et permettent d'observer une part significative du fluage et de la relaxation des matériaux.

VII - EXPLOITATION DES MESURES PRISES SUR LE CAISSON

1 - Thermocouples

Durant les essais la température de la cavité intérieure a fréquemment varié et les régimes thermiques dans le béton ont gardé un caractère transitoire. On peut toutefois noter que les modifications de température se propagent plus vite que ne le laissent prévoir les essais de conductivité thermique en laboratoire : on peut voir là l'influence des éléments métalliques noyés. Il a été également possible de constater que le calorifuge avait d'excellentes qualités. Pendant ce temps les canalisations extérieures chauffaient l'air du hall abritant le réacteur. En conséquence, les gradients thermiques tendaient à disparaître, voir à s'inverser par rapport aux hypothèses du calcul. Lors des essais en CO2 en septembre 1971, tous les gradients étaient négligeables (voir figure 5).

Cette circonstance remarquable permet d'attribuer aux variations de pression seules, les variations des lectures des capteurs à cette époque. Il n'a pu en être de même lors de l'essai final (voir figure 5), mais le caisson ayant été dégonflé rapidement la température n'a pas sensiblement évoluée pendant cette opération et encore une fois les capteurs n'ont enregistré que l'effet de la chute de pression.

2 - Dynamomètres

La figure 6 montre l'évolution dans le temps des forces mesurées au moyen des dynamomètres, c'est-à-dire la tension des câbles instrumentés au voisinage de leurs ancrages. Les courbes correspondent à la moyenne des observations pour les câbles verticaux et horizontaux. Lors du blocage initial la force est de 275 t, celle-ci s'abaisse début 1972 à 235 t pour les cerces et 240 t pour les câbles longitudinaux. Ces valeurs sont supérieures de 7% et de 5% respectivement à celles calculées pour les conditions de service à long terme.

- Essais en pression et température
- Pressure and temperature tests
- Druck und Temperatur prüfung

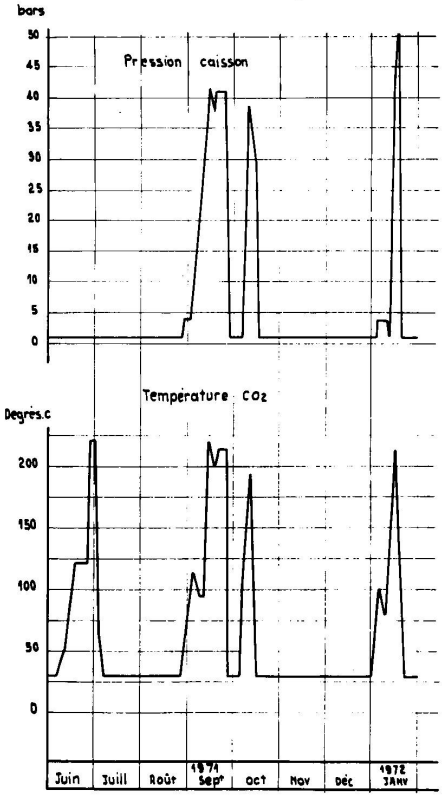

Figure.4.

- Températures dans le béton
- Temperatures in the concrete
- Temperature im Beton

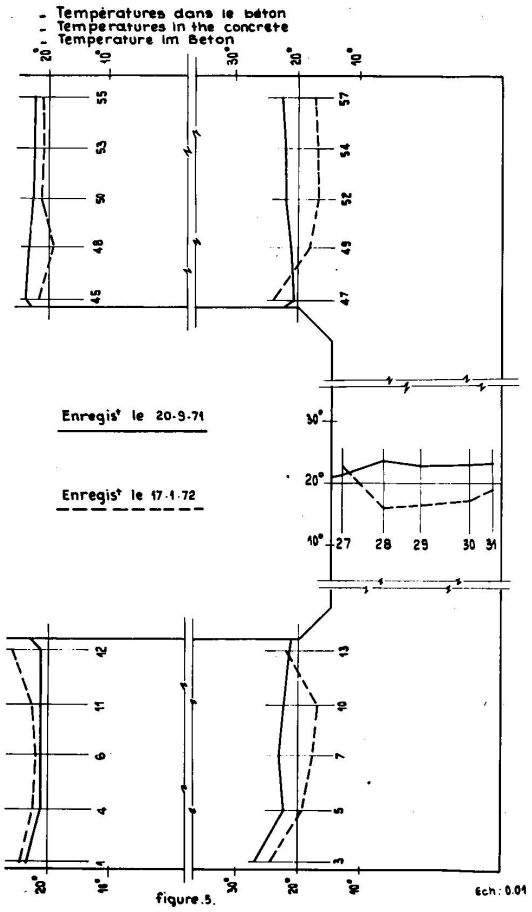

figure.5.

Ech: 0.01

Compte tenu des causes d'imprécision de la comparaison calcul-mesure, notamment en ce qui concerne l'effet de la température sur la relaxation de l'acier, on peut considérer que les hypothèses prises pour le calcul ont été convenables. Conformément aux prévisions, l'élévation de la température de l'ouvrage fait baisser la tension des dynamomètres, du fait de la différence des coefficients de dilatation entre l'acier et le béton. Les valeurs observées varient de 1 à 3 t. L'effet de la mise en pression sous 41 b entraîne d'autre part une surtension des cerces, (à mi hauteur), de 2, 34 t. Enfin, comme on le verra plus loin, les dynamomètres permettent le "calage" des modules de déformation utilisés pour l'exploitation des lectures des témoins sonores.

3 - Pendules inversés

Les observations en température sans pression sont peu intéressantes (sauf pour le contrôle de la verticalité de l'ouvrage), car les déformations tant calculées que mesurées sont inférieures au millimètre. La figure 7 montre la variation d'un rayon correspondant à deux essais en pression accompagnés de variations thermiques négligeables. La linéarité et la réversibilité des déformations sont satisfaisantes. Celles-ci correspondent à un module de déformation global de l'ordre de 400 000 b.

4 - Extensomètres sur peau d'étanchéité

Les jauges étaient groupées en panneau dans la partie courante du fût -. EDF (DTG) a procédé à l'exploitation des lectures. A la fin de la mise en précontrainte du caisson les résultats étaient les suivants :

σ_C (circonférentielle) = $16,2 \pm 0,7$ hb

σ_Z (longitudinale) = $10,4 \pm 0,7$ hb

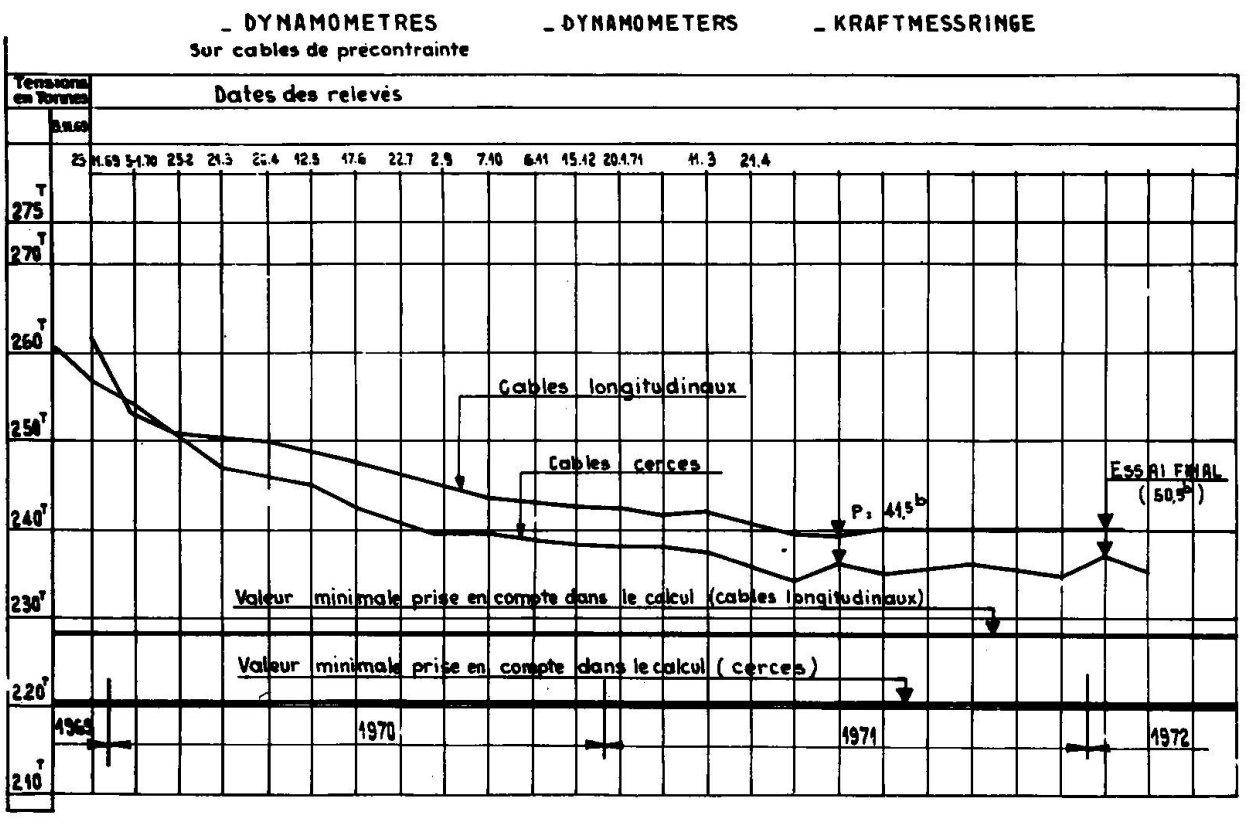

figure . 6.

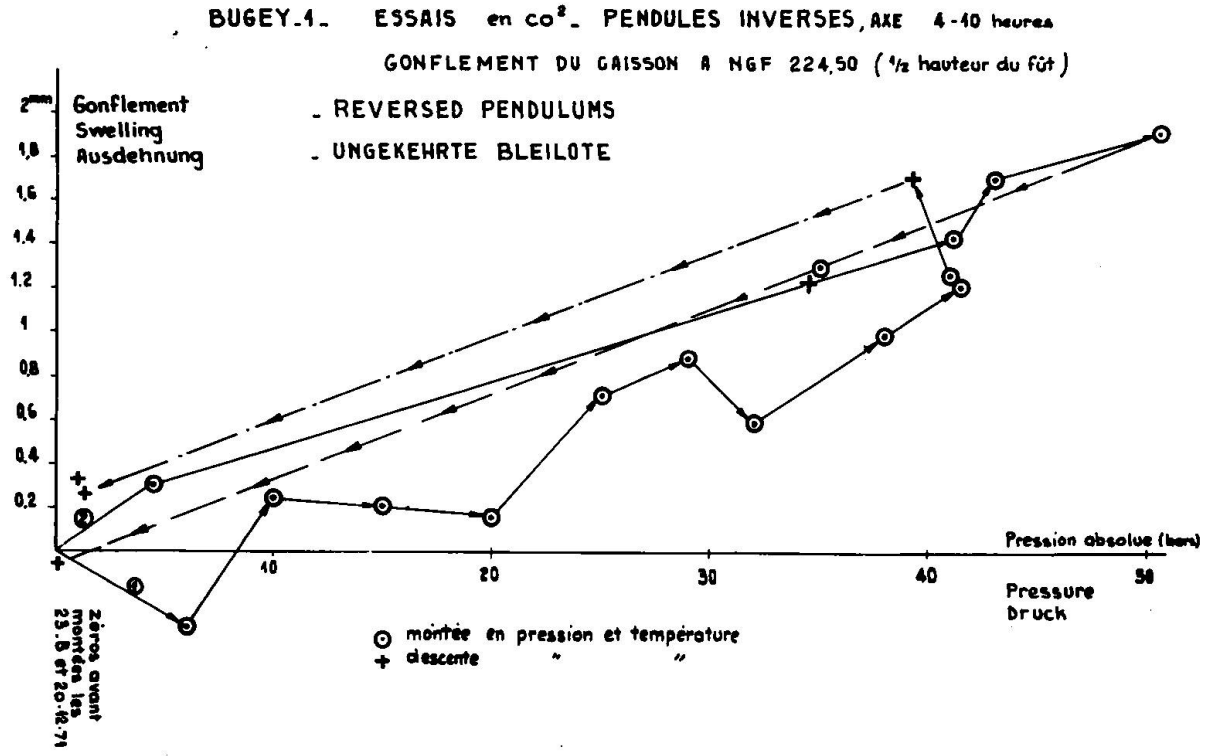

figure . 7.

Les déformations enregistrées par les jauges collées sur le métal et les témoins sonores noyés dans le béton les plus proches étaient remarquablement concordantes (651×10^{-6} et 624×10^{-6} pour σ_c par exemple). Il y a une correspondance convenable entre calculs et mesure si l'on affecte au béton un module de déformation partiellement différé de 250 000 b à cette époque, cette dernière valeur étant par ailleurs en accord avec les indications des dynamomètres.

On a pu observer également une bonne correspondance entre les valeurs calculées et mesurées lors des essais, puis les jauges ont été abandonnées en raison notamment de leur dérive.

6 - Témoins sonores

La figure 8 montre l'implantation des 171 témoins sonores, groupés en 72 points de mesure, qui ont fait l'objet des lectures les plus fréquentes pendant les essais. Les informations ainsi recueillies ont été utilisées pour le pilotage des essais, c'est-à-dire la conduite avec sécurité des opérations de mise en température et pression. Il fallait donc procéder à l'exploitation immédiate des lectures.

Dans ce but, EDF (DTG) et CITRA ont établi un programme de calcul sur ordinateur, baptisé "TSONO". Celui-ci calcule les déformations et les contraintes à partir des fréquences des cordes vibrantes et de leur température. Il fait appel aux formules de l'élasticité et nécessite certaines données numériques. Les valeurs suivantes ont été fixées :

Coefficient de dilatation acier	12×10^{-6}
Coefficient de dilatation béton	8×10^{-6}
Coefficient de POISSON	0,20

Le module de déformation E doit être adapté au cas de chargement concerné. La validité de la valeur prise est vérifiée en comparant la résultante des efforts internes déduits de l''exploitation des témoins et la force extérieure appliquée (précontrainte d'après les dynamomètres, ou pression).

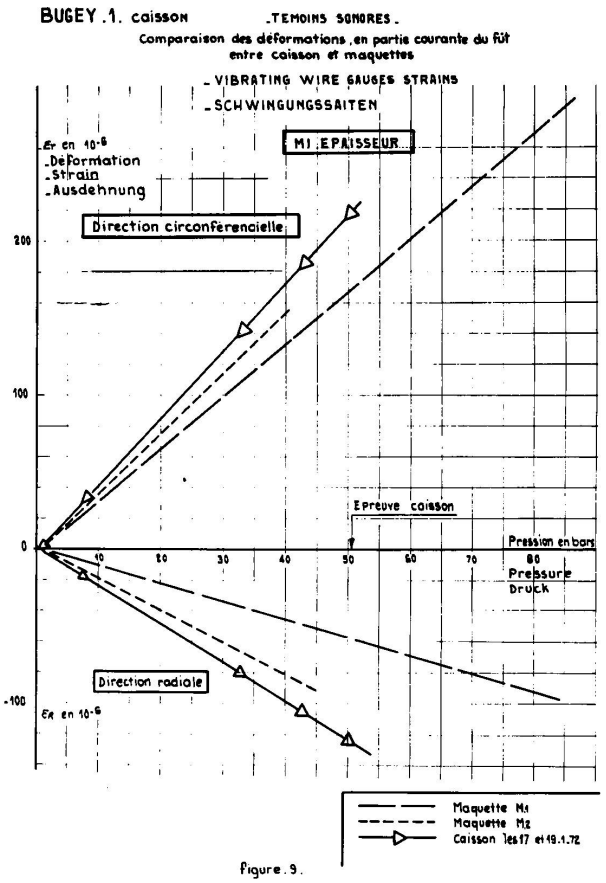

Figure.9.

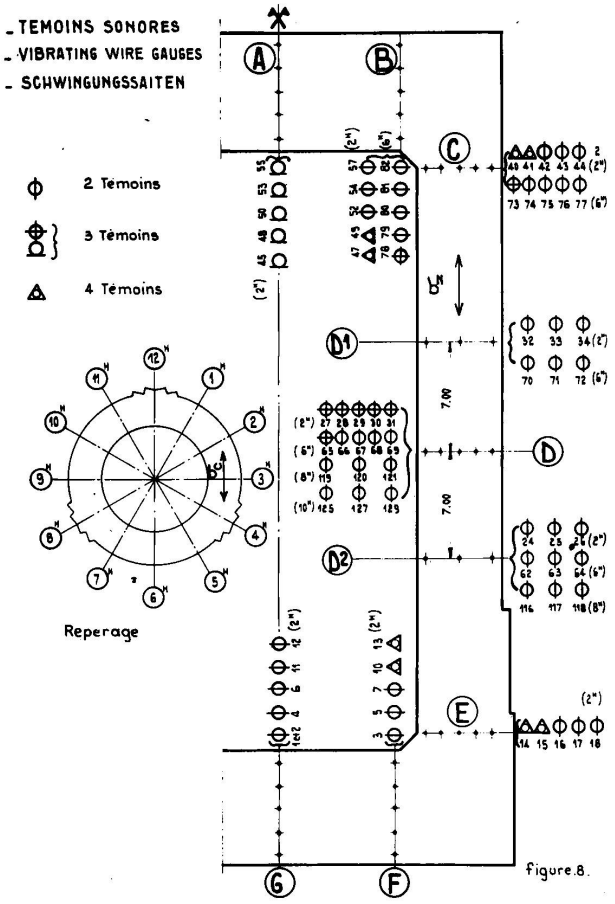

Figure.8.

Les valeurs suivantes de E se sont montrées les plus convenables :

- Pour la pression seule $E_C = E_Z =$ 370 000 b

- Pour la précontrainte à l'époque des essais
  $E_C =$ 170 000 b
  $E_Z =$ 140 000 b

On voit donc apparaître une certaine anisotropie. D'autre part, pour enlever plus rapidement les raidisseurs de la peau d'étanchéité, on a coulé d'abord autour de celle-ci un "corset" de 70 cm d'épaisseur intégré ultérieurement au béton du fût cylindrique. Les témoins sonores placés dans ce corset ont enregistré au cours de la mise en précontrainte de l'ouvrage des déformations correspondant à un module inférieur au module moyen de la structure.

La figure 9 montre les déformations notées en partie courante du fût, à mi-épaisseur du béton. On peut noter la remarquable linéarité des diagrammes.

Les figures 10 et 11 montrent la comparaison calcul-mesure pour σ_c et σ_z à mi-fût dans les cas précontrainte seule et précontrainte plus essai à 41,5 b (avec gradient thermique négligeable, comme on l'a vu en VII. 1).

VIII - EXPLOITATION DES MESURES PRISES SUR LES MAQUETTES, COMPARAISON AVEC LE CAISSON

Nous ne détaillerons pas l'exploitation des mesures prises sur les maquettes, travail similaire à celui exposé en VII. La comparaison calcul-mesure s'est montrée satisfaisante. Il est difficile de pouvoir comparer avec exactitude maquette et prototype : l'histoire des bétons et les états thermiques sont toujours différents aux époques des mesures. La figure 9 groupe des déformations correspondant au caisson et aux deux maquettes.

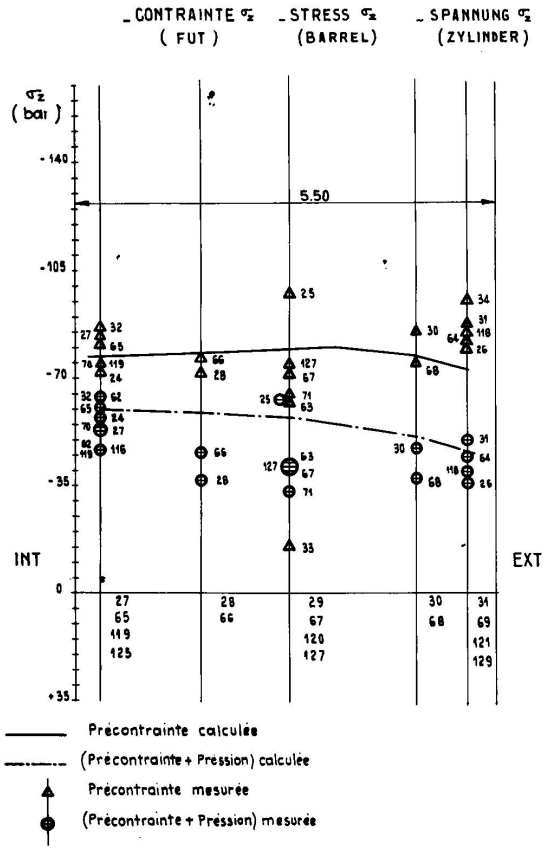

Figure.11.

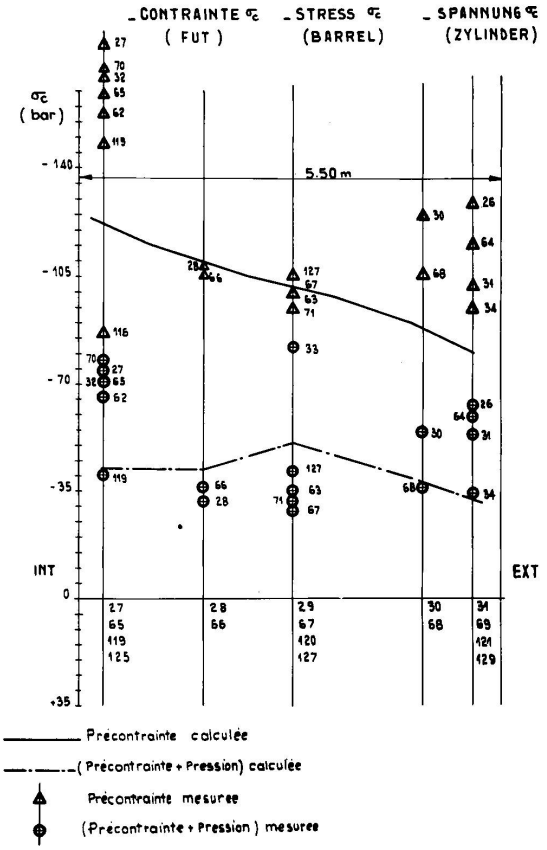

Figure.10.

RESUME

Le caisson en béton précontraint de la centrale nucléaire BUGEY 1 a été construit de 1967 à 1970. Ses caractéristiques principales sont : diamètre intérieur 17,10 m, pression interne 46 b, poids des câbles de précontrainte 4 200 t.

La dalle supérieure ne comporte aucun câblage transversal en raison de la présence d'un bloc tubulaire.

Les études ont été accompagnées d'une large expérimentation comprenant deux maquettes à l'échelle du 1/5e. En raison du caractère exceptionnel de la structure de nombreux dispositifs de mesure ont été installés : pendules inversés, thermocouples, cordes vibrantes, jauges à fil résistant, dynamomètres etc, ...

La présente contribution analyse les informations fournies par ces appareils pendant les essais du caisson, de juin 1971 à janvier 1972.

Les résultats des mesures et des calculs sont comparés, la concordance est satisfaisante.

SUMMARY

The Prestressed Concrete Pressure Vessel of BUGEY I Nuclear Power Reactor was erected between 1967 and 1970, the main features of which being :

- Internal diameter : 17.10 m
- Operating pressure : 45 bars
- 4,200 t of prestressing tendons.

The upper slab has no transverse cabling because of the shape of the standpipes unit.

The studies involved a wide range of tests, including tests performed on two 1/5 scale models. Owing to its unique features, numerous measuring devices such as "reversed pendulums", thermocouples, vibrating wires, electrical strain-gauges and dynamometers etc... were placed in the concrete structure.

This paper analyses the results obtained by means of these devices during the tests period, from June 1971 to January 1972. Concordance of the test results with calculations is satisfactory.

ZUSAMMENFASSUNG

Der Spannbetondrückbehälter des Kernkraftwerks BUGEY I ist in den Jahren 1967 bis 1970 gebaut worden. Die wichtigsten Merkmale folgen hier :

Innendurchmesser : 17,10 M
Betriebsdrück : 46 Bars
Gewicht der Spannglieder : 4200 T

Die Deckplatte enthält keine Querbewehrung infolge der Anwesenheit eines Hohlzylinderblocks.

Die Untersuchungen umfassten viele Prüfungen und die Ausprobung von zwei auf 1/5 verkleinerten Versuchsmodellen. Der ausserordentlichen Art des Bauwerks wegen, wurden zahlreiche Prüfungsgeräte eingesetzt, wie zum Beispiel : umgekehrte Bleilote, Temperaturgeber, Schwingungssaiten. Dehnungsmeszstreifen, Kraftmessringe, usw.

Dieser Bericht analysiert die Ergebnisse dieser Geräte während der Prüfungszeit des Behälters, ab Juni 1971 bis Januar 1972.
Der Vergleich der Ergebnisse der Bemessungen entsprach den Berechnungen zur Genüge.

Leere Seite
Blank page
Page vide

IABSE
AIPC
IVBH

SEMINAR on:
« CONCRETE STRUCTURES SUBJECTED TO TRIAXIAL STRESSES »
17th - 19th MAY, 1974 - ISMES - BERGAMO (ITALY)

Analysis of Podded Boiler Type PCPV with Reference to the Analysis of Solid of Revolution

Analyse d'un caisson en béton précontraint du type «Podded Boiler» avec référence à l'analyse d'un solide de révolution

Die Berechnung eines «Podded Boiler Type PCPV» als Umdrehungs Körper

S. KAWAMATA
Associate Professor, Institute of Industrial Science
University of Tokyo, Tokyo, Japan

SUMMARY

Simplified finite element three-dimensional elastic analysis of the podded boiler type PCPV is discussed.

The first part deals with consistent method of assessing the effective rigidity of standpipe zone, where finite element analyses of the unit area of regular hole pattern are utilized.

In the second part "method of sliced substructures", a new method of simplified three-dimensional analysis of PCPV is proposed. The stiffness of PCPV is evaluated as the combination of stiffness matrix of modified axi-symmetric problems and two-dimensional stiffness matrices of horizontally sliced substructures. This method enables us to analyze the three-dimensional problems of PCPV allowing for the effect of boiler pods within the same degrees of freedom as the axi-symmetric analysis.

The validity of the new method is shown by numerical examples.

1. INTRODUCTION

The finite element method has been widely accepted in the structural analysis for the design of PCPV because of its efficiency, accuracy and adaptability to the general purpose programs. Starting from elastic analysis, the scope of the finite element analysis in the PCPV design has been broadened to wider fields of heat conduction problem, time dependent creep problem, tracing of cracking and failure process, etc.

For the design of PCPV of the gas-cooled reactors and the advanced gas-cooled reactors, the finite element analysis in the form of axi-symmetric problems of body of revolution was efficiently adapted, resulting high accuracy with small degrees of two-dimensional freedom.

However, as discussed in the review by Argyris et.al.[1], having various kinds of openings such as standpipe zone in the top slab and coolant circulator deposits, stress in PCPV has some discrepancies from the axi-symmetric condition.

The effect of the multiple perforations of standpipe zone has been taken into account by simply reducing the elastic constant within the framework of the axi-symmetric analysis [2,3,4]. But the consideration of the stress disturbance induced by major openings gives rise to necessity of three-dimensional analysis [5].

In the early stage, the three-dimensional finite element analysis, having very large degrees of freedom and band width of the system stiffness matrices, required huge amount of memory, computing time, labour for input data preparation and consequently high cost of analysis. The development of the iso-parametric element technique [6] put the cost of the three-dimensional elastic analysis of PCPV in the range of reasonable investment for the design purpose [1,7].

The geometry of the podded boiler type PCPV recently developed for AGR and HTGR, having vertical cavities within the thickness of vessel wall, leads to the indispensable practice of the three-dimensional analysis for each phase of design, i.e. elastic, time-dependent and failure analyses. Even the most efficient program of three-dimensional elastic analysis seems to require more than ten times of computation time compared with the corresponding axi-symmetric analysis of the same accuracy. Even if this situation is acceptable for the elastic analysis, the cost of three-dimensional creep and failure analyses, which involve numerous repetition of stress redistribution process, will amount to unrealistic one as a tool for the structural design. Lewis et.al.[4] discussed this problem and suggested the use of simply rough mesh of element idealization. But rather poor representation of strain distribution shown in his example cautions us to the possibility of getting inaccurate results which will be caused by the errors accumulated in the course of repeated steps.

Thus, when considering the step analyses for the long-term and failure situation, the type of finite element three-dimensional treatment must be determined on the balance between the cost and labour of computation and the accuracy of the results obtainable at these expense. In this sense, more efficient scheme of the three-dimensional finite element elastic analysis of PCPV, which can provide

the acceptable accuracy within computing time not much exceeding the one required for the axi-symmetric problems, is worth searching.

The object of this paper is to present a new scheme of simplified finite element three-dimensional elastic analysis of the podded boiler type PCPV, in which a modified axi-symmetric treatment of solids of revolution combined with condensed stiffness matrices of two-dimensional "sliced substructures" is utilized.

The first part of the paper describes the transformation of the standpipe zone of top slab into an equivalent homogeneous transversely isotropic medium which enables more consistent treatment of axi-symmetric analysis than in the case of simple reduction of Young's modulus done in the previous practices [4]. By the two-dimensional finite element analyses of the unit area formed by the regular patterns of perforations, each of the elastic constants of the equivalent transversely isotropic body is assessed. The same type of the unit zone analysis was done by Meijers [8,9]. The present method has been developed by the author with collaborators since 1967 [10]. It includes the evaluation of the equivalent transverse shear modulus and constitutes an important part of the new method of modified axi-symmetric analysis.

The latter half of the paper devoted to the description of "method of sliced substructures". In the method of sliced substructures, the three-dimensional portion to be analysed is divided into a number of horizontally sliced layers which have the shape of partial rings having a circular opening of the boiler pod in them.

A dual system of assumed displacement field is adopted. For the system of the structural resistance in the direction of the vertical z-axis and the shearing resistance of the vertical r-z plane, the well known displacement mode of axi-symmetric problems is assumed, i.e. two-dimensional displacements u and w which are constant along the circumference are taken. Similarly to the axi-symmetric case, the stiffness based on this system of resistance is evaluated with regard to the nodal points in the vertical plane of symmetry with regard to the specified resistance.

On the other hand, the resistance formed by the strain in horizontal plane is evaluated separately for each layer of the horizontal slices; each slice is devided into a two-dimensional finite element mesh in r-θ plane and the stiffness matrix for the total slice area is formed as the ordinary plane stress problem. Then the unknown displacements of the interior part of the slice are eliminated by the static condensation, only the nodal displacements in the radial direction u on the plane of symmetry being retained as unknowns. The displacement assumed for this system of horizontal resistance has two-dimensional freedom in r-θ plane but is constant within the thickness of the slice.

Both stiffness matrices, one representing axial and shearing resistance and the other the resistance in the horizontal plane, are combined on the vertical section of symmetry, taking the nodal displacements u in the both system as the same unknown. This means the final system equation has the same degrees of freedom as the

axi-symmetric problems, i.e. twice the number of nodes in the vertical section of symmetry.

In this scheme, dual mode of the displacement is assumed, namely different assumptions of displacements are adopted for the two groups of stresses.

Therefore, the present method can be interpreted as a kind of the method of partial approximation, which has lately been investigated by Kikuchi in the field of finite element shell analysis [11-13]. The assumed horizontal displacement fields in the sliced substructures contain incompatibility in the boundary surfaces between upper and lower layers, and the convergence criteria is not yet clear for the present scheme of approximation. Therefore, the validity and the efficiency of the method must be investigated by numerical experiments on the actual problems of podded boiler PCPV.

2. EFFECTIVE ELASTIC COEFFICIENTS OF STANDPIPE ZONE

A method of evaluating the effective elastic constants of the homogeneous medium equivalent to the standpipe zone of triangular hole pattern is described here. Because of the regular pattern of hole arrangement the effective rigidity in respective directions can be assessed by finite element two-dimensional analysis of the constituent unit area of the zone.

Transformed homogeneous body is in general anisotropic. As the cylindrical openings have the axis in the vertical z-direction, it is clear that the equivalent continuum has the different elastic coefficients in z-direction and in r-θ plane. In the r-θ plane, it will have anisotropy of different kind according to the hole pattern. When applying the three-dimensional finite elements for this zone in the analysis of the total vessel, any kind of orthotropy can be assigned to this part. But in order to apply the axi-symmetric analysis for the vessel, transformation into an equivalent transversely isotropic body is required and the averaging of the coefficients is neccessary, when they have different values in different directions.

Fortunately, a triangular hole pattern, having three equiangular lines of symmetry, necessarily leads to isotropy in the horizontal plane, resulting the unique solution of equivalence for the transformed transversely isotropic body. This condition of the triangular pattern allows us to obtain all the elastic coefficients by analyzing the single unit area.

The elastic coefficients for the transversely isotropic body contain 5 parameters and can be given in the following form [14-16].

$$\begin{Bmatrix} \sigma_x \\ \sigma_y \\ \sigma_z \\ \tau_{yz} \\ \tau_{xz} \\ \tau_{xy} \end{Bmatrix} = \begin{bmatrix} d_1 & & & & & \\ d_2 & d_1 & & & \text{symmetry} & \\ d_3 & d_3 & d_4 & & & \\ & & & d_5 & & \\ & & & & d_5 & \\ & & & & & (d_1-d_2)/2 \end{bmatrix} \begin{Bmatrix} \varepsilon_x \\ \varepsilon_y \\ \varepsilon_z \\ \gamma_{yz} \\ \gamma_{xz} \\ \gamma_{xy} \end{Bmatrix} \tag{1}$$

In contrast, in the case of isotropy, we have two-parameter coefficients as

$$\begin{Bmatrix}\sigma_x\\ \sigma_y\\ \sigma_z\\ \tau_{yz}\\ \tau_{xz}\\ \tau_{xy}\end{Bmatrix} = \begin{bmatrix} d_1^0 & & & & & \\ d_2^0 & d_1^0 & & \text{symmetry} & & \\ d_2^0 & d_2^0 & d_1^0 & & & \\ & & & (d_1^0-d_2^0)/2 & & \\ & & & & (d_1^0-d_2^0)/2 & \\ & & & & & (d_1^0-d_2^0)/2 \end{bmatrix} \begin{Bmatrix}\varepsilon_x\\ \varepsilon_y\\ \varepsilon_z\\ \gamma_{yz}\\ \gamma_{xz}\\ \gamma_{xy}\end{Bmatrix} \qquad (2\text{-a})$$

where

$$d_1^0 = \frac{(1-\nu)\,E}{(1+\nu)(1-2\nu)}, \qquad d_2^0 = \frac{\nu\,E}{(1+\nu)(1-2\nu)} \qquad (2\text{-b})$$

Let the perforated zone of top slab shown in Fig.1(a) be considered. The hole pattern shown in Fig.1(b) is assumed to be infinitively spread in the x-y plane and the shaded unit area is to be analyzed. The depth of the slab is assumed also to be infinitive in z-direction.

In order to give the infinitive medium the unit strain in the sense of mean value, relative displacements are subjected between a paticular pair of opposite edges of the unit area, while the boundary faces being kept plane because of the conditions of symmetry. The mean stress evaluated from the boundary face reactions yields the neccesary effective coefficients of elasticity.

1) d_4 : Effective Elastic Coefficient for Normal Stress in z-direction

The effective coefficient d_4 for σ_z can be evaluated, in principle, from the resultant reaction R_z which is caused by prescribing vertical displacement $\delta_z = h$ to the top surface as shown in Fig.2(a).

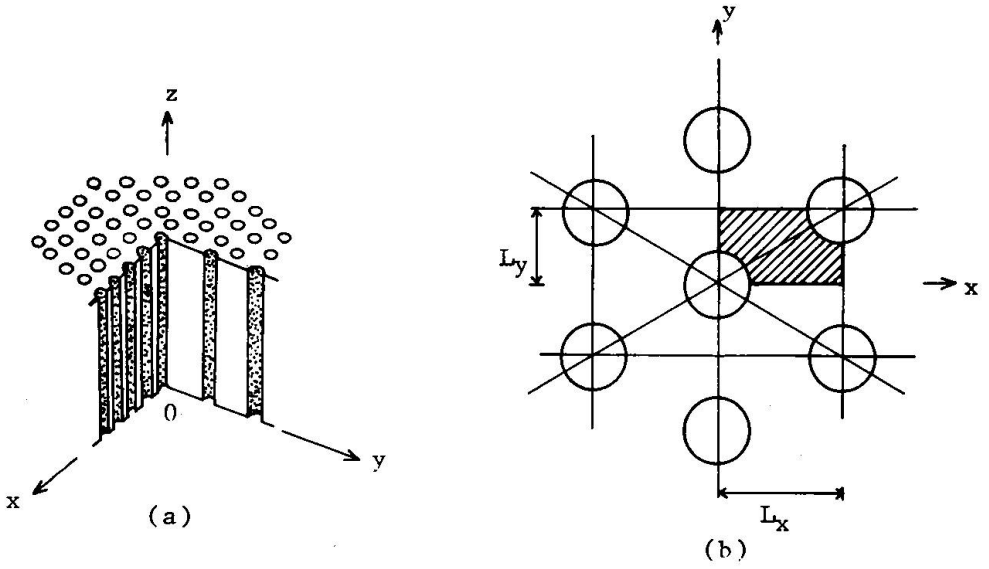

Fig.1 Standpipe Zone and its Hole Pattern

While, this state of stress can be realized also by giving the same displacement to the body, in which the surfaces of the cylindrical holes are constained by rollers, the constraint forces subsequently being released as shown in Fig.2(b). The latter release of constraint will not cause any significant reaction in z-direction when the hole is not very large. Therefore the effective coefficient can be approximately represented by

$$d_4 = \alpha\, d_1^{\circ} \qquad (3\text{-a})$$

where d_1° : coefficient for isotropic case given in Eq.(2-b)

$$\alpha = A/A_o : \qquad (3\text{-b})$$

ratio of perforated to unperforated areas shown in Fig.2(c)

2) d_1, d_2, d_3, : Effictive Elastic Coefficient Derived from Strain in the Plane of Slab

When we put $\varepsilon_x = 1$ in Eq.(1), we have

$$\begin{Bmatrix} \sigma x \\ \sigma y \\ \sigma z \end{Bmatrix} = \begin{Bmatrix} d_1 \\ d_2 \\ d_3 \end{Bmatrix} \qquad (4)$$

Therefore, prescribing displacement $\delta_x = L_x$ as shown in Fig.3, these coefficients can be determined as the mean intensities of the reactions in three directions, i.e.

$$\begin{aligned} d_1 &= \bar{\sigma}_x = R_x/L_y h \\ d_2 &= \bar{\sigma}_y = R_y/L_x h \\ d_3 &= \bar{\sigma}_z = R_z/L_x L_y \end{aligned} \qquad (5)$$

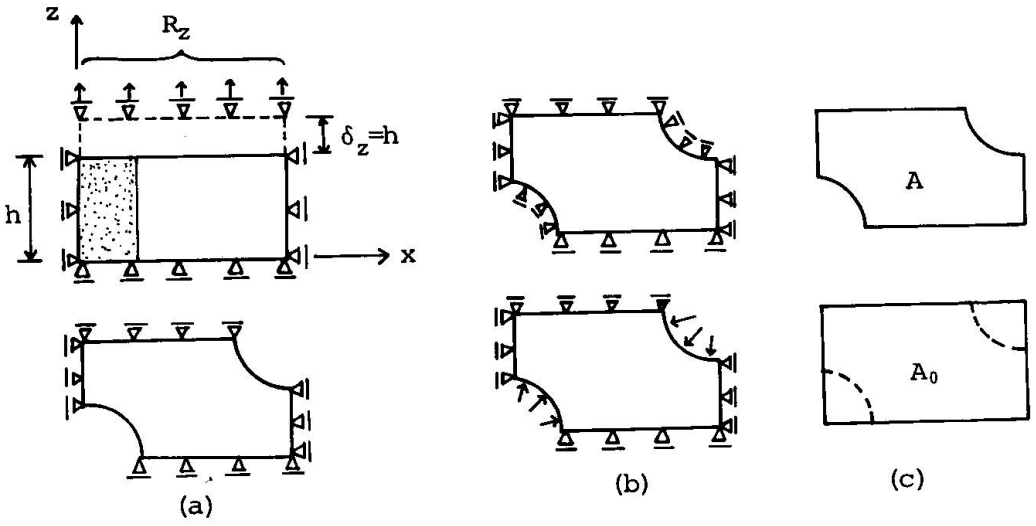

Fig.2 Assessment of Diagonal Coefficient for z-Direction

Besides this, giving $\varepsilon_y = 1$ in the same manner, we have another relation as

$$\begin{Bmatrix} \sigma x \\ \sigma y \\ \sigma z \end{Bmatrix} = \begin{Bmatrix} d_2 \\ d_1 \\ d_3 \end{Bmatrix} \qquad (6)$$

But the coefficients become equal to the ones obtained by the above analysis as the result of the reciprocal theorem.

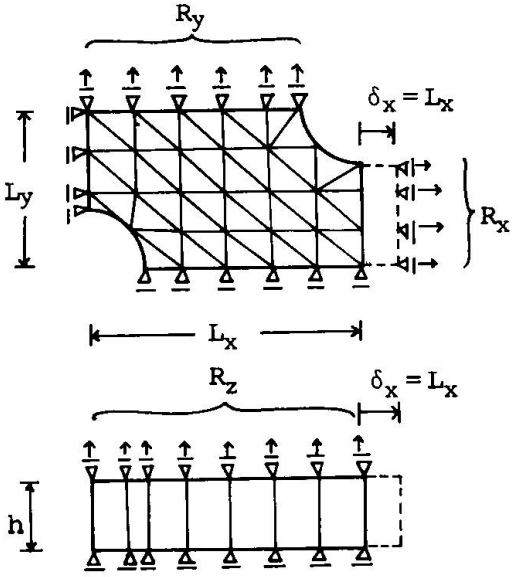

Fig.3 Assessment of Elastic Coefficients d_1, d_2 and d_3

3) d_5 : Coefficient for Transverse Shear

In the infinitive perforated body, an uniform (mean) shearing strain $\bar{\gamma}_{xz}$ is to be prescribed as indicated by Fig.4(a). In order to realize this state, we prescribe $\delta_z = \pm L_x/2$ at the both ends of the solid unit as shown in Fig.4 (b) and (c).

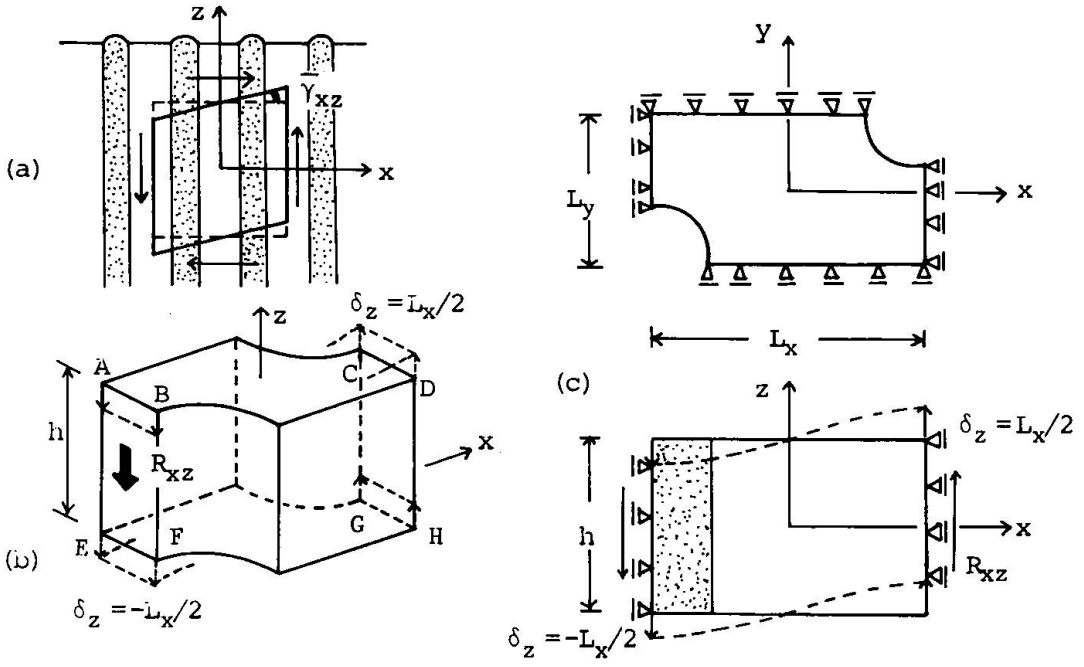

Fig.4 Assessment of Transverse Shear Coefficient, d_5

The resultant vertical force R_{xz} divided gross area of the vertical end face corresponds to the mean shearing stress $\bar{\tau}_{xz}$, leading to the following result :

$$\bar{\tau}_{xz} = \frac{R_{xz}}{L_y h} = d_5 \qquad (7)$$

Though the actual analysis of the solid unit must be carried out by the use of three-dimensional elements, there is no variation of variables in the direction of z-axis from the condition of uniform strain.

Thus, applying the condition of

$$u = u(x,y), \quad v = v(x,y), \quad w = w(x,y) \qquad (8)$$

to the three dimensional nodal displacements, the problem is reduced to two-dimensional one with the stiffness matrix being condensed.

Example of Analysis of Effective Elastic Coefficients

As an example, the effective coefficients for standpipe zone of triangular pattern having the dimensions of

$$\left.\begin{aligned} &L_x = 83\text{cm}, \quad L_y = 48\text{cm} \\ &D = 60\text{cm (diameter of holes)} \end{aligned}\right\} \qquad (9)$$

were analysed. The original moduli of elasticity of the concrete were assumed as

$$E = 3.52 \times 10^6 \text{ kg/cm}^2, \quad \nu = 0.17 \qquad (10)$$

The ratio of perforated to unperforated areas for this example is

$$\alpha = A/A_o = A/L_x L_y = 0.645 \qquad (11)$$

From Eqs.(3) and (11) we obtain

$$d_4 = \alpha d_1' = 0.645 \cdot \frac{(1-\nu)\, E}{(1+\nu)(1-2\nu)} \qquad (12)$$

For obtaining the coefficients d_1, d_2, and d_3, the finite element model shown in Fig.5(a) was analyzed in plane strain state. Prescribed displacements of $\delta_x = L_x$ caused the boundary reactions shown in Figs.5(b) and (c). Vertical reaction resultant R_z was obtained from σ_z in each element using the ralation of

$$\sigma_z = \nu (\sigma_x + \sigma_y) \qquad (13)$$

in the plane strain problem. The final results were calculated as follows :

$$d_1 = \frac{R_x}{L_y h} = \frac{7.23 \times 10^6 \text{kg}}{48.0\text{cm} \times 1\text{cm}} = 1.50 \times 10^5 \text{kg/cm}^2 \qquad (14\text{-a})$$

$$d_2 = \frac{R_y}{L_x\, h} = \frac{3.65 \times 10^6 \text{kg}}{83.0\text{cm} \times 1\text{cm}} = 0.440 \times 10^5 \text{kg/cm}^2 \qquad (14\text{-b})$$

$$d_3 = \frac{R_z}{L_x L_y} = \frac{131.2 \times 10^6 \text{kg}}{48.0\text{cm} \times 83.0\text{cm}} = 0.329 \times 10^5 \text{kg/cm}^2 \qquad (14\text{-c})$$

The reduction of the elastic coefficient from the original solid caused by the perforations can be represented by the following relations :

$$\left.\begin{aligned} d_1 &= 0.396 \times d_1^0 = 0.396 \times \frac{(1-\nu)\,E}{(1+\nu)(1-2\nu)} \\ d_2 &= 0.568 \times d_2^0 = 0.568 \times \frac{\nu E}{(1+\nu)(1-2\nu)} \\ d_3 &= 0.579 \times d_3^0 = 0.579 \times \frac{\nu E}{(1+\nu)(1-2\nu)} \end{aligned}\right\} \qquad (15)$$

The equivalent Young's modulas and Poisson's ratio in x-y plane are correlated to those of the original solid as

$$\left.\begin{aligned} E_1 &= 0.37\, E \\ \nu_1 &= 1.34\, \nu \end{aligned}\right\} \qquad (16)$$

For the analysis of the transverse shear coefficient d_5, a finite element mesh shown in Fig.6(a) was used, where the iso-parametric solid elements of 20 nodes were incorpotated. Prescribing $\delta_z = \pm 1/2\text{cm}$ on both end faces, the nodal vertical reactions shown in Fig.6(d) were obtained. From the resultant $\bar{R}_{xz}$ of these reactions, the shear coefficient was obtained as

$$d_5 = \frac{R_{xz}}{L_y\, h} = \frac{\bar{R}_{xy} L_x}{L_y\, h} = \frac{22.63 \times 10^6 \text{kg/cm} \times 83.0\text{cm}}{48.0\text{cm} \times 564\text{cm}}$$

$$= 0.0694 \times 10^6 \text{kg/cm}^2 \qquad (17)$$

The reduction of the shear coefficient is indicated by the relation

$$d_5 = 0.461\, G \qquad (18)$$

where

$$G = E/2(1+\nu) = (d_1^0 - d_2^0)/2 \;:$$

shear modulas of the unperforated solid

The distribution of the vertical displacement is shown in Fig.6 (b). Fig.6(c) shows the resultant vectors of shear stress component τ_{xz} and τ_{yz} together with its intensity represented by the factor to the mean shearing stress $\bar{\tau}_{xz}$.

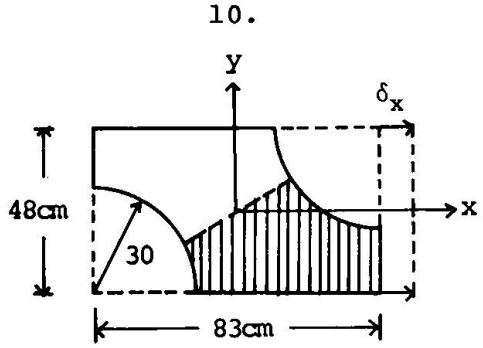

108 elements
73 nodes
for tot. area

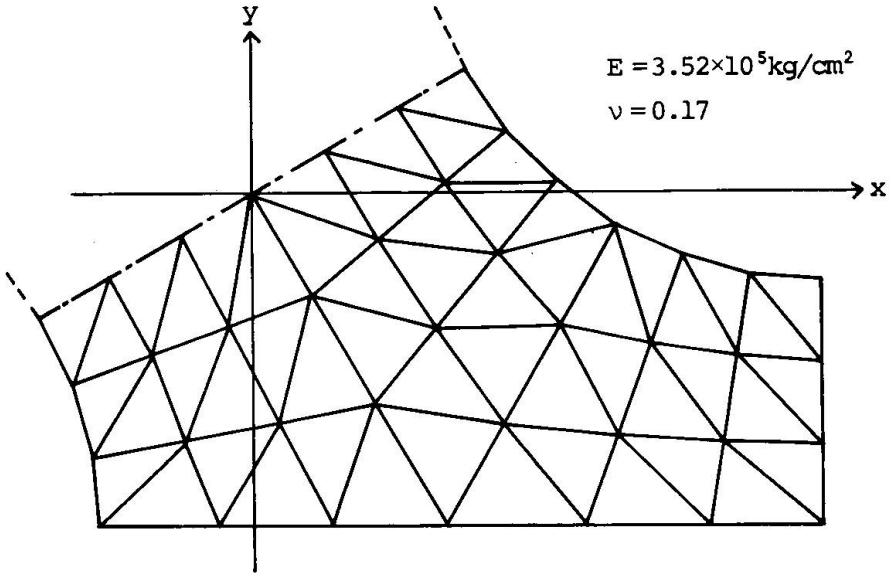

(a) Mesh Division (Plain Strain Problem)

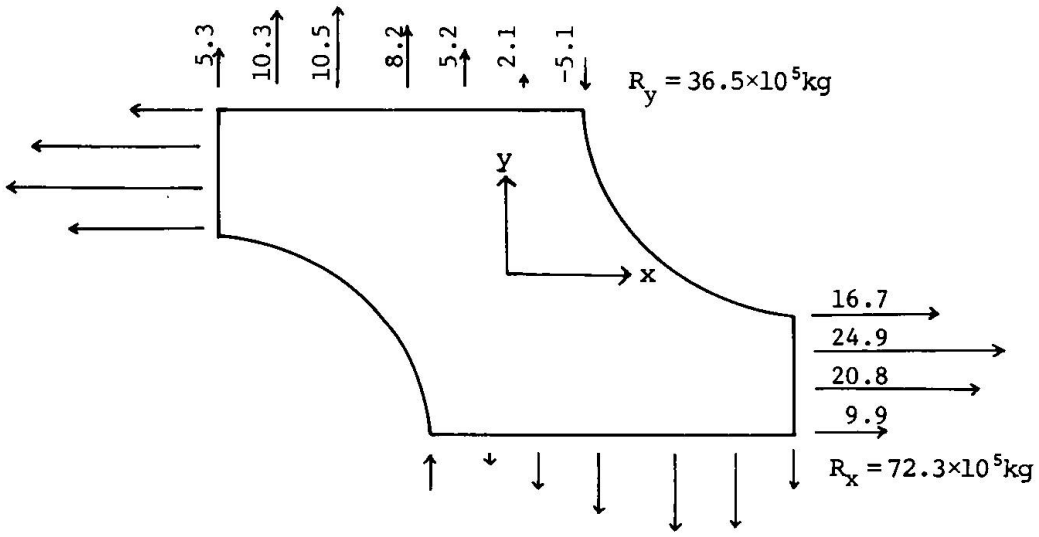

(b) Reactions for Prescribed Displacement $\delta_x = 83$cm

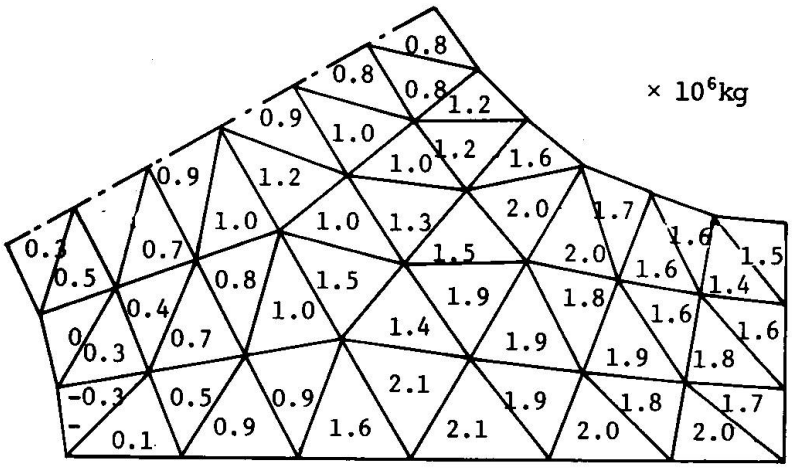

(c) Stress Resultants in z-Direction

Fig.5 Plain Strain Analysis of Unit Area for d_1, d_2 and d_3

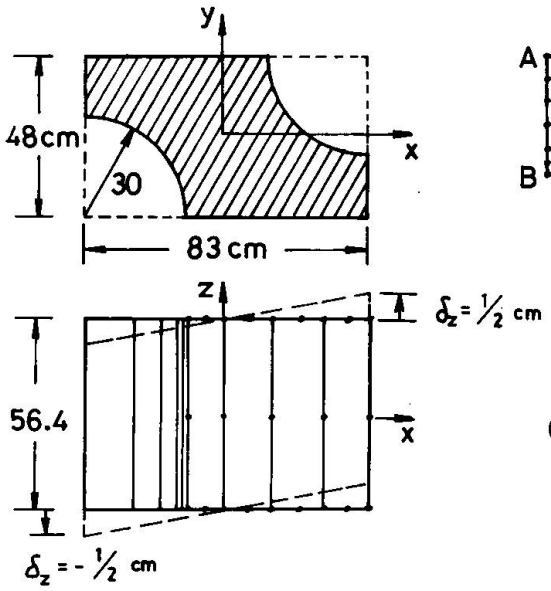

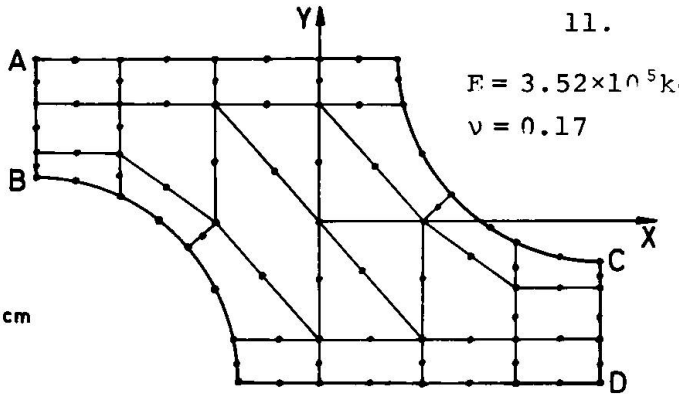

(a) Prescribed Displacements and Idealization by Iso-Parametric Elements

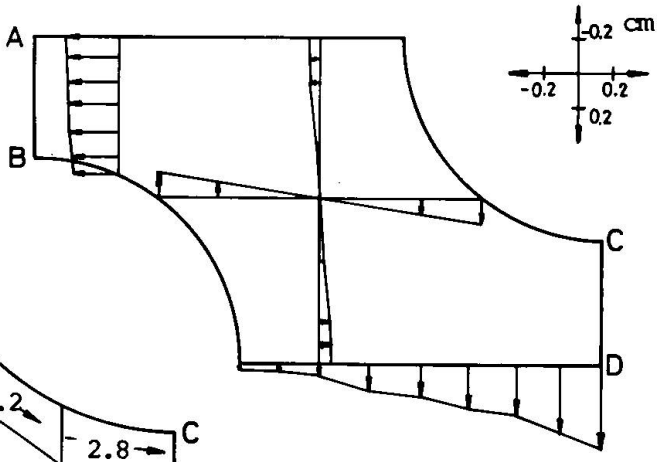

(b) Distribution of Vertical Displacement

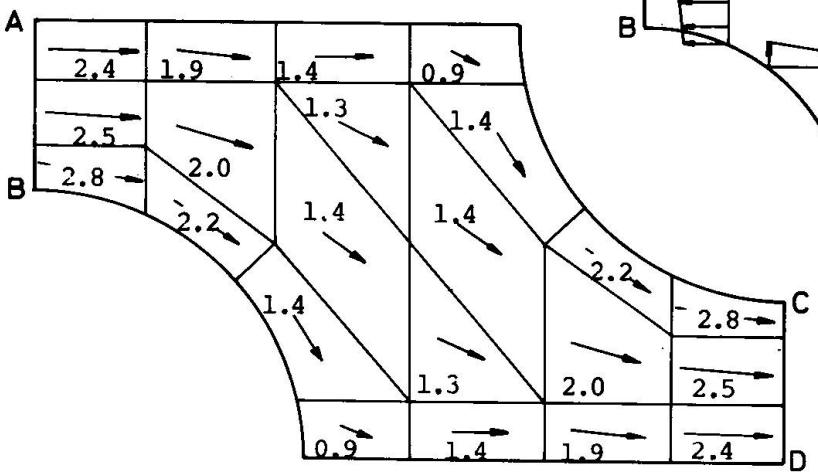

(c) Resultant of τ_{xz} and τ_{yz} figures : ratio to mean stress $\bar{\tau}_{xz}$

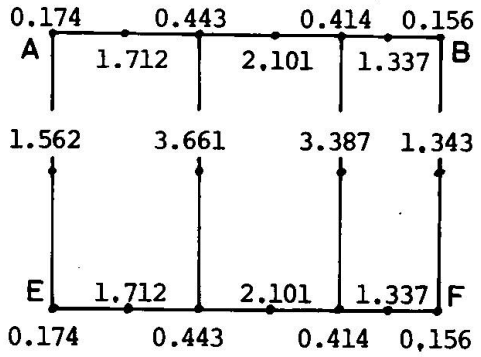

(d) Vertical Modal Reactions, $\times 10^6$kg

Fig.6 Shearing Stress Analysis of Unit Solid for d_5

As indicated in this example, the finite element analysis of the unit area enables consistent assessment of the equivalent elastic coefficients for the perforated solids with regular hole pattern. It must be also noted as one of the advantages of this method that it provides the factors of stress concentration relative to the mean stress intensity which will be obtained from the analysis of the transformed homogeneous field. The effect of the steel liner or reinforcement arround the holes to the effective stiffness can be allowed for by incorporating the corresponding elements in the finite element analysis.

3. METHOD OF SLICED SUBSTRUCTURES

In this section "the method of sliced substructures", a new method of simplified three-dimensional elastic analysis for podded boiler type PCPV, is proposed.

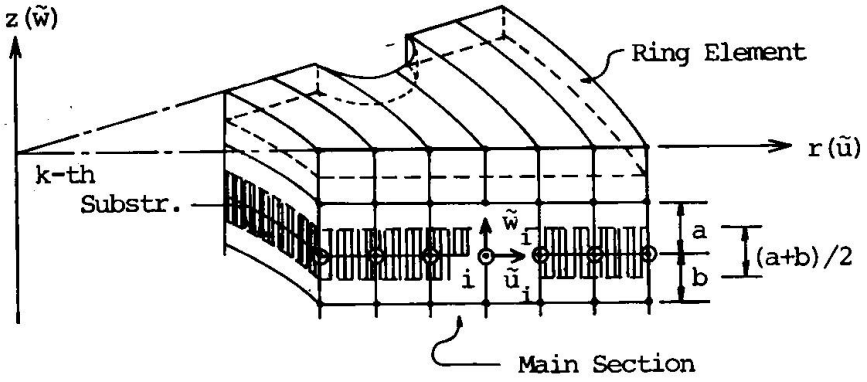

(a) Finite Element Mesh for Main Section

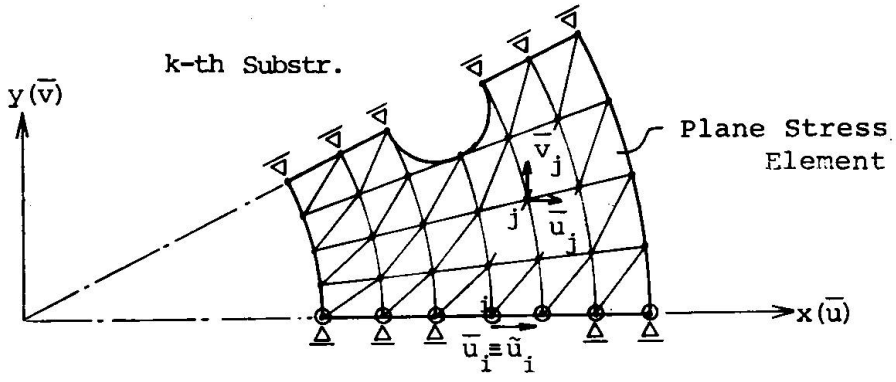

(b) Finite Element Mesh for Sliced Substructure

Fig. 7 Dual System of Idealization

1) Dual System of Finite Element Idealization

Let the vertical plane of symmetry located between two boiler pods be called the main section.

Let us idealize the solid portion to be analysed as the combination of two different kinds of finite element mesh.

The one system of the idealization is to divide the main section into a rectangular lattice pattern as shown in Fig.7(a), and to assign two-dimensional degrees of freedom, $\tilde{u}_i$ and $\tilde{w}_i$, to each nodes. This is the same practice as in the axi-symmetric analysis and the solid is represented as an assemblies of ring elements. It must be noted that the arc length of some ring elements is reduced from normal arc length by the existence of the opening for boiler.

As another system of the idealization, the solid is divided into layers of horizontal slices. As shown in Fig.7(a), the boundaries of the sliced layers are situated at the middle height of each lattice of the mesh for the main section. Therefore the thickness of the slice becomes $h=(a+b)/2$, where a and b represent the height of the upper and the lower lattice, respectively. The reference surface of the sliced layer is the horizontal plane on the end of which the nodes of the main section are resting.

Each sliced layer is now subdivided into a two dimensional mesh in the horizontal plane as shown in Fig.7(b). To each node of this mesh freedom of displacements $\bar{u}_j$ and $\bar{v}_j$, in x- and y-direction respectively, is assigned. It must be noted that displacement $\bar{u}_i$ of the node on one edge of the slice, which is the only component of displacement as the result of the condition of symmetry, is identical with the displacement $\tilde{u}_i$ assigned for the node of the main section.

2) Stiffness Matrix for Axial and Shearing Resistances

For the evaluation of the element stiffness based on the normal resistance in z-direction and the shearing resistance in r-z plane, we assume the displacement of axi-symmetric distribution

$$\tilde{u} = \tilde{u}(r, z)$$
$$\tilde{v} = \tilde{v}(r, z) \qquad (19)$$

which is shown in Fig.8. From this displacement field, the axi-symmetric distribution of strain is resulted as shown in Fig.8.

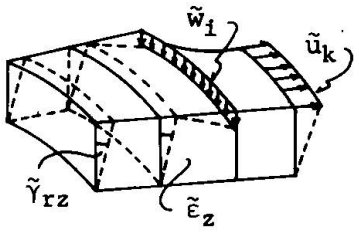

Fig.8 Distribution of Axi-symmetric Displacement and Strain

The important point is that, in evaluating the element stiffness, stress components σ_r and σ_θ caused by ε_r and ε_θ are not taken into account, because these components of resistance are supplemented later in the form of the stiffness of the sliced layers.

Thus, the element stiffness matrix is obtained by the formula

$$[\tilde{K}_e] = \int_{vol} [B]^T [\tilde{D}_1] [B] \, dV \qquad (20)$$

where [B] is strain matrix, $[\tilde{D}_1]$ is modified elasticity matrix, both for the axi-symmetric problem.

This formulation is basically the same to the element stiffness matrix of the axi-symmetric problem excepting the following two points.

i) In order to exclude the contribution of the resistance in r-θ plane, we use the elasticity matrix $[\tilde{D}_1]$ of the following form:

$$\{\tilde{\sigma}\} = [\tilde{D}_1] \{\tilde{\varepsilon}\} \qquad (21\text{-a})$$

$$\begin{Bmatrix} \tilde{\sigma}_r \\ \tilde{\sigma}_\theta \\ \tilde{\sigma}_z \\ \tilde{\tau}_{rz} \end{Bmatrix} = \begin{bmatrix} 0 & 0 & d_{13} & 0 \\ 0 & 0 & d_{23} & 0 \\ d_{31} & d_{32} & d_{33} & 0 \\ 0 & 0 & 0 & d_{44} \end{bmatrix} \begin{Bmatrix} \tilde{\varepsilon}_r \\ \tilde{\varepsilon}_\theta \\ \tilde{\varepsilon}_z \\ \tilde{\gamma}_{rz} \end{Bmatrix} \qquad (21\text{-b})$$

Eq.(21-b) means that we suppress the four coefficients in the ordinary [D] matrix for the axi-symmetric problem, and

ii) For the ring elements which cross the opening for boiler, the integration is carried out with regard to the actual volume reduced by the opening.

3) Stiffness Matrix for Sliced Substructures

The sliced layers are a kind of substructures which represents the partial components of the structural resistance, i.e. the resistance in the horizontal plane. The resistance of these substructures is to be combined with the axial and shearing resistances to form a total stiffness written in terms of the nodal freedom of the main section.

To each sliced substructure, two-dimensional degrees of freedom were assigned, that is we assumed the distribution of u and w which is constant within the thickness of the slice as shown in Fig.9. This means that the assumed distribution for the sliced substructures contains discontinuity in the boundaries of layers.

For each sliced substructure, the following stiffness ralation is formulated:

$$[\bar{K}] \{\bar{d}\} = \{f_s\} \qquad (22)$$

where $\{\bar{d}\}$: two-dimensional nodal displacements for the whole area of a sliced substructure

$\{f_s\}$: external forces in x and y directions applied to the nodes in a sliced substructure

$[\bar{K}]$: system stiffness matrix for plane stress problem of a sliced substructure

It must be noted that the stiffness matrix $[\bar{K}]$ in Eq.(22) is not the one for plane strain but that of plane stress. The reason can be explained by the fact that the constraint forces existing in plane strain state was already taken into account in the stiffness of the axi-symmetric resistance by taking the coefficients d_{13}, d_{23}, d_{31} and d_{32} in Eq.(21-b), and stiffness based on the plane stress state is to be su-perimposed.

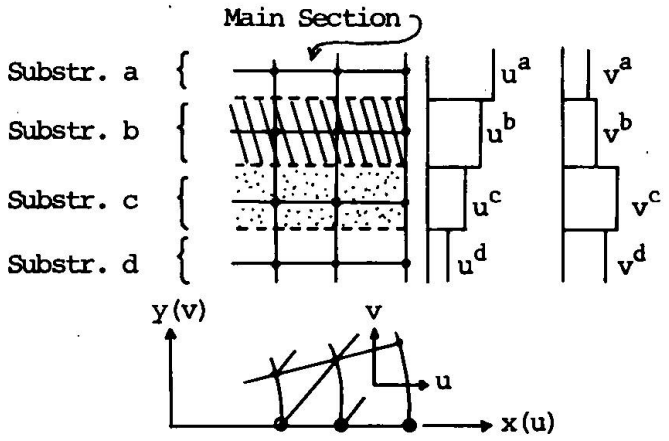

Fig.9 Assumed Distribution of Displacement for Sliced Substructures

Now, let us divide the nodal degrees of freedom of sliced substructure into two groups as shown in Fig.10, namely $\{\bar{u}_I\}$, a group of the radial displacements of the nodes resting on the main section and $\{\bar{d}_{II}\}$, a group of displacement components of all the other nodes.

In order to eliminate the freedom $\{\bar{d}_{II}\}$, Eq.(22) is rearranged into the following form:

$$\left[\begin{array}{c|c} \bar{K}_{11} & \bar{K}_{12} \\ \hline \bar{K}_{21} & \bar{K}_{22} \end{array}\right] \left\{\begin{array}{c} \bar{u}_I \\ \hline \bar{d}_{II} \end{array}\right\} = \left\{\begin{array}{c} f_{sI} \\ \hline f_{sII} \end{array}\right\} \qquad (23)$$

where

u_I : radial displacement of the nodes on the main section
: all the other nodal degrees of freedom
f_{sI} : external force of the nodes on the main section
f_{sII} : external force of the other nodes

The well-known procedure of the static condensation leads to the stiffness relation with regard to the retained freedom $\{\bar{u}_I\}$ as follows:

$$[\bar{K}_I]\{\bar{u}_I\} = \{\bar{f}_I\} \qquad (24\text{-a})$$

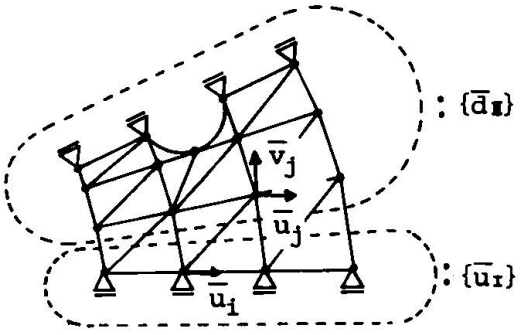

Fig. 10 Retained and Eliminated Displacements in Static Condensation

where $$[\bar{K}_I] = [\bar{K}_{11}] - [\bar{K}_{12}][K_{22}]^{-1}[\bar{K}_{21}] \qquad (24\text{-b})$$

: condensed stiffness matrix for $\{\bar{u}_I\}$

$$\{\bar{f}_I\} = \{f_I\} - [K_{12}][K_{22}]^{-1}\{f_{II}\} \qquad (24\text{-c})$$

: reduced external force corresponding to $\{\bar{u}_I\}$

The dimension of $[\bar{K}_I]$ matrix is $(m \times m)$, where m is twice the number of nodes contained in one horizontal line of the mesh of the main section.

4) Final Equation of Equilibrium

Basing on the fact that the retained degrees of freedom $\{\bar{u}_1\}$ of each sliced substructure are identical with the radial components of the nodal displacements $\{\tilde{d}\}$ of the main section, the final equilibrium equation with regard to the nodes in the main section can be composed by the superposition of the both stiffness relation derived in the above.

The composition of the final equation can be indicated by the following form:

$$\{[\tilde{K}]+[\bar{K}]\}\{\tilde{d}\} = \{\tilde{f}\}+\{\bar{f}\} \qquad (25)$$

where
- $\{\tilde{d}\}$: two-dimensional nodal degrees of freedom of the main section
- $\{\tilde{f}\}$: nodal external force in z-direction evaluated for the total arc length of the ring element
- $\{\bar{f}\}$: nodal external force in r-direction reduced from distributed external force on sliced substructure ,c.f. Eq.(24-c)
- $[\tilde{K}]$: stiffness matrix representing the axi-symmetric system of resistance
- $[\bar{K}]$: stiffness matrix representing the resistance in the horizontal plane derived from sliced substructures

In the final equation, the system stiffness matrix $[\tilde{K}]$ composed from the element stiffness matrix given in Eq.(20) has the same dimension and band structure as in the ordinary axi-symmetric problem of the given idealization of the main section. While, matrix $[\bar{K}]$ of the system stiffness matrix is composed of the condensed stiffness matrices $[\bar{K}_I]$ given in Eq.(24-b) for each substructure by placing them diagonally.

The composition of $[\bar{K}]$ matrix can be illustrated with respect to a simple layout of the main section and the slices shown in Fig.11. For this model, when we put $\{\tilde{d}\}$ vector as

$$\{\tilde{d}\} = \{\tilde{u}_1 \ \tilde{w}_1 \ \tilde{u}_2 \ \tilde{w}_2 \ \tilde{u}_3 \ \cdots\cdots\} \tag{26}$$

$[\bar{K}]$ matrix and load vectors take the following form:

$$[\bar{K}] = \begin{array}{c} \begin{array}{ccc} \tilde{d}_{1\sim4} & \tilde{d}_{5\sim8} & \tilde{d}_{9\sim12} \end{array} \\ \left[\begin{array}{c|c|c} \bar{K}^a & & \\ \hline & \bar{K}^b & \\ \hline & & \bar{K}^c \end{array}\right] \end{array} \tag{27-a}$$

where

$$[\bar{K}^a] = \begin{array}{c} \begin{array}{cccccccc} \tilde{u}_1 & \tilde{w}_1 & \tilde{u}_2 & \tilde{w}_2 & \tilde{u}_3 & \tilde{w}_3 & \tilde{u}_4 & \tilde{w}_4 \end{array} \\ \left[\begin{array}{cc|cc|cc|cc} * & 0 & * & 0 & * & 0 & * & 0 \\ 0 & 0 & 0 & 0 & 0 & 0 & 0 & 0 \\ \hline * & 0 & * & 0 & * & 0 & * & 0 \\ 0 & 0 & 0 & 0 & 0 & 0 & 0 & 0 \\ \hline * & 0 & * & 0 & * & 0 & * & 0 \\ 0 & 0 & 0 & 0 & 0 & 0 & 0 & 0 \\ \hline * & 0 & * & 0 & * & 0 & * & 0 \\ 0 & 0 & 0 & 0 & 0 & 0 & 0 & 0 \end{array}\right] \end{array} \tag{27-b}$$

* : non-zero element

and

$$\tilde{f} = \{0 \ f_{z1} | 0 \ f_{z2} | 0 \ f_{z3} | \cdots\cdots | 0 \ f_{z12}\} \tag{28}$$

$$\bar{f} = \{\bar{f}_1^a \ 0 | \bar{f}_2^a \ 0 | \bar{f}_3^a \ 0 | \bar{f}_4^a \ 0 | \bar{f}_5^b \ 0 | \bar{f}_6^b \ 0 | \cdots\cdots | \bar{f}_8^b \ 0 | \bar{f}_9^c \ 0 | \cdots\cdots | \bar{f}_{12}^c \ 0\} \tag{29}$$

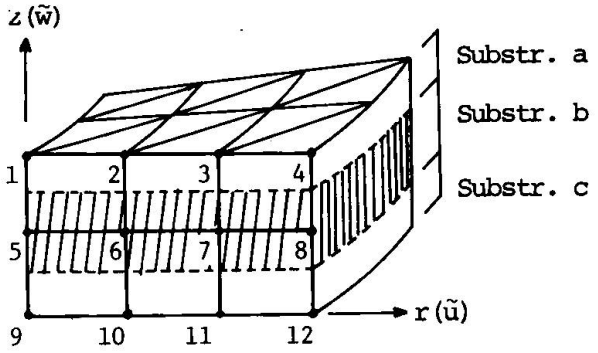

Fig. 11 Example of Layout of Main Section and Substructures

5) Evaluation of Stresses

The nodal displacements of the main section $\{\tilde{d}\}$, being substituted back into $\{\bar{u}_I\}$ in Eq.(23), yields the nodal displacement of the substructures. In evaluating the stress in the elements of each slice, the effect of Pisson's ratio i.e. σ_x and σ_y caused by $\tilde{\varepsilon}_z$ must be superimposed to the plane stress. Thus the final form of the stress of the slices is given as follows:

$$\{\sigma_e\} = \{\tilde{\sigma}(\tilde{\varepsilon}_z)\} + \{\bar{\sigma}\} \tag{30-a}$$

where $$\{\bar{\sigma}\} = \{\bar{\sigma}_x \ \bar{\sigma}_y \ \bar{\tau}_{xy}\} : \tag{30-b}$$

stress of an element of sliced substructure obtained by using stress matrix for plane stress problem

$$\{\tilde{\sigma}(\tilde{\varepsilon}_z)\} = \begin{Bmatrix} \tilde{\sigma}_x \\ \tilde{\sigma}_y \\ 0 \end{Bmatrix} = \begin{bmatrix} E_{13} \\ E_{23} \\ 0 \end{bmatrix} \tilde{\varepsilon}_z : \tag{30-c}$$

stress induced by $\tilde{\varepsilon}_z$ of the ring elements

It must be noted that, in Eqs.(30), $\{\bar{\sigma}\}$ is calculated with respect to the each element of the substructures while $\{\tilde{\sigma}(\tilde{\varepsilon}_z)\}$ is calculated with respect to the each ring element of the main section, both being to be superimposed according to the geometrical co-relation.

4. EXAMPLES OF ANALYSIS BY THE METHOD OF SLICED SUBSTRUCTURES

In order to illustrate the application of the method of sliced substructures and to show its validity and efficiency, the following two simple problems were analysed.

Example 1: Analysis of a Thick-Walled Cylinder without Hole

Thick-walled cylinder partially subjected to inner pressure, shown in Fig.12(a), was analyzed using both of the ordinaly axi-symmetric and sliced substructure methods. As the problem is purely axi-symmetric the method of sliced substructure must lead to the same result to that of the axi-symmetric analysis. Finite element idealization shown in Fig.12(b) was used.

Figs.12(c) and (d) shows the comparison of the both analyses with regard to displacement and stress distribution, respectively, of the main section. It can be seen that almost identical results were obtained from both method.

Table I indicates the comparison of computing time for axi-symmetric and sliced substructure analyses.

	Axi-Symmetric	Sliced Substructures
Data Input and Stiffness Matrix	3.3 sec.	38.4 sec.*
Solving Eq.	2.3	4.0
Back Substitution and Out Put	1.5	4.6
Total	7.1 sec.	47.0 sec.

* including 24.0 sec. of matrix inversion for a substructure

Table I Computing Time for Example 1, IBM 360/195

Example 2: Analysis of a Thick-Walled Cylinder with Holes

A thick-walled cylinder of the same dimensions and loading as Example 1 but having vertical holes like boiler pods was analyzed. The problem is three-dimensional in this case and the solution obtained by the method of sliced substructures was compared with that of the ordinary three-dimensional analysis by the use of iso-parametric elements.

Fig.13(a) shows the definition of the problem. The finite element idealization used in both method is shown in Fig.13(b).

The comparison between the results from both method is presented in Figs.13(c) and (d).

CONCLUSIONS

In this paper a simplified method of elastic analysis for podded boiler type PCPV was presented.

A finite element analyses of the unit area of the hole pattern enable consistent method of evaluating the coefficients of elasticity of the transversely isotropic body equivalent to the stand pipe zone of top slab.

Also, a newly developed "method of sliced substructures" enables us to analyze the three-dimensional problems of PCPV within the same degrees of freedom as the axi-symmetric problems, where the disturbance of stress by the boiler pods is fully allowed for.

For the problems of the same scale experienced in the examples, the ratio of necessary computing time of axi-symmetric / sliced substructures/ was 7 / 47 , respectively. The computing time for the method of substructure can be further reduced by introducing the iso-parametric two-dimensional elements in the idealization of the sliced substructures, because a large part of the total computing time was occupied by the matrix inversion contained in the static condensation of the substructures.

ACKNOWLEDGEMENTS

The sincere appreciation is expressed to Dr. Y. Hangai, University of Tokyo; Mr. S. Shioya, Nihon University; Mr. Y. Isobata, Mr. N. Tanaka and Mr. H. Akiyama, Shimizu Construction Co. Ltd. to whom the author greatly indepted for their collaboration in all phases of this research.

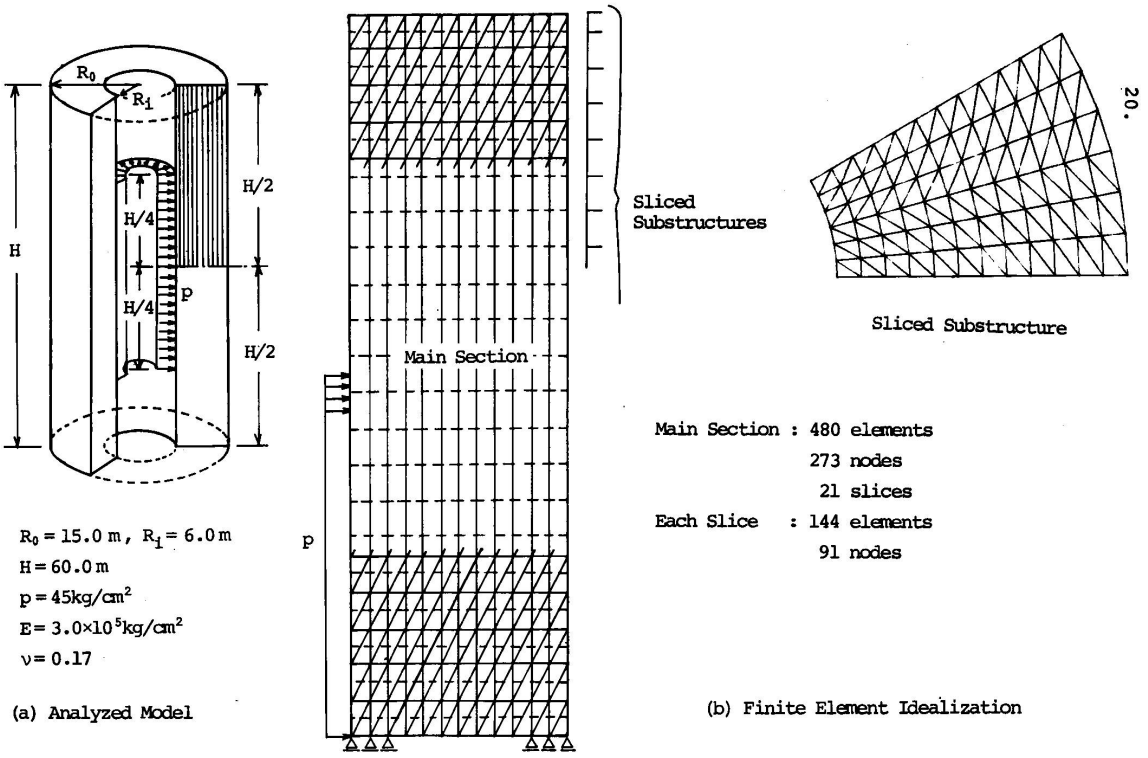

Fig. 12 Analysis of a Thick-Walled Cylinder Partially Loaded by Inner Pressure

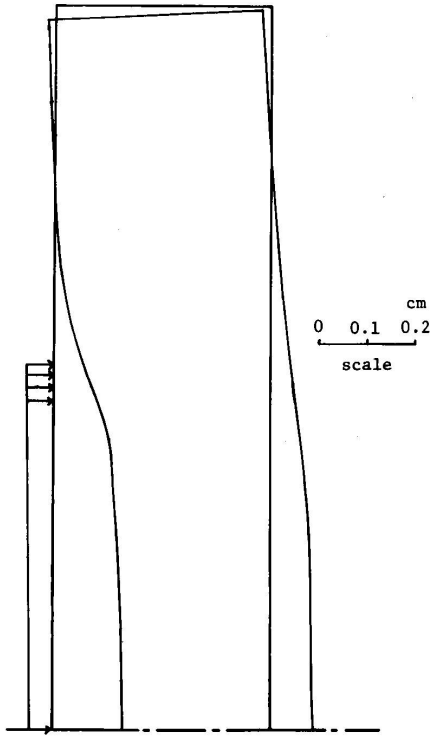

(c) Displacement

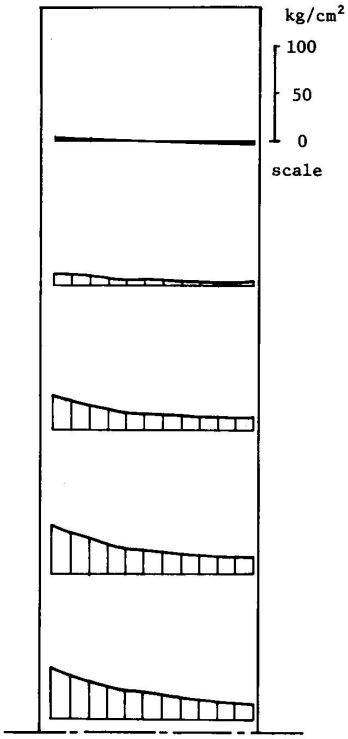

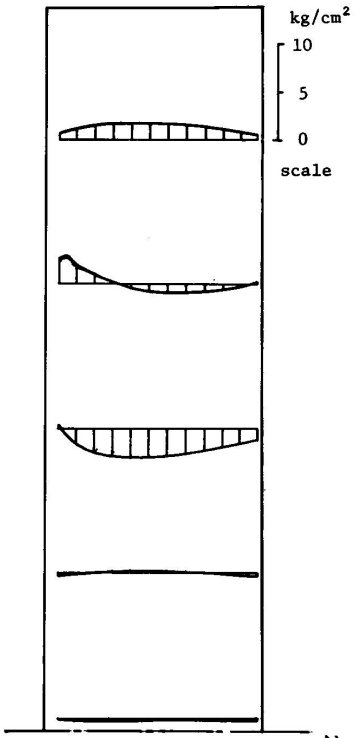

(d) Stresses

Fig 12 Analysis of a Thick-Walled Cylinder Partially Loaded by Inner Pressure
(Difference of results from both methods is invisible in the diagrams)

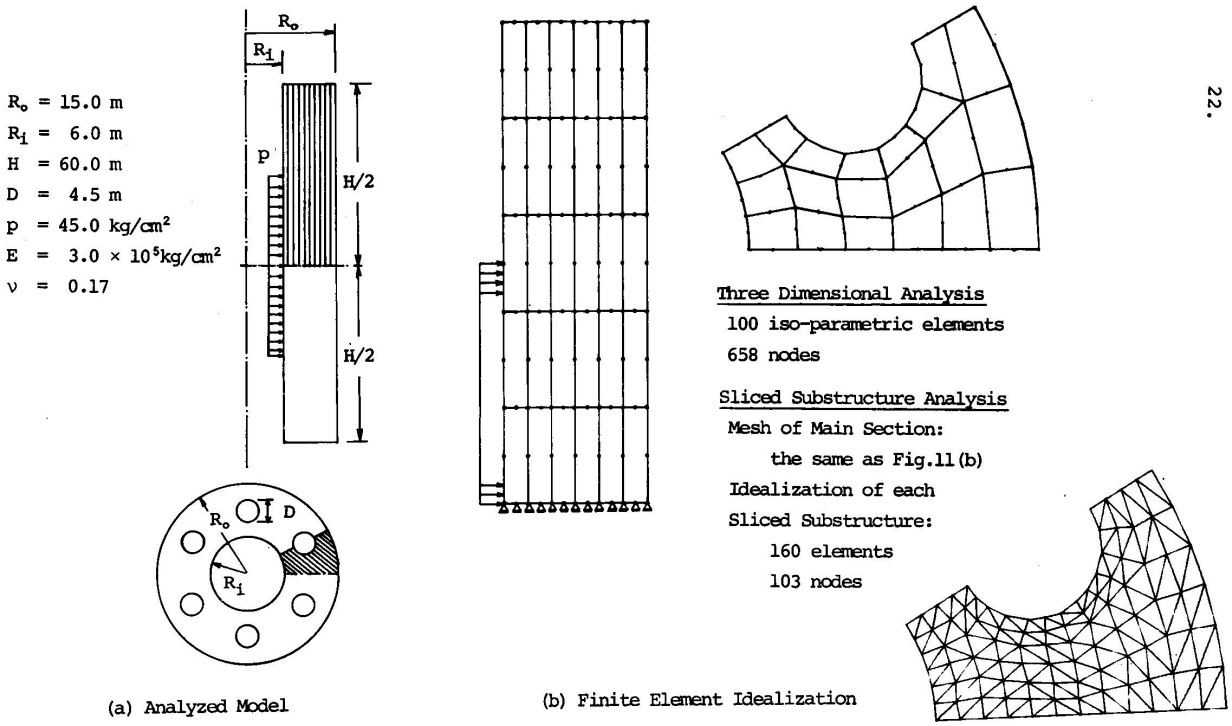

(a) Analyzed Model

(b) Finite Element Idealization

Fig.13 Analysis of Thick-Walled Cylinder with Holes

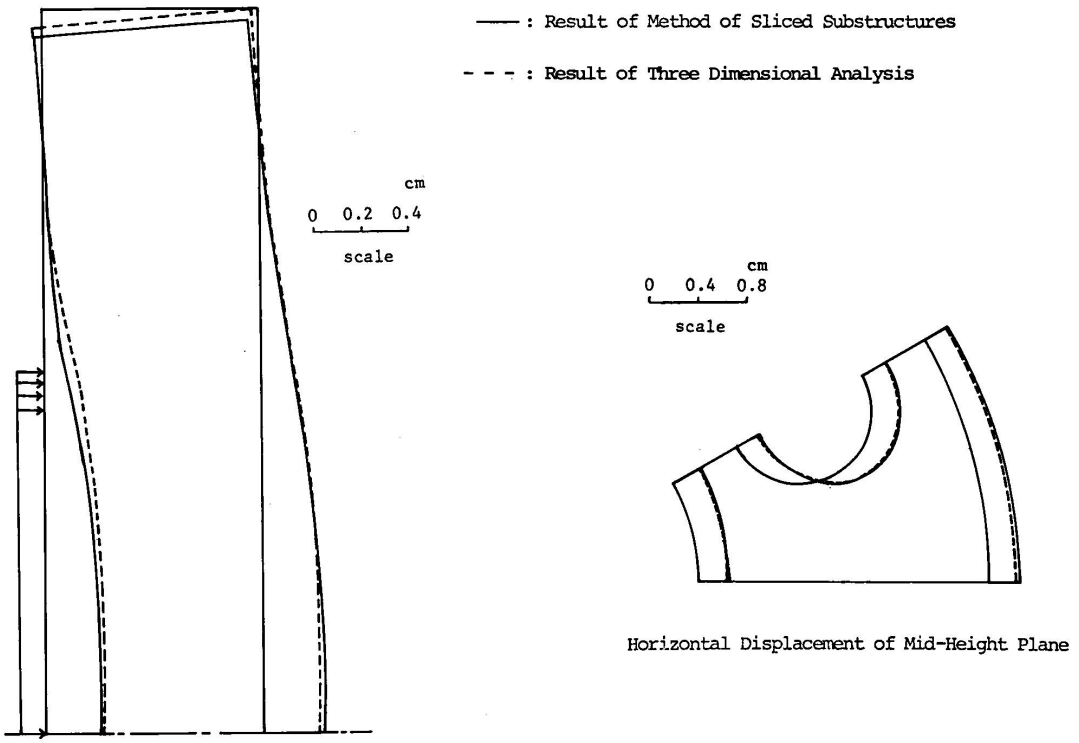

(c) Distribution of Displacement

Fig. 13 Analysis of Thick-Walled Cylinder with Holes

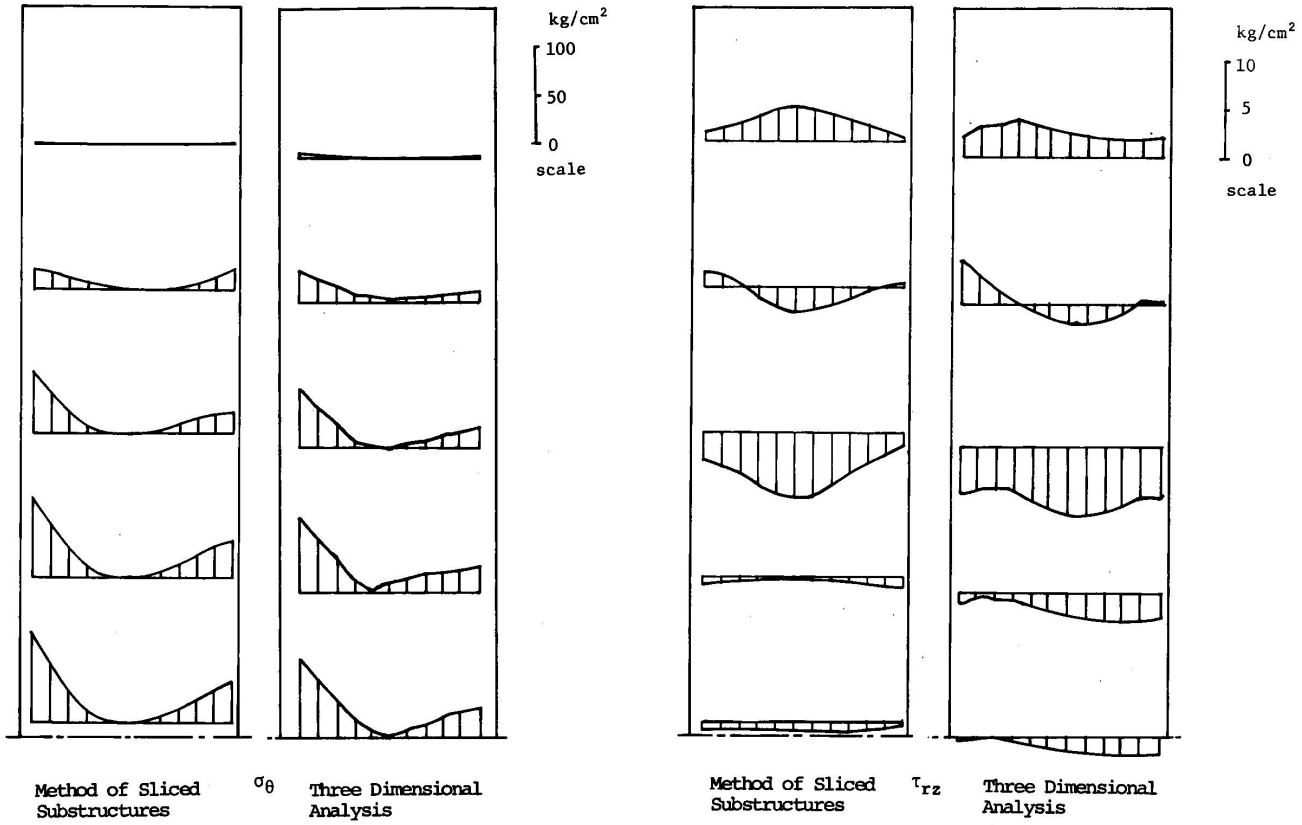

(d) Stress Distribution

Fig. 13 Analysis of Thick-Walled Cylinder with Holes

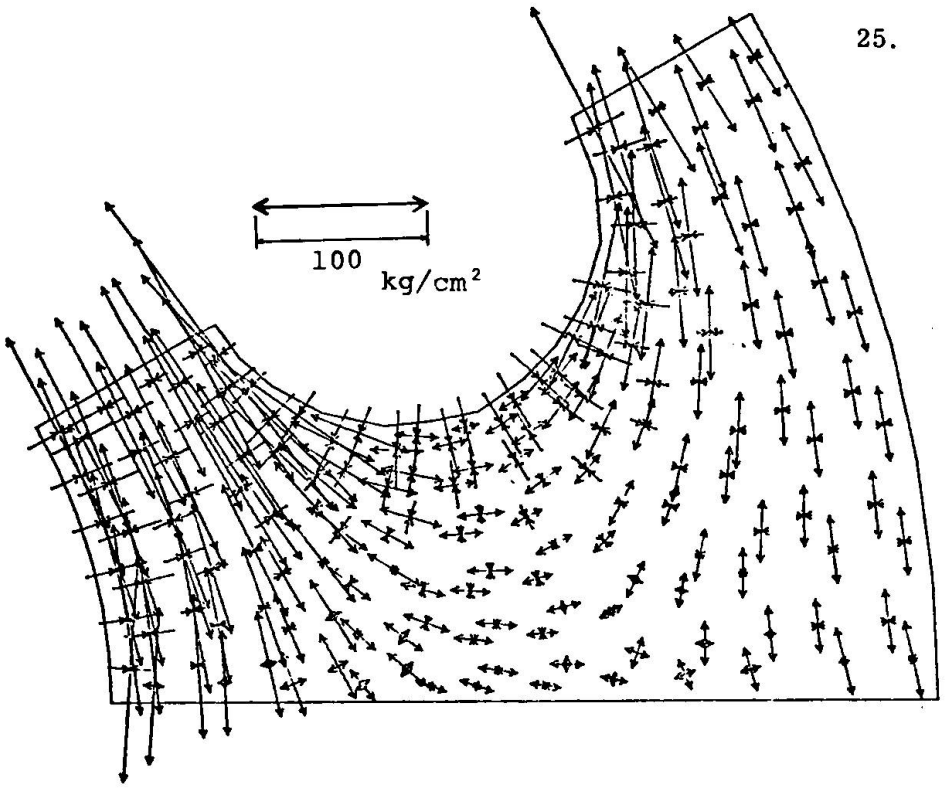

Result by Method of Sliced Substructures

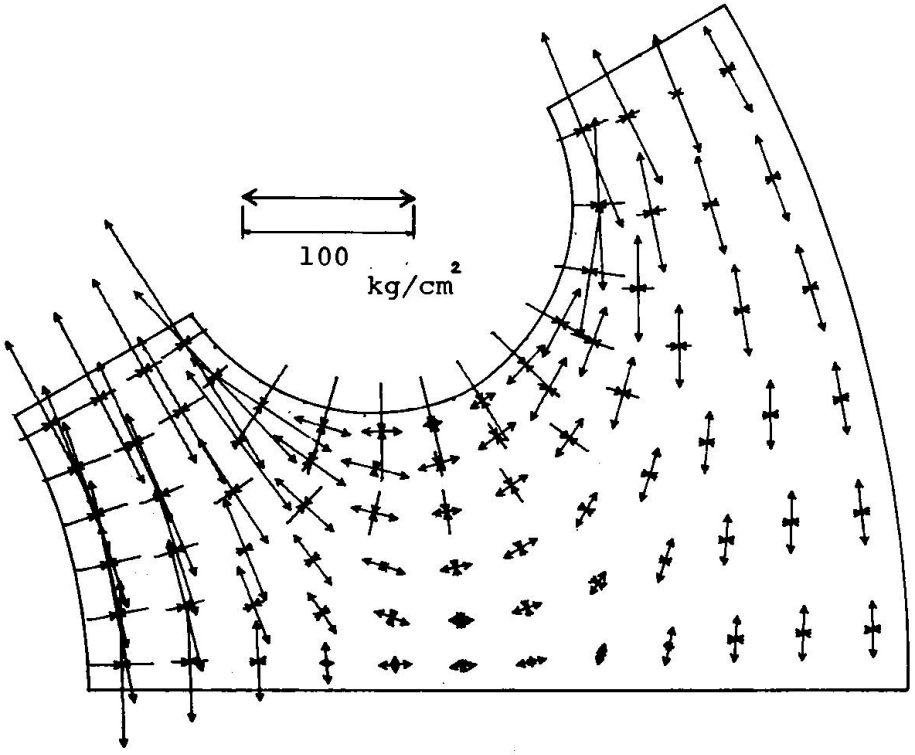

Result by Three Dimensional Analysis

(d) Principal Stress Distribution

Fig. 13 Analysis of Thick-Walled Cylinder with Holes

REFERENSES

[1] J.H.Argyris, K,E.Buck, D,W.Scharpf and K.J.Willam, "Linear Methods of Structural Analysis", 1st SMIRT Conference, Berlin, 1971; Nuclear Engineering and Design, Vol.19, 1972, pp.139-167.

[2] R.W.Bailey and R.Fidler, "Stress Analysis of Plates and Shells Containing Patterns of Reinforced Holes", Nuclear Engineering and Design, Vol.3, 1966, pp.41-53.

[3] H.M.S. Abdul-Wahab and J.Harrop, "The Rigidity of Perforated Plates with Reinforced Holes", Nuclear Engineering and Design, Vol. 5, 1967, pp.134-141.

[4] D.J.Lewis, J,Irving and G,D,T.Carmichael, "Advances in the Analysis of Prestressed Concrete Pressure Vessels", 1st SMIRT Conference, 1971; Nuclear Engineering and Design, Vol.20, 1972, pp.543-573.

[5] Y.R.Rashid and W.Rockenhauser, "Pressure Vessel Analysis by Finite Element Techniques", Proc. Conf.on PCPV, London, 1967, Inst. Civil Engrs., 1968, pp.375-383.

[6] O.C.Zienkiewicz, B.M.Irons, J,Ergatoudis, S.Ahmad and F.C.Scott, "Iso-Parametric and Associated Element Families for Two-and Three-Dimensional Analysis", Finite Element Methods in Stress Analysis, ed. I.Holand and K,Bell, TAPIR, Trondheim, 1969, pp.383-432.

[7] O.C,Zienkiewicz, D.R.J.Owen, D.V.Phillips and G.C.Nayak, "Finite Element Methods in the Analysis of Reactor Vessels", 1st SMIRT Conference, Berlin, 1971; Nuclear Engineering and Design, Vol.20, 1972, pp.507-541.

[8] P.Meijers, "Three-dimensional Stress Analysis for Perforated Plates with a Regular Triangular Hole Pattern", Inst. TNO for Mechanical Construction, Delft, Rep. No.81290, 1971.

[9] P.Meijers, "Review of ASKA Program", Numerical and Computer Methods in Structural Mechanics, Proc. Conf., Urbana, 1971, ed. S,J.Fenves, N.Perone, A,R.Robinson and W.C.Schnobrich, Academic Press, 1973, pp.123-149.

[10] Y.Tsuboi, S.Kawamata, N,Tanaka, "Finite Element Analysis of Continua —— Effective Rigidity of Perforated Body, Proc. Annual Convention, Architectural Institution of Japan, Oct. 1967

[11] F,Kikuchi, "An Example of Partial Approximation in the Finite Element Method, Proc. 23rd Japan Nat. Congr. Theo. Appl. Mech, 1973, to be published.

[12] F.Kikuchi, "On the Validity of an Approximation Available in Finite Element Shell Analysis, to appear, 1974.

[13] F.Kikuchi, "Theory and Example of Partial Approximation in the Finite Element Method, to appear, 1974.

[14] A.E.Green and W.Zerna, "Theoretical Elasticity", Oxford at the Clarendon Press, 1960, p.159.

[15] S.G.Lekhnitskii, "Theory of Elasticity of an Anisotropic Elastic Body", Holden-Day, 1963.

[16] O,C,Zienkiewicz and Y,K,Cheung, "The Finite Element Method in Structural and Continuum Mechanics", McGraw-Hill, 1967, p.50.

RESUME

On discute une méthode simplifiée pour l' analyse élastique tridimensionnelle par éléments finis d' un caisson en béton précontraint du type "Podded Boiler".

La première partie traite une méthode pour l' évaluation de la rigidité efficace de la zone avec pénétrations, où l' on utilise des analyses tridimensionnelles par éléments finis de la surface unitaire de un système régulier de trous.

Dans la deuxième partie on propose la nouvelle méthode des sous-structures coupées pour l' analyse tridimensionnelle simplifiée des caissons.

La rigidité du caisson vient déterminée comme combinaison de la matrice de problèmes axial-simmétriques modifiés et des matrices de rigidité bidimensionnelles de sous-structures coupées horizontalement. La méthode permet l' analyse tridimensionnelle des problèmes de caissons en tenant compte de l' effet des "Boiler Pods", et en maintenant les mêmes degrés de liberté que dans l' analyse axial-simmétrique.

La validité de la méthode est prouvée par des exemples numériques.

ZUSAMMENFASSUNG

Im ersten Teil wird ein Verfahren beschrieben, das es erlaubt die effektive Festigkeit von perforierten Zonen zu bewerten mit Hilfe von Analysen mit endlichen Elementen einer Einheitsfläche von regelmässigen Perforationssystemen.

Im zweiten Teil wird eine neue vereinfachte Methode für tridimensionale Analysen von Spannbeton-Druckbehältern, die sogenannte "Sliced-Structures Method" erklärt. Die Steifigkeitsberechnung für diese Behälter ist eine Kombination der Festigkeitsmatrix von modifizierten axialsymmetrischen Problemen und der zweidimensionalen Festigkeitsmatrix von Querschnitten von Unterkonstruktionen; bei der Berücksichtigung des "Boiler Pod" Effekts ist der selbe Grad von Freiheit gestattet wie bei der axialsymmetrischen Analyse. Die Gültigkeit der neuen Methode wird mit einigen Zahlenbeispielen belegt.

Leere Seite
Blank page
Page vide

IABSE
AIPC
IVBH

SEMINAR on:
«CONCRETE STRUCTURES SUBJECTED TO TRIAXIAL STRESSES»
17th-19th MAY, 1974 - ISMES - BERGAMO (ITALY)

Ein Berechnungsverfahren für dickwandige, rotationssymmetrische Konstruktionen, am Beispiel eines Reaktordruckbehälters aus Spannbeton

A calculation system for rotation-symmetric constructions with thick walls, shown by a model of an reactor vessel in prestressed concrete

Un procédé de calcul pour constructions rondes, à paroi épaisse à l'exemple d'un réservoir de réacteur sous pression en béton précontraint

D. JUNGWIRTH, Dr. Ing. - O. SEIDL, Dipl. Ing.
Fa. Dyckerhoff & Widmann AG
Deutschland

1. Einleitung

Bei der Deckung des progressiv ansteigenden Energiebedarfes unserer Industriegesellschaft werden in Zukunft die Kernkraftwerke eine bedeutende Stellung einnehmen. Zu den ursprünglich dominierenden Problemen, die kernphysikalischen Vorgänge durch geeignete maschinentechnische Anlagen zu beherrschen, kommen nun im Zuge weiteren Ausbaues neue bautechnische Aufgaben hinzu, die die Wirtschaftlichkeit solcher Kraftwerke nicht unwesentlich beeinflussen.

Bei Kernreaktoren läuft die Kernspaltung in einem Druckbehälter gesteuert ab, wobei ein Kühlmittel die entstehende Wärme direkt oder über Wärmetauscher zum Betreiben von Turbinen abführt.
In Deutschland (siehe auch [1]) baut bzw. entwickelt man hauptsächlich den Leichtwasserreaktor als Siedewasser - (z.B. AEG) und Druckwasserreaktor (z.B. Siemens) bzw. den gasgekühlten Reaktor als Hochtemperaturreaktor. Ein schematischer Aufbau dieser 3 Typen wird in Bild 1 gezeigt. Während man bei den Leichtwasserreaktoren mit Drücken von 80 bis 180 atü und Temperaturen bis 350° C arbeitet, treten bei den gasgekühlten Reaktortypen Drücke von nur 40 atü, dafür Temperaturen bis zu 800° C auf.

Der bislang überwiegenden Ausführung der Druckbehälter aus Stahl mußte ein weiterer biologischer Schild, vorwiegend aus Beton zur

Abschirmung der Strahlung beigeordnet werden. Es war naheliegend, dem Beton nicht nur eine Abschirmfunktion, sondern in Form des Spannbetondruckbehälters auch die Aufgabe der Druckaufnahme zuzuweisen. Diese Spannbetondruckbehälter lassen sich dem Trend zu größeren Leistungseinheiten besser anpassen als Stahlbehälter, außerdem wird das Risiko des Sprödbruches bei Stahl umgangen. Alle 3 in Bild 1 angesprochenen Reaktortypen können in Spannbeton wirtschaftlich ausgeführt werden. Stahlbeton wird den Sicherheitsanforderungen nicht gerecht.
Der typische Aufbau eines Spannbetondruckbehälters wird in Bild 2 gezeigt. Der sog.Liner soll gasdicht sein. Je nach Lage spricht man vom kalten oder heißen Liner. Die Isolierung und die Kühlung dient als Hitzeschild, sodaß der Spannbetonbehälter auf seiner Innenseite neben dem Innendruck und der Strahlung nur noch einer Temperaturbeanspruchung von ca. 80° C widerstehen muß. An seiner Außenseite herrscht Raumtemperatur von ca. 25° C.

Solche dickwandige Spannbetonbehälter müssen den Beanspruchungen im Bau- und Betriebszustand bis zum Grenzzustand mit hypothetisch überhöhten Innendrücken gerecht werden. Die hierzu erforderlichen Berechnungen sind am dreidimensionalen rotationssymmetrischen Tragwerk zu untersuchen. Störzonen und unsymmetrische Beanspruchungen sind abzuschätzen [1,2]. Die einzelnen Lastfälle werden im folgenden Abschnitt eingehender erläutert.

2. Zu untersuchende Lastfälle und zulässige Beanspruchungen beim Spannbetondruckbehälter.

Neben den üblichen Lastfällen wie Eigengewicht, Wind gegf.Erdbeben usw. sind betriebsspezielle Belastungen zu untersuchen. Sofern kein Containment (Schutzhülle) benötigt wird, müssen wegen der katastrophalen Folgen auch nahezu unwahrscheinliche Ereignisse wie z.B. Absturz eines Flugkörpers, Explosionswellen und Flächenbrände als zusätzliche Lastfälle untersucht werden. Ansonsten ist das Containment u.a. für diese Lastfälle sowie für Strahlkräfte aus möglichen Rohrbrüchen zu bemessen.
Die der Tabelle 1 zu entnehmende Zusammenstellung der Lastfälle für Spannbetondruckbehälter wurde im wesentlichen aus einem Normvorschlag [2] gewonnen. Dabei wird zwischen Bauzustand, Betriebszustand und Grenzzustände unterschieden. In der rechten Hälfte der Tabelle werden in Anlehnung an [2] die jeweils zulässigen Spannungen angegeben.

Die Größe und der zeitliche Verlauf der Kriech- und Schwindverformung ist bei dicken Körpern und bei den lokal auftretenden Temperaturen bis zu 80° C noch nicht abschließend geklärt. Die sich nach den neuen Spannbetonrichtlinien [3] ergebenden Werte gelten für Temperaturen bis zu 30° C. Sie sind, soweit dem Kriechen und Schwinden besondere Bedeutung zukommt, zur Erfassung möglicher Grenzwerte um 20 % zu erhöhen oder zu verringern. Die Bereiche mit hoher Temperatur sind mit Zuschlägen zu versehen.

3. Berechnungsverfahren

3.1 Allgemeines

Die folgenden Untersuchungen befassen sich hauptsächlich mit der Berechnung des Bau- und Betriebszustandes dickwandiger Behälter. Für den Bruchzustand wird im allgemeinen ein Bruchmodell zugrundegelegt und das Problem nach den Regeln der Bruchlinientheorie gelöst (siehe auch [1]) oder ein Modellversuch durchgeführt. Für die Berechnung des Gebrauchszustandes wird von der E-Theorie ausgegangen, d.h. es werden homogenes isotropes Werkstoffverhalten, das Hookesche Gesetz und kleine Formänderungen unterstellt. Die Dickwandigkeit der Konstruktion muß berücksichtigt werden.

Für die Berechnung der Behälter als dreidimensionales Bauteil stehen im wesentlichen 2 Verfahren zur Verfügung:

V e r f a h r e n d e r f i n i t e n E l e m e n t e .

Das Tragwerk wird im allgemeinen in kleine, einfach berandete Flächen bzw. Körper wie Dreiecke, Rechtecke oder Tetraeder unterteilt und die Verträglichkeit sowie das Gleichgewicht zwischen den einzelnen Elementen hergestellt z.B. [4] und [5] . In [6] wird dagegen mit Streifenelementen gerechnet, die sich über die gesamte Länge des Tragwerkes erstrecken.

M e t h o d e d e r d y n a m i s c h e n R e l a x a t i o n .

Dieses Differenzen-Verfahren wird in [1] und [7] ausführlich beschrieben. An den Kreuzungspunkten der mit einem räumlichen Rasternetz überzogenen Konstruktion werden die unbekannten Spannungen und Verschiebungen bestimmt. Dabei geht man nicht nur vom statischen Gleichgewicht aus, sondern vom elasto-dynamischen. Die die Temperaturspannungen erfassende und die veränderlichen Materialeigenschaften berücksichtigende Differentialgleichung wird in die entsprechende Differenzengleichung übergeführt und numerisch gelöst.

In der Firma Dyckerhoff & Widmann wurde in den Sechziger Jahren ein Rechenverfahren ausgearbeitet, das in die Verfahren der finiten Elemente eingeordnet werden kann. Man stellte sich dabei die Aufgabe, ein einfaches anschauliches, ausreichend genaues und flexibles Rechenverfahren zu finden, das mit normalen Rechenanlagen und mit weitgehend bekannten Programmen gelöst werden kann. Eine dicke rotationssymmetrische Behälterwand wird in ihrem statischen Verhalten durch mehrere konzentrisch angeordnete untereinander gekoppelte dünne Schalen erfaßt.
Die einzelne Schale kann wiederum durch einen räumlich gekrümmten Trägerrost ersetzt werden. Die Wirkung der Ringstäbe kann durch Federn bzw. Radialstäbe erfaßt werden. Damit wird das räumliche System für rotationssymmetrische Belastung auf ein ebenes zurückgeführt. Für die dicke Platte gilt Entsprechendes.

Die folgende Beschreibung des Rechenganges befaßt sich zunächst mit der dünnen Konstruktion und leitet anschließend auf die Lösung bei dickwandigen Konstruktionen über.

3.2 Beschreibung des Rechenganges

3.2.1 Rotationssymmetrische dünne Konstruktionen wie Schalen und Platten unter rotationssymmetrischer Belastung

a) Transformation der dünnen Schalen bzw. Platten in ein ebenes Rahmensystem:

Der die Schale ersetzende räumlich gekrümmte Trägerrost (Bild 3) setzt sich aus Ring- und Meridianstäben zusammen, die sich unter 90° kreuzen. Bei rotationssymmetrischer Belastung verformt sich jeder Meridianstab gleich. Es kann also ein Meridianstab stellvertretend für alle betrachtet werden. Bei der Platte liegen die Verhältnisse entsprechend.

Führt man nun anstelle der Ringstäbe Federn bzw. Radialstäbe ein, die das gleiche Verformungsverhalten wie die Ringstäbe aufweisen, wird das räumliche System in ein ebenes Rahmensystem (elastisch gelagerter Stabzug) übergeführt (Bild 4).

Bei entsprechend enger Teilung geht der Meridianstab in einen elastisch gebetteten Balken über. Nachdem zwischen der Differentialgleichung für die Lösung des elastisch gebetteten Balkens und der Rotationsschale eine Analogie besteht [8] und [9] , die bereits im siebzehnten Jahrhundert von L.Euler erkannt wurde, geht das vorgesehene Rechenverfahren bei dichter Teilung in die Schalen-Lösung über.
Die Ergebnisse werden also umso genauer je feiner die Unterteilung in Ring- und Meridianstäbe ist. Der Rechenaufwand steigt. Da aber das Tragverhalten des vorgeschlagenen Ersatzsystemes kaum von dem des endgültigen Systems abweicht und außerdem eine mathematische Analogie zwischen den beiden Systemen besteht, ist die Rechengenauigkeit sehr groß.

In Bild 5 wird am Beispiel einer Zylinderschale unter rotationssymmetrischer Randbelastung gezeigt, daß beim Rechnen mit dem elastisch gelagerten Stabzug sich die grobe Intervalleinteilung weniger nachteilig auf das Rechenergebnis auswirkt als bei anderen Verfahren wie z.B. der normalen finiten Element Methode ([4], Seite 145). Hier bleiben die Spannungen innerhalb der Elemente konstant, außerdem weicht das statische System der finiten Elemente stark vom endgültigen System ab. Neuerdings kann jedoch der Spannungsverlauf innerhalb eines finiten Elementes nach einer beliebigen Funktion angesetzt werden, wodurch die Rechengenauigkeit erhöht wird.

b) Ermittlung der Querschnittswerte:

Nach Bild 4 lautet die Querschnittsfläche des M e r i d i a n s t a b e s n

$$F_n = b_n \times d_n \qquad (1)$$

das Trägheitsmoment

$$J_n = \frac{1}{12} \times F_n \times d_n^2 \qquad (2)$$

Es bedeuten

$i+1, i, i-1$	Knoten des Meridianstabes
$n+1, n, n-1$	Stababschnitte in Meridianrichtung
l_n	Länge des Stabes n
b_i	Breite des Meridianstabes im Knoten i
d_i	Schalendicke im Knoten i
b_n	Breite des Meridianstabes n $\quad b_n = \frac{1}{2}(b_i + b_{i-1})$
d_n	Schalendicke des Meridianstabes n $\quad d_n = \frac{1}{2}(d_i + d_{i-1})$

Die Querschnittsfläche F_{ki} des R a d i a l s t a b e s ist so festzulegen, daß sein Verformungsverhalten Δk_i in Stabrichtung dem des zu ersetzenden Ringstabes Δr_i unter einer Linienlast p entspricht. Nach Bild 6 ist:

$$\Delta r_i = \frac{p \times r_i^2}{E \times h_i \times d_i} = \Delta k_i = \frac{p \times b_i \times l_{ki}}{E \times F_{ki}} \qquad (3)$$

daraus folgt

$$F_{ki} = \frac{b_i \times l_{ki} \times h_i \times d_i}{r_i^2} \text{ oder } \frac{b_i \times l_{ki} \times F_{Ring}}{r_i^2} \qquad (4)$$

Für $b_i = l_{ki} = r_i$ wird $F_{ki} = F_{Ring}$ (5)

Eine entsprechende Bedingung ist für die Bestimmung des Trägheitsmomentes J_{ki} anzusetzen. Es ist die Verdrehung ϕ_r unter einem Krempelmoment m gleichzusetzen mit dem Enddrehwinkel ϕ_{ki} des Radialstabes unter einem Moment $m \cdot b_i$ (siehe Bild 7). Bei der Auswertung der Rechenergebnisse müssen, besonders bei flachen Schalen, die Radialstabmomente M zur Erlangung der Schalenmomente M_ϕ in die Schalenebene transformiert werden.

$$\phi_r = \frac{m \times r_i^2}{E \times J_{x,Ring}} = \phi_{ki} = \frac{m \times b_i \times l_{ki}}{E \times J_{ki}} \qquad (6)$$

Daraus folgt

$$J_{ki} = \frac{b_i \times l_{ki} \times J_{x,Ring}}{r_i^2} \qquad (7)$$

Für $b_i = l_{ki} = r_i$ wird

$$J_{ki} = J_{x,Ring} \quad \text{oder} \tag{8}$$

$$J_{ki} = J_{1\text{-}1,Ring} \times \sin^2\alpha + J_{2\text{-}2,Ring} \times \cos^2\alpha \tag{9}$$

Es bedeuten:

k_i	Radialstab
l_{ki}	Länge des Radialstabes
h_i	Höhe des Ringstabes
r_i	Radius des Ringstabes (Parallelkreis)
$J_{x,Ring}$	Trägheitsmoment des Ringstabes in x-Richtung

d) Schlußbemerkung

Meridian- und Radialstäbe bilden einen Rahmen und ersetzen eine rotationssymmetrische Konstruktion wie z.B. eine Schale unter rotationssymmetrischer Belastung in ihrer Tragwirkung. Mit einem entsprechenden Rahmenprogramm können Schnittgrößen, Spannungen und Verformungen für beliebige rotationssymmetrische Beanspruchungen elektronisch berechnet werden.

Die Belastungen sind in Knotenlasten zusammenzufassen. Das Temperaturfeld bzw. die Zwangverformungen können jeweils über Temperaturverformungen der Stäbe in meridianer und radialer Richtung eingegeben werden.

Der Einfluß der Querkontraktion kann über modifizierte Querschnittswerte bzw. Federn iterativ bzw. genähert berücksichtigt werden. Selbst wenn die Querdehnung vernachlässigt wird, erhält man in vielen Fällen bessere Übereinstimmung mit der E-Theorie als vom System anderer Verfahren überhaupt möglich ist (Bild 5, 16 und f.f.).

3.2.2 Rotationssymmetrische dickwandige Konstruktionen

a) Ersatz der rotationssymmetrischen dickwandigen Konstruktion durch konzentrisch dünne Systeme.

Die dickwandige Konstruktion wird durch gekoppelte dünne Schalen und Platten ersetzt. Jede Schale wird in einem Meridianstab und in Radialstäbe übergeführt. Die Koppelung erfolgt durch sog. Verbindungsstäbe. Verbindungsstäbe und Meridianstäbe bilden demnach einen Rahmen, in dessen Knoten die Radialstäbe (elastisch gelagerter Rahmen) angreifen (Bild 8). Die Verhältnisse bei Platten sind entsprechend. Der Verbindungsstab soll möglichst senkrecht zum Meridianstab verlaufen.

Im Hinblick auf eine genaue Extrapolation der Randspannungen sollten die äußeren Schalen nicht wesentlich dicker als $1/10 \times r$ sein (r=Radius). Die Zwischenschalen können dagegen den doppelten bis dreifachen Wert aufweisen. Wie die Gegenüberstellung mit der exakten Lösung nach Lamé [1o] beim Beispiel "Dickwandiger Kreisring unter Innendruck" (Bild 9) zeigt, liegt der Fehler bei dieser relativ groben Teilung unter 3 %.

b) Ermittlung der Querschnittswerte

Die Querschnittswerte der Meridian- und Radialstäbe werden wie in Abschn. 3.2.1 gezeigt, gefunden.
Die Länge des Verbindungsstabes l_{i-k} ergibt sich aus der Teilung der Dicke der Behälterwand in einzelne Schalendicken d_i, d_k ...

$$l_{i-k} = \frac{1}{2}(d_i + d_k) \qquad (1o)$$

Für die Fläche gilt

$$F_{i-k} = \frac{1}{2}(h_i + h_k) \times \frac{1}{2}(b_i + b_k) \qquad (11)$$

und für das Trägheitsmoment

$$J_{i-k} = \frac{1}{12} F_{i-k} \times \frac{1}{4}(h_i + h_k)^2 \qquad (12)$$

3.3 Elektronisches Rechenprogramm

Für die Ermittlung der Schnittgrößen, Spannungen und Verformungen des elastisch gelagerten Rahmens steht wiederum ein elektronisches Rechenprogramm zur Verfügung. Ein Vorprogramm ermittelt die System- und Querschnittswerte, sodaß lediglich die Eingabe der Koordinaten der "Elementeckpunkte" erforderlich ist. Eingabefehler werden somit auf ein Minimum reduziert. Die Ergebnisse können über Plotter aufgezeichnet werden.

3.4 Sonderfälle

3.4.1 Die Vorspannung, Kriechen und Schwinden

Es ist ein wesentliches konstruktives Problem, die Vielzahl an Spanngliedverankerungen bei den vorgespannten Reaktoren unterzubringen. Beim Wickelverfahren wird dies zunächst umgangen. Bei doppelt gekrümmten Schalen muß die Oberfläche jedoch gegen das Abgleiten beim Wickeln mit besonderer Profilierung versehen werden. Die den Spannstahl vor Korrosion schützende äußere Betonschicht ist nicht vorgespannt.

Ein in der Firma Dyckerhoff & Widmann entwickeltes Verfahren bringt eine optimale Lösung (Bild 1o). Über einen äußeren Wandring wird mit Hilfe von Radialspanngliedern ein innenliegendes Spanngliedbündel vorgespannt. Nach dem Betonieren

und Erhärten des inneren Betonringes kann die Umlagerung der Druckkraft im äußeren Ring auf den inneren erfolgen. Durch Korrektur der Kraft in den Radialspanngliedern läßt sich gegf. die Vorspannung beliebig steuern, sodaß z.B. der heiße Liner durch Kriechumlagerung keine Überbeanspruchung erfährt.

Diese verschiedenen Last- und Bauzustände bedürfen aber einer genauen Nachrechnung unter Berücksichtigung von Kriechen und Schwinden, was mit dem vorliegenden Programm kein Problem ist. Man wird zweckmäßig mit einem wahrscheinlichen oberen und unteren Kriech- und Schwindwert rechnen, um den Temperatureinfluß (Abschnitt 2) auf die Größe von Kriechzahl und Schwindmaß einigermaßen abzugrenzen.

Es erweist sich dabei als zweckmäßig, innerhalb der Zeitintervalle mit mittleren kriecherzeugenden Spannungen zu rechnen. Neben den elastischen Verformungsgliedern sind dann lediglich noch die plastischen Glieder sowie das Schwinden zu berücksichtigen. Eine ausführliche Beschreibung dieses Rechenverfahrens kann [3] entnommen werden. Das vorliegende Rechenprogramm wurde entsprechend erweitert.

3.4.2 Untersuchung des Einflusses örtlicher Fehlstellen

Das Rechenprogramm ermöglicht durch Variation der Eingaben entweder nach statistischen Methoden [11] (Monte Carlo-Prinzip) oder gezielt die Auswirkung örtlicher Fehlstellen zu verfolgen. So kann durch Ausfall eines Meridianstabes der Einfluß eines örtlichen Versagens (Riß) untersucht werden. Der entsprechende Spaltendruck kann berücksichtigt werden. Auf diese Weise läßt sich sukzessive ein Bruchbild entwickeln.

3.4.3 Unsymmetrische Lastfälle

Unsymmetrische Lastfälle treten bei Spannbetonreaktoren bis auf Erdbebenbeanspruchungen nur selten auf. Dies gilt jedoch nicht für das Containment bzw. im allgemeinen Schalenbau. Man wird dann diesen Lastfall in einen symmetrischen und in einen antimetrischen Anteil zerlegen. Der symmetrische Anteil wird wie beschrieben gelöst. Für die Untersuchung des antimetrischen Lastfalles muß der räumliche gekrümmte Trägerrost (Bild 3 b) in seiner Gesamtheit betrachtet werden. Bei dickwandigen Schalen nimmt jedoch die Zahl der Unbestimmten rasch zu. Die Rechenkapazität der EDV-Anlage reicht dann in vielen Fällen nicht mehr aus.

Es empfiehlt sich dann einen ersten Rechenschritt am Gesamtsystem mit einem groben Raster durchzuführen. Der darauf folgende zweite Rechenschritt wird an einem Teilausschnitt mit entsprechend feinem Raster vollzogen, wobei die Randbedingungen vom ersten Rechenschritt übernommen werden.

4. Beispiele

Es ließe sich eine Vielzahl von bereits gerechneten Beispielen aufführen, angefangen von der Platte zur Schale bis zum dickwandigen Behälter, mit der Absicht, die Ergebnisse der exakten Theorie, anderen Rechenverfahren oder Messungen gegenüber zu stellen. Die Zahl der Beispiele soll aber auf die folgenden beiden beschränkt bleiben.

4.1 Zylindrischer Wasserbehälter

Der in Bild 11 gezeigte Wasserbehälter wird mit dem in Bild 12 aufgetragenem Ersatz-System gerechnet. In Bild 13 sind die Ergebnisse denjenigen nach der Elastizitätstheorie 12 gegenübergestellt. Der maximale Fehler ist kleiner 3 %.

4.2 Reaktordruckbehälter aus Spannbeton

Es handelt sich hier um einen Versuchsreaktor [13] (Bild 14), bei dem die errechneten Beanspruchungen mit Messungen verglichen werden konnten. Bild 15 zeigt das statische Ersatz-System und Bild 16 die Richtung und Größe der Spannungstrajektorien im Störbereich infolge Innendruck. In Bild 17 sind die Ringzugspannungen im Zylinderschaft aufgetragen. Die Übereinstimmung mit den Messungen kann als sehr gut bezeichnet werden.

5. Schlußwort

Am Beispiel des Reaktordruckbehälters wird ein sehr flexibles Rechenverfahren zur Erfassung des Tragverhaltens rotationssymmetrischer, dickwandiger Konstruktionen beschrieben. Das Tragwerk wird dabei in dünne gekoppelte konzentrische Tragsysteme (Bild 8) unterteilt. Die einzelnen dünnwandigen Systeme werden durch einen elastisch gelagerten ebenen Stabzug erfaßt. Es geht die Analogie der Schale zum elastisch gebetteten Balken ein. Mit diesem Ersatzsystem kann der Bau- und Betriebszustand vom Reaktor-Druckbehälter aus Spannbeton mit großer Genauigkeit gerechnet werden. Dynamische Lasten werden durch statische Ersatzlasten berücksichtigt. Das Kriechproblem wird durch die Annahme einer mittleren kriecherzeugenden Spannung vereinfacht. Asymmetrische Lasten können durch die Wahl geeigneter Randbedingungen berücksichtigt werden.

Herrn Dr.Neunert sei an dieser Stelle für seine wertvollen Anregungen, den Herren Bercea und Knell für die Mitarbeit gedankt.

6. Schrifttum

1 Konstruktiver Ingenieurbau, Berichte, Bautechnische Aufgaben bei Kernkraftwerken, Heft 1o, Vulkanverlag Essen 1971

2 DNA, Reaktordruckbehälter aus Spannbeton, Studie für einen Norm-Entwurf 1972

3 Rüsch H., Jungwirth D., Hilsdorf H. — Kritische Sichtung der Verfahren zur Berücksichtigung der Einflüsse von Kriechen und Schwinden des Betons auf das Verhalten der Tragwerke. Beton und Stahlbetonbau 1973/3,4 und 6

4 Zienkiewicz O.C. und Cheung Y.K. — The finite Element Method. Mc. Graw Hill. London 1967

5 Fette H. — Gekrümmte finite Elemente zur Berechnung von Schalentragwerken. Dissertation 1969, Werner-Verlag Düsseldorf

6 Rudy du Preez — Berechnung prismatischer Flächentragwerke mit Hilfe finiter Streifenelemente. Bautechnik 1972/5

7 Zerna W., Schellenbach G. — Zur Berechnung von Spannbeton-Reaktordruckbehälter. Beton- und Stahlbetonbau 197o/11

8 Ackert U., Kreuzinger H. — Numerische Berechnung von Rotationsschalen unter rotationssymmetrischer Last. Der Bauingenieur 1971/6.

9 Starke P. — Biegesteife Rotationsschale. Verlag W.Ernst & Sohn 1968

1o Worch G. — Elastische Scheiben. Betonkalender Teil II, 1967, Wilhelm Ernst & Sohn, Berlin

11 Grasser E., Kraemer U. — Arbeitstagung: Sicherheit von Betonbauten. Deutscher Beton Verein 1973

12 Girkmann K. — Flächentragwerke. 5.Auflage Wien 1959, S.454.

13 Dorner H., Gruhl H. — Spannbeton-Reaktordruckbehälter für 1oo atü Innendruck. Technische Überwachung, Siemens, 1966/1.

Tabelle 1: Lastfälle und zulässige Beanspruchungen bei Spannbetondruckbehälter in Anlehnung an [2]

	BAUTEIL	LASTFALL	ZUL. BEANSPRUCHUNG BETON	ZUL. BEANSPRUCHUNG STAHL
BAUZUSTAND (E-Theorie)	Behälter	verschiedene Herstellphasen	nach DIN 4227 bzw. Spannbetonrichtlinien	DIN 4227 bzw. Spannbetonrichtlinien und Stahlbauvorschriften
BETRIEBSZUSTAND (E-Theorie)	Behälter+Liner	Eigengewicht g Vorspannung v mit Kriechen k und Schwinden s Innendruck p_o (Bemessungsdruck, An- und Abschalten sowie Schnellabschalten) Innendruck beim Störfall p_s Innendruck beim Prüfen p_p Temperatur T Kriech- und Schwind-Umlagerung Erdbeben (über statische Ersatzlast) Verformungsberechnung für Liner-Integrität mit oberen und unteren Grenzwerten aus k*s	In der Regel gilt zul $\sigma = \beta_c/2{,}1$ für Druckspannungen. Bei mehrachsiger Druckbeanspruchung dürfen die entsprechenden Laborergebnisse berücksichtigt werden mit $\nu = 2{,}1$, aber nicht größer als $1{,}5 \cdot \beta_{w,5}/2{,}1$ ($\beta_{w,5}$ = 5% Fraktile der Zylinderfestigkeit nach 90 Tagen) Bei instationärer Temperaturbeanspruchung $\nu = 1{,}8$ Bei normalem Betriebszustand wird in jedem Schnitt ein Druckkräfte gefordert Zugbeanspruchung im Normalfall, zentrisch: zul $\sigma = \beta_c/3o$, Zugbeanspruchung in Außenflächen: zul $\sigma = \beta_c/1o$ Zugbeanspruchung in Störungszone: keine Begrenzung von zul σ	Spannstahl: zul. $\sigma_z = o{,}7 \cdot \beta_z \leq o{,}95 \cdot \beta_{o,o1}$; bei Randspannungen $+15\% \leq \beta_{o,o1}$ Kurzzeitiges Überspannen zul $\sigma_z = \beta_{o,o1}$ Relaxation des Spannstahles ist zu beachten Betonstahl: DIN 1o45
GRENZZUSTÄNDE (E-Theorie, besser aber mit Bruchmodell [1]; z.B. kinematische Kette oder Modell-Versuch)	für Liner-Integrität	Lastkombinationen: $g+1{,}8 \cdot p_o$ $g+1{,}8 \cdot p_o + T$ mit k,s $g+1{,}8 \cdot p_o + o{,}8 \cdot T$ mit k,s + $o{,}2 \cdot T$ ohne k,s (wenn $1{,}6 \cdot p_s > 1{,}8 \cdot p_o$, dann mit $1{,}6 \cdot p_s$ rechnen)	σ_{gr} = o,9 · Mehrachsige Druckfestigkeit bzw. $o{,}9 \cdot \beta_c$ im Druck-Zugbereich wenn $\sigma_{Zug} > \beta_c/3o$, Zug voll abdecken	Spannstahl: $\sigma_{gr} = o{,}95 \cdot \beta_s$ Betonstahl: $\sigma_{gr} = \beta_s$
	für Behälter	Erhöhung des Betriebsdruckes auf das 2,5+3fache je nach Genehmigungsbehörde	$\sigma_{gr} = o{,}9\ \beta_c$ bzw. β_c je nach Genehmigungsbehörde	$\sigma_{gr} = \beta_s$ bzw. β_z je nach Genehmigungsbehörde
	am Behälter-Ersatzsystem, wenn Containment fehlt	Stat. Ersatzlasten für Druckstoß (Explosion), für Prallstoß (Absturz)	Anzustreben lokal in den plastischen Bereich zu kommen ohne schwerwiegende Zerstörung auszulösen.	

BILD 1: REAKTORTYPEN IN DEUTSCHLAND

Reactor types in Germany

Erläuterung zu a,b, und c,:
1 Core
2 Dampferzeugung, Wärmetauscher
3 Frischdampf
4 Druckwasser
5 Druckhalter
6 Turbine
7 Generator
8 Kondensator
9 Pumpe
10 Speisewasser
11 Abschirmbehälter, Containment
12 Druckbehälter
13 Sicherheitsanlagen,
Anlage zum Wechseln der Brennerelemente
14 Primärkreis
15 Sekundärkreis

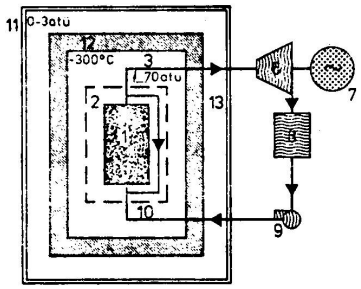

a. SIEDEWASSERREAKTOR Boiling water reactor
(LEICHTWASSERREAKTOR) (Light water reactor)

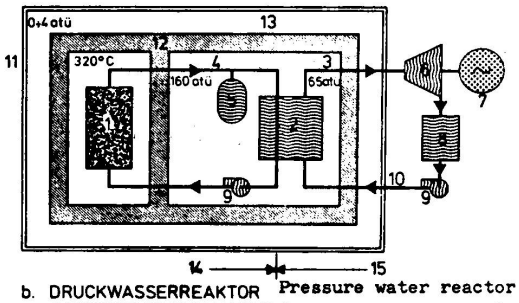

b. DRUCKWASSERREAKTOR Pressure water reactor
(LEICHTWASSERREAKTOR) (Light water reactor)

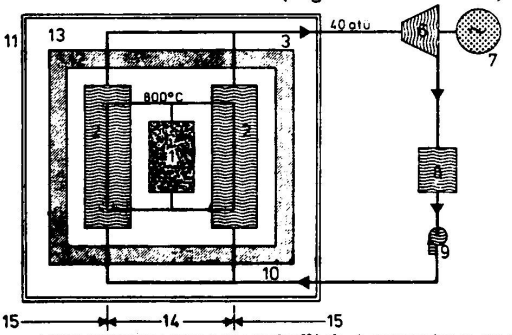

c. HOCHTEMPERATURREAKTOR High temperature reactor
(GASGEKÜHLTER REAKTOR) (reactor cooled with gas)

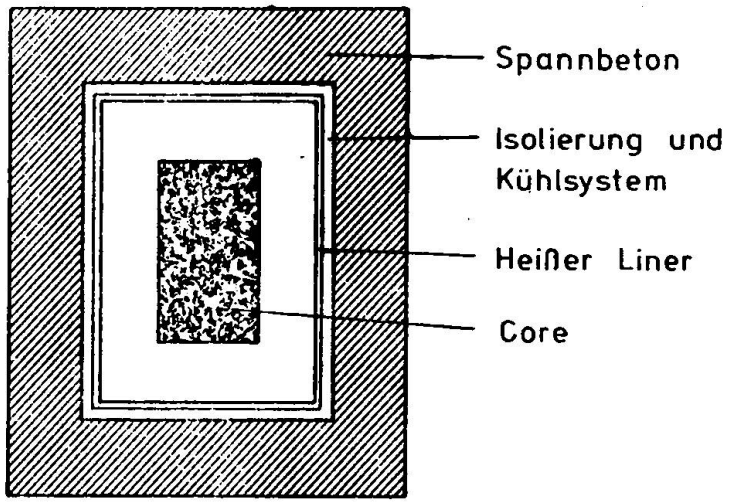

Bild 2: Spannbeton-Druckbehälter
Pressure vessel in prestressed concrete

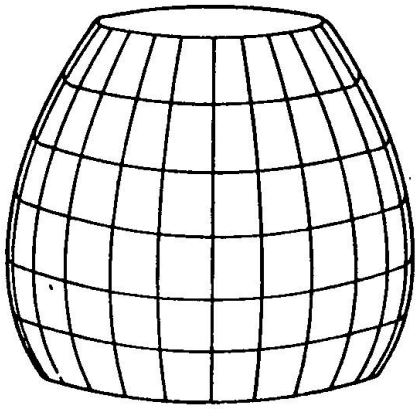

a) Schale
shell

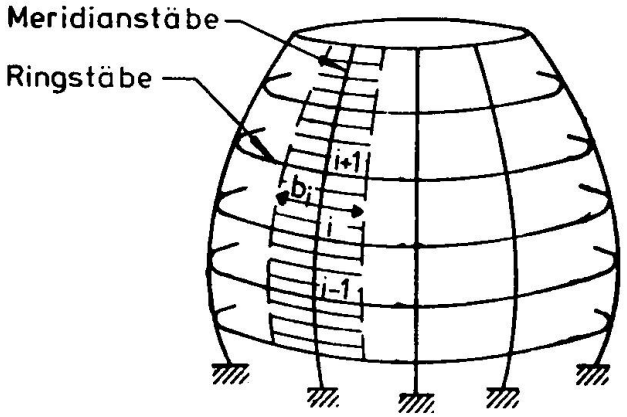

b) räumlich gekrümmter
Trägerrost
locally curved
girder grillage

Bild 3: Von der Schale zum räumlich gekrümmten Trägerrost
From the shell to the locally curved girder grillage

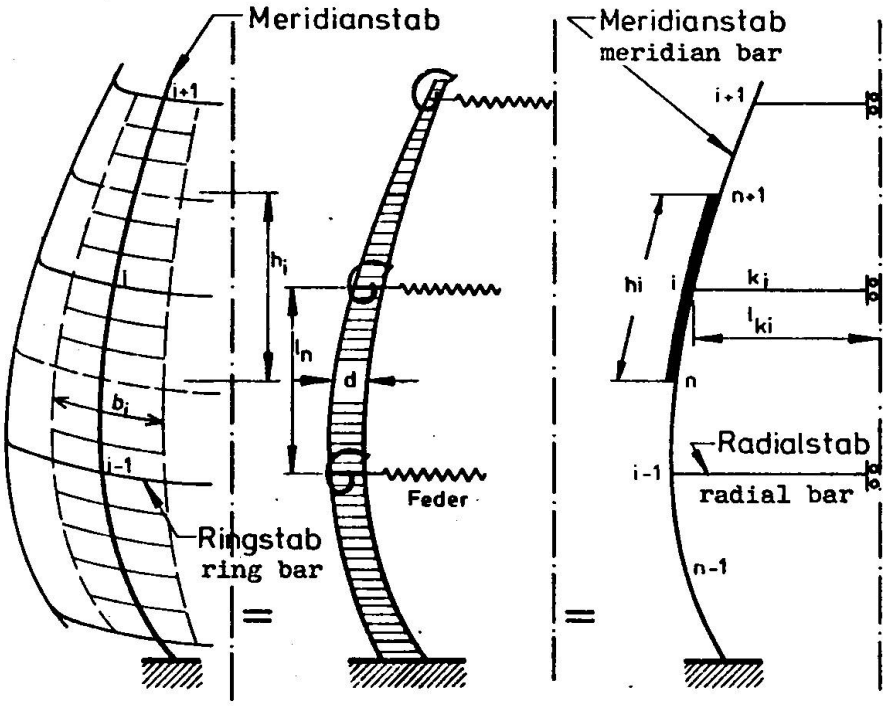

a) räumlich gekrümmter Trägerrost
a) locally curved girder grillage

b) elastisch gelagerter Stabzug
b) elastically placed bar

c) Ersatzsystem
c) system for replacement

Bild 4: Vom räumlich gekrümmten Trägerrost zum Ersatzsystem
From the locally curved girder grillage to the system of replacement

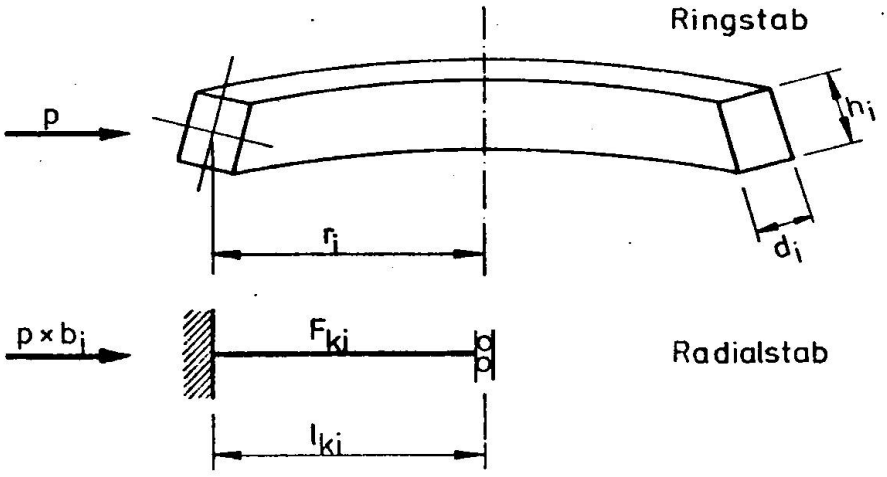

Bild 6: Bedingung zur Bestimmung der Fläche des Radialstabes
Condition for determination of the area for the radial bar

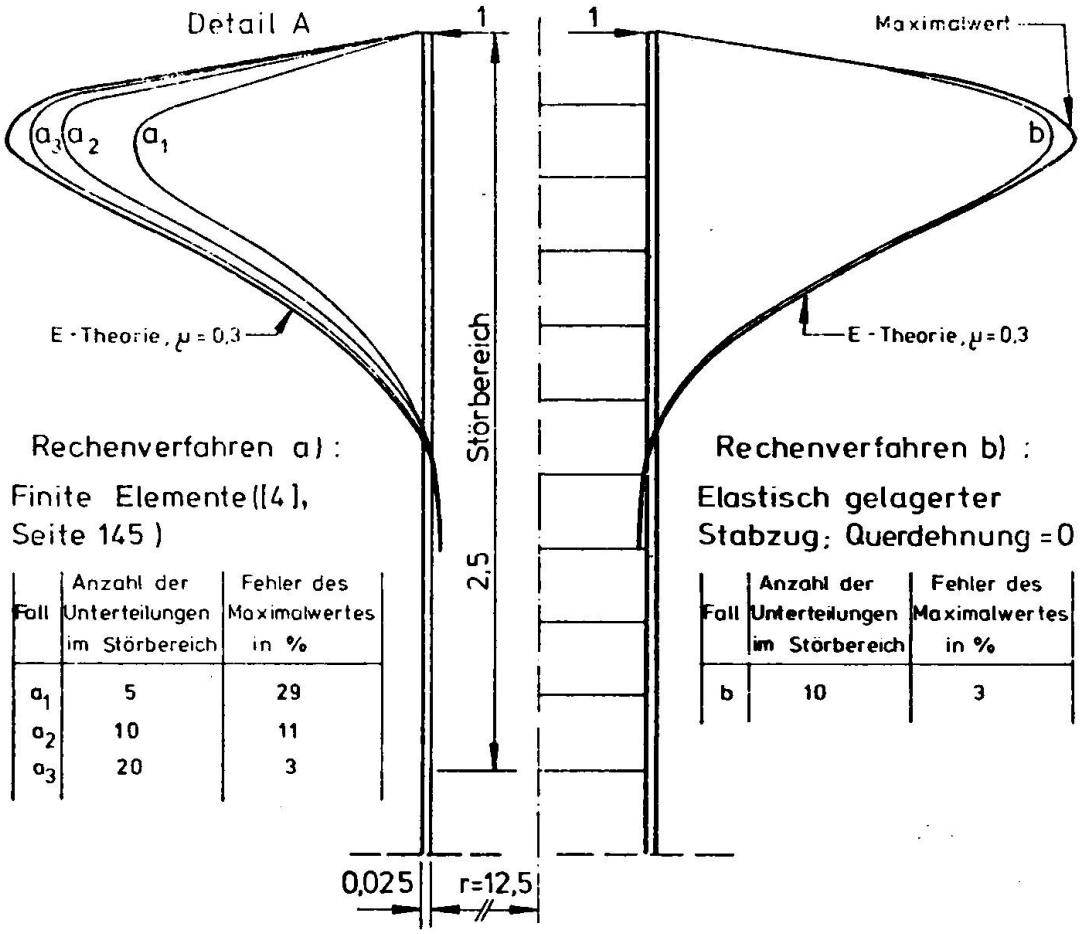

Rechenverfahren a) :

Finite Elemente ([4], Seite 145)

Fall	Anzahl der Unterteilungen im Störbereich	Fehler des Maximalwertes in %
a_1	5	29
a_2	10	11
a_3	20	3

Rechenverfahren b) :

Elastisch gelagerter Stabzug; Querdehnung = 0

Fall	Anzahl der Unterteilungen im Störbereich	Fehler des Maximalwertes in %
b	10	3

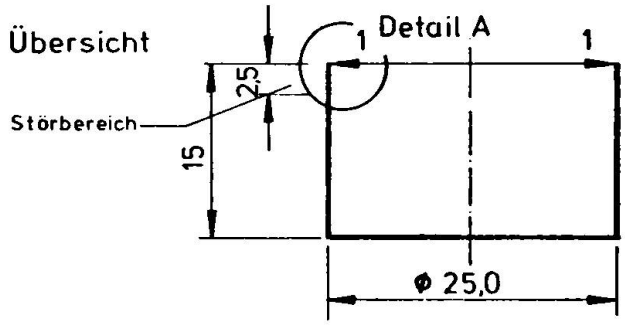

Bild 5 : Fehler verschiedener Rechenverfahren in % Bezogen auf die exakte Lösung am Beispiel einer randbelasteten Zylinderschale

Errors of different calculation systems in percentage referred to the exact solution with the sample of a cylinder shell loaded a the edge

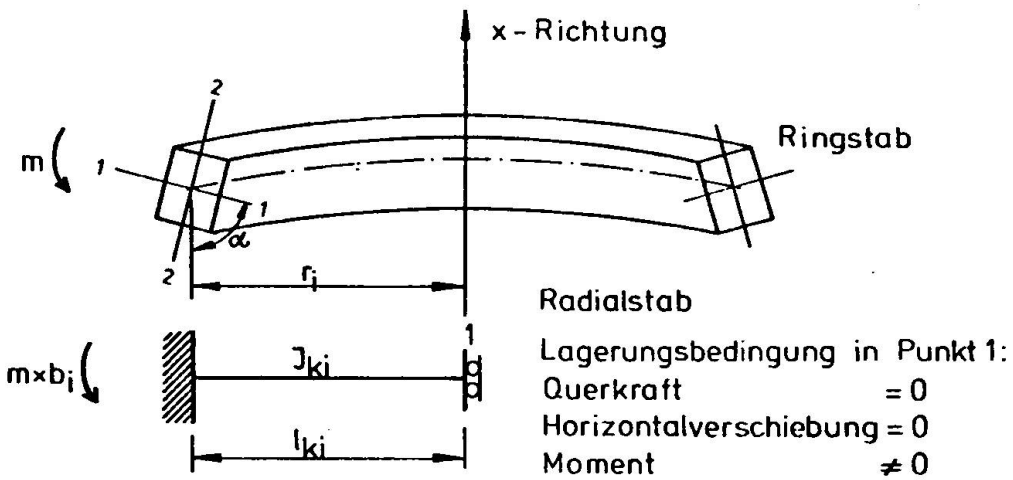

Bild 7: Bedingung zur Bestimmung des Trägheitsmoments des Radialstabes

Condition for determination of the moment of inertia of the radial bar

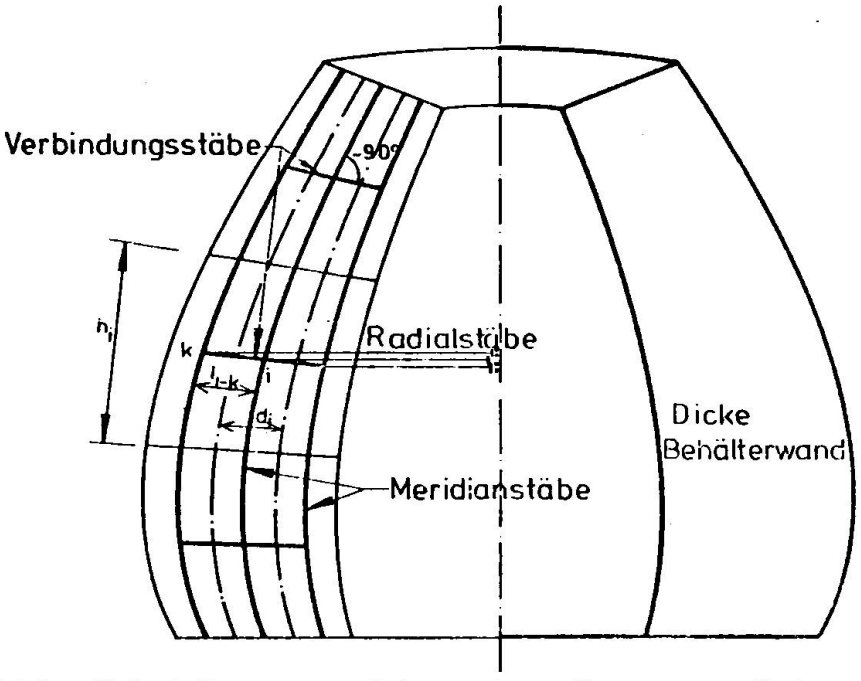

Bild 8: Unterteilung der dickwandigen Schale in zB. 3 konzentrisch dünne Schalen

Splitting up the thick-walled shell - for example in 3 concentric thin shells

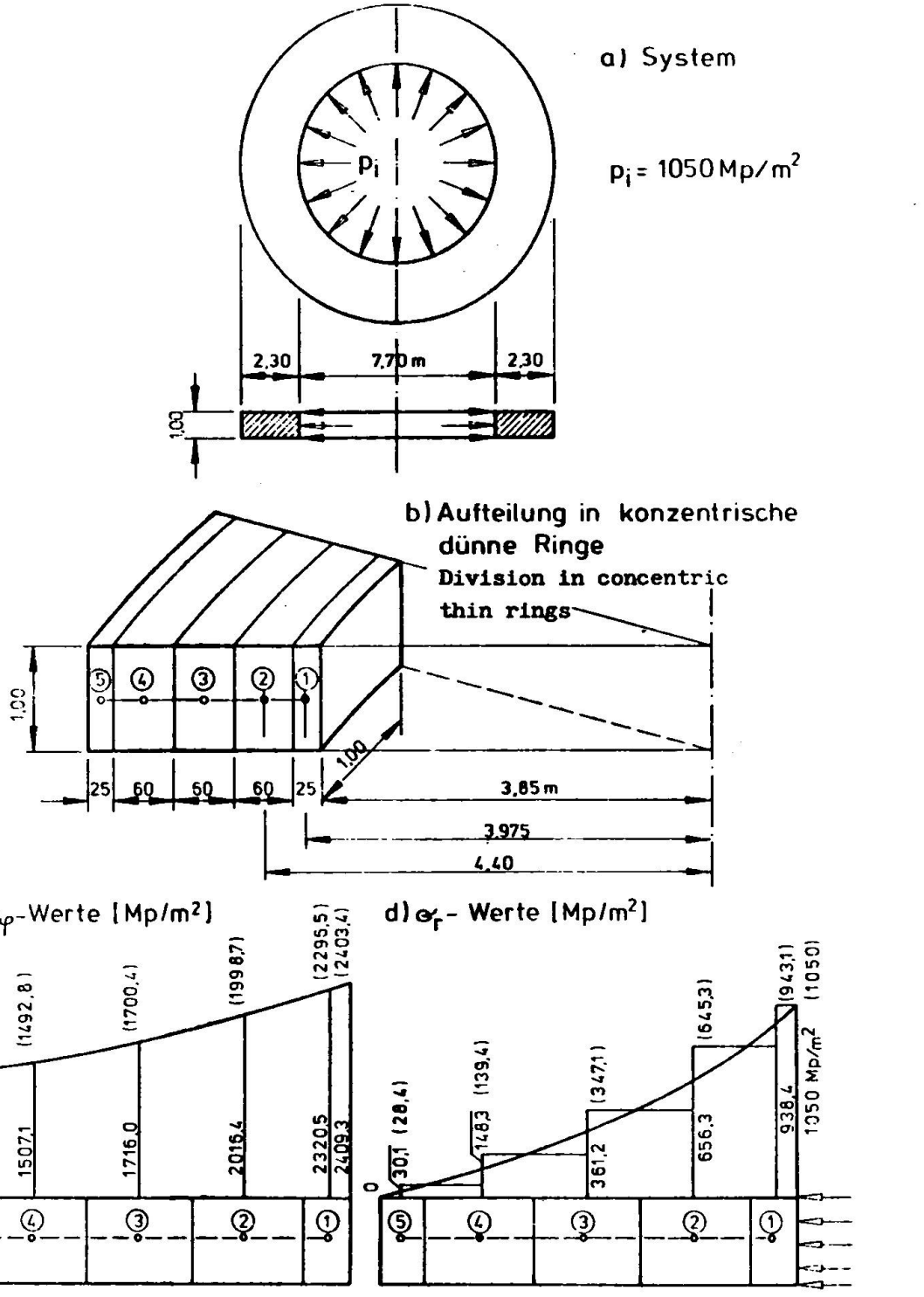

Die Klammerwerte entsprechen der exakten Lösung nach Lamé [10] $_{\mu=0,3}$

Bild 9: Dickwandiger Kreisring unter Innendruck

Circle ring with thick walls under internal pressure

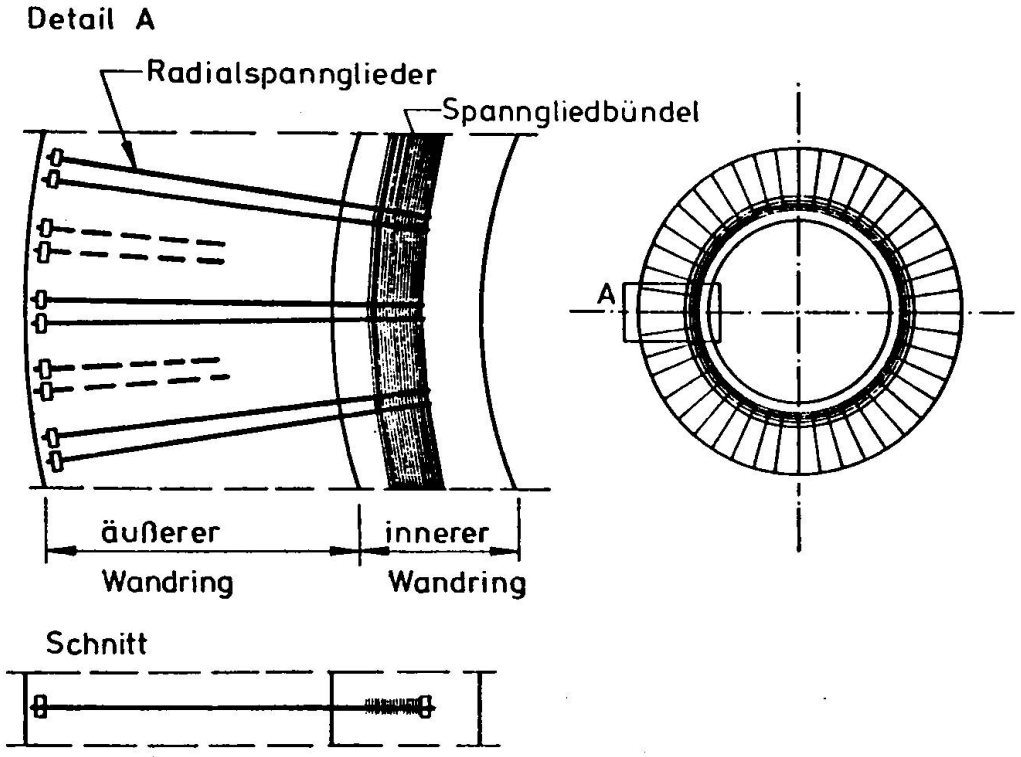

Bild 10: Neuartige Vorspannung eines Spannbeton-Druckbehälters
Novel type of prestressing of p.c. pressure vessel

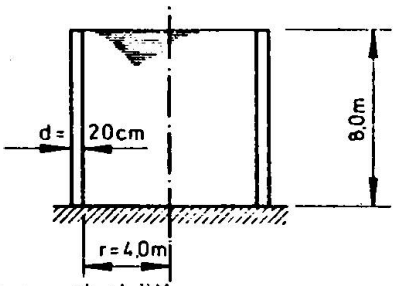

Bild 11: Zylindrischer Wasserbehälter
cylindrical water reservoir

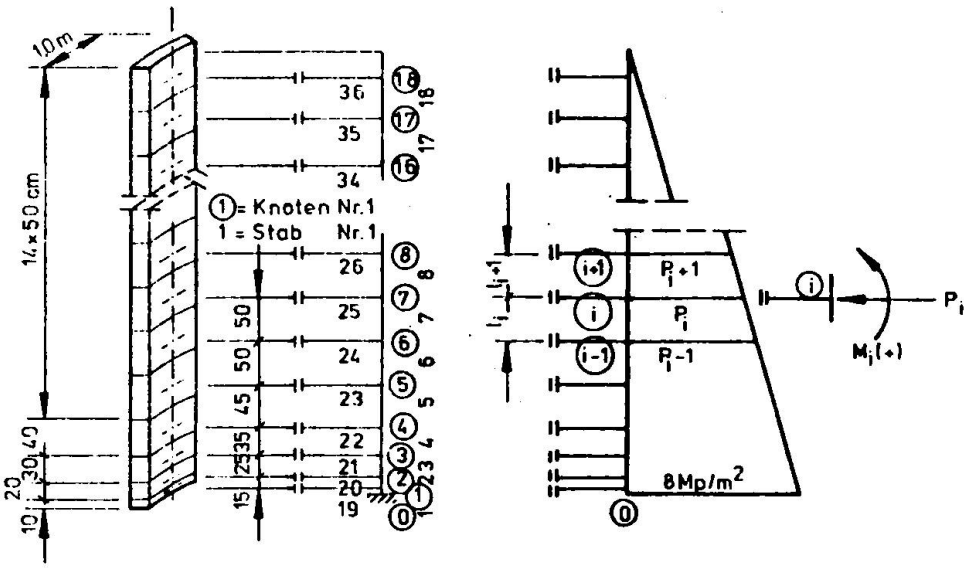

Bild 12: Statisches System und Belastung

Statics and loading

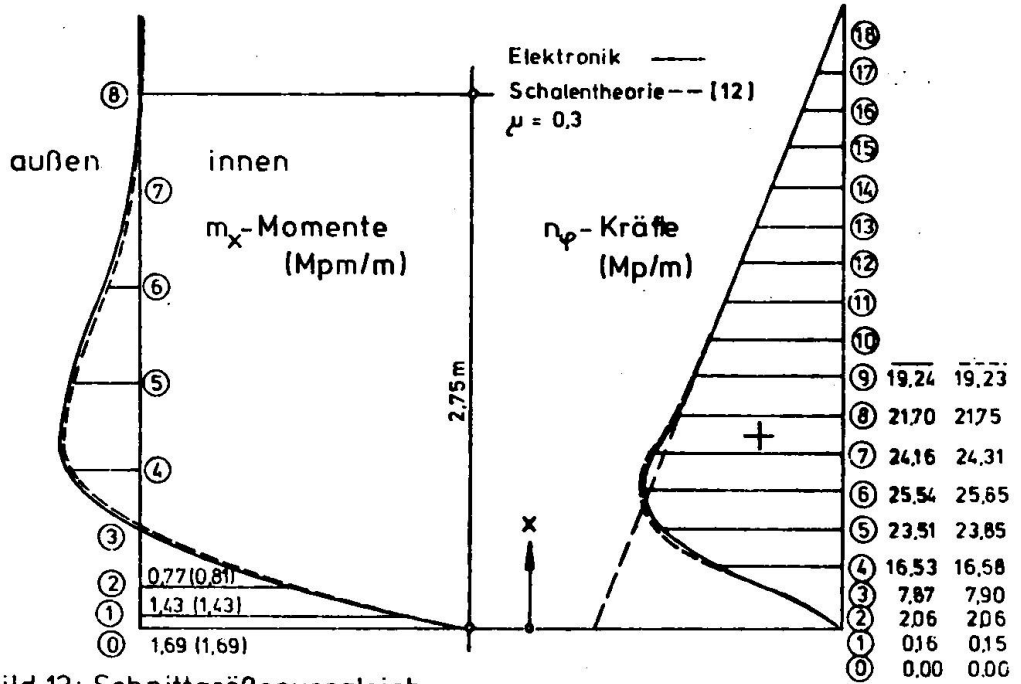

Bild 13: Schnittgrößenvergleich

Comparison of section sizes

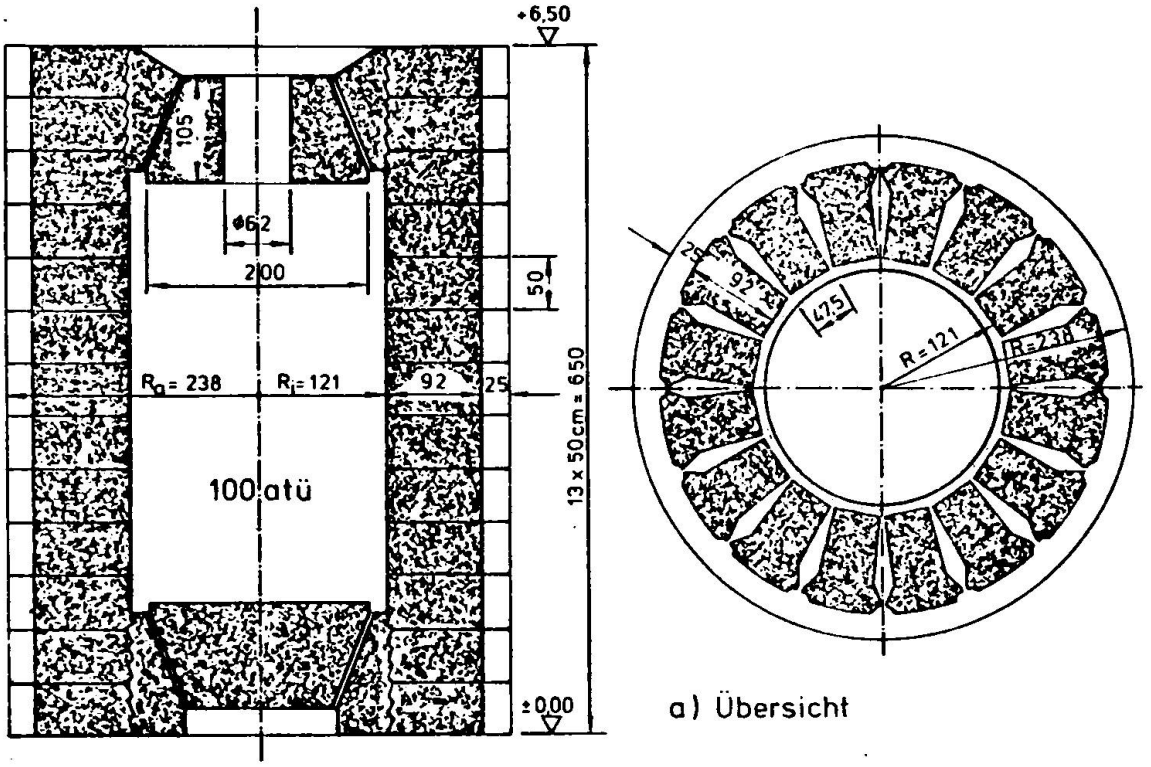

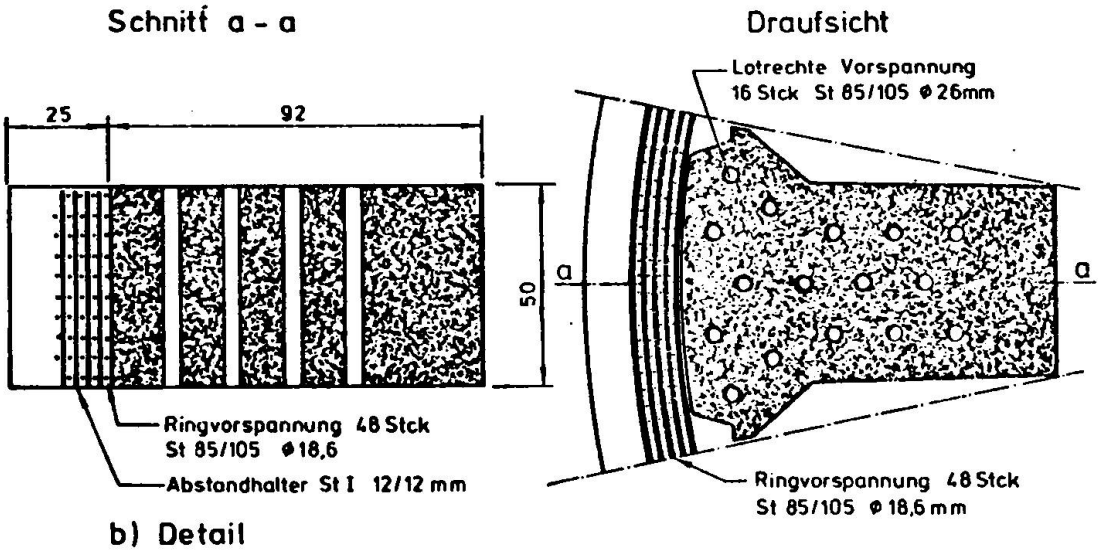

Bild 14: Versuchsreaktor Erlangen

Test Reactor Erlangen

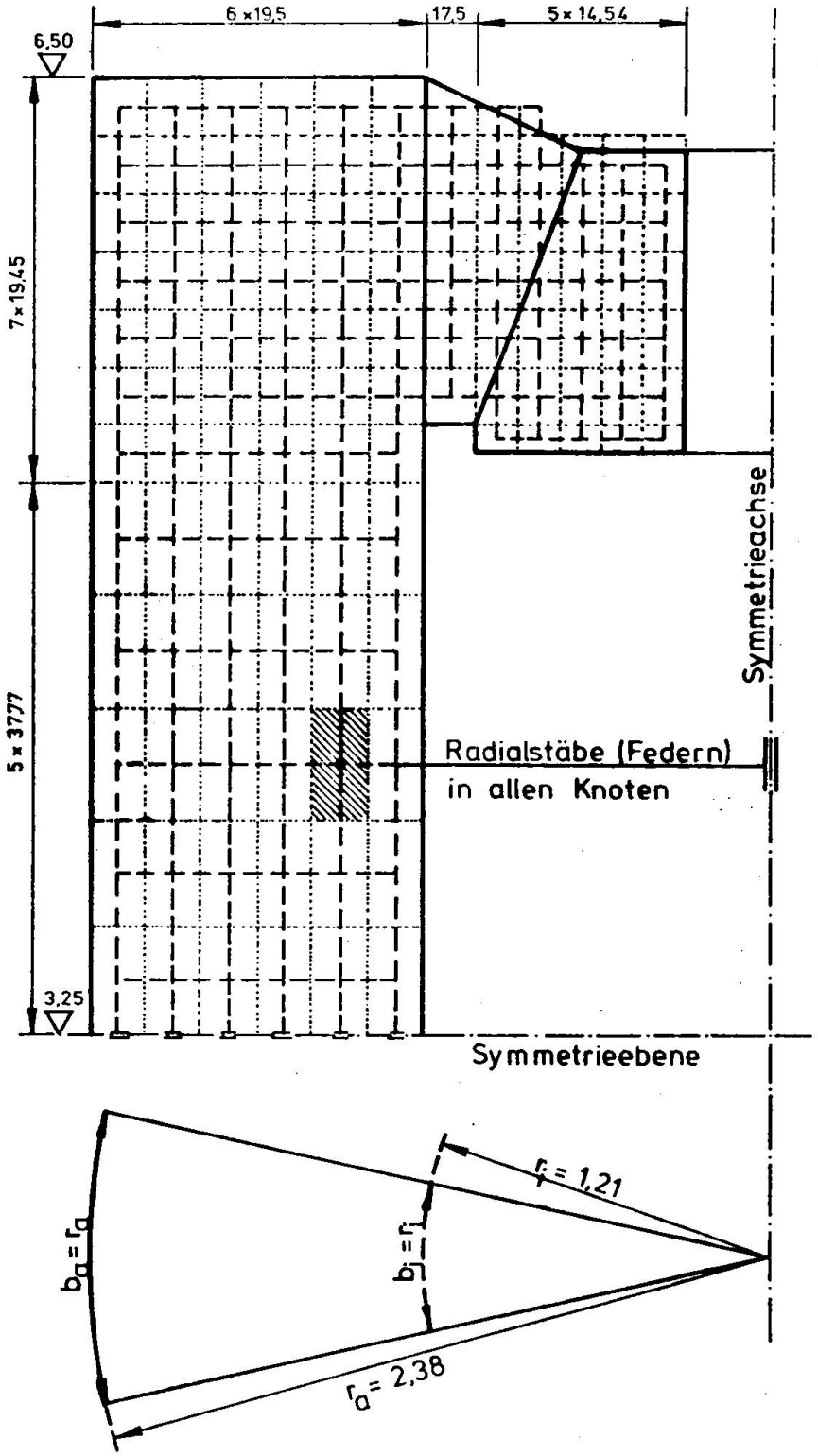

Bild 15: Statisches Ersatz-System

Equivalent static system

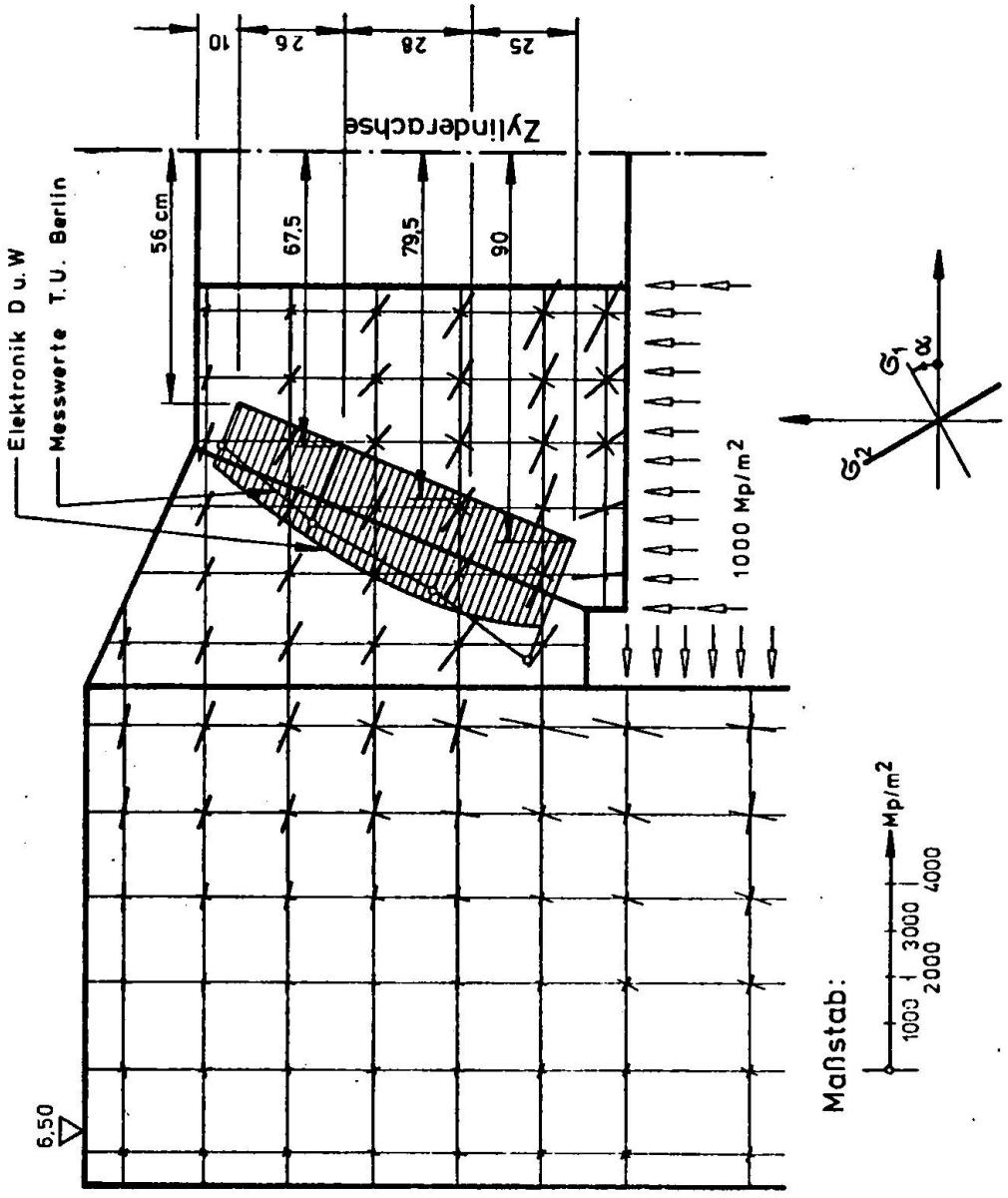

Bild 16: Schiefe Hauptspannungen im Störungsbereich - Lastfall Innendruck Vergleich Messung mit Rechnung

Inclined main stresses in the upper edge of the vessel - loading case internal pressure - comparing measurements with calculation

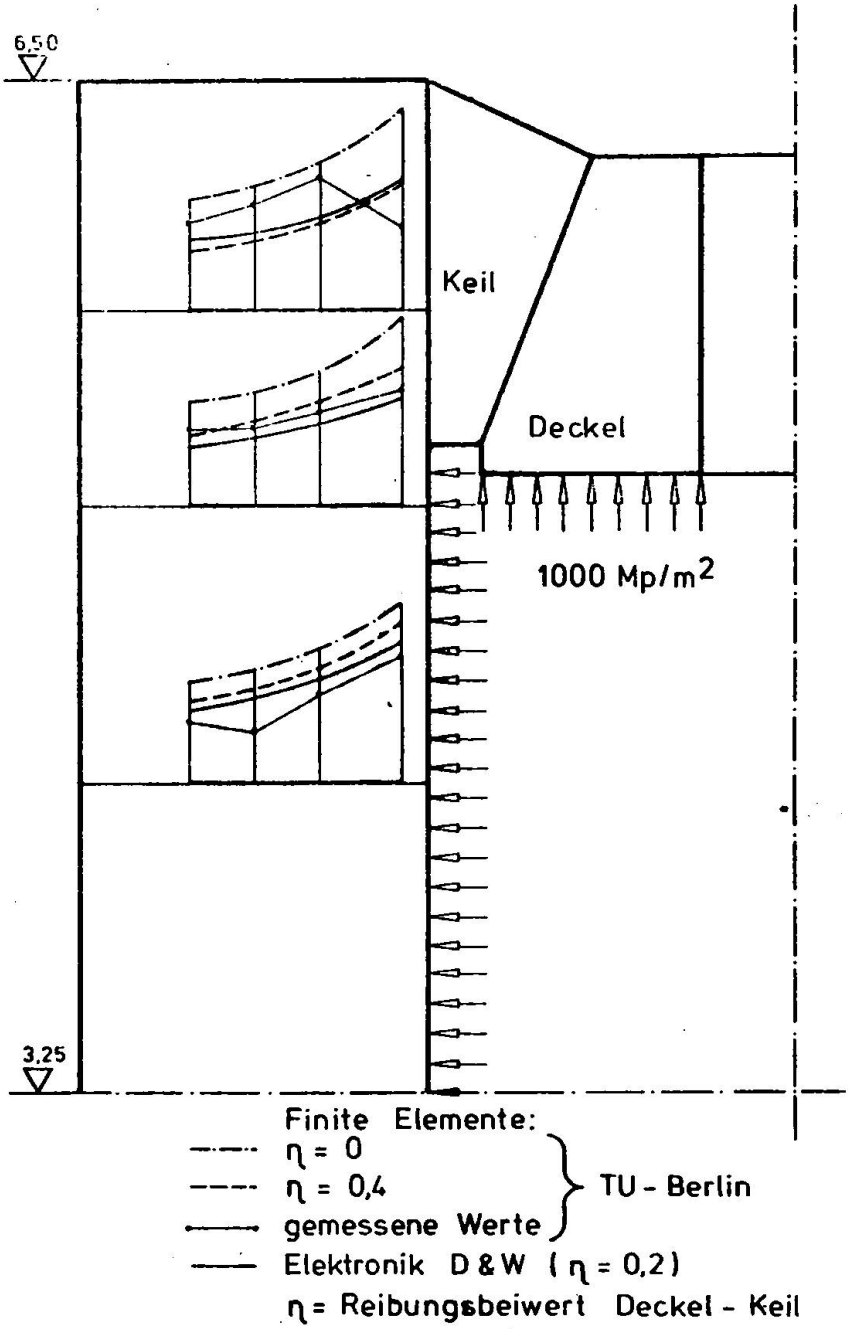

Bild 17: Betonringspannungen σ_φ kp/cm² im Schaftbereich, Lastfall Innendruck, Vergleich Messung mit Rechnung

Stresses of concrete ring σ_φ kp/sq.cm in the zone of the shaft, loading case internal pressure, comparing measurement with calculation

Zusammenfassung

Der Beschreibung verschiedener Reaktortypen und der zu führenden Rechennachweise folgt die Ableitung eines weiteren Berechnungsverfahrens für dickwandige, rotationssymmetrische Konstruktionen. Die Behälterwand wird in ihrem statischen Verhalten durch untereinander gekoppelte Schalen ersetzt; diese werden durch räumlich gekrümmte Trägerroste erfaßt, deren Ringstäbe ins Rechenprogramm über Federn eingehen. Als Anwendungsbeispiel dient ein neuartiger Reaktordruckbehälter aus Spannbeton.

Summary

The description of different reactor types and of the calculation which have to be carried out is followed by the description of a further calculation system for rotation-symmetric constructions with thick walls. For its static behaviour the thick tank wall will be divided in different thin shells coupled to each other; these will be changed into curved girder grillages; the ring bars of which are entering into the technical data programme by means of springs. As a model of application may serve a new type of a reactor vessel in prestressed concrete.

Résumé

La description de différents types de réacteurs avec les correspondantes preuves de calcul est suivie de la dérivée d'un autre procédé de calcul pour constructions rondes, à paroi épaisse. Le comportement statique de la paroi épaisse est remplacé par des voiles minces couplées les unes avec les autres. Ces voiles minces sont remplacées par des grilles de poutres spatialement courbées. Les barres à anneau de ces grilles de poutres entrent dans le programme de calcul à l'aide de ressorts. Un nouveau réservoir de réacteur sous pression en béton précontraint sert d'exemple d'application.

IABSE
AIPC
IVBH

SEMINAR on:
«CONCRETE STRUCTURES SUBJECTED TO TRIAXIAL STRESSES»
17th-19th MAY, 1974 - ISMES - BERGAMO (ITALY)

Grenzbelastungen rotationssymmetrischer Kontinua

Ultimate load of axi-symmetric continua

Sollicitations ultimes des continu symétriques rotatifs

Dipl. Ing. Dr. techn. Wolfram WALLUSCHEK-WALLFELD
Technische Hochschule Graz
Rechbauerstraße 12, A-8010 Graz, Austria

1. Einleitung

Bei der Berechnung von Reaktordruckgefäßen steht mehr als bei anderen Bauwerken die Sicherheit des Druckgefäßes im Vordergrund. Neben den von Land zu Land verschiedenen zulässigen Spannungen beim Gebrauchslastverfahren werden auch Traglastuntersuchungen, z.B. als Nachweis der Dichthautintegrität, und auch Bruchlastberechnungen gefordert. Als Bruchsicherheit wird das Verhältnis von der Grenzlast zufolge eines hypothetisch ansteigenden Innendruckes zum Betriebsdruck definiert. Der ansteigende Innendruck simuliert den Ausfall von Spannkabeln und die üblichen Unsicherheiten von Material, Geometrie, Rechenungenauigkeit usw.

Für genaue Untersuchungen des Bruchvorganges werden die Finite Element Methode (Lit. 1,2,3) oder das Rechenverfahren der dynamischen Relaxation verwendet (Lit. 4). Diese Verfahren benötigen einen sehr großen Aufwand an Maschinenzeit, der durch viele Iterationen im plastischen Bereich der Stahlteile und der nur schrittweise erfaßbaren Rißfortpflanzung bei Steigerung des Innendruckes bedingt ist. Der Rechenaufwand der Methode der kinematischen Bruchmodelle (Lit. 5) ist dazu relativ gering.

Die neuesten Entwicklungen (Lit. 6,7,8) von Spannbetondruckbehältern für Leichtwasserreaktoren weisen folgende, typischen, geometrischen Merkmale auf:

- o zylindrische Form des Behälters;
- o oberer Abschluß als Deckel mit ungefähr gleichem Durchmesser wie Behälterinnendurchmesser;
- o Ausrundung des Überganges von Zylinderwand zu Behälterboden;
- o Bodenplattendurchmesser wesentlich größer als Zylinderwandstärke.

Auf Grund dieser Merkmale kann man annehmen, daß ein Versagen der Tragfähigkeit des Behälters durch Bruch des zylindrischen Teiles eintritt. Die Deckelabstützung und der Deckel selbst müssen gesondert untersucht werden.

Für die näherungsweise Berechnung der Grenzlast wird für den Mittelteil des zylindrischen Behälterteiles ein einfaches Rechenverfahren gezeigt. Dieses eignet sich auch ausgezeichnet zur Vorberechnung des zylindrischen Teiles von Druckbehältern und zur Festlegung von Wandstärke und Spannkräften (Lit. 3).

2. Die Methode des unendlichen Zylinders

Den folgenden Entwicklungen wird das Rechenmodell eines unendlich langen, dickwandigen, vollkommen rotationssymmetrischen Zylinders zugrunde gelegt. Das bedeutet Ebenbleiben des Querschnittes senkrecht zur Rotationsachse. Die axiale Ausdehnung ist jedoch nicht behindert - es können zwängungsfreie, gleichmäßige Temperatur- und Kriechverformungen auch in axialer Richtung auftreten.

Die Rotationssymmetrie bedingt Schubspannungsfreiheit in der Vertikal-Tangentialebene und in der Querschnittsebene.

Die Annahme eines unendlich langen Zylinders bedingt ferner, daß die Schubspannungen in der Radial-Axialebene Null werden und die drei Normalspannungen in radialer, tangentialer und axialer Richtung gleichzeitig die entsprechenden Hauptspannungen sind.

Die Methode des unendlichen Zylinders hat unter den obigen Voraussetzungen gegenüber der Finiten Element Methode folgende Vorteile:

- Die Spannungen werden direkt aus dem Gleichungssystem gewonnen.
- Um zwängungsfreie, axiale Ausdehnung infolge gleichmäßiger Temperatur bei ebenbleibendem Querschnitt zulassen zu können, sind bei einer Berechnung mit der Finiten Element Methode zwei Vorberechnungen zur Ermittlung der gleichmäßigen, axialen Verschiebung für die benötigten Randbedingungen erforderlich. Mit den daraus errechneten Knotenverschiebungen kann erst in einer dritten Rechnung die Spannungsermittlung durchgeführt werden.

Der inhomogene Zylinder wird je nach gewünschter Genauigkeit in eine Zahl von Teilzylindern (Abb. 1) aufgelöst, wobei jeder Teilzylinder für sich als homogener Zylinder mit besonderen Materialeigenschaften aufgefaßt wird. Für jeden Teilzylinder werden Gleichgewichtsbedingungen, und für jede Begrenzungsfläche zwischen je zwei Teilzylindern Kontinuitätsbedingungen aufgestellt. Als Lösung ergeben sich die drei Hauptspannungen.

Radiale Kontinuitätsbedingung

An der Berührungsfläche zweier Teilzylinder darf keine Klaffung auftreten. Das bedeutet, daß dort die Verschiebung beider Teilzylinder in radialer Richtung (u_i, u_{i-1}) gleich sein muß.

Die Verschiebungen hängen von den Dehnungen in radialer und in tangentialer Richtung ab.

Die in Abb. 2 eingezeichneten Verschiebungen und Richtungen werden durch positive Dehnungen in radialer und tangentialer Richtung hervorgerufen.

Für die Gesamtverschiebungen zweier benachbarter Teilzylinder i und i-1 ergibt sich für die Begrenzungsfläche i die Bedingung:

$$u_{t,i} - u_{r,i} = u_{r,i-1} + u_{t,i-1} \qquad (1)$$

Nimmt man die radiale Dehnung in einem Teilzylinder näherungsweise konstant an, so erhält man für den Teilzylinder i-1 auf der Innen- und Außenseite die Verschiebung

$$u_{r,i-1} = \varepsilon_{r,i-1} \cdot \frac{r_i - r_{i-1}}{2} \tag{2}$$

und für den Teilzylinder i

$$u_{r,i} = \varepsilon_{r,i} \cdot \frac{r_{i+1} - r_i}{2} \tag{3}$$

Der Verschiebungsanteil aus der tangentialen Dehnung bewirkt eine Umfangsvergrößerung und daher eine Vergrößerung des Radius.

Ist ΔU_i die mittlere Umfangsvergrößerung bei Änderung des Radius $r_m = (r_i + r_{i+1}) \cdot 0{,}5$ um u_t, so gilt

$$2\,(r_m + u_{t,i}) \cdot \pi = 2\,r_m \cdot \pi + \Delta U_i \tag{4}$$

Die Zunahme des Umfanges infolge der mittleren Dehnung $\varepsilon_{t,i}$ beträgt:

$$\Delta U_i = \varepsilon_{t,i} \cdot 2\,\frac{(r_{i+1} + r_i)}{2} \cdot \pi \tag{5}$$

Man erhält somit

$$u_{t,i} = \varepsilon_{t,i}\,\frac{(r_{i+1} + r_i)}{2} \tag{6}$$

und

$$u_{t,i-1} = \varepsilon_{t,i-1}\,\frac{(r_i + r_{i-1})}{2} \tag{7}$$

Damit erhält man die Kontinuitätsbedingung

$$\varepsilon_{t,i} \cdot \frac{(r_{i+1} + r_i)}{2} - \varepsilon_{r,i} \cdot \frac{(r_{i+1} - r_i)}{2} = \\ = \varepsilon_{t,i-1} \cdot \frac{(r_i + r_{i-1})}{2} + \varepsilon_{r,i-1} \cdot \frac{(r_i - r_{i-1})}{2} \tag{8}$$

Berücksichtigt man Temperaturdehnungen $\varepsilon_{T,i}$ und $\varepsilon_{T,i-1}$ in den Teilzylindern, so gilt

$$(\varepsilon_{t,i} + \varepsilon_{T,i}) \cdot \frac{r_{i+1} + r_i}{2} - (\varepsilon_{r,i} + \varepsilon_{T,i}) \cdot \frac{r_{i+1} - r_i}{2} - \\ - (\varepsilon_{t,i-1} + \varepsilon_{T,i-1}) \cdot \frac{r_i + r_{i-1}}{2} - (\varepsilon_{r,i-1} + \varepsilon_{T,i-1}) \cdot \\ \cdot \frac{r_i - r_{i-1}}{2} = 0 \tag{9}$$

Mit Hilfe des Hooke'schen Gesetzes werden nun die Dehnungen durch die Spannungen ersetzt. Man kann mit guter Genauigkeit für einen Teilzylinder i die Tangentialspannungen σ_t und Axialspannungen σ_z als Mittelwert über die Wanddicke des Teilzylinders in die Rechnung einführen. Bei den Radialspannungen $\sigma_{r,i}$ und $\sigma_{r,i+1}$ wird ihre Abhängigkeit vom Radius berücksichtigt (Abb. 3).

Äußere Kräfte, wie z.B. Vorspannkräfte, zwischen den Teilzylindern werden hälftig auf den äußeren und inneren Teilzylinder aufgeteilt.

Es wird die Vorzeichenfestlegung getroffen, daß äußere, radiale Belastungen $V_{B,r}$ positiv sind, wenn sie von innen nach außen wirken.

Die radiale Kontinuitätsbedingung an der Kontaktfläche i lautet somit:

$$\sigma_{r,i-1} \cdot {}^{D}S_{,i-1} + \sigma_{z,i-1} \cdot {}^{E}S_{,i-1} + \sigma_{t,i-1} \cdot {}^{F}S_{,i-1} + \sigma_{r,i} \cdot {}^{G}S_{,i} + \\ + \sigma_{z,i} \cdot {}^{H}S_{,i} + \sigma_{t,i} \cdot {}^{J}S_{,i} + \sigma_{r,i+1} \cdot {}^{K}S_{,i+1} = {}^{B}K_{,r,i} \qquad (10)$$

Es ist

$${}^{B}K_{,r,i} = {}^{V}T_{,r,i} + {}^{V}B_{,r,i-1} \cdot {}^{D}B_{,r,i} + {}^{V}B_{,r,i} \cdot {}^{G}B_{,i} + \\ + {}^{V}B_{,r,i+1} \cdot {}^{K}B_{,i+1}$$

Die einzelnen Koeffizienten lauten:

$${}^{D}S_{,i-1} = \frac{1}{4\,E_{i-1}} \left[(r_i + r_{i-1}) \cdot \nu_{i-1} - (r_i - r_{i-1})\right]$$

$${}^{E}S_{,i-1} = \frac{r_i \cdot \nu_{i-1}}{E_{i-1}}$$

$${}^{F}S_{,i-1} = \frac{1}{2\,E_{i-1}} \left[(r_i - r_{i-1}) \cdot \nu_{i-1} - (r_i + r_{i-1})\right]$$

$${}^{G}S_{,i} = \frac{1}{4\,E_{i-1}} \left[(r_i + r_{i-1}) \cdot \nu_{i-1} - (r_i - r_{i-1})\right] - \frac{1}{4\,E_i} \cdot \\ \cdot \left[(r_{i-1} + r_i) \cdot \nu_i + (r_{i+1} - r_i)\right]$$

$${}^{H}S_{,i} = -\frac{r_i \cdot \nu_i}{E_i}$$

$${}^{J}S_{,i} = \frac{1}{2\,E_i} \left[(r_{i+1} + r_i) + (r_{i+1} - r_i) \cdot \nu_i\right]$$

$$K_{S,i+1} = -\frac{1}{4\,E_i}\left[(r_{i+1}+r_i)\cdot\nu_i + (r_{i+1}-r_i)\right]$$

$$V_{T,r,i} = r_i\,(\varepsilon_{T,i-1} - \varepsilon_{T,i}) = r_i\,(\alpha_{T,i-1}\cdot T_{i-1} - \alpha_{T,i}\,T_i)$$

Es ist ν_i die Querdehnzahl, E_i der Elastizitätsmodul und $\alpha_{T,i}$ der Wärmeausdehnungskoeffizient, T_i die Temperatur des Teilzylinders i.

$$D_{B,i-1} = D_{S,i-1}$$

$$G_{B,i} \neq G_{S,i}$$

$$G_{B,i} = \frac{1}{4\,E_{i-1}}\left[(r_i - r_{i-1}) - (r_i + r_{i-1})\cdot\nu_{i-1}\right] -$$

$$- \frac{1}{4\,E_i}\left[(r_{i+1}+r_i)\cdot\nu_i + (r_{i+1}-r_i)\right]$$

$$K_{B,i+1} = -K_{S,i+1}$$

<u>Axiale Kontinuitätsbedingung</u>

Da an einem unendlich langen Hohlzylinder die Schnittebene senkrecht zur Rotationsachse eben bleiben muß, gilt dies auch für zwei benachbarte Teilzylinder.

$$\varepsilon_{z,i} = \varepsilon_{z,i-1} \tag{11}$$

Für die axialen Dehnungen der Teilzylinder i und i-1 erhält man

$$\varepsilon_{z,i} = \frac{1}{E_i}\left[\sigma_{z,i} - (\sigma_{t,i} + \frac{\sigma_{r,i+1}+\sigma_{r,i}}{2})\cdot\nu_i\right] + \alpha_{T,i-1}\cdot T_{i-1}$$

$$\varepsilon_{z,i-1} = \frac{1}{E_{i-1}}\left[\sigma_{z,i-1} - (\sigma_{t,i-1} + \frac{\sigma_{r,i}+\sigma_{r,i-1}}{2})\cdot\nu_{i-1}\right] +$$

$$+ \alpha_{T,i-1}\cdot T_{i-1} \tag{12}$$

Die axiale Kontinuitätsbedingung für den Teilzylinder i-1 und i ergibt sich zu

$$\sigma_{r,i-1}\cdot L_{S,i-1} + \sigma_{z,i-1}\cdot M_{S,i-1} + \sigma_{t,i-1}\cdot N_{S,i-1} +$$

$$+ \sigma_{r,i}\cdot O_{S,i} + \sigma_{z,i}\cdot P_{S,i} + \sigma_{t,i}\cdot Q_{S,i} + \sigma_{r,i+1}\cdot R_{S,i+1} = B_{K,z,i}$$

(13)

Es ist

$$B_{K,z,i} = V_{T,z,i} + V_{B,r,i-1} \cdot L_{B,i-1} + V_{B,r,i} \cdot O_{B,i} + V_{B,r,i+1} \cdot R_{B,i+1}$$

mit den Koeffizienten

$$L_{S,i-1} = \frac{\nu_{i-1}}{2\,E_{i-1}}$$

$$M_{S,i-1} = -\frac{1}{E_{i-1}}$$

$$N_{S,i-1} = \frac{\nu_{i-1}}{E_{i-1}}$$

$$O_{S,i} = \frac{\nu_{i-1}}{2\,E_{i-1}} - \frac{\nu_i}{2\,E_i}$$

$$P_{S,i} = \frac{1}{E_i}$$

$$Q_{S,i} = -\frac{\nu_i}{E_i}$$

$$R_{S,i+1} = -\frac{\nu_i}{2\,E_i}$$

$$V_{T,z,i} = \alpha_{T,i-1} \cdot T_{i-1} - \alpha_{T,i} \cdot T_i$$

$$L_{B,i-1} = L_{S,i-1}$$

$$O_{B,i} = -\frac{\nu_i}{2\,E_i} - \frac{\nu_{i-1}}{2\,E_{i-1}}$$

$$R_{B,i+1} = -R_{S,i+1}$$

Radiale Gleichgewichtsbedingung

Mit den obigen Voraussetzungen erhält man mit Abb. 3 und der Bedingung, daß die Summe aller radialen Kräfte Null sein muß:

$$\sigma_{r,i} \cdot r_i \cdot d\varphi - \sigma_{r,i+1} \cdot r_{i+1} \cdot d\varphi + 2 \cdot \sigma_{t,i} \cdot (r_{i+1} - r_i) \cdot \sin\frac{d\varphi}{2} = 0 \qquad (14)$$

Mit $\sin \frac{d\varphi}{2} \approx \frac{d\varphi}{2}$ erhält man

$$\sigma_{r,i} \cdot A_{S,i} + \sigma_{t,i} \cdot B_{S,i} + \sigma_{r,i+1} \cdot C_{S,i+1} = B_{G,r,i} \qquad (15)$$

$$B_{G,r,i} = V_{B,r,i} \cdot A_{B,i} + V_{B,r,i+1} \cdot C_{B,i+1}$$

mit den Koeffizienten

$$A_{S,i} = r_i$$

$$B_{S,i} = (r_{i+1} - r_i)$$

$$C_{S,i+1} = - r_{i+1}$$

$$A_{B,i} = A_{S,i} = r_i$$

$$C_{B,i+1} = - C_{S,i+1} = r_{i+1}$$

Axiale Gleichgewichtsbedingung

Die Bedingung lautet, daß die resultierende, äußere, axiale Kraft gleich der Summe der inneren Kräfte sein muß. Eine äußere Zugkraft $V_{B,z}$ wird positiv, eine äußere Druckkraft negativ eingeführt.

$$\sum_{i=1}^{n} \sigma_{z,i} \cdot (r_{i+1}^2 - r_i^2) \cdot \pi = V_{B,z} \qquad (16)$$

Mit

$$S_{S,i} = (r_{i+1}^2 - r_i^2) \cdot \pi$$

und

$$B_{G,z} = V_{B,z}$$

lautet die Gleichgewichtsbedingung

$$\sum_{i=1}^{n} \sigma_{z,i} \cdot S_{S,i} = B_{G,z} \qquad (17)$$

Teilzylinder mit Rißflächen

Treten in einem Teilzylinder i nach Abb. 4 Radialfugen auf, so ist hiefür $\sigma_{t,i} = 0$. Treten horizontale Fugen auf, so wird $\sigma_{z,i} = 0$. Es können radiale und horizontale Fugen auch gleichzeitig auftreten.

Nach Abb. 4 treten im Teilzylinder i mit beschränkter Tragfähigkeit Dehnungen $\varepsilon_{z,i}$ und $\varepsilon_{t,i}$ nur aus Quer- und Temperaturdehnung auf. Da Spannungen $\sigma_{z,i}$ und $\sigma_{t,i}$ infolge der Risse nicht auftreten können, entstehen gegenüber den nichtgerissenen Teilzylindern Differenzen $\Delta\varepsilon_{z,i}$ und $\Delta\varepsilon_{t,i}$ der Dehnungen aus den Kontinuitätsbedingungen.
In die weitere Rechnung werden diese ideellen Rißdehnungen $\Delta\varepsilon_{z,i}$ und $\Delta\varepsilon_{t,i}$ als Unbekannte anstelle der Spannungen $\sigma_{z,i}$ und $\sigma_{t,i}$ eingeführt. Durch diese Maßnahme brauchen nur wenige Koeffizienten im Gleichungssystem geändert zu werden.

Horizontale Rißebenen ($\sigma_{z,i} = 0$)

In den radialen Kontinuitätsbedingungen fallen die Anteile der Axialspannung $\sigma_{z,i}$ weg.

$K_{r,i}$:

$$\sigma_{r,i-1} \cdot D_{S,i-1} + \sigma_{z,i-1} \cdot E_{S,i-1} + \sigma_{t,i-1} \cdot F_{S,i-1} + \sigma_{r,i} \cdot G_{S,i} + \sigma_{t,i} \cdot J_{S,i} + \sigma_{r,i+1} \cdot K_{S,i+1} = B_{K,r,i} \qquad (18)$$

$K_{r,i+1}$:

$$\sigma_{r,i} \cdot D_{S,i} + \sigma_{t,i} \cdot F_{S,i} + \sigma_{r,i+1} \cdot G_{S,i+1} + \sigma_{z,i+1} \cdot H_{S,i+1} + \sigma_{t,i+1} \cdot J_{S,i+1} + \sigma_{r,i+2} \cdot K_{S,i+2} = B_{K,r,i+1} \qquad (19)$$

Aus der axialen Kontinuitätsbedingung der Teilzylinder i und i-1 ergibt sich nach Abb. 4

$$\Delta\varepsilon_{z,i} + \varepsilon_{z,i} = \varepsilon_{z,i-1} \qquad (20)$$

Für den Teilzylinder mit beschränkter Tragfähigkeit ist statt $\sigma_{z,i} \cdot P_i$ nun $\Delta\varepsilon_{z,i}$ einzuführen und man erhält die Kontinuitätsgleichung:

$K_{z,i}$:

$$\sigma_{r,i-1} \cdot L_{S,i-1} + \sigma_{z,i-1} \cdot M_{S,i-1} + \sigma_{t,i-1} \cdot N_{S,i-1} + \sigma_{r,i} \cdot O_{S,i} + \Delta\varepsilon_{z,i} + \sigma_{t,i} \cdot Q_{S,i} + \sigma_{t,i+1} \cdot R_{S,i+1} = B_{K,z,i} \qquad (21)$$

Für die axiale Kontinuitätsbedingung zwischen den Teilzylindern i und i+1 ergibt sich mit ($-\Delta\varepsilon_{z,i}$) statt

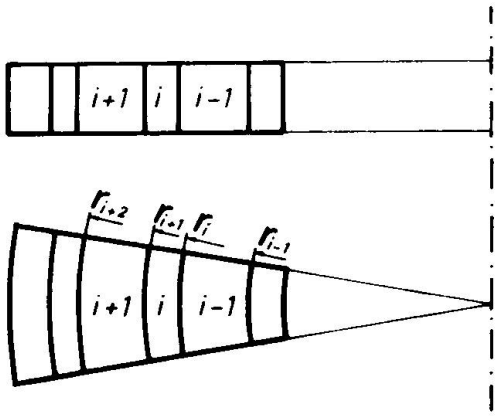

ABB. 1

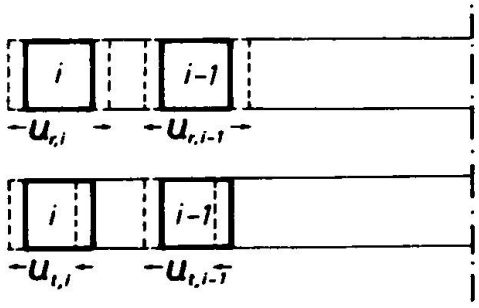

ABB. 2

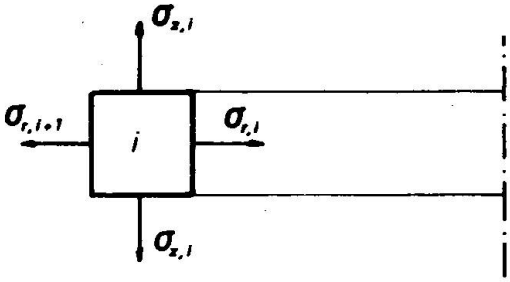

ABB. 3

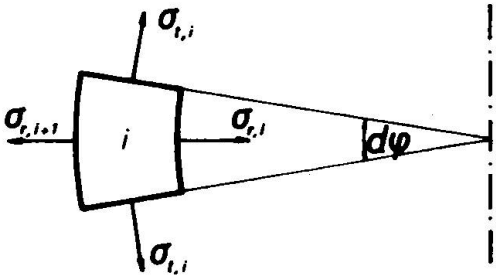

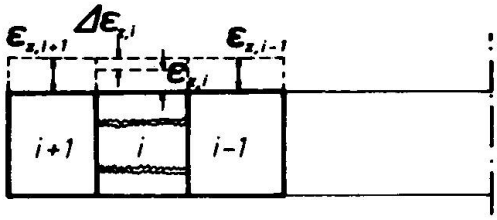

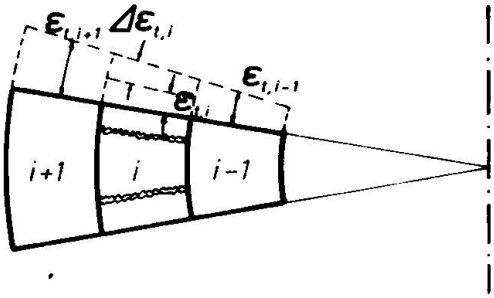

ABB. 4

$\sigma_{z,i} \cdot M_{S,i}$ zu

$K_{z,i+1}$:

$$\sigma_{r,i} \cdot L_{S,i} + (-1) \cdot \Delta\varepsilon_{z,i} + \sigma_{t,i} \cdot N_{S,i} + \sigma_{r,i+1} \cdot O_{S,i+1} +$$

$$+ \sigma_{z,i+1} \cdot P_{S,i+1} + \sigma_{t,i+1} \cdot Q_{S,i+1} + \sigma_{r,i+2} \cdot R_{S,i+2} = B_{K,z,i+1} \quad (22)$$

In der axialen Gleichgewichtsgleichung entfällt der Ausdruck $\sigma_{z,i} \cdot S_{S,i}$.

Die radialen Gleichgewichtsgleichungen bleiben unverändert.

Radiale-vertikale Rißebene ($\sigma_{t,i} = 0$)

Die mittlere, ideelle Dehnung des Teilzylinders i mit beschränkter Tragfähigkeit in tangentialer Richtung beträgt

$$(\varepsilon_{t,i} + \Delta\varepsilon_{t,i}) \cdot \frac{(r_{i+1} + r_i)}{2} \quad (23)$$

Damit erhält man in der radialen Kontinuitätsbedingung der Teilzylinder i-1 und i anstelle des Ausdruckes $\sigma_{t,i} \cdot J_{S,i}$ den Wert $\Delta\varepsilon_{t,i} \cdot J_{\Delta\varepsilon,i}$.

$$J_{\Delta\varepsilon,i} = \frac{(r_{i+1} + r_i)}{2}$$

$K_{r,i}$:

$$\sigma_{r,i-1} \cdot D_{S,i-1} + \sigma_{z,i-1} \cdot E_{S,i-1} + \sigma_{t,i-1} \cdot F_{S,i-1} + \sigma_{r,i} \cdot G_{S,i} +$$

$$+ \sigma_{z,i} \cdot H_{S,i} + \Delta\varepsilon_{t,i} \cdot J_{\Delta\varepsilon,i} + \sigma_{r,i+1} \cdot K_{S,i+1} = B_{K,r,i} \quad (24)$$

In die radiale Kontinuitätsgleichung für die Teilzylinder i und i+1 muß man für den Ausdruck $\sigma_{t,i} \cdot F_{S,i}$ nun $\Delta\varepsilon_{t,i} \cdot F_{\Delta\varepsilon,i}$ einführen.

$$F_{\Delta\varepsilon,i} = -\frac{(r_{i+1} + r_i)}{2}$$

$K_{r,i+1}$:

$$\sigma_{r,i} \cdot D_{S,i} + \sigma_{z,i} \cdot E_{S,i} + \Delta\varepsilon_{t,i} \cdot F_{\Delta\varepsilon,i} + \sigma_{r,i+1} \cdot G_{S,i+1} +$$

$$+ \sigma_{z,i+1} \cdot H_{S,i+1} + \sigma_{t,i+1} \cdot J_{S,i+1} + \sigma_{r,i+2} \cdot K_{S,i+2} = B_{K,r,i+1}$$

(25)

In der axialen Kontinuitätsbedingung der Teilzylinder i-1 und i fällt der Ausdruck $\sigma_{t,i} \cdot Q_{S,i}$ weg. In der axialen Kontinuitätsbedingung der Teilzylinder i und i+1 fällt der Ausdruck $\sigma_{t,i} \cdot N_i$ heraus. In der radialen Gleichgewichtsbedingung für den Teilzylinder i fällt der Ausdruck $\sigma_{t,i} \cdot B_{S,i}$ weg. Die vertikale Gleichgewichtsbedingung bleibt unverändert.

Gleichungssystem

Bei n Teilzylindern erhält man 3 . n - 1 Gleichungen für n Tangential-, n Axial- und n-1 Radialspannungen. Diese werden zweckmäßi nach dem Schema in Abb. 5 geordnet.

Für gerissene Teilzylinder sind die Koeffizienten entsprechend obigen Entwicklungen zu ändern.

3. Bruchkriterium

Bei einem Bruchsicherheitsnachweis unter hpothetisch ansteigende Innendruck hat der Spannungszustand an der Außenseite des zylindrischen Teiles des Druckbehälters die Form

$$+\sigma_3 = +\sigma_t > +\sigma_1 \approx +\sigma_z > -\sigma_2 \approx -\sigma_r$$

(+ Zugspannung; - Druckspannung)

Man sieht, daß die Tangentialspannung (σ_t), die auf Grund der rotationssymmetrischen Idealisierung die dritte Hauptspannung (σ_3) ist, wie nachfolgend gezeigt wird, maßgebend für die Rißbildung ist. Axial- und Radialspannung (σ_z, σ_r) fallen hier mi den Hauptspannungen (σ_1, σ_2) zusammen. Ein Vergleich der Reche ergebnisse der Methode des unendlichen Zylinders mit den Ergebnissen aus einer Berechnung des gesamten Behälters mit der Finiten Element Methode bestätigen dies (Lit. 9).

Für die Anstrengung des Betons bei Spannungszuständen oben angeführter Art geben alle Verformungsenergiehypothesen (v. Mises, Huber, Hencky, Beltrami), die Hypothese der maximalen Schubspannung (Tresca), der maximalen (Navier, St. Venant) und resultierenden (Sandel) Dehnung unbrauchbare Grenzwerte.

		1	2	3	4	5	6	7	8	9	10	11	12	13	14	15	16	17	18	19	20	21	22	23
	Gleichung	$G_{z,1}$	$G_{t,1}$	$G_{r,2}$	$G_{z,2}$	$G_{t,2}$	$G_{r,3}$	$G_{r,i-1}$	$G_{z,i-1}$	$G_{t,i-1}$	$G_{r,i}$	$G_{z,i}$	$G_{t,i}$	$G_{r,i+1}$	$G_{z,i+1}$	$G_{t,i+1}$	$G_{r,i+2}$	$G_{r,n-1}$	$G_{z,n-1}$	$G_{t,n-1}$	$G_{r,n}$	$G_{z,n}$	$G_{t,n}$	Belastung
1	G_z	$S_{s,1}$			$S_{s,2}$				$S_{s,i-1}$			$S_{s,i}$			$S_{s,i+1}$				$S_{s,n-1}$			$S_{s,n}$		$B_{G,z}$
2	$G_{r,1}$		$B_{s,1}$	$C_{s,2}$																				$B_{G,r,1}$
3	$K_{r,2}$	$E_{s,1}$	$F_{s,1}$	$G_{s,2}$	$H_{s,2}$	$J_{s,2}$	$K_{s,3}$																	$B_{K,r,2}$
4	$K_{z,2}$	$M_{s,1}$	$N_{s,1}$	$O_{s,2}$	$P_{s,2}$	$Q_{s,2}$	$R_{s,3}$																	$B_{K,z,2}$
5	$G_{r,i-1}$							$A_{s,i-1}$		$B_{s,i-1}$	$C_{s,i}$													$B_{G,r,i-1}$
6	$K_{r,i}$							$D_{s,i-1}$	$E_{s,i-1}$	$F_{s,i-1}$	$G_{s,i}$	$H_{s,i}$	$J_{s,i}$	$K_{s,i+1}$										$B_{K,r,i}$
7	$K_{z,i}$							$L_{s,i-1}$	$M_{s,i-1}$	$N_{s,i-1}$	$O_{s,i}$	$P_{s,i}$	$Q_{s,i}$	$R_{s,i+1}$										$B_{K,z,i}$
8	$G_{r,i}$										$A_{s,i}$		$B_{s,i}$	$C_{s,i+1}$										$B_{G,r,i}$
9	$K_{r,i+1}$										$D_{s,i}$	$E_{s,i}$	$F_{s,i}$	$G_{s,i+1}$	$H_{s,i+1}$	$J_{s,i+1}$	$K_{s,i+2}$							$B_{K,r,i+1}$
10	$K_{z,i+1}$										$L_{s,i}$	$M_{s,i}$	$N_{s,i}$	$O_{s,i+1}$	$P_{s,i+1}$	$Q_{s,i+1}$	$R_{s,i+2}$							$B_{K,z,i+1}$
11	$G_{r,i+1}$													$A_{s,i+1}$		$B_{s,i+1}$	$C_{s,i+2}$							$B_{G,r,i+1}$
12	$K_{r,n}$																	$D_{s,n-1}$	$E_{s,n-1}$	$F_{s,n-1}$	$G_{s,n}$	$H_{s,n}$	$J_{s,n}$	$B_{K,r,n}$
13	$K_{z,n}$																	$L_{s,n-1}$	$M_{s,n-1}$	$N_{s,n-1}$	$O_{s,n}$	$P_{s,n}$	$Q_{s,n}$	$B_{K,z,n}$
14	$G_{r,n}$																				$A_{s,n}$		$B_{s,n}$	$B_{G,r,n}$

ABB. 5

Die Unterschiede der Bruchspannungen nach den Theorien von Mohr, Leon, Coulomb sowie nach den Untersuchungen von Weigler-Becker an Scheiben, Rosenthal-Glucklich an Hohlzylindern zu der Normalspannungshypothese sind in diesem Spannungsbereich gering (Lit. 10,11,12). Es liegt daher nahe, für die Rißbildung die größte Zugspannung, in diesem Fall die Tangentialspannung, verantwortlich zu machen und senkrecht auf diese die Bruchfläche anzunehmen. Der mögliche Fehler durch Nichtbeachtung der zwei anderen Spannungen dürfte gegenüber den Unsicherheiten der Materialkenntnisse, wie Elastizitätsmodul, Querdehnzahl, mehrachsiges Kriechen, vagabundierende Spannungen aus Abbindewärme usw., vernachlässigbar klein sein.

Literatur

(1) Y.R. Rashid: "Ultimate Strength Analysis of Prestressed Concrete Pressure Vessels"; Nuclear Engineering and Design 7 (1968), 334 - 344; North-Holland Publishing Comp., Amster

(2) W. Walluschek-Wallfeld: "Beitrag zur Berechnung von Druckbehältern aus Spannbeton"; Dissertation, Techn. Hochschule Graz 1973.

(3) H.H. Hofmann: "Grenztragfähigkeitsanalyse - Verbindung statistischer Methoden (Monte Carlo Methode) mit der Finite Element Analysis, z.B. für die Bruchberechnung von Spannbeton-Reaktordruckgefäßen"; Proc. of the 1st Intern. Conf. on Structural Mechanics in Reactor Technology, H 3/6 Berlin 1971.

(4) G. Schnellenbach: "Allgemeine Berechnung von Spannbeton-Reaktordruckbehältern unter Berücksichtigung von nichtlinearen Spannungs-Dehnungsgesetzen nach der Methode der dynamischen Relaxation"; Proc. of the 1st Intern. Conf. on Structural Mechanics in Reactor Technology, H 1/3, Berlin

(5) K. Schimmelpfennig, V. Hansson: "Untersuchungen zur Grenztragfähigkeit von Spannbeton-Reaktordruckbehältern"; Preprints of the 2nd Intern. Conf. on Structural Mechanics in Reactor Technology, H 2/3, Berlin 1973.

(6) J. Németi: "Status Report on the Austrian PCRV Model with Hot Liner"; 2nd Intern. Conf. on Structural Mechanics in Reactor Technology, H 3/8, Berlin 1973.

(7) F. Bremer, W. Fürste: "Entwicklung eines Spannbetondruckbehälters für Leichtwasserreaktoren und zugehörige Komponenten"; Techn. Mitt. Krupp - Forschungsberichte, Band 31 (1973) Heft 3.

(8) S. Menon et al.: "Scandinavian PCRV Development: Present Status and Planned Work, 1973 - 1975"; Preprints of the 2nd Intern. Conf. on Structural Mechanics in Reactor Technology, H 3/9, Berlin 1973.

(9) A. Nesitka, W. Walluschek-Wallfeld: "Statische Berechnung, Sicherheitsüberlegungen und Untersuchungen des Bruchvorganges von Reaktordruckbehältern aus Spannbeton"; Preprints of the 2nd Intern. Conf. on Structural Mechanics in Reactor Technology, H 2/7, Berlin 1973.

(10) H. Kupfer: "Das Verhalten des Betons unter mehrachsiger Kurzzeitbelastung unter besonderer Berücksichtigung der zweiachsigen Beanspruchung"; Deutscher Ausschuß für Stahlbeton, Heft 229, Berlin 1973.

(11) H. Weigler, G. Becker: "Über das Bruch- und Verformungsverhalten von Beton bei mehr-achsiger Beanspruchung"; Bauingenieur 36 (1961), Heft 10, S. 390 - 396.

(12) I. Rosenthal, J. Glucklich: "Strength of Plain Concrete under Biaxial Stress"; ACI Journal, November 1970, S. 903 - 914.

ZUSAMMENFASSUNG

Reaktordruckgefäße aus Spannbeton sind zum großen Teil Behälter von zylindrischer Form. Für den zylindrischen Mittelteil wird ein Näherungsverfahren gezeigt, das gut zur Festlegung von Wandstärke und Spannkräften geeignet ist und eine Abschätzung der Bruchsicherheit ermöglicht. Die Verwendung der Normalspannungshypothese als Bruchkriterium für den Beton wird begründet.

SUMMARY

In general, prestressed concrete pressure vessels are vessels of cylindric shape. The paper shows a simple method with good accuracy for calculating the middle cylindric part of pressure vessels.

This method is well suited to determine the thickness of the wall and the tendons as well as to estimate the ultimate load. The paper explains the reason for the application principal stress hypothesis as failure criterion for concrete.

RÉSUMÉ

La plupart des caissons en béton précontraint pour des réacteurs nucléaires est d'une forme cylindrique. Pour la partie cylindrique du caisson une méthode approximative est présentée, particuliereme appropriée à déterminer l'epaisseur de la paroi et les précontrain Par la même méthode, il est possible d'estimer la sécurité de rupture. L'application de l'hypothèse de la contrainte principale pour le critère de rupture du béton est motivée.

Rapports complémentaires
Ergänzende Berichte
Complementary Report

II-2 Prof. E. FUMAGALLI

Monsieur le Président, Mesdammes et Messieurs, en tenant compte que mon rapport est déjà à vos mains, pour mieux documenter l' activité de l' ISMES dans le domaine des modèles de conténiteurs nucléaires en précontraint, je me permets d' utiliser le temps à disposition pour vous proposer la projection d' un bref documentaire relatif à deux modèles récemment essayés à l' ISMES. A ce sujet je donne la parole à M. Verdelli qui a suivi personellement l' éxécution et les essais des modèles susdits.

II-2 Mr. G. VERDELLI

A short film is shown to illustrate the tests dealt with in Report II-2 more effectively; it summarizes the most interesting aspects of the construction and the tests carried out at ISMES during the last year on thin models in the scale 1 : 20. The film is divided into two parts. The first part shows the most important construction stages and the tests carried out on thin model no. 2 (see paper). The collapse of this model occurred at a pressure of 120 Kg/cm^2 with the breaking of a large number of the hoop cables of the barrel. The second part of the film has no commentary and illustrates the ultimate tests carried out in successive stages on thin model no. 3 described in detail in the report in question and only recently finished. In the initial stage of the ultimate tests the maximum pressure reached was 90 Kg/cm^2 corresponding to the first clearly visible cracks which concerned the central part of the barrel. In the two overpressure tests up to 115 Kg/cm^2 which were later carried out, although there were an increased number of cracks (limited however to the central part of the barrel) the elastic behaviour of the prestressing cables was still evident. Final collapse, at 140 Kg/cm^2, occurred with the collapse of the central part of the upper slab. This type of unexpected collapse is caused by the yield of the wires of the slab hoop cables, the diameter - in this third model - not having been increased as were the wires in the other cable systems.

II-3 Ing. R. RICCIONI

Mr. Chairman, Ladies and Gentlemen; I trust you will allow me to apologize not only for myself but also on behalf of Prof. Fanelli and Dr. Robutti for the delay in presenting our paper. A delay hardly justified by the fact of our being in an own house here, but perhaps excusable on account of our work, based on numerical methods, is only a simple chess piece, dependent on the other pieces in the game - that is to say - the project, the available information of the physical model and the specified rheological input.

The substance of our work is not only a verification of the structure of a nuclear vessel with finite element method - as it would seem to appear at first sight - but is infact an exact indication of the necessity and possibility of complementarity for those involved in the designing, verification of physical and numerical modelling, as well as for those who provide information on rheological behaviour of materials.

In our case the information obtained from the physical model suggested an investigation in the elastic linear field and has allowed an evaluation of the elastic modulus of concrete. The results of tests carried out on samples of concrete of the same type as that used in the physical model - elaborated with the matematical one - allowed evaluation of the elastic modulus by other means. The compatibility between the figures obtained through completely different methods was morethansatisfactory.

The determination of the optimum prestressing sequence of cables and of local safety factors, complete the picture of information available and confirm a "modus operandi" which must be considered fundamental for structures, such as nuclear vessels, whose safety must not be in doubt.

II - 4 Dr. F.K. GARAS

I must apologize for not giving the participants enough time to read my paper, but if you work for a commercial organization you will realize it is not always easy to find time to write papers. However, I will try in the next few minutes to highlight some of the key points mentioned in the paper. The paper deals mainly with the problem of high shear stresses which have to be accommodated in the design of prestressed concrete pressure vessels as shown in figure 1 of the paper. This shows a section through the Hartlepool/Heysham podded boiler type pressure vessel. There are four vessels of this design under construction at present in the U.K.

Pressure vessels for the containment of nuclear reactors include structural members which rely for their safety on the capacity of concrete to resist high shear stresses. Typical examples are end slabs, the barrel wall and boiler closures. These members are geometrically deep in relation to their span and subject to flexure, but the large deformations which would normally be induced are restricted by lateral restraint in the form of either prestressing or the continuity of the structure around the element considered. The first part of the paper is a summary of an experimental investigation into circular end slabs. Figure 7 in the paper shows the type of model which was used. To date we have tested 23 models to failure. They varied in scale between 1/24th and 1/8th scale. The parameters studied included the amount of hoop prestress, bonded reinforcement, span to depth ratio, boundary conditions, penetration liners, sustained temperature and concrete strength.

Figure 6 in the paper shows the general behaviour of a typical model. Here we plotted the percentage of ultimate pressure versus the percentage of maximum central deflection. The flexural behaviour can be divided into three stages. The first, the elastic stage, was determined by the pressure at which the first crack occurred, the next stage, elastoplastic, where boundary reinforcement started to yield and we got higher deflections and the last stage is the plastic stage. This behaviour was overcome by a shear type failure which is shown in Figure 7 in the paper. This is a typical failure in which a shear plug is formed with the exit of the plug determined by the position of the vertical prestress. The angle of shear plane was found to be determined by the span to depth ratio and the amount of hoop prestress.

In analysing the behaviour of end slabs we found that the ultimate shear strength was influenced by three components (figure 3 in the paper) - the compression zone, the small zone at the bottom, the aggregate interlock - which most people ignore in their analyses - and the third one, whose contribution is fairly small, the dowel action of the rebar.

In the end slab models a large number of internal and surface strain measurements were taken during the various stages of the tests and Slide 1 gives typical results.
The slide shows the development of the compressive and tensile zones as the pressure is increased. It can be seen that the reduction in depth of the compression zone can be determined from slab measurements. The first figure shows the stress distribution at 43% of the ultimate pressure. Although high tensile stresses of the order of 3000 microstrain were developed at the outer surface of the model it was still considered elastic. Figure 4 in the paper shows how the depth of the compression zone was reduced as the pressure was increased up to about 95% of the ultimate pressure. Prior to ultimate, the depth of the compression zone varied between 10 and 15% of the total depth depending on the type of model tested.

To give an idea of the breakdown of the total shear force between the three components previously mentioned, the compression zone represents about 45% of the total shear force, aggregate interlock as much as 50% and dowel action about 2 to 3%.

In the paper, an empirical expression is given which predicts the results of our experimental work and most of the published data. This is shown on page 5.

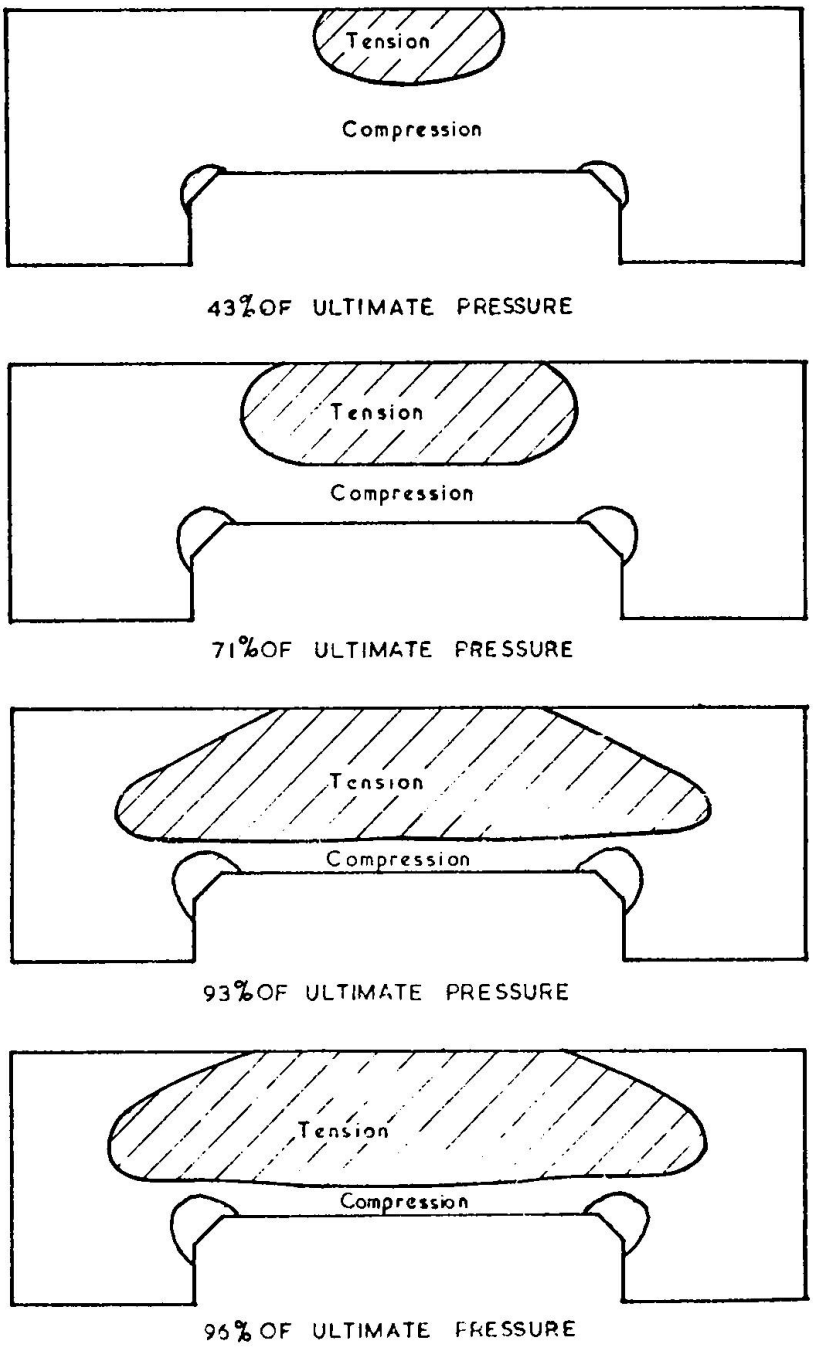

Development of Zones of Tensile Stress

SLIDE 1

The second part of the paper describes part of the development work carried out on the boiler closures for the Hartlepool and Heysham vessels. In each vessel there are 8 boiler pods, having a corresponding number of closures. Figure 2 in the paper shows the arrangement and various details. The paper describes the design philisophy behind these components.

To support the development of the design, models of 2 different scales were tested. Firstly 60 No. 1/10th scale models were tested and these were used to optimise on the design parameters and to examine their likely effects on the operational and overload behaviour. Figure 8 in the paper shows the test arrangement of the small scale models. The test programme is described in the paper. A typical mode of failure is shown in figure 10 in the paper. One of the significant results of the tests was the difference between the contribution of the active and passive restraint. This is one of the parameters which was examined and some of the models were tested with active and some with passive restraint. Figure 9 in the paper shows that the ultimate shear strength was 50% higher in the case of models with active prestress.

The results obtained from the 1/10th scale models were used in the final design of the closure but as a confirmatory measure 4 No. 1/3rd scale models were tested to examine the short and long term behaviour, using the test arrangement shown in figure 11 in the paper. The models were initially prestressed down and most of the components were scaled accurately. We used a hydrostatic pressure loading system. The test programme is described in Table 2 of the paper. M1 and M2 were tested in the short term at ambient temperature with passive and active prestress, respectively. In model M3, elevated temperature was sustained for a period of 9 months and M4 was temperature and load-cycled. Figure 15 shows a comparison between the measured and predicted hoop, creep strains for model M3 using a prediction based on Dr. Browne's work on the specific strain data for the Hartlepool concrete. Finally it is worth noting that generally there was good correlation between the behaviour of the two scales of model.

Prof. R. N. WHITE

The first question is from Prof. Baker, on Prof. Fumagalli's paper II-2. "Were cables bonded? Could long term pressure load and temperature effects be assessed from the test? "

Ing. F. SCOTTO reply

As concerns the first question the answer is: the cables (monowire type) were not bonded.

In so far the second question is concerned our experience on long term effects was just devoted to follow the variations in the prestressing: see Fig. 6 of the paper II-2. The figure reports the losses up to 10 days (in our tests we were more interested in the ultimate condition and related safety factors than in the long term effect) but the tests went on along 3 months without remarkable changes in results.

In any case we believe that in principle, it is possible on our models to follow the behaviour of the structure along a reasonable period of time (i. e. one year) in the sense that realibility of the instrumentation can be ascertained, and the temperature in the test room can be satisfactorily kept constant. (this test is very expensive).

In the reality the actual structure will experience any kind of operational and accidental conditions along its life: this cannot be simulated on models. It must be taken in mind that it is already a great problem to assess the variation in the prestressing forces due to intricate loading and thermal hystory of PCPV. This in turn will change the state of stress of the structure and the corresponding long term effects. For the above we believe that this problem must be studied on the basis of a mathematical approach with simplified conservative assumptions.

Prof. R. N. WHITE

A second question from Prof. Baker, on Dr. Garas' s paper II-4: "Did the shear cracks start as bending cracks? Test of short unreinforced beams give deviations of shear strength several times greater than typical deviations for bending strength. Will this also apply to pressure vessels and slabs? "

Dr. F. K. GARAS

As an aid to further understanding of the shear compressive failure of restrained end slabs, we have tried to simplify the problem by examining visually the inclined crack patterns leading to the two-dimensional mode of failure of restrained deep beams.

A number of restrained beams representing a strip of an end slab, having a span to depth ratio of 2.5, were loaded under different degrees of restraint and using similar loading conditions to those adopted in the end slab tests.

The investigation has shown that the nominal shearing stresses at failure were similar to those which occurred in end slabs. Typical values were given in the national report (paper no. I-5) Table 1.

Prof. R.N. WHITE

Could I also ask a question while you are here? You mentioned the breakdown of shearing force was about 45% in the concrete compression zone, 50% in the interlock and maybe a few percent in dowel action. How did you determine this breakdown?

Dr. F.K. GARAS

The contribution of each component in resisting shear forces was assessed using experimental data: (i) Compression zone: the shear resistance of this component was abstracted from our experimental work on restrained deep elements failing in shear compression. Part of this work was published in an earlier paper. A relationship between the amount of hoop restraint and the shear strength was developed. In end slab models the biaxial compression was directly derived from the hoop prestress forces above the tip of the haunch crack. Using this information the shear resistance of the compression zone was about 45% of the total.

(ii) Aggregate Interlock in Tension Zone: the magnitude of this component is a function of crack width and crack displacement. From end slab tests the cracks widths just prior to failure were derived by substracting a value for the elastic strain, based on a linear extension, from the total radial deformation of the slab. By extrapolation using Fenwick's work on aggregate interlock and the measured crack width and shear displacement from our models the aggregate interlock component was about 50% of the total shear force.

Prof. R.N. WHITE

Next paper for the questions is no.5: the question in for Prof. Hornby, from Prof. Baker, who has supplied us with many good questions. This question runs like this: cables on British reactors are non-bonded, therefore with accidental overload splitting the liner, gas pressure will spread in wide cracks. Is the disappearance of vapour pressure analogous?

Mr. I.W. HORNBY

The reference I made in the introduction of our paper to the vapour pressure during the heating up is a totally different condition to gas pressurising cracks after the splitting of the liner.

The vapour pressure is analogus to gas which has got behind the liner through, say, a small undetected pin hole in a weld. This gas, if it did not dissipate, could cause a pressure build up behind the liner or in cracks (if, in fact, any cracks exist at working pressure). The vapour pressure in the hot spot test dissipated very rapidly (see fig. 12 of Irving et. al. 1974) and other more recent tests with gas, have measured large flows away from a liner concrete interface. Consequently the possibility of a build up of pressure behind the liner is very unlikely.

Reference: Irving, J., Carmichael, G. D. T., and Hornby, I. W.
A full-scale model test of hot-spots in the prestressed concrete pressure vessels of Oldbury Nuclear power station. Proc. Inst. Civ. Engrs. 1974, 57 (June) 331-351.

Prof. R. N. WHITE

The next question on paper 7 is directed to Mr. Lemasson; this is also from Prof. Baker: "French vessels have bonded cables, British have non-bonded. Do you still think non-bonded cables are better? "

Mr. M. LEMASSON

Je pense que le sujet est inépuisable et je crois que pendant très longtemps on parlera encore des câbles injectés et des câbles non injectés. Il y a effectivement deux techniques possibles, qui ont chacune leurs avantages et leurs inconvénients, mais je ne pense pas que quelqu' un ait trouvé de conclusion définitive. C' est tout ce qu' on peut dire. Dans le cas de la précontrainte par enroulement de fils ou câbles ("wire winding") des caissons du type HTGR, je crois que là effectivement il serait très difficile de protéger autrement que par de la graisse. Mais pour les câbles sous gaine en France nous continuons à les injecter et nous avons toujours pensé que l' adhérence qui existait de ce fait entre le câble et la structure apportait un complément de sécurité. Je pense que c' est tout ce qu' on peut dire à ce sujet qui je crois ne sera pas épuisé tout de suite.

CHAIRMAN

Are there more remarks on this subject? You know, from the very beginning when prestressed reactor pressure vessels came into the idea, this question about the grouting or not grouting was very important. I think more or less every country now has a particular philosophy on this point. For instance in Germany we grout mainly from the viewpoint of the protection against corrosion, because we have the feeling there is no better way to have a good corrosion protection. And then we have all the benefits which grouting gives. We think in any case there is no need to change a cable at a later time.

Prof. A. L. L. BAKER

Could I pose one supplementary question? I just wanted to ask whether anyone has had experience of removing a non bonded cable, examining it and putting it back again. Has that been done yet after these ten years or so? and if so, how does it work? I mean, can it be done fairly simply or is it very difficult?

Mr. I. W. HORNBY

In Britain, a system of cable inspection has been in operation from the completion of the first concrete pressure vessel. The inspection includes the destressing and total withdrawal, of a number of cables every year. These cables then undergo a through examination particularly for evidence of corrosion. The operation is relatively straight forward and has to date presented no difficulties. The cables that are withdrawn are not reused but replaced with new ones.

Prof. A.D. ROSS

I think two points ought to be made. Grouting in conventional civil engineering structures has not invariably protected the tendons from corrosion. I think that is a point that is worth making. What Mr. Hornby said about stray electric currents, of course we do understand and this is a risk we are aware of in Great Britain. If there are tendons or other corrodable materials at risk, electric welding and especially direct current welding should be avoided on the construction. One point only I would like to add: if at any time, 10 years, 15 years hence, you are concerned that the pre-stress in your vessel may have declined too much it is very simple to re-tension and restore the full prestress. This is one of the major advantages of ungrouted tendons.

Dr. R.D. BROWNE

I would like to ask Dr. Scotto whether there is any guarantee that a grouted cable under conditions of modest temperature will inhibit the formation of macro-electrolytic cells over a long period of time? We have been looking at the mechanisms of corrosion of reinforcement in concrete in relation to offshore structures. It appears that there are instances where certain materials can contaminate concrete, giving a reduction to the passivation of the reinforcing by the alkalis in cement: a corrosion macrocell can develop with the steel. I am wondering whether perhaps I can throw it back to Dr. Scotto to ask whether any work has been done on grouted cables to establish that over a substantial period of time under site operational conditions, rather than under laboratory conditions, that the grouted cable has shown to be satisfactory.

Ing. F. SCOTTO

If I have understood it correctly, you said that in your country your opinion is to grout the cables with cement mortar. As far as the "winding system" is concerned, which is your opinion assuming that you cannot grout these cables?

I would just like to give you the results of the famous enquiry we made in Berlin, on the subject "to grout or not to grout". We divided the people who where talking about this argument in categories, that is to say, the purchasers, the authorities and suppliers. It is clear that the suppliers liked to grout and not to speak about these problems in the future, while the purchasers were of different opinion, because they are committed to keep these structures for their whole life, and finally the authorities, who are people grouted of doubts, were reluctant on the subject. Generally speaking authorities and purchasers were against grouting while the suppliers were in favour of it.

We have known of negative experience in the French famous first pressure vessel. They were oobliged to change some cables because difficulties arised during the construction. Steel was not suitably protected, but this is something that happens. In fact it is very difficult during the construction stage to be 100% safe, on the quality of the work, especially nowadays, that we have troubles for strikes and so on. So the probability of corrosion, because we have to talk in terms of probabilities, the probability to loose the vessel or the overall plant, to loose millions of dollars, is very high.

If I had to decide about this question, I believe I would decide to be against grouting, just to tell you my present position.

CHAIRMAN

I think it is a very interesting question we are discussing now, but strictly speaking it is not the subject of our seminar, because it has nothing to do with tri-axial stresses. As we have no more written questions I ask the audience if there are questions on the papers. We have some time left for the discussion. I hope that you will use this time.

Ing. F. SCOTTO

I was very much interested in the French paper by Mr. Lemasson. They say that they have made some frictional tests. Can you kindly give us some figures and the method followed to ascertain these frictions?

Mr. M. LEMASSON

Nous avions effectivement construit un anneau à l' échelle 1 par rapport au caisson, c' est à dire un anneau de 25 m de diamètre environ avec une gorge circulaire dans laquelle nous pouvions placer différents câbles de précontrainte, introduits dans différents types de gaines. Celles-ci pouvaient être des gaines rigides, des gaines souples en feuillard, revêtues on non revêtues. Dans le cas du câble BBR et avec une gaine souple revêtue de zinc nous avons obtenu 0,16 comme coefficient de frottement global: ce coefficient était un peu plus important dans le cas de tubes rigides et je crois qu' il était de l' ordre de 0.20.

Prof. R.N. WHITE

I'd like to address a question to Mr. Kawamata. One of your slides showed the comparison of normal stresses and shear stresses; the shear stresses did not agree nearly as well as the others. Is this an inherent difficulty with this layered substructure?

Dr. S. KAWAMATA

I think Prof. White is pointing out a difference in the shear stress distributions from the method of sliced substructure and from the ordinary three dimensional analysis using isoparametric elements shown in fig. 13 (d).

Last evening I asked Prof Zienkiewicz about the latter distribution of shearing stress. The result is not natural because the shearing stress does not vanish at the free surface. Prof. Zienkiewicz opinion is that this result may be based on the way by which we are representing the value of the stress. When we use some points near the boundary of the elements, we will often have irregular distribution of stress. His suggestion is to use the values at the Gauss points in linear or parabolic interpolation of the stress distribution. Therefore, a part of the difference may be attributed to the wrong interpretation of the solution by the iso-parametric elements.

Using the IBM 360/195 axi-symmetric analysis required 7 seconds of CPU time. For our new system of substructure analysis, we used 47 seconds. The letterCPU time includes 27 seconds of matrix inversion during the condensation procedure. I think this is a rather big amount which we have experienced so far and I think something is wrong in the inversion procedure. So this will be further reduced. But for the three dimensional iso-parametric method we cannot make comparison because we used the Gauss-Seidel's iteration using the initial value, which was the results we got from the method of sliced substructure, and it converged very rapidly.

Prof. A.D. ROSS

I have a very brief question relevant to the splendid films of the tests of the models that we saw. Having seen many model tests over the years this is the first time that I have seen a top cap fail so suddenly in a hydraulic test. I wanted to ask if there was a long pipeline which might have stored a fair amount of strain energy in the system.

Ing. F. SCOTTO

First of all, I must explain the reason why you have assisted to this kind of ultimate condition in this model. The final collapse you have assisted to in the film was related to the third model. This final condition was reached at 140 atm. The difference between the third and the second model (that is the first that you have seen with all the hooping cables that were broken at 120 atm) was simply due to the fact that we improved the diameter of the wires from 6 to 7 mm, from 7 to 8 mm, etc. just to try to find out what were the results, in terms of safety, of this wasting of steel. In terms of costs we are talking of half a million $, a very big amount of money.

Coming in the question, because we had an hydraulic pressurization and the pressurized copper bag that was inside to allow the deformation of the concrete did not fail at all, as you have seen, we were able to assist to the collapse of the internal portion of the cap slab, non reinforced, and to the explosive effects of the releasing strain energy. It resulted a sort of opening like a flower of the upper outer ring of the barrel and then a cutting out in pieces of the internal portion of the slab and consequently, finally, the explosive failure. The reason of this strange collapse was due to the fact that we did not improve (as per the rest of the structure) the cap slab hooping cable system.

CHAIRMAN

It seems that there are no more questions, then it is left to me to thank all the authors, to thank those who have taken part in the discussion.

The session is closed. Thank you very much.

Leere Seite
Blank page
Page vide